



UNIVERSITY OF
BIRMINGHAM

Enzyme-responsive nanomaterials for the delivery of antimicrobial peptides

by

Alexander Antropenko

A thesis submitted to the
University of Birmingham
for the degree of
DOCTOR OF PHILOSOPHY

School of Chemistry

College of Engineering and Physical Sciences

University of Birmingham

April 2024

UNIVERSITY OF
BIRMINGHAM

University of Birmingham Research Archive

e-theses repository

This unpublished thesis/dissertation is copyright of the author and/or third parties. The intellectual property rights of the author or third parties in respect of this work are as defined by The Copyright Designs and Patents Act 1988 or as modified by any successor legislation.

Any use made of information contained in this thesis/dissertation must be in accordance with that legislation and must be properly acknowledged. Further distribution or reproduction in any format is prohibited without the permission of the copyright holder.

Abstract

The rate of resistance to antibiotics that are commonly used in the clinic is escalating rapidly, surpassing the introduction of new antimicrobial drugs. To address this problem, alternative strategies are being explored, such as the re-evaluation of antibiotics, that have not yet gained widespread clinical application. Antimicrobial peptides (AMPs) represent one of those antibiotics, offering remarkable antimicrobial efficacy against various pathogens. However, in clinical settings, AMPs are typically considered a last-resort option due to their off-target effects and poor stability *in-vivo* resulting from their cationic and amphiphilic peptide nature. Therefore, most of current strategies addressing these limitations focus primarily on the control and shielding of the cationic charge and the amphiphilic nature of AMPs. These can potentially be achieved through encapsulation of AMPs inside stimuli-responsive polyelectrolyte complexes (PECs) by combining the cationic drug with anionic polyelectrolytes. Stimuli-responsive polymers can be employed as encapsulation materials in PECs to design systems that activate drug release in response to specific changes encountered during microbial infection, such as variations in pH, enzyme activity, or temperature.

The overarching aim of this Thesis was to explore the creation of PECs capable of encapsulating the clinically approved antimicrobial peptide, Polymyxin B and its subsequent enzyme-induced release. In Chapters 2 and 3, the aims were: Firstly, to synthesize anionic and helical polymers incorporating enzyme-degradable peptide side chains (Aim 1.1), followed by evaluation of the degradation properties of these polymers in response to the enzyme released by gram-negative bacterium *Pseudomonas aeruginosa* (Aim 1.2). In Chapter 4, the first objective (Aim 1.3) was to assemble Polymyxin B and the anionic enzyme-degradable polymers into PECs. The next objective (Aim 1.4) involved investigating the *P. aeruginosa*-induced drug release from these PECs, while Aim 1.5 focused on assessing the antimicrobial activity of the developed PECs against *P. aeruginosa* strains.

Chapter 1 provides a review of the current developments in the field of the stimuli-responsive delivery of AMPs using polyelectrolyte complexes. Chapters 2 and 3 discuss the synthesis of polymers with poly(methacrylamide) and poly(acetylene) backbones respectively coupled to enzyme-degradable peptide side chains. Of the synthesized materials, two poly(methacrylamide) polymers from Chapter 2 were found to be the most effective in terms of degradation by the enzyme released by *P.aeruginosa*, while none of the synthesized acetylene-containing peptides from Chapter 3 polymerized. Subsequently, the poly(methacrylamide) polymer with the highest multivalency was used to form PECs with Polymyxin B in Chapter 4. Eight different formulations of PECs were created, with one being the most optimized in terms of encapsulation efficacy and physiological stability. The stability of the particles was further improved by the addition of Tannic Acid, which acted as a protective coating and a cross-linker. The Thesis then evaluated the ability of the PECs to release Polymyxin B under enzymatic degradation. Finally, the preliminary evaluation of the antimicrobial activity of the PECs against various *P.aeruginosa* strains were presented.

Preface

- Chapter 1 (Introduction) of this Thesis has been published in the following article: Alexander Antropenko, Frank Caruso and Paco Fernandez-Trillo, Stimuli-Responsive Delivery of Antimicrobial Peptides Using Polyelectrolyte Complexes, *Macromol. Biosci.*, 2023, e2300123.
- In Chapter 2 and 3 of this Thesis Paco Fernandez-Trillo provided helpful discussion which helped with experimental design and planning, including help with language editing. Overall, these chapters contain 85 % of my original work.
- In Chapter 4 of this Thesis Dr Sara Hadjigol performed antimicrobial activity testing of PECs, which included bacterial culturing and measurement of the growth curves and MICs; Paco Fernandez-Trillo and Professor Frank Caruso provided helpful discussion which helped with experimental design and planning, including help with language editing. Overall, this chapter contains 80 % of my original work.

Acknowledgements

I want to start by thanking my two supervisors, Dr. Francisco Fernández-Trillo and Prof. Frank Caruso, for giving me the opportunity to work on this research in their groups in Birmingham and Melbourne. They provided continuous guidance and support throughout my Ph.D. journey. My supervisors were a great source of motivation and advice for me, empowering me to take on challenges and explore new avenues. I would like to thank Paco for his countless hours and energy spent providing constructive feedback and being a mentor in both scientific and personal matters. I would also like to thank Frank for giving me hope during difficult times and allowing me to finish the project in Melbourne.

I also want to express my gratitude to the members of Paco's and Frank's groups, both past and present. They made the research experience special and unforgettable. Thank you for your humor, positive energy and care. I would like to mention two post-docs, Sameh and Andrey, for teaching me essential synthetic methods that I used in the project.

I want to extend my thanks to everyone else who contributed to this thesis, both scientifically and personally: Dr. Sara Hadjigol for her assistance with antimicrobial testing; the analytical technicians in Birmingham (Chris, Allen, and Cécile) and Melbourne (Shuai and Sergey), who provided valuable support. Special thanks to Steve and Fran for their management of the laboratory. I extend my sincere appreciation to Maryline for her help with manuscripts and administrative tasks. Furthermore, I want to acknowledge and thank my committee chair, Prof. Sally Gras, for her invaluable advice during the confirmation and progress review meetings.

I also acknowledge the School of Chemical and Biomolecular Engineering at the University of Melbourne, the School of Chemistry, and the EPS College at the University of Birmingham for their financial support through the Priestley Joint PhD Scholarship and the facilities they provided to conduct the research. To make the research environment a safe and pleasant place to work.

I want to acknowledge the editorial work done by Wiley-VCH GmbH on the published work presented in this thesis.

Lastly, I would like to thank my parents, grandparents and all my fluffy friends, who always believed in me more than I did, for your support and everything you do to make me feel happy.

Contents

Abstract	i
Declaration of Authorship	ii
Preface	iii
Acknowledgements	iv
1 Introduction - Stimuli-Responsive Delivery of Antimicrobial Peptides Using Polyelectrolyte Complexes	1
1.1 Manuscript	2
1.2 Scope of Thesis	18
1.3 References	22
2 Preparation and evaluation of enzyme-degradable polymers for encapsulation of AMPs	24
2.1 Aim	26
2.2 Introduction	26
2.3 Experimental Section	30
2.3.1 Materials	30
2.3.1.1 Peptide synthesis	30
2.3.1.2 Polymerization reactions	30
2.3.1.3 Enzyme degradation studies	30
2.3.2 Instrumentation	31
2.3.3 Solid-phase peptide synthesis of enzyme-degradable sequences	32
2.3.3.1 Characterization of the synthesized peptides	33
2.3.4 Synthesis of poly(methacrylamide) polymers with enzyme-degradable peptide side chain	34
2.3.4.1 Characterization of the enzyme-degradable polymers	35
2.3.5 Enzymatic degradation testing procedure	36
2.4 Results and discussion	38
2.4.1 Peptide synthesis	38

2.4.1.1	Coupling of methacrylate group	42
2.4.1.2	Further optimization of solid-phase peptide synthesis of P1/2 peptides	47
2.4.2	Synthesis of the polymers bearing enzyme-degradable side chains	48
2.4.3	Enzymatic degradation of poly(methacrylamides) with peptide side chain	55
2.5	Conclusions	59
2.6	Supporting Information	60
2.7	References	68
3	Synthesis of stimuli-responsive helical polymers	71
3.1	Aim	73
3.2	Introduction	73
3.3	Experimental Section	77
3.3.1	Materials	77
3.3.1.1	Peptide synthesis	77
3.3.1.2	Polymerization reactions	77
3.3.2	Instrumentation	77
3.3.3	Solid-phase peptide synthesis of acetylene-containing peptides	78
3.3.3.1	Specific for synthesis of P4	79
3.3.3.2	Specific for synthesis of P5	79
3.3.3.3	Specific for synthesis of P6	79
3.3.3.4	Specific for synthesis of P7	80
3.3.4	Characterization of the synthesized peptides	80
3.3.5	Synthesis of poly(acetylene) polymers with enzyme-degradable peptide side chain	82
3.3.5.1	Characterization of the poly(acetylene) polymers	82
3.4	Results and discussion	84
3.4.1	Synthesis of an anionic acetylene-containing peptide (P4) from previous design of P1	84
3.4.2	Polymerization of P4 peptide	88
3.4.3	Synthesis of phenylacetylene-containing peptide P5	94
3.4.4	Polymerization of P5 peptide	96
3.4.5	Synthesis of propargyl containing peptides P6 and P7	98
3.4.6	Polymerization of P6 and P7 peptides	104
3.5	Conclusions	110
3.6	Supporting information	112
3.7	References	122

4	Polyelectrolyte complexes for enzyme-responsive delivery of AMPs	124
4.1	Aim	127
4.2	Introduction	127
4.3	Experimental Section	130
4.3.1	Materials	130
4.3.1.1	Assembly of PECs nanoparticles	130
4.3.1.2	Enzymatic degradation studies	130
4.3.1.3	Evaluation of antimicrobial activity of PECs	130
4.3.2	Instrumentation	131
4.3.3	Assembly of PECs nanoparticles	131
4.3.4	Characterization of PECs nanoparticles.	132
4.3.4.1	Dynamic Light Scattering (DLS) ¹⁶	132
4.3.4.2	Standard operating procedure parameters for DLS measurements	133
4.3.4.3	Standard operating procedure parameters for ζ -potential measurements	133
4.3.4.4	TEM imaging of PECs particles	134
4.3.5	PECs particles disassembly and physiological stability assays	134
4.3.6	Estimation of encapsulation efficacy of Polymyxin B in PECs	134
4.3.7	Enzymatic degradation testing procedure	135
4.3.8	<i>In-vitro</i> release of Polymyxin B from PECs in presence of thermolysin	136
4.3.9	<i>In-vitro</i> evaluation of antimicrobial activity PECs against <i>P. aeruginosa</i>	136
4.4	Results and discussions	138
4.4.1	Assembly and characterization of PECs nanoparticles loaded with AMP	138
4.4.2	Estimation of encapsulation efficacy of Polymyxin B in PECs	147
4.4.3	Investigating physiological stability and dominant interactions in selected PECs	149
4.4.3.1	Enhancing physiological stability of PolB: Poly-P2 PECs nanoparticles	152
4.4.4	Evaluation of enzyme degradation properties of PolB: Poly-P2 PECs nanoparticles	156
4.4.5	<i>In-vitro</i> release of Polymyxin B from PolB: Poly-P2 PECs nanoparticles	161
4.4.6	Antimicrobial activity of PolB: Poly-P2 PECs nanoparticles against <i>P. aeruginosa</i>	168
4.5	Conclusions	172

4.6	Supporting information	174
4.7	References	185
5	Conclusions	189
5.1	References	196

List of Figures

	Page
2.1 a) Assembly and oxidative cross-linking of Polyelectrolyte Complexes (PECs) nanoparticles from P4 _{SH} (Ac-CEECE-GLA-EEEC-OH) and antimicrobial Branched poly(ethylene imine) (B-PEI). Degradation of PECs nanoparticles by LasB and subsequent PEI release, previously developed by Insua et al. ¹ b) Enzyme degradation products of the LasB-degradable peptide sequence P4 _{SH} . c) Assembly of non enzyme-responsive PECs nanoparticles using clinically-approved Antimicrobial Peptide (AMP) - Polymyxin B. Indicating how the stability and antimicrobial efficacy of PECs can be tuned by changing the polyanion size.	27
2.2 a) Schematic representation of previously developed enzyme-responsive polymer compared to a newly proposed design discussed in this Chapter. Both polymers contain the core enzyme-responsive peptide sequence - GLA-. b) The figure also includes schematics of enzyme degradation products for both polymers are shown for comparison purposes.	28
2.3 a) Structure of previously developed LasB-degradable peptide (P4 _{SH}), developed by Insua et al. ¹ b) Schematic representation of disulfide cross-linking between the LasB-degradable peptide sequences, only for representation purposes.	39
2.4 a) Enzyme degradation products of the LasB-degradable peptide sequence (P4 _{SH}) developed by Insua et al. ¹ b) Schematic representation of the enzymatic degradation of cross-linked LasB-degradable peptide sequences, only for representation purposes.	39
2.5 a) The design (<i>i.e.</i> , chemical structure) of newly developed polymer with enzyme-degradable peptide side chain Poly-P2 . b) Schematic representation of a Poly-P2 structure with degree of polymerization (Dp) = 6. c) Enzyme degradation products of Poly-P2 . d) Schematic representation of the enzymatic degradation of a Poly-P2 structure with Dp = 6. . . .	40
2.6 Reaction scheme for coupling of methacrylic acid with Ac-EEGLAK-Resin to produce a final structure of P2 (Ac-EEGLAK(COC(CH₃)CH₂)-NH₂) sequence.	42

2.7	a) RP-HPLC chromatogram of a) crude and b) purified P2 (Ac-EEGLAK-(COC(CH₃)CH₂)-NH₂) sequence, where methacrylate group coupled with methacrylic acid.	43
2.8	Fully assigned ¹ H-NMR (400 MHz, DMSO- <i>d</i> ₆) spectrum of peak at 13.91 min (from Figure 2.7) - P2 (Ac-EEGLAK(COC(CH₃)CH₂)-NH₂)	43
2.9	Fully assigned ¹ H-Nuclear magnetic resonance (NMR) (400 MHz, DMSO- <i>d</i> ₆) spectrum of peak at 22.28 min (from Figure 2.7) SP-1 - side product of 1,4-addition to the double bond of methacrylic acid.	44
2.10	Proposed mechanism of a) 1,2 and b) 1,4-addition during the methacrylic acid coupling to the lysine side chain.	45
2.11	Mass spectrometry (MS) traces for SP-1 with proposed masses of different peptide adducts in negative ion mode. SP-1 represents the unknown peak, which eluted at 22.28 min (Figure 2.7a) during the analytical HPLC of the crude sample of P2	45
2.12	Schematic representation of the coupling mechanism of the methacrylate group to the main peptide sequence (Ac-EEGLAK-NH₂) using methacrylic anhydride and DIPEA.	46
2.13	RP-HPLC chromatograms a) to c) of crude P2 (Ac-EEGLAK(COC(CH₃)CH₂)-NH₂) with improving purities.	47
2.14	RP-HPLC chromatograms a) to b) of crude P2 (Ac-EEGLAK(COC(CH₃)CH₂)-NH₂) with improving purities.	47
2.15	Reaction scheme for RAFT polymerization of P2 monomer, represents synthesis of Poly-P2-R1 and R2	49
2.16	Comparison of ¹ H-NMR (400 MHz, DMSO- <i>d</i> ₆) spectra of P2 (Ac-EEGLAK-(COC(CH₃)CH₂)-NH₂) with RAFT polymerization reaction products Poly-P2-R-1 and Poly-P2-R-2	51
2.17	Reaction scheme for the synthesis of Poly-P2 (poly(Ac-EEGLAK(COC(CH₃)CH₂)-NH₂)) . The same reaction scheme applies for Poly-P1 (poly(Ac-EEGLAK(COC(CH₃)CH₂)-NH₂))	52
2.18	Comparison of ¹ H-NMR (400 MHz, DMSO- <i>d</i> ₆) spectra of P2 (Ac-EEGLAK-(COC(CH₃)CH₂)-NH₂) with the polymerization reaction product Poly-P2 (poly(Ac-EEGLAK(COC(CH₃)CH₂)-NH₂))	53
2.19	GPC chromatograms of synthesized Poly-P2 (poly(Ac-EEGLAK(COC(CH₃)CH₂)-NH₂)) polymers. Molecular masses were calculated based on a standard calibration method using poly(ethylene glycol) standards.	54
2.20	Schematic representation of enzymatic degradation of Poly-P2 which leads to the creation of degradation products DP-1 and DP-2	55

2.21	Relative amine content (%) in samples of thermolysin-responsive polymers Poly-P1 (poly(Ac-EGLAK(COC(CH₃)CH₂)-NH₂)) and Poly-P2 (poly(Ac-EEGLAK(COC(CH₃)CH₂)-NH₂)) evaluated in this work. The relative amine content was calculated from fluorescamine conjugates formed after incubation with enzymes for 5 hours and normalized to the fluorescence observed with a model degradation peptide (P3). Emissions normalized for Poly-P1 and Poly-P2 , HEPES, CaCl ₂ , Na ₂ B ₄ O ₇ buffer (Buffer), Thermolysin as enzyme control (Therm.), succinyl casein (SC) as a control for enzymatic activity, degradation peptide H ₂ N-LA-NH ₂ (P3) as a control to normalize fluorescence intensity. For unnormalized data, see Figure S2.29. Incubation time: 5 hours. <i>n</i> = 3.	56
2.22	Enzymatic degradation of a) Poly-P1 (poly(Ac-EGLAK(COC(CH₃)CH₂)-NH₂)) and b) Poly-P2 (poly(Ac-EEGLAK(COC(CH₃)CH₂)-NH₂)) monitored with ζ-potentials. Average data is presented from 3 technical replicates ± standard deviation (<i>n</i> = 3). For enzyme degradation procedure, see Section 2.3.5.	57
S2.23	Summary of RP-HPLC chromatograms of P1 (Ac-EGLAK(COC(CH₃)CH₂)-NH₂)) and P2 (Ac-EEGLAK(COC(CH₃)CH₂)-NH₂)).	60
S2.24	MS traces for P1 (Ac-EGLAK(COC(CH₃)CH₂)-NH₂)) and P2 (Ac-EEGLAK(COC(CH₃)CH₂)-NH₂)) in negative ion mode.	61
S2.25	¹ H-NMR (top) and ¹³ C (bottom) NMR (400 MHz, DMSO- <i>d</i> ₆) spectra of P1 (Ac-EGLAK(COC(CH₃)CH₂)-NH₂)).	62
S2.26	¹ H-NMR (top) and ¹³ C (bottom) NMR (400 MHz, DMSO- <i>d</i> ₆) spectra of P2 (Ac-EEGLAK(COC(CH₃)CH₂)-NH₂)).	63
S2.27	¹ H-NMR (400 MHz, DMSO- <i>d</i> ₆) (top) of Poly-P1 (poly(Ac-EGLAK(COC(CH₃)CH₂)-NH₂)), ¹ H-NMR (400 MHz, DMSO- <i>d</i> ₆) (bottom) of Poly-P2 (poly(Ac-EEGLAK(COC(CH₃)CH₂)-NH₂)).	64
S2.28	GPC chromatogram of Poly-P1 (poly(Ac-EGLAK(COC(CH₃)CH₂)-NH₂)) with key polymerization reaction conditions.	65
S2.29	Emissions intensity (λ _{exc} 355 nm, λ _{em} 470 nm) of fluorescamine conjugates for: HEPES, CaCl ₂ , Na ₂ B ₄ O ₇ buffer (Buffer), thermolysin as enzyme control (Therm.), succinyl casein (SC) as a control for enzymatic activity, degradation peptide P3 (H ₂ N-LA-NH ₂) as a control to normalize fluorescence intensity, thermolysin-responsive polymers Poly-P1 (poly(Ac-EGLAK(COC(CH₃)CH₂)-NH₂)) and Poly-P2 (poly(Ac-EEGLAK(COC(CH₃)CH₂)-NH₂)). All substrates were evaluated in the absence and presence of thermolysin. Incubation time: 5 hours. <i>n</i> = 3.	66

S2.30	Solid phase Fourier transform infrared spectroscopy (FTIR) spectra of the antibiotic Polymyxin B (PolB), P2 peptide and its polymer Poly-P2 . $n = 1$	67
3.1	a) Chemical structure of methacrylamide polymer Poly-P2 (poly(Ac-EEGLAK(COC(CH₃)CH₂)-NH₂)). b) Chemical structures of DP-1 and DP-2 - an enzyme degradation products of Poly-P2	74
3.2	Representation of different stereoisomers of poly(acetylenes), which arise from polymerization of substituted acetylenes. The dynamic helical properties of poly(acetylenes) are presented, allowing the helical chirality (P versus M) to change via stimuli post-polymerization. Adapted with permission. ⁷ Copyright © 2020, Springer Nature Limited.	75
3.3	a) Schematic illustration of the LasB-degradable helical polymers. b) Schematic illustration of the potential pathways of degradation of helical polymers derived from the P1 peptide.	76
3.4	Reaction scheme for coupling propargyl chloroformate to the lysine side chain, producing P4 (Ac-EGLAK(COOCH₂CCH)-NH₂)	84
3.5	RP-HPLC chromatogram of crude P4 (Ac-EGLAK(COOCH₂CCH)-NH₂) sequence.	85
3.6	a) ¹ H-NMR (400 MHz, DMSO- <i>d</i> ₆) spectra of the peak at 15.62 min - P4 (Ac-EGLAK(COOCH₂CCH)-NH₂) . b) ¹ H-NMR (400 MHz, DMSO- <i>d</i> ₆) spectra of peak at 19.53 min P4-SP-1 (Ac-EGLAK-NH₂) . For fully assigned NMR spectra see S3.27.	86
3.7	RP-HPLC chromatogram of purified P4 (Ac-EGLAK(COOCH₂CCH)-NH₂) sequence.	87
3.8	a) Chemical structures of two Rh catalysts used in polymerizations of acetylene-containing peptides. Cat.1 - [Rh(nbd)Cl] ₂ , its activation using a triethylamine (TEA) base. Cat.2 - Rh(nbd)(nPh-BPh ₃), no activation required. b) Reaction scheme of polymerization P4 (Ac-EGLAK(COOCH₂CCH)-NH₂) peptide sequence using Cat.1 . The same reaction scheme applies for polymerization with Cat.2 but without the addition of TEA.	89
3.9	Comparison of ¹ H-NMR (400 MHz, DMSO- <i>d</i> ₆) spectra of P4 (Ac-EGLAK(COOCH₂CCH)-NH₂) with products of polymerization reactions Poly-P4-1 and Poly-P4-2	91
3.10	Left: Syntheses and chemical structures of PA-1- 4. Right: Schematic representations of poly(acetylene) polymers. Highlighted in red are the novel, unsaturated and conjugated, polymeric backbones. Reused with permission. ¹⁵ Copyright©, 2018 Wiley Periodicals, Inc.	93

3.11	Reaction scheme for coupling 4-ethynylbenzoic acid to -GLA-Resin sequence producing P5 (CHC₆H₄-GLA-NH₂)	95
3.12	RP-HPLC chromatogram of a) crude and b) purified P5 (CHC₆H₄-GLA-NH₂) sequence.	95
3.13	¹ H-NMR(400 MHz, DMSO- <i>d</i> ₆) spectrum of the peak at 20.69 min (Figure 3.12) - P5 (CHC₆H₄-GLA-NH₂) . For fully assigned NMR spectra see S3.34.	96
3.14	Reaction scheme of polymerization P5 (CHC₆H₄-GLA-NH₂) peptide sequence using Cat.1	97
3.15	Comparison of ¹ H-NMR (400 MHz, DMSO- <i>d</i> ₆) spectra of P5 (CHC₆H₄-GLA-NH₂) with products of polymerization reactions Poly-P5-1 and Poly-P5-2	97
3.16	Reaction scheme for coupling propargyl amine to -GLA-Resin sequence through imidazole-peptide intermediate, forming P6 and P7 peptide. . . .	99
3.17	Schematic representation of a) parallel and b) anti-parallel β -sheet formation between the monomers of P6	100
3.18	RP-HPLC chromatogram of a) crude and b) purified P6 (CHCCH₂NHCO-GLA-OH) sequences. b) RP-HPLC chromatogram of c) crude and d) purified P7 (CHCCH₂NHCO-GLA-OCH₃)	101
3.19	¹ H-NMR (400 MHz, DMSO- <i>d</i> ₆) spectrum of P6 (CHCCH₂NHCO-GLA-OH) sequence. For fully assigned NMR spectra see S3.35.	102
3.20	¹ H-NMR (400 MHz, DMSO- <i>d</i> ₆) spectrum of P7 (CHCCH₂NHCO-GLA-OCH₃) sequence. For fully assigned NMR spectra see S3.36.	103
3.21	Turbidity changes of P6 samples under different monomer concentration in THF.	103
3.22	Reaction scheme of polymerization P7 (CHCCH₂NHCO-GLA-OCH₃) peptide sequence using Cat.1 . The same scheme can be applied for polymerization of P6 (CHCCH₂NHCO-GLA-OH)	104
3.23	Comparison of ¹ H-NMR (400 MHz, DMSO- <i>d</i> ₆) spectra of P6 (CHCCH₂NHCO-GLA-OH) with the product of polymerizations Poly-P6-1 and Poly-P6-2	106
3.24	Comparison of ¹ H-NMR (400 MHz, DMSO- <i>d</i> ₆) spectra of P7 (CHCCH₂NHCO-GLA-OCH₃) with product of polymerizations Poly-P7-1 to Poly-P7-4	106
3.25	Proposed chemical structure of <i>cis</i> -transoidal conformation of Poly-P7	107
3.26	Zoomed in ¹ H-NMR (400 MHz, DMSO- <i>d</i> ₆) spectrum of Poly-P7-3	108
S3.27	a) Fully assigned ¹ H-NMR (400 MHz, DMSO- <i>d</i> ₆) spectra of the peak at 15.62 min - P4 (Ac-EGLAK(COOCH₂CCH)-NH₂) . b) Fully assigned ¹ H-NMR (400 MHz, DMSO- <i>d</i> ₆) spectra of peak at 19.53 min P4-SP-1 (Ac-EGLAK-NH₂)	112

S3.28	2D-COSY ^1H -NMR (400 MHz, DMSO- d_6) spectra of P4 (Ac-EGLAK(CO-OCH₂CCH)-NH₂) and of a side product P4-SP-1 (Ac-EGLAK-NH₂)	113
S3.29	Summary of RP-HPLC chromatograms of a) P4 , b) P5 , c) P6 , d) P7	114
S3.30	MS traces for P5 (CHC₆H₄-GLA-NH₂) in negative ion mode.	115
S3.31	MS traces for P6 (CHCCH₂NHCO-GLA-OH) in negative ion mode.	115
S3.32	MS traces for P7 (CHCCH₂NHCO-GLA-OCH₃) in positive ion mode.	116
S3.33	^1H -NMR (top) and ^{13}C (bottom) NMR (400 MHz, DMSO- d_6) spectra of P4 (Ac-EGLAK(COOCH₂CCH)-NH₂)	117
S3.34	^1H -NMR (top) and ^{13}C (bottom) NMR (400 MHz, DMSO- d_6) spectra of P5 (CHC₆H₄-GLA-NH₂)	118
S3.35	^1H -NMR (top) and ^{13}C (bottom) NMR (400 MHz, DMSO- d_6) spectra of P6 (CHCCH₂NHCO-GLA-OH)	119
S3.36	^1H -NMR (top) and ^{13}C (bottom) NMR (400 MHz, DMSO- d_6) spectra of P7 (CHCCH₂NHCO-GLA-OCH₃)	120
S3.37	FTIR spectra of P7 (CHCCH₂NHCO-GLA-OCH₃) in solid state (top) and in liquid state in THF (bottom). $n = 1$	121
4.1	a) Schematic representation of the formation of PECs nanoparticles by self-assembly of cationic Polymyxin B (PolB) with poly(styrene sulphonate) (PSS) and effect of the different multivalency of anionic polymer on physiological stability and antimicrobial activity. b) Schematic representation of anionic polymer bearing enzyme-degradable side chain Poly-P2, poly(Ac-EEGLAK(COC(CH₃)CH₂)-NH₂) , represented as a key component in an active delivery system, solution to passive drug delivery.	128
4.2	Schematic representation of enzyme-responsive PECs-based delivery system.	129
4.3	Schematic representation of the laboratory method for preparation of PECs particles.	138
4.4	Summary of DLS autocorrelation function (ACF) curves of PECs nanoparticles prepared with Poly-P2 and PolB at $[n^+/n^-]$ ratios of 1.13, 1.00, 0.750, 0.606, 0.500, 0.438, 0.375, 0.125. N1 - ACF curves directly after 24 hours of mixing. The results are presented as an average of 3 technical replicates for each sample.	141
4.5	Summary of DLS size-intensity plots of PECs nanoparticles prepared with Poly-P2 and PolB at $[n^+/n^-]$ ratios of 1.13, 1.00, 0.750, 0.606, 0.500, 0.438, 0.375, 0.125. N1 - size-intensity plots directly after 24 hours of mixing. The results are presented as an average of 3 technical replicates for each sample.	142

4.6	ζ -potential values for all of the formulations of PECs-N1, presented as a table and as a graph. Results are shown as means \pm standard deviation ($n = 3$).	143
4.7	Size variation of different batches of PECs-F3 ($[n^+/n^-] = 0.750$ ratio), monitored with DLS. B1, B2, B3 and B4 are used to represent batch numbers. PECs were prepared in 15 mM HEPES buffer (pH 7.45). The results are presented as an average of 3 technical replicates for each sample.	144
4.8	a) DLS results of PECs-F3 ($[n^+/n^-] = 0.750$ ratio) prepared in Milli-Q water. The results are presented as an average of 3 technical replicates for each sample. b,c) TEM micrographs of the selected PECs-F3 ($[n^+/n^-] = 0.750$ ratio) prepared in Milli-Q water, $n = 1$	146
4.9	Schematic representation of PolB encapsulation using Poly-P2 , R - represents the rest of Poly-P2 chemical structure. Dab - diaminobutyric acid.	147
4.10	a) Estimated encapsulation efficacy of PolB in PECs using fluorescamine assay. b) Polymyxin B loading in each PECs formulation, based on encapsulated efficacy. The results are presented as an average of 3 technical replicates for each sample.	148
4.11	Summary of DLS size-intensity plots as well as autocorrelation functions (ACF) of PECs nanoparticles with $[n^+/n^-] =$ a) 1.13 (F1) and b) 0.750 (F3) in presence of 154 mM NaCl at 37 °C over 4 hours. The results are presented as an average of 3 technical replicates for each sample.	150
4.12	Summary of DLS data: a) autocorrelation functions (ACF) as well as b) size-intensity plots of PECs nanoparticles with $[n^+/n^-] = 0.750$ (F3) in presence of 100 mM Urea, EDTA, Tween 20 and NaCl at 37 °C after 24 hours of incubation. c) Comparison of hydrodynamic radii (D_H) for PECs after incubation with 100 mM Urea, EDTA, Tween 20 and NaCl. d) Interactions rated in terms of their influence on PECs assembly and stability. The results are presented as an average of 3 technical replicates for each sample.	151
4.13	Schematic representation of multi-binding properties of Tannic Acid (TA) with Polymyxin B (PolB) used as an example. R_1 - represents the rest of the chemical structure of Polymyxin B.	153
4.14	Summary of DLS autocorrelation functions (ACF), size-intensity plots and ζ -potential data of PECs-F3 (PECs-N1) and PECs-F3 + TA (PECs-N2) nanoparticles with $[n^+/n^-] = 0.750$ (F3). The results are presented as an average of 3 technical replicates for each sample.	154

4.15	Summary of DLS size-intensity plots as well as autocorrelation functions (ACF) of PECs nanoparticles with $[n^+/n^-] = 0.750$ (F3) a) with added Tannic Acid (TA), b) without added Tannic Acid (TA) in presence of 154 mM NaCl at 37 °C over 4 hours. The results are presented as an average of 3 technical replicates for each sample.	155
4.16	Relative amine content (%) in samples of thermolysin-responsive PECs evaluated in this work. The relative amine content was calculated from fluorescamine conjugates formed following incubation of PECs with $[n^+/n^-] = 1.13$ ratio (F1) and $[n^+/n^-] = 0.750$ ratio (F3) with enzymes for 5 hours and normalized to the fluorescence observed with a model degradation peptide. Emissions normalized for HEPES, CaCl_2 , $\text{Na}_2\text{B}_4\text{O}_7$ buffer (Buffer), Thermolysin as enzyme control (Therm.), succinyl casein (SC) as a control for enzymatic activity, degradation peptide $\text{H}_2\text{N-LA-NH}_2$ (P3) as a control to normalize fluorescence intensity. All substrates were evaluated in the absence and presence of thermolysin. Incubation time: 5 hours, $n = 3$. For unnormalized data, see Figure S4.32.	157
4.17	Enzymatic degradation of PECs with $[n^+/n^-] = 0.750$ a) without b) with Tannic Acid (TA) monitored with ζ -potentials. Incubation time: 6 hours, 3 technical replicates were recorded for each sample. For enzyme degradation procedure see Section 4.3.7.	159
4.18	Schematic representation of a dialysis set-up for investigating enzyme-induced Polymyxin B release from PECs-F3. Therm. - thermolysin. . . .	161
4.19	Thermal stability of PECs-F3 ($[n^+/n^-] = 0.750$ ratio), monitored with DLS. The results are presented as an average of 3 technical replicates for each sample as an ACF curves.	162
4.20	Relative amine content (%) in the dialysate collected during the enzyme-induced release experiment, which is representative of the release of Polymyxin B (PolB) from PECs with $[n^+/n^-] = 0.750$ ratio (F3). Emission intensities were normalized to the fluorescence of fluorescamine-PolB (0.0373 mg/mL), a total concentration of PolB which was presumed to pass (100 %) through the dialysis membrane. Thermolysin control (Therm.) was also included, which represents the relative amine content of thermolysin-fluorescamine adducts. A sample of PolB (Free PolB) with a concentration of 0.209 mg/mL was used to monitor the efficacy of the dialysis membrane to pass PolB. Incubation time: 24 hours. Time points collected at 1,2,3,4,5 and 24 hours, $n = 3$. For unnormalized data, see Figure S4.33.	164

4.21	Polymyxin B content in a dialysate collected during the enzyme-induced release experiment, data based on relative amine content from Figure 4.20, $n = 1$.	165
4.22	RP-HPLC chromatograms of a control sample of Polymyxin B sulfate in water at a concentration of 0.0250 mg/mL overlaid with chromatograms of HEPES buffer with added NaCl for reference. $n = 1$.	166
4.23	RP-HPLC chromatograms of dialysate samples at 1 - 5 and 24 hours from <i>in-vitro</i> release study, including PolB (0.0373 mg/mL) and HEPES control samples. $n = 1$.	167
4.24	The MIC of PECs-F1 and PECs-F3 including free Polymyxin B (PolB-Control) against normal pathogenic <i>P.aeruginosa</i> (ATCC-47085 - P.a) and MDR (FADDI-PA067 P.a - MDR) strains. For the OD ₆₃₀ plots see S4.35 and S4.36. MIC were derived from the linear regression analysis of the relationship between percentage of relative bacterial growth against theoretical PolB concentration, which is shown in Figures S4.35 c - e and S4.36 c - e. Data is presented as mean and \pm standard deviation of two replicates.	169
4.25	Chemical structures of proposed enzyme degradation products of Poly-P2 polymer with peptide side chain.	170
S4.26	Summary of DLS autocorrelation function (ACF) curves of PECs nanoparticles prepared with Poly-P2 and PolB at $[n^+/n^-]$ ratios of 1.13, 1.00, 0.750, 0.606, 0.500, 0.438, 0.375, 0.125. N1 - ACF curves directly after 24 hours of mixing, N2 - ACF curves directly after 24 hours following the addition of Tannic Acid (TA). The results are presented as an average of 3 technical replicates for each sample.	175
S4.27	Summary of DLS size-intensity plots of PECs nanoparticles prepared from Poly-P2 at $[n^+/n^-]$ ratios of 1.13, 1.00, 0.750, 0.606, 0.500, 0.438, 0.375, 0.125. N1 - size-intensity plots directly after 24 hours of mixing, N2 - size-intensity plots directly after 24 hours following the addition of Tannic Acid (TA). The results are presented as an average of 3 technical replicates for each sample.	176
S4.28	DLS data for the samples of controls: Polymyxin B (PolB), Poly-P2 and Tannic Acid (TA) in 10 mM HEPES solution at pH 7.45. The results are presented as an average of 3 technical replicates for each sample.	177
S4.29	FTIR spectra of Tannic Acid (TA), free drug Polymyxin B (PolB), peptide monomer P2 , enzyme degradable polymer Poly-P2 , PECs + TA with $[n^+/n^-] = 1.00$ ratio (F2), PECs with $[n^+/n^-] = 1.13$ ratio (F1), $[n^+/n^-] = 0.750$ ratio (F3). $n = 1$.	177

S4.30	UV-Vis spectra of Tannic Acid (TA), Polymyxin B (PolB), polymer with enzyme-degradable peptide side chain (Poly-P2) and PECs + TA with $[n^+/n^-] = 0.750$ ratio. $n = 1$.	178
S4.31	a) The standard curve of Free Polymyxin B-fluorescamine conjugates based on 7 Polymyxin B standards at different concentrations, $n = 3$. b) Polymyxin B concentration in each formulation of PECs. c) Emission Intensity of fluorescamine conjugates for PECs prepared with different PolB concentrations <i>i.e.</i> , at different $[n^+/n^-]$ ratios. $n = 3$.	179
S4.32	Emissions intensity (λ_{exc} 365 nm, λ_{em} 470 nm) of fluorescamine conjugates formed for HEPES, $CaCl_2$, $Na_2B_4O_7$ buffer (Buffer), Thermolysin as enzyme control (Therm.), succinyl casein (SC) as a control for enzymatic activity, degradation peptide $H_2N-LA-NH_2$ (P3) as a control to normalize fluorescence intensity, enzyme-responsive PECs: PECs-F1 ($[n^+/n^-] = 1.13$), PECs-F3 ($[n^+/n^-] = 0.750$). All substrates were evaluated in the absence and presence of thermolysin. Incubation time: 5 hours. $n = 3$.	180
S4.33	Emissions intensity (λ_{exc} 365 nm, λ_{em} 470 nm) of fluorescamine conjugates found in the dialysate during the enzyme-induced release experiment, which are representative of the release of Polymyxin B (PolB) from PECs with $[n^+/n^-] = 0.750$ ratio (F3). Thermolysin control (Therm.) was also included, which represents the emission intensity caused by the thermolysin-fluorescamine adducts. A sample of PolB (Free PolB) with a concentration of 0.209 mg/mL was used to monitor the efficacy of the dialysis membrane to pass PolB. Incubation time: 24 hours. Time points collected at 1,2,3,4,5 and 24 hours, $n = 3$.	181
S4.34	Additional data from <i>in-vitro</i> release experiment. DLS Size-Intensity distributions of PECs-F3 $[n^+/n^-] = 0.750$ suspensions inside the dialysis membrane over time points = 1,3,24 and 51 hours. a) PECs-F3 control, without added thermolysin, b) PECs-F3 + thermolysin. c) Normalized count rates of PECs-F3 and PECs-F3-control samples inside the dialysis membrane over time points = 1,3,24 and 51 hours. The results are presented as an average of 3 technical replicates for each sample.	182
S4.35	a) Growth curve (OD_{630}) of <i>P.aeruginosa</i> (ATCC-47085) in the absence of PECs and PolB, representing negative control. b) OD_{630} at 570 min of PECs-F3, PECs-F1 and PolB-control samples at different drug content concentrations (serial two-fold dilutions). c - e) Relative bacteria growth of samples (%) at different drug content and linear regression analysis for determining MIC. The results are shown as means \pm standard deviations ($n = 2$).	183

S4.36 a) Growth curve (OD ₆₃₀) of MDR - <i>P.aeruginosa</i> (FADDI-PA067) in the absence of PECs and PolB, representing negative control. b) OD ₆₃₀ at 840 min of PECs-F3, PECs-F1 and PolB-control samples at different drug content concentrations (serial two-fold dilutions). c - e) Relative bacteria growth of samples (%) at different drug content and linear regression analysis for determining MIC. The results are shown as means ± standard deviations (<i>n</i> = 2).	184
---	-----

List of Tables

	Page
2.1 Summary of free-radical polymerization conditions and reactant concentrations, where P2 (Ac-EEGLAK(COC(CH₃)CH₂)-NH₂) is a monomer and V-501 (4,4'-Azobis(4-cyanopentanoic acid)) is a thermal initiator. . . .	35
2.2 Summary of the concentrations and conditions used in enzymatic degradation testing.	37
2.3 Peptides and their structures evaluated in this Chapter in the deprotonated state.	41
2.4 Summary of the concentrations and conditions of attempted RAFT polymerizations. P2 (Ac-EEGLAK(COC(CH₃)CH₂)-NH₂) used as a monomer, CTA-1 (2-((Ethylthio)carbonothioyl)thio-2-methylpropanoic acid) as a chain transfer agent and V-501 (4,4'-Azobis(4-cyanopentanoic acid)) as thermal initiator.	50
2.5 Summary of free-radical polymerization conditions and reactant concentrations, where P2 (Ac-EEGLAK(COC(CH₃)CH₂)-NH₂) is a monomer and V-501 (4,4'-Azobis(4-cyanopentanoic acid)) is a thermal initiator. . . .	52
3.1 Chemical structures the acetylene-containing peptides, synthesized in this Chapter.	78
3.2 Summary of polymerization conditions and reactant concentrations for the reaction of acetylene-containing peptide sequences P4 - P7	83
3.3 Summary of polymerization conditions and reactant concentrations for the reaction of P4 with Cat.1 - [Rh(nbd)Cl] ₂ and Cat.2 - Rh(nbd)(nPh-BPh ₃).	89

3.4	Chemical structures of the acetylene-containing peptide monomers, evaluated in this Chapter.	94
3.5	Summary of polymerization conditions and reactant concentrations for the reaction of P5 with Cat.1 - [Rh(nbd)Cl] ₂ using acetonitrile (ACN) and tetrahydrofuran (THF) solvents.	96
3.6	Chemical structures of the P6 and P7 peptides.	100
3.7	Summary of polymerization conditions and reactant concentrations for the reaction of P6 and P7 monomers with Cat.1 - [Rh(nbd)Cl] ₂ and Cat.2 , Rh(nbd)(nPh-BPh ₃) using tetrahydrofuran (THF) solvent.	105
4.1	Summary of the concentrations and conditions used in enzymatic degradation testing.	135
4.2	Summary of DLS data for the formulations of PECs evaluated in this work. For Autocorrelation functions (ACFs), see Figure 4.4 and for size-intensity plots, see Figure 4.5.	139
4.3	Summary of DLS data for the PECs-N1 and PECs-N2 (PECs-N1 + Tannic Acid (TA)) formulations evaluated in this work. Average data is presented from 3 technical replicates ± standard deviation (<i>n</i> = 3). For autocorrelation functions (ACF), see Figure S4.26 and for size-intensity plots, see Figure S4.27.	174

Abbreviations

ACF Autocorrelation function. [xiv–xvii](#), [xx](#), [132](#), [134](#), [139–141](#), [143](#), [145](#), [149–151](#), [154](#), [155](#), [162](#), [174](#), [175](#)

ACN Acetonitrile. [xx](#), [82](#), [96](#), [193](#)

Alloc Allyloxycarbonyl. [32](#), [41](#), [45](#), [46](#), [79](#)

AMP Antimicrobial Peptide. [ix](#), [18–21](#), [26–29](#), [38–40](#), [48](#), [49](#), [52](#), [58](#), [59](#), [73–75](#), [110](#), [111](#), [127–129](#), [138](#), [153](#), [160](#), [168](#), [170](#), [172](#), [173](#), [190](#), [192](#), [194](#), [195](#)

ATCC American Type Culture Collection. [xvii](#), [xviii](#), [137](#), [168](#), [169](#), [183](#)

ATRP Atom transfer radical polymerization. [48](#)

B-PEI Branched poly(ethylene imine). [ix](#), [27](#)

CD Circular dichroism. [104](#)

CDI 1,1'-Carbonyldiimidazole. [77](#), [79](#), [99](#), [102](#)

COSY Correlation spectroscopy. [xiv](#), [85](#), [113](#)

CTA-1 2-((Ethylthio)carbonothioyl)thio-2-methylpropanoic acid. [xix](#), [30](#), [34](#), [49](#), [50](#)

DCM Dichloromethane. [33](#), [80](#)

DIPEA N,N-diisopropylethylamine. [x](#), [30](#), [32](#), [40](#), [42](#), [46](#), [77–79](#), [87](#), [94](#)

DLS Dynamic light scattering. [xiv–xviii](#), [xx](#), [132–134](#), [136](#), [138–142](#), [144–147](#), [149–151](#), [153–155](#), [159](#), [162](#), [163](#), [172](#), [174–177](#), [182](#)

DMAP 4-Dimethylaminopyridine. [92](#)

DMF Dimethylformamide. [30](#), [32](#), [48](#), [77–80](#), [82](#), [90](#), [193](#)

DMSO Dimethyl sulfoxide. [x–xiv](#), [31](#), [33–36](#), [43](#), [44](#), [51](#), [53](#), [62–64](#), [77](#), [80](#), [81](#), [86](#), [91](#), [96](#), [97](#), [102](#), [103](#), [106](#), [108](#), [112](#), [113](#), [117–120](#)

Dp Degree of polymerization. ix, 40, 53, 54, 59, 73, 128

DPBS Dulbecco's Phosphate-Buffered Saline. 30, 31

EDTA Ethylenediaminetetraacetic acid. xv, 30, 36, 77, 133–135, 151, 152

EE Encapsulation efficacy. 148, 149

ESI Electrospray ionization. 31, 77

Et₂O Diethyl ether. 33, 80

FA Formic Acid. 30, 31

FDA Food and Drug Administration. 20, 27, 129, 172, 192

Fmoc Fluorenylmethyloxycarbonyl. 30, 32, 40–42, 77–79

FRP Free-radical polymerization. 48, 52–54, 192

FTIR Fourier transform infrared spectroscopy. xii, xiv, xvii, 31, 67, 78, 121, 131, 145, 177

GPC Gel permeation chromatography. x, xi, 31, 35, 53, 54, 65, 82

HATU Hexafluorophosphate azabenzotriazole tetramethyl uronium. 92

HBTU Hexafluorophosphate benzotriazole tetramethyl uronium. 30, 32, 40, 42, 46, 77–79, 84, 94

HEPES 4-(2-hydroxyethyl)-1-piperazineethanesulfonic acid. xi, xv–xviii, 30, 36, 56, 66, 130–132, 134–136, 143–145, 157, 161–163, 166, 167, 177, 180

HLE Human leukocyte elastase. 59

HOBt Hydroxybenzotriazole. 92

HPLC High performance liquid chromatography. x, 31, 33, 34, 36, 42–45, 47, 48, 78, 81, 82, 84, 87, 95, 101, 136, 165, 166, 168, 194

HR-MS High resolution-mass spectrometry. 33, 34, 81, 82

LasB Elastase B from *Pseudomonas aeruginosa*. ix, xii, 19, 26–28, 38–41, 48, 55, 57, 59, 76, 94, 127, 157, 190

LB Luria–Bertani broth. 130, 137

LCST Lower critical solution temperature. 92

MBHA 4-Methylbenzhydramine hydrochloride. 30, 32, 77, 78

MDR Multi drug resistant. xvii, xix, 168–170, 184

MHB Mueller-Hintin broth. 130, 137

MIC Minimum inhibitory concentration. xvii–xix, 127, 137, 148, 168–170, 172, 183, 184, 192

Milli-Q Ultrapure water. xv, 30, 34, 130, 131, 134, 145, 146

MS Mass spectrometry. x, xi, xiv, 31, 33, 34, 36, 42, 43, 45, 61, 77, 78, 81, 82, 95, 108, 115, 116

MTT 3-(4,5-Dimethylthiazol-2-yl)-2,5-Diphenyltetrazolium Bromide. 194

NMM N-methylmorpholine. 30, 32, 77, 79

NMR Nuclear magnetic resonance. x–xiv, 31, 35, 36, 42–46, 50, 51, 53, 62–64, 77, 80–82, 84–86, 90, 91, 95–98, 102–108, 112, 113, 117–120

NNLS Non-negative least squares. 132

NP Nanoparticles. 131

OD Optical density. xvii–xix, 137, 169, 183, 184

PDI Polydispersity index. 131, 132, 140, 144, 145, 154, 162, 172

PECs Polyelectrolyte Complexes. ix, xiv–xx, 18–21, 26–28, 38, 48, 54, 58, 59, 73, 75, 127–132, 134–145, 147–165, 168–170, 172–181, 183, 184, 190–195

PEI Poly(ethylene imine). ix, 26, 27

PoIB Polymyxin B. xii, xiv–xix, 27, 67, 127–130, 134, 136, 138–145, 147–154, 156, 158–172, 175, 177–179, 181, 183, 184, 191–195

PPAs poly(phenylacetylenes). 92

PSS Polystyrene sulfonate. xiv, 27, 54, 127, 128

RAFT Reversible addition-fragmentation chain transfer. x, xix, 34, 48–53

RI Refractive index. 32, 133

RP-HPLC Reversed-phase high performance liquid chromatography. x–xiv, xvii, 31, 43, 47, 60, 78, 85, 87, 95, 101, 114, 131, 166, 167

SC Succinyl casein. [xi](#), [xvi](#), [xviii](#), [36](#), [56](#), [66](#), [135](#), [157](#), [180](#)

SEC Size exclusion chromatography. [31](#)

SPPS Solid-phase peptide synthesis. [100](#), [192](#)

TA Tannic acid. [xv–xviii](#), [xx](#), [130](#), [153–156](#), [158–160](#), [172](#), [174–178](#), [191](#)

TEA Triethylamine. [xii](#), [88](#), [89](#)

TEM Transmission electron microscopy. [xv](#), [130](#), [131](#), [134](#), [144–147](#), [172](#)

TFA Trifluoroacetic acid. [30](#), [31](#), [33](#), [77](#), [78](#), [80](#), [84](#), [91](#)

THF Tetrahydrofuran. [xiii](#), [xiv](#), [xx](#), [82](#), [88](#), [90](#), [93](#), [96](#), [97](#), [103–105](#), [110](#), [121](#)

TOF Time-of-flight. [31](#), [33](#), [34](#), [77](#)

Tween 20 Polysorbate 20. [xv](#), [130](#), [133](#), [134](#), [151](#)

UCST Upper critical solution temperature. [92](#)

UV-Vis Ultraviolet-visible. [xviii](#), [31](#), [78](#), [131](#), [145](#), [178](#)

V-501 4,4'-Azobis(4-cyanopentanoic) acid. [xix](#), [30](#), [34](#), [35](#), [49](#), [50](#), [52](#), [53](#)

WHO World Health Organization. [26](#)

Chapter 1

Introduction - Stimuli-Responsive Delivery of Antimicrobial Peptides Using Polyelectrolyte Complexes

Format: Review article.

Information: A. Antropenko, F. Caruso and P. Fernandez-Trillo, Stimuli-Responsive Delivery of Antimicrobial Peptides Using Polyelectrolyte Complexes, *Macromol. Biosci.*, 2023, e2300123.

Published by Wiley-VCH GmbH, shared with the Creative Commons Attribution-NonCommercial License (CC-BY-NC): <https://creativecommons.org/licenses/>

Contributions: Alexander Antropenko wrote sections 2, 3, and 4, including the first draft, and drew all the figures. Paco Fernandez-Trillo wrote sections 1,2 and 5, planned and organized the first draft. Frank Caruso contributed to discussions and input on content, including reviewing of the manuscript. All authors revised the manuscript and contributed to the final version.

Contents

1.1 Manuscript	2
1.2 Scope of Thesis	18
1.3 References	22

1.1 Manuscript

Stimuli-Responsive Delivery of Antimicrobial Peptides Using Polyelectrolyte Complexes

Alexander Antropenko, Frank Caruso, and Paco Fernandez-Trillo*

Antimicrobial peptides (AMPs) are antibiotics with the potential to address antimicrobial resistance. However, their translation to the clinic is hampered by issues such as off-target toxicity and low stability in biological media. Stimuli-responsive delivery from polyelectrolyte complexes offers a simple avenue to address these limitations, wherein delivery is triggered by changes occurring during microbial infection. The review first provides an overview of pH-responsive delivery, which exploits the intrinsic pH-responsive nature of polyelectrolytes as a mechanism to deliver these antimicrobials. The examples included illustrate the challenges faced when developing these systems, in particular balancing antimicrobial efficacy and stability, and the potential of this approach to prepare switchable surfaces or nanoparticles for intracellular delivery. The review subsequently highlights the use of other stimuli associated with microbial infection, such as the expression of degrading enzymes or changes in temperature. Polyelectrolyte complexes with dual stimuli-response based on pH and temperature are also discussed. Finally, the review presents a summary and an outlook of the challenges and opportunities faced by this field. This review is expected to encourage researchers to develop stimuli-responsive polyelectrolyte complexes that increase the stability of AMPs while providing targeted delivery, and thereby facilitate the translation of these antimicrobials.

Escherichia coli and *Pseudomonas aeruginosa*, the development rate of new antibiotics is superseded by the development of antimicrobial resistance.^[2] For example, based on recent data from the World Health Organization, out of the eleven phase 3 antimicrobial agents developed to date, only two have displayed confirmed activity against *P. aeruginosa*.^[3] Therefore, alternative strategies need to be explored to address this emergence in antimicrobial resistance.^[4–6] One of these strategies is the re-evaluation of antibiotics that have not currently found widespread clinical use.

An example of such a category of antibiotics is AMPs. Although AMPs have excellent antimicrobial properties, their potential has not been fully realized.^[7–9] Natural and synthetic AMPs are often positively charged peptides with hydrophobic and hydrophilic moieties, which confer them with antimicrobial properties. These peptides tend to show excellent antimicrobial activity against some of the more challenging Gram-negative pathogens.^[10]

However, because of their cationic nature and amphiphilicity, they are often toxic to mammalian cells. Moreover, peptides are expensive to manufacture and have short half-lives in biological media owing to degradation by proteases. These limitations make the translation of AMPs into clinical practice challenging, and only a few AMPs have found clinical use, often as last-resort antibiotics.^[9,11] Although several strategies have been explored to optimize the pharmacokinetic and pharmacodynamic properties of AMPs, these strategies often

1. Introduction

Antimicrobial resistance presents an ongoing growing threat to global health. In 2019, over 3.5 million deaths were associated with antimicrobial resistant strains, with the highest number of cases reported in sub-Saharan Africa.^[1] As observed, particularly in non-fermenting Gram-negative pathogens, such as

A. Antropenko, P. Fernandez-Trillo
School of Chemistry
University of Birmingham
Edgbaston, Birmingham B15 2TT, UK
E-mail: f.ftrillo@udc.es

A. Antropenko, P. Fernandez-Trillo
Institute of Microbiology and Infection
University of Birmingham
Edgbaston, Birmingham B15 2TT, UK

A. Antropenko, F. Caruso
Department of Chemical Engineering
The University of Melbourne
Parkville, VIC 3010, Australia

P. Fernandez-Trillo
Departamento de Química
Facultade de Ciencias and Centro de Investigacións Científicas
Avanzadas (CICA)
Universidade da Coruña
A Coruña 15071, Spain

The ORCID identification number(s) for the author(s) of this article can be found under <https://doi.org/10.1002/mabi.202300123>

© 2023 The Authors. Macromolecular Bioscience published by Wiley-VCH GmbH. This is an open access article under the terms of the Creative Commons Attribution-NonCommercial License, which permits use, distribution and reproduction in any medium, provided the original work is properly cited and is not used for commercial purposes.

DOI: 10.1002/mabi.202300123

rely on the chemical modification of the peptides via either using chemical moieties that can temporarily mask the cationic charge^[12] or conjugating the AMP to a suitable carrier.^[13–16] However, these strategies come at the expense of changing the chemical nature of the AMPs, which inherently changes its antimicrobial profile. Masking the cationic charge will reduce the affinity for negatively charged membranes while modifying the other residues may affect the secondary structure and the hydrophobicity of the AMP. Moreover, the efficiency of these chemical modifications can be hard to control, as AMPs present multiple cationic residues that need masking, leading to variability between batches and manufacturers.^[17,18] For example, colistin methanesulfonate, produced by the sulfomethylation of cationic residues in colistin,^[19] has different percentages of colistin or methanosulfonated derivatives depending on the manufacturer.^[20–22] Since in vitro antibacterial potency is decreased by sulfomethylation, the antimicrobial activity of colistin methanesulfonates is hard to predict.

Alternatively, drug delivery vehicles can protect AMPs from degradation while protecting mammalian cells from AMP toxicity. In this case, the native chemical structure of the AMP is preserved so that, if released, it will keep its original antimicrobial mode of action. The challenge in this approach is to optimize the rate and site of delivery so that therapeutic doses of the AMP are achieved. To date, a wide range of materials have been explored as drug delivery vehicles for AMPs, including liposomes, nanoparticles, and hydrogels.^[18,23–31] As most AMPs are cationic molecules, complexation with oppositely charged polyelectrolytes is an attractive and simple method for preparing nanostructured materials from AMPs. For example, layer-by-layer deposition has been employed to immobilize AMPs on surfaces,^[32] while complexation in solution can result in the formation of polyelectrolyte complexes and coacervates, including particles and micelles.^[33–36] Several factors affect the morphology and stability of the formed polyelectrolyte complexes, including the molecular weight of the polyelectrolytes, their charge density and concentration, or the pH and ionic strength of the solutions used in their preparation. A discussion of these factors is outside this review's scope and has been comprehensively reviewed elsewhere.^[32–36] Interested readers are encouraged to check this literature.

Although most of polyelectrolyte complexes can effectively protect AMPs from degradation and shield their toxicity, they provide a passive mechanism of delivery, which can result in low activity, off-target effects, and the development of resistance. However, the presence of pathogenic microorganisms in healthy tissues leads to changes in their microenvironment, including changes in pH, the presence of elevated amounts of specific enzymes secreted by a pathogen, or an increase in the concentration of reactive oxygen species such as hydrogen peroxide. Therefore, the development of stimuli-responsive nanomaterials that can respond to these changes and selectively deliver AMPs at the site of infection is a potential strategy to minimize the limitations of AMPs while addressing the growing concern of antimicrobial resistance.

This review aims to provide an overview of the state-of-the-art in the delivery of AMPs using stimuli-responsive nanomaterials based on polyelectrolyte complexes. In Section 2, we provide examples of AMP delivery systems that use changes in pH as a trig-

ger for delivery as electrostatically assembled nanomaterials are inherently pH-responsive. These systems include pH-responsive delivery from surfaces as well as nanoparticulate systems. We also provide examples highlighting the role of electrostatic interactions between the AMP and the rest of the system on the responsive properties as well as on the delivery of the antimicrobial. In Sections 3 and 4, we provide examples of enzyme- and temperature-responsive materials, respectively. These materials may have a greater potential in realizing targeting against pathogen-mediated stimuli, as infection is associated with the expression of degrading enzymes or changes in temperature. These latter two areas are still in their infancy, with only a handful of examples that use polyelectrolyte complexation to encapsulate AMPs. Thus, we also include examples that demonstrate the potential of targeting these two stimuli to develop smart delivery systems for AMPs that should restrict the release of the AMP to the microenvironment of the pathogen. In Section 5, we conclude with a summary and an outlook of the field. Here, we highlight the key features that make stimuli-responsive polyelectrolyte complexes an ideal platform to deliver AMPs, while also indicating some of the challenges and opportunities for the field. This review is expected to encourage researchers to develop stimuli-responsive PECs that can address the current limitations in the translation of AMPs.

2. pH-Responsive AMP Delivery Systems

2.1. pH-Responsive Delivery of AMPs from Surfaces

Egles and co-workers were the first to demonstrate that polyelectrolyte complexes could be used to encapsulate AMPs using layer-by-layer deposition. Defensin, an AMP collected from *Anopheles gambiae*, was deposited within polyelectrolyte complex multilayers consisting of poly(ethyleneimine), poly(sodium 4-styrenesulfonate), poly(allylamine hydrochloride), poly(L-glutamic acid), and poly(L-lysine).^[37] In an attempt to prepare multilayered films with antimicrobial properties, defensin was deposited close to the final layer and the polyelectrolyte assembly was capped with either poly(L-lysine) or poly(L-glutamic acid). Antimicrobial activity was observed only for the system that used poly(L-lysine) as the final layer, and this difference was attributed to the better adhesion of the negatively charged bacteria to the cationic groups of poly(L-lysine). Furthermore, at the working pH (6.5–7.0), poly(L-lysine) showed antimicrobial activity owing to the protonation of its amines. A similar approach has been used to develop a variety of systems to deliver AMPs from surfaces but none of the studies to date specifically evaluates the pH-responsive properties of such systems.^[38–40]

Sukhishvili and collaborators were the first to report a pH dependence on the release of an AMP using poly(methacrylic acid) as the pH-responsive component.^[41] In this work, a model AMP, L5 peptide (containing approximately five positive charges at physiological pH, i.e., 7.4),^[42] was loaded onto poly(methacrylic acid) hydrogels through electrostatic interactions between the carboxylate groups of poly(methacrylic acid) and the amines of the L5 peptide (**Figure 1A**). The cross-linker that was used to prepare the hydrogels played a significant role on the pH-responsive release properties of the AMP. When adipic acid dihydrazide (AADH) was used, the hydrogels were weakly pH-sensitive with

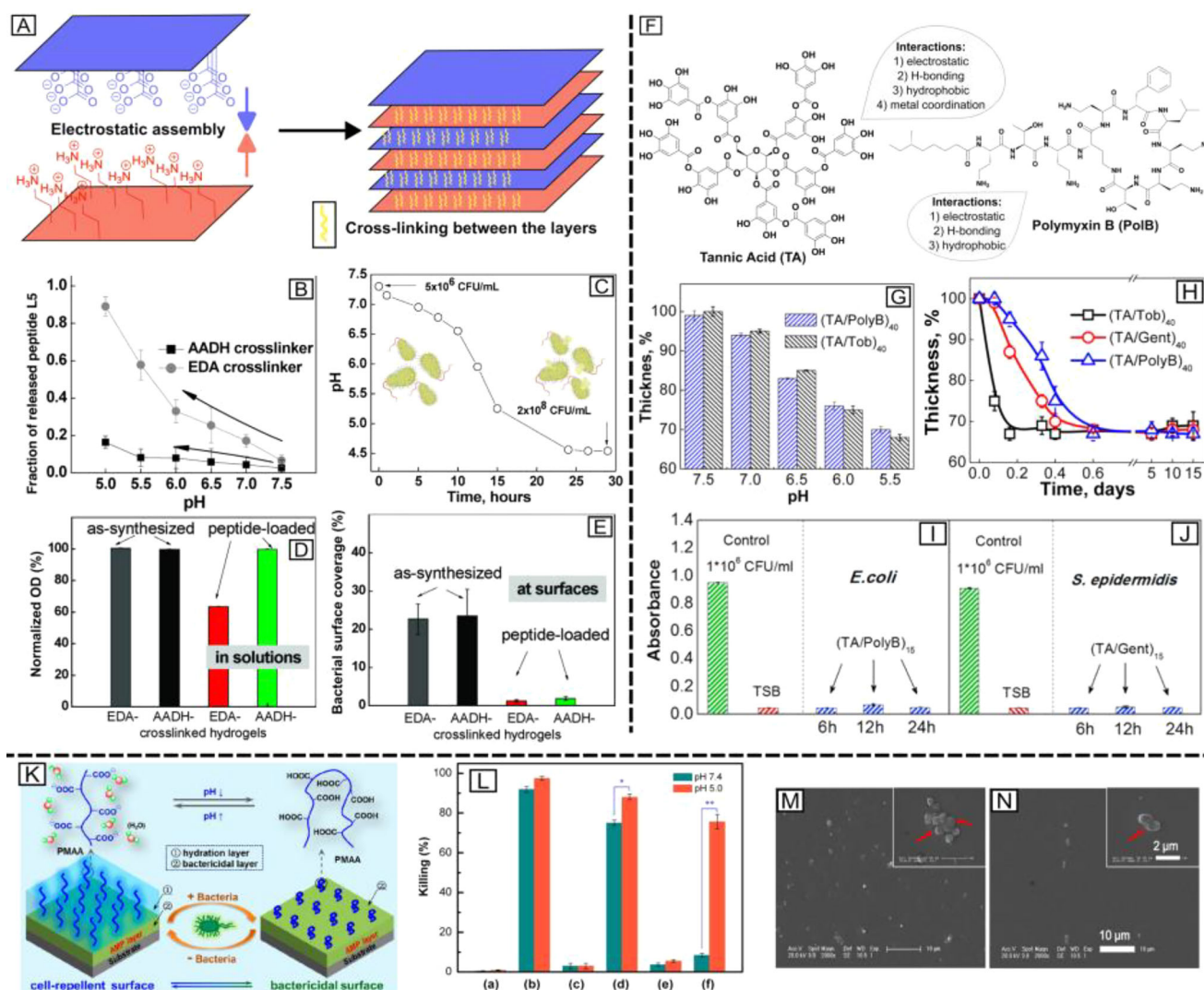


Figure 1. A) Schematic representation of polyelectrolyte complex multilayer film formation using oppositely charged electrolytes. B) Effect of pH on the retention of L5 from EDA- and AADH-stabilized poly(methacrylic acid) hydrogels (degree of polymerization = 10). Error bars represent the average standard deviations obtained from three separate experiments. C) Variation in pH during growth of *S. epidermidis* in tryptic soy broth (TSB). D) Normalized optical density at 600 nm (OD_{600}) of *S. epidermidis* in TSB after incubation for 4 h in the presence of the as-synthesized or peptide-loaded hydrogels. E) Surface coverage of *S. epidermidis* after incubation for 4 h in TSB. F) Chemical structures of tannic acid (TA) and polymyxin B (PolyB). G) Ellipsometry data of long-term pH-triggered release from (TA/PolyB)₄₀ (blue) and (tannic acid/tobramycin)₄₀ (TA/Tob)₄₀ (black) films, deposited at pH 7.5 and immersed in 0.01 M phosphate buffer solution containing 0.2 M NaCl in the pH range of 7.5–5.5. (H) Time evolution of normalized thickness (as measured by ellipsometry) of (tannic acid/gentamycin)₄₀ (TA/Gen)₄₀, (TA/Tob)₄₀, and (TA/PolyB)₄₀ films deposited at pH 7.5 and immersed at pH 5.5. Error bars are within symbol size if not shown. I, J) Growth of *E. coli* (I) and *S. epidermidis* (J) in solution in the presence of (TA/PolyB)₁₅- and (TA/Gen)₁₅-coated wafers after different incubation times in 2 mL of 1×10^6 CFU mL⁻¹ bacterial suspension at 37 °C; bacterial growth in the presence of uncoated silicon wafers after incubation for 24 h and TSB (controls) is also shown. K) Schematic diagram of bacteria-responsive hierarchical antibacterial surface that can switch from cell-repellent to bactericidal properties upon environment acidification. L) Killing efficiencies of different coating formulations: (a) pristine silicon, (b) AMP, (c) poly(methacrylic acid), (d) one-layer architecture, (e) non-responsive hierarchical architecture, and (f) responsive hierarchical architecture; * $p < 0.05$, ** $p < 0.01$. M, N) Representative scanning electron microscopy images of *Staphylococcus aureus* attachment to one-layer architecture (M) or responsive hierarchical architecture (N). Samples were incubated in growth medium containing 10^6 bacterial cells mL⁻¹ for 24 h. Red arrows indicate intact bacterial cells, and red arrows indicate lesions and distortions on the cell membrane of microorganisms. A–E) Adapted with permission.^[41] Copyright 2010 American Chemical Society, F–J) Adapted with permission.^[43] Copyright 2014 American Chemical Society, K–N) Adapted with permission.^[44] Copyright 2016 American Chemical Society.

only 15% of L5 released upon lowering the pH from 7.5 to 5.0 (Figure 1B). This relatively weak pH response was attributed to the strong hydrogen bond interactions between the L5 peptide and the amide groups of AADH. In contrast, when ethylenediamine (EDA) was used as the cross-linker, the hydrogels were

more sensitive to changes in pH and released 90% of the loaded L5 across the pH range examined (Figure 1B). Moreover, the majority of the AMP ($\approx 60\%$) was released between pH 6.0 and 5.0 with an additional 30% released between pH 7.5 and 6.0 (Figure 1B), creating a release profile that favors a low pH.

Further, when compared with hydrogels prepared using cross-linker AADH, the hydrogels that were prepared using EDA as the cross-linker displayed a higher antimicrobial activity in inhibiting growth of *Staphylococcus epidermidis* in media (Figure 1D). This higher antimicrobial activity was likely due to *S. epidermidis* lowering the pH in the culture media once it reached a certain cell density (Figure 1C). However, this effect was mild, with only a 40% reduction in growth of the pathogen observed (Figure 1D). Nevertheless, both AMP delivery systems inhibited colonization of hydrogel-coated surfaces, suggesting that these AMP delivery systems may be more suitable for applications where prolonged delivery is preferred (e.g., antibacterial coatings) (Figure 1E).

In subsequent work, Sukhishvili and co-workers reported an improved antimicrobial delivery system based on tannic acid (TA) (Figure 1F).^[43] TA is a naturally occurring polyphenol with multiple binding modalities (i.e., hydrophobic interactions, hydrogen bonding, metal coordination, and/or electrostatic interactions) owing to the presence of the catechol and gallol groups.^[45,46] In particular, TA exhibits multiple charges at slightly basic pH (e.g., -6 at pH 9, -3.5 at pH 8.5, and -1 at pH 8)^[42] and becomes neutral at most physiological pHs ($\text{pH} \leq 7.4$) and therefore electrostatic interactions can be easily disrupted. Taking advantage of the unique properties of TA, Sukhishvili and co-workers developed layer-by-layer films that encapsulated either an antimicrobial peptide (polymyxin B, PolyB)^[47] or an aminoglycoside antibiotic (tobramycin (Tob)^[48] or gentamicin (Gen)^[49]), all currently in clinical use as last-resort antibiotics. The TA-derived films displayed a high drug loading capacity ($300 \mu\text{g mm}^{-3}$) and a steady degradation profile with a decrease in pH (Figure 1G,H). Of all three systems, the PolyB-containing films inhibited the growth of *E. coli* after 6 h of incubation in a bacteria-containing solution (Figure 1I) despite having the slowest pH-induced drug release (5% of PolyB released at pH 5.5 after 6 h, Figure 1H). The additional stabilization of the TA/PolyB system was attributed to stronger hydrogen bonding and hydrophobic interactions present in this system than in the other two systems, which was believed to play a key role in the slow-release kinetics observed. The findings of this study illustrate some of the challenges faced when developing an optimized AMP delivery system, in particular the need to balance antimicrobial efficacy and stability of the system under physiological conditions.

Yin and co-workers developed a pH-responsive surface coating that could switch from displaying cell-repellent properties at physiological pH to bactericidal properties under the acidic conditions caused by bacterial colonization.^[44] To realize such switchable properties, a hierarchical polymer brush architecture was used that combined a pH-responsive poly(methacrylic acid) outer layer with an AMP-modified poly(methacrylic acid) inner layer (Figure 1K). Cecropin B, an AMP first isolated from the hemolymph of the giant silk moth *Hyalophora cecropia*, was used as the model antimicrobial.^[50,51] Under normal physiological conditions (i.e., pH 7.45), the poly(methacrylic acid) outer layer was negatively charged and hydrophilic, effectively shielding the cationic and hydrophobic AMP, rendering the surface more biocompatible and cell-repellent (Figure 1K). However, with the acidification of the microenvironment caused by bacterial growth, the carboxylate groups of poly(methacrylic acid) became protonated. This protonation rendered the polymer hydrophobic, causing polymer chain collapse and thus exposing the AMP-containing

layer (Figure 1K). The study showed that the antimicrobial properties of the polymer brushes containing poly(methacrylic acid) had a high pH sensitivity, resulting in a 65% increase in killing efficacy of *S. aureus* when the pH of the environment changed from 7.45 (15% killing efficiency) to 5.0 (80% killing efficiency) (Figure 1L). In comparison, coatings prepared using a more traditional one-layer approach (i.e., using a copolymer of AMP-modified monomer and methacrylic acid) were only 20% more efficient in bacterial killing at pH 5.0 (90% killing efficiency) than at pH 7.45 (70% killing efficiency) (Figure 1L). As a result, the poly(methacrylic acid)-based polymer brush system showed the best biocompatibility toward blood pellets under physiological conditions (Figure 1M,N). Although this work uses covalent immobilization rather than polyelectrolyte complexation to localize the AMP within the inner layer, this strategy ensures that the cytotoxic nature of AMPs is shielded from healthy tissues when placed in the body, and while at ambient temperature protects the implant from bacterial colonization.

2.2. pH-Responsive AMP Delivery from Nanoparticulate Systems

As demonstrated in Section 2.1, delivering AMPs from surfaces may reduce their efficacy in suspension, as a result of the limited diffusion of the antimicrobial from the films. To address this limitation while still protecting these peptides from degradation, systems that can be suspended in biological fluids, such as liposomes or nanoparticles, have been developed.^[6,18,27–30] Under the appropriate conditions, polyelectrolyte complexation in solution can produce colloiddally stable nanoparticles, often termed PECs, polyionic complexes (PICs), or interpolyelectrolyte complexes. If one of the complexing polyelectrolytes is a block copolymer that carries a neutral block, such as poly(ethylene glycol) (PEG), these nanoaggregates are often termed PIC micelles.^[33,52–54]

The first example of an AMP loaded inside a polyelectrolyte complex nanoparticle was reported by Devore and colleagues.^[55] KSL-W, a synthetic AMP identified from a combinatorial library,^[56] formed colloiddally stable particles of 100–200 nm in size with an anionic graft copolymer synthesized via derivatization of poly(acrylic acid) or poly(methacrylic acid) with Jeffamine M-2070 (Figure 2A-a).^[55] Polymers with different backbones and grafting densities were prepared to control the hydrophilicity and charge density in the polymer backbone. Among the polymers studied, the anionic graft copolymer (PPAAg1), derived from poly(acrylic acid) (PPAA) and with $\approx 0.5\%$ grafting density (1% grafting density was targeted), performed the best at protecting KSL-W from proteolytic degradation in human plasma, reducing AMP degradation by 30% in 4 h compared to the free peptide (Figure 2B). However, the improved stability caused by shielding was accompanied with a reduction in antimicrobial efficacy of 50% as a result of charge masking, demonstrating the challenge in preparing both active and stable polyelectrolyte complex nanomaterials derived from AMPs (Figure 2C).

In 2017, Fernandez-Trillo and collaborators used a similar approach to encapsulate clinically relevant PolyB with anionic polymer poly(styrene sulfonate) (PSS) (approved by the US Food and Drug Administration) to prepare polyelectrolyte complex particles (Figure 2A-b).^[34] Nanoparticles that were stable in physiological media were obtained when an excess of the anionic

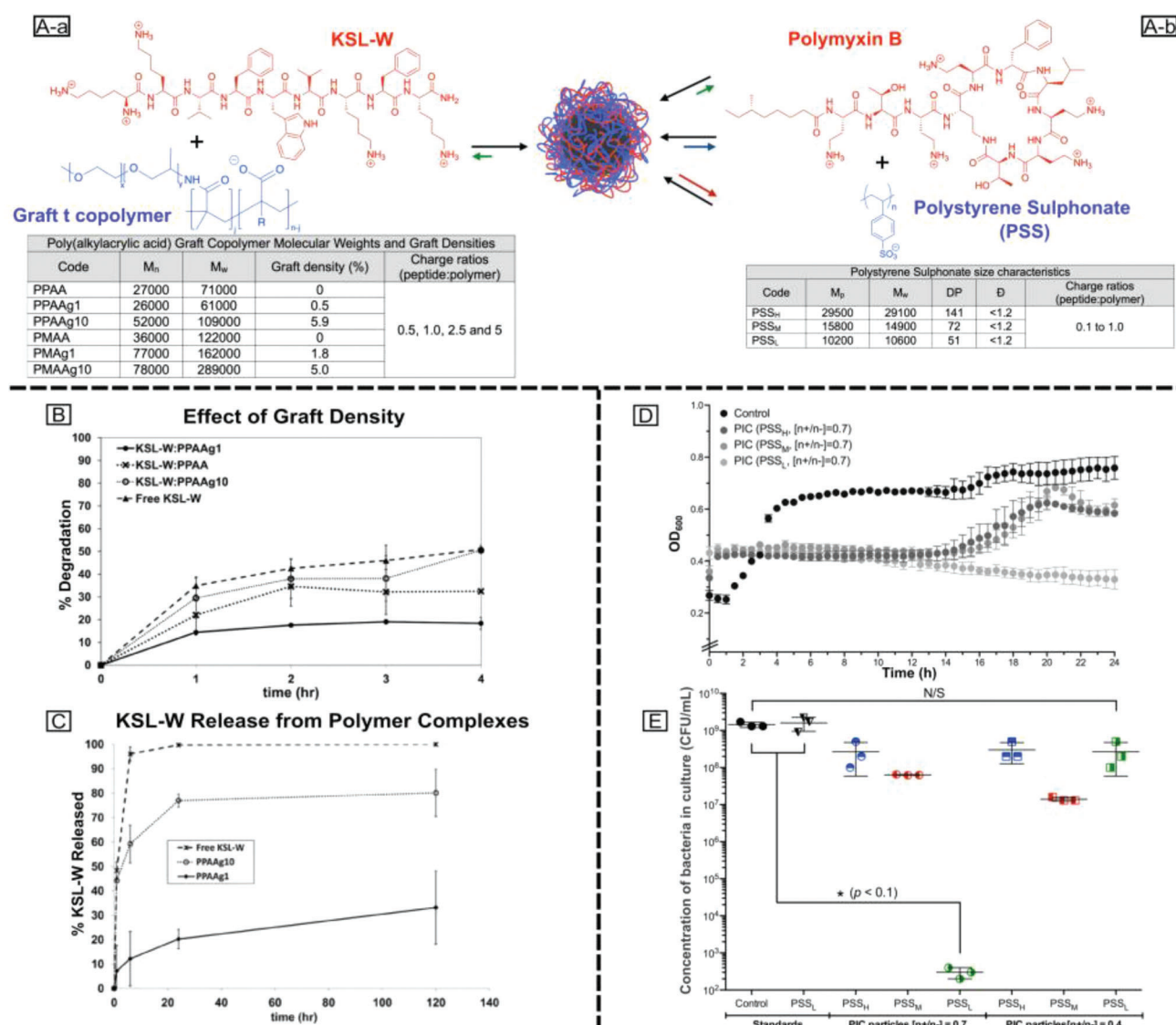


Figure 2. A-a) Schematic representation of the formation of polyelectrolyte complex nanoparticles by self-assembly of cationic KSL-W with anionic graft copolymer ($R = \text{H}$, $-\text{CH}_3$, or $\text{CH}_2-\text{CH}_2-\text{CH}_3$) and effect of the change in multivalency. A-b) Schematic representation of the formation of polyelectrolyte complex nanoparticles by self-assembly of cationic PolyB with PSS and effect of the change in multivalency including size characteristics of polyanions used to assemble the polyelectrolyte complexes. B) Degradation of free KSL-W and KSL-W complexed with anionic copolymer in 50:50 (v/v) human plasma:water. Error bars are standard deviations of 3 samples. C) Release kinetics of free and complexed KSL-W from polyelectrolyte complex nanoparticles made from KSL-W and anionic graft copolymer (PPAAg1—graft density 0.5% and PPAAg10 graft density 5.9%) at 37°C in water (charge ratio = 0.5, $[\text{KSL-W}]_0 = 66 \text{ mg mL}^{-1}$). Error bars are standard deviations of 2 samples. D) Change in OD_{600} for *P. aeruginosa* cultures in the absence (Control) and presence of PSS containing polyelectrolyte complex nanoparticles prepared at $\{n+/n-\}$ ratio (i.e., ratio between positive charges of ammonium groups in PolyB over the negative charges of acidic groups in PSS) of 0.7. Error bars represent the standard deviation, $n = 3$. E) Concentration (CFU mL^{-1}) of *P. aeruginosa* in the absence (Control) and presence of polyelectrolyte complex nanoparticles prepared from different PSS sources at different $\{n+/n-\}$ ratios, calculated from the colonies detected on the agar plates (one-way analysis of variance (ANOVA), Tukey test, confidence interval (CI) = 95%); N/S, not significant. Error bars represent the standard deviation, $n = 3$. A-a, B, C) Adapted with permission.^[55] Copyright 2012 Wiley Periodicals Inc., A-b) Adapted with permission under terms of the CC-BY 4.0 license.^[34] Copyright 2016, The Authors. Published by Elsevier Ltd. D,E) Adapted with permission under terms of the Creative Commons CC-BY 4.0 license.^[57] Copyright 2017, The Author(s). Published by Springer Nature.

component was present, resulting in the formation of a “protective” anionic corona around the positively charged AMP therapeutic (Figure 2D).^[34] The polyelectrolyte complex nanoparticle loaded with PolyB degraded slowly, providing a passive release of the cationic antimicrobial, and thus inhibiting the growth of *P. aeruginosa* (Figure 2D). Furthermore, by changing the degree of

polymerization of PSS, the stability and antimicrobial activity of these polyelectrolyte complex nanoparticles could be fine-tuned (Figure 2A-b,E).^[57]

Although the above studies showcase the challenges faced during the preparation of colloiddally stable and active polyelectrolyte complexes with AMPs, the effect of pH on the release and

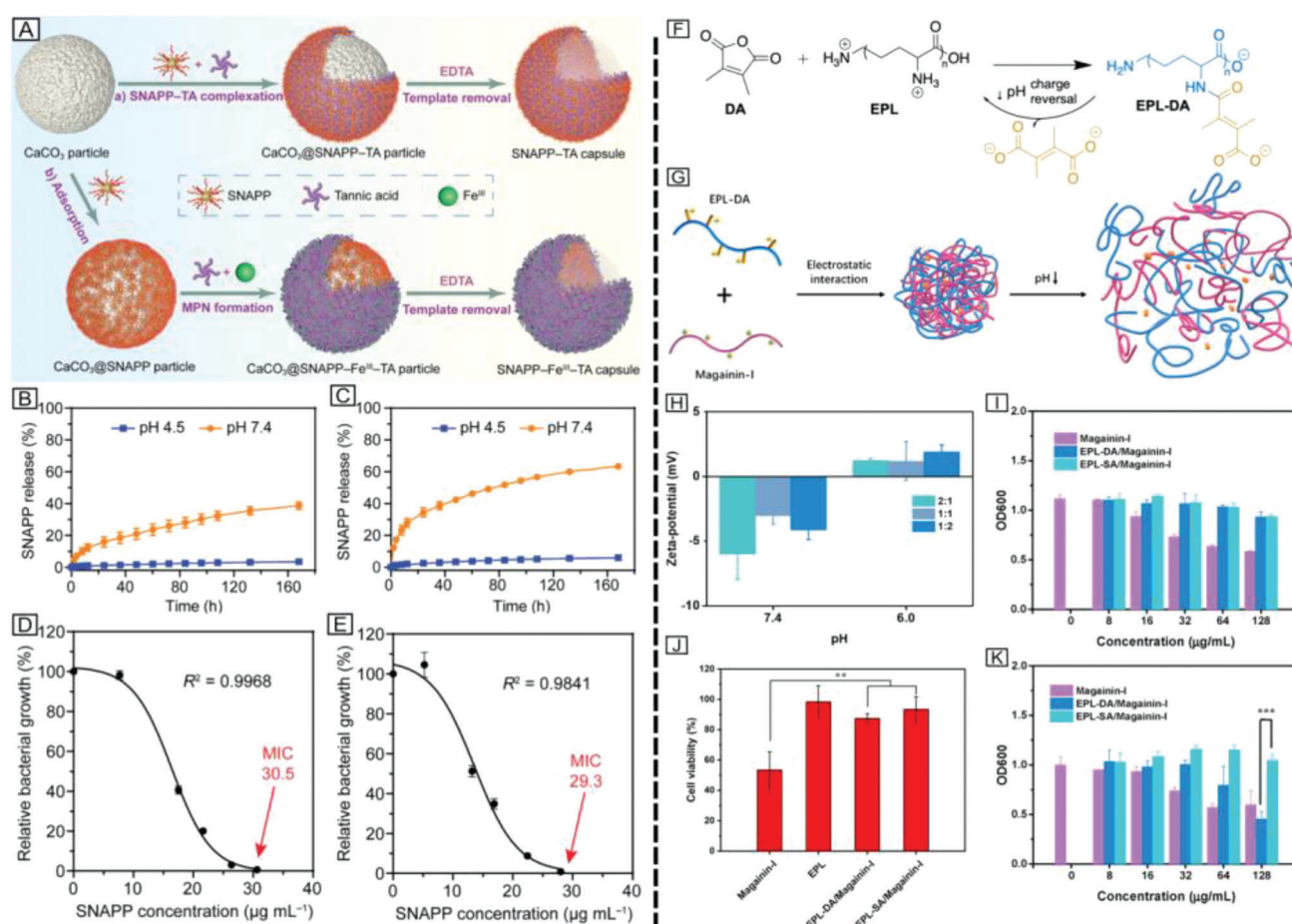


Figure 3. A) Schematic representation of the immobilization of SNAPPs via the assembly of SNAPP-TA or SNAPP-Fe^{III}-TA capsules onto sacrificial CaCO₃ particle templates. B,C) Release of SNAPPs from SNAPP-Fe^{III}-TA capsules (B) or SNAPP-TA capsules (C) at pH 4.5 and 7.4. The results are shown as means ± standard deviations (*n* = 3). D,E) Relative growth (%) of *E. coli* as a function of the concentration of SNAPPs released from SNAPP-TA (D) or SNAPP-Fe^{III}-TA capsules (E). The results are shown as means ± standard deviations (*n* = 3). F) Synthesis of EPL-DA and its pH-triggered degradation. G) Schematic representation of the preparation of polyelectrolyte complex nanoparticles and the stimuli-responsive release of AMP Magainin-I. H) Zeta-potential of EPL-DA/Magainin-I with different compositions at pH 7.4 and 6.0. I,K) Inhibitory effect of Magainin-I, EPL-DA/Magainin-I, and succinic anhydride-modified ε-polylysine (EPL-SA)/Magainin-I against *P. aeruginosa* at pH 7.4 (I) and pH 6.0 (K). J) Cytotoxicity of Magainin-I, EPL, EPL-DA/Magainin-I, and EPL-SA/Magainin-I against NIH/3T3 cells. The concentration of Magainin-I was 128 μg mL⁻¹. (H,I,J,K) Data were expressed as mean ± standard deviations. A-E) Adapted with permission.^[59] Copyright 2021 Wiley-VCH, F-K) Adapted with permission.^[61] Copyright 2022 Wiley Periodicals LLC.

antimicrobial activity of these systems was not examined. Moreover, in some cases, strong electrolytes were used (e.g., PSS) which are fully charged under most physiological relevant conditions (pH ≤ 7.4).^[42] Similarly, most AMPs carry lysine (pK_a of side chain ≈ 10.7) and arginine (pK_a of side chain ≈ 12.1) residues, which are fully protonated under these conditions. As such, changes in pH will have a minimal effect on the charge density of these polyelectrolytes, thereby resulting in considerably weak pH-responsive delivery systems.

The first reported pH-responsive polyelectrolyte complex nanoparticles were derived from tannic acid that, much like the system developed by Sukhishvili and coworkers for surfaces,^[43] was used to prepare nano systems capable of encapsulating either an AMP—colistin sulphate^[19]—or one of two aminoglycoside antibiotics, gentamicin^[49] and gatifloxacin.^[58] Out of the three antimicrobials tested, the nanoparticles containing colistin sulphate

were the most stable at pH 7.4, with only ≈ 39% of the drug being released at this pH. However, at pH 4.5 the electrostatic interactions between the AMP and the tannic acid were neutralized, leading to complete particle disassembly, and the release of ≈ 98% of the AMP in < 2 h of incubation. Moreover, the minimum inhibitory concentration of these colistin-containing nanoparticles at pH 7.4 was 50% higher (i.e., weaker antimicrobial activity) than at pH 4.5 and, at this pH, the antimicrobial activity of the polyelectrolyte complex nanoparticles was equivalent to that of free colistin sulphate demonstrating the pH-responsiveness of the system.

Tannic acid has also been used by Caruso and collaborators to develop microcapsules that incorporated structurally nanoengineered antimicrobial peptide polymers (SNAPPs),^[59] an AMP mimic (Figure 3A). SNAPPs are star-shaped poly(amino acids) containing hydrophilic lysine and hydrophobic valine residues

and exhibit antimicrobial activity (submicromolar range) against multidrug-resistant bacteria.^[60] Two types of SNAPP-containing microcapsules were prepared using a template-mediated approach: 1) polyelectrolyte complexation of SNAPPs and tannic acid onto porous CaCO₃ (SNAPP–TA capsules) (Figure 3A, route a) and 2) adsorption of SNAPPs on CaCO₃ and subsequent encapsulation within a metal–phenolic coating (SNAPP–Fe^{III}–TA capsules) (Figure 3A, route b).^[59] Both SNAPP-containing systems were more stable at lysosomal pH 4.5 (up to 160 h) than at extracellular pH (i.e., 7.4), at which sustained AMP release was observed (Figure 3B,C), thus inhibiting the growth of model pathogen *E. coli* (Figure 3D,E). The higher stability observed at pH 4.5 was attributed to the formation of stronger H-bonding and ionic interactions between SNAPPs and tannic acid at pH 4.5 when compared to 7.4, possibly due to the star shape architecture of the antimicrobial polymer and the very high charge density of this AMP mimic. Furthermore, the capsules were successfully nebulized into inhalable aerosol droplets, thus demonstrating their potential in pulmonary delivery applications. Compared with the microcapsules formed via route b, the SNAPP–TA capsules (formed via route a) showed higher endosomal/lysosome colocalization, indicating potential to target bacteria that commonly reside within endo/lysosomes (e.g., *Mycobacterium tuberculosis*).

In another study, Ji and co-workers reported a different strategy to prepare pH-responsive polyelectrolyte complex nanoparticles, which exploits the decomposition of 2,3-dimethylmaleic acid amides under acidic conditions.^[61,62] A pH-responsive polymer (EPL-DA) was designed by derivatization of ϵ -polylysine (EPL) with 2,3-dimethylmaleic anhydride (DA) (Figure 3F, forward reaction), and the resulting anionic polymer was used to encapsulate a natural AMP, Magainin-I (Figure 3G).^[61,63] When the pH of the environment was lowered from 7.4 to 6.0, the charge of the Magainin-I-containing particles changed from negative to positive (Figure 3H), suggesting the hydrolysis of the negatively charged EPL-DA to yield positively charged EPL (Figure 3F, backward reaction). This hydrolysis resulted in charge repulsion between both cationic EPL and Magainin-I, leading to the disassembly of the polyelectrolyte complex particles and consequent release of the AMP. The EPL-DA/Magainin-I nanoparticles displayed minimal antibacterial activity against *P. aeruginosa* at pH 7.45. Notably, at pH 6.0, the EPL-DA/Magainin-I particles retained $\approx 75\%$ of the antimicrobial efficacy of free Magainin-I at concentrations of 32 and 64 $\mu\text{g mL}^{-1}$ while exceeding the efficacy of free AMP at 128 $\mu\text{g mL}^{-1}$ (Figure 3I,K). Furthermore, EPL-DA/Magainin-I particles were considerably less cytotoxic than the free drug—cell viability of EPL-DA/Magainin-I was 87% compared with that (50%) of free Magainin (Figure 3J). These AMP delivery systems were effective at shielding the toxicity of the AMP while triggering its release at low pH.

3. Enzyme-Responsive AMP Delivery Systems

3.1. Enzyme-Responsive Delivery of AMPs from Surfaces

Although the inherent pH responsive behavior of polyelectrolytes can be exploited to develop AMP delivery systems, challenges remain in preparing stable and active nano systems that can release AMPs as a function of pH, as highlighted in Section 2. Further,

as mentioned previously, owing to being strong polyelectrolytes, the charge density of AMPs barely changes within physiological pH. Moreover, changes in pH are not always driven by infection, as there are pH gradients between organs, tissues, and/or cellular compartments. Though these changes can be exploited to develop targeted systems, such as intracellular delivery as shown above,^[59] these changes can also lead to off-target effects, such as AMP release in the extracellular milieu. As an alternative approach, changes specifically driven by infections can be used as stimuli. For instance, bacteria often secrete a variety of enzymes, which are virulence factors designed to facilitate colonization of the host and overwhelm its defenses. These enzymes (Figure 4A) commonly degrade tissues and biomolecules, often targeting peptide sequences and biopolymers that are not targeted by host enzymes. Therefore, the use of enzyme-responsive antimicrobial delivery systems presents potential to more precisely target and release a variety of antibiotics, including AMPs.^[64–66]

Boulmedais and collaborators designed a hyaluronidase-degradable polyelectrolyte complex multilayer coating^[67] that incorporated cateslytin (Figure 4B), an AMP that is produced upon proteolysis of chromogranin A, an acidic protein stored in the secretory vesicles of numerous neuroendocrine and immune cells.^[68] Hyaluronidase, which is a common enzyme secreted by a variety of pathogens, catalyzes the degradation of hyaluronic acid (HA), a key structural component of the extracellular matrix.^[69] As such, hyaluronidases are versatile targets for developing enzyme-responsive delivery systems for a variety of pathogens. Similarly, to the pH-responsive system developed by Egles and co-workers,^[37] the AMP was embedded in multilayered films prepared from polyelectrolytes HA and chitosan (CHI). The latter cationic polysaccharide is commonly used in the preparation of polyelectrolyte complex multilayers^[70,71] and has antimicrobial properties.^[72,73] In this enzyme-responsive system, the AMP was covalently coupled to HA, which resulted in stronger drug retention on the surface. To evaluate the response to hyaluronidase, the antimicrobial activity against *C. albicans* was compared between the HA-based system and a hyaluronidase-resistant system that used polyacrylic acid and cateslytin-functionalized poly(allylamine hydrochloride). The system resistant to hyaluronidase showed minimal antimicrobial effects, whereas the system using HA fully inhibited the growth of *C. albicans* after 24 h of incubation (Figure 4C). Moreover, the versatility of the system was demonstrated by inhibiting the growth of *M. luteus* (Figure 4D) and *S. aureus* (Figure 4E), two hyaluronidase-producing bacteria. Of note, *S. aureus* is a leading cause of pneumonia and other respiratory infections, as well as infections in surgical sites, artificial joints, and cardiovascular tissues.^[74]

3.2. Enzyme-Responsive Delivery of AMPs from Nanoparticulate Systems

Using similar principles to those discussed above, Fernandez-Trillo and colleagues developed highly selective polyelectrolyte complex nanoparticles by combining a peptide that could be degraded by LasB (a protease secreted by pathogen *P. aeruginosa*) with cationic antimicrobial polymer polyethyleneimine.^[75,76] Glutamic acids were incorporated into

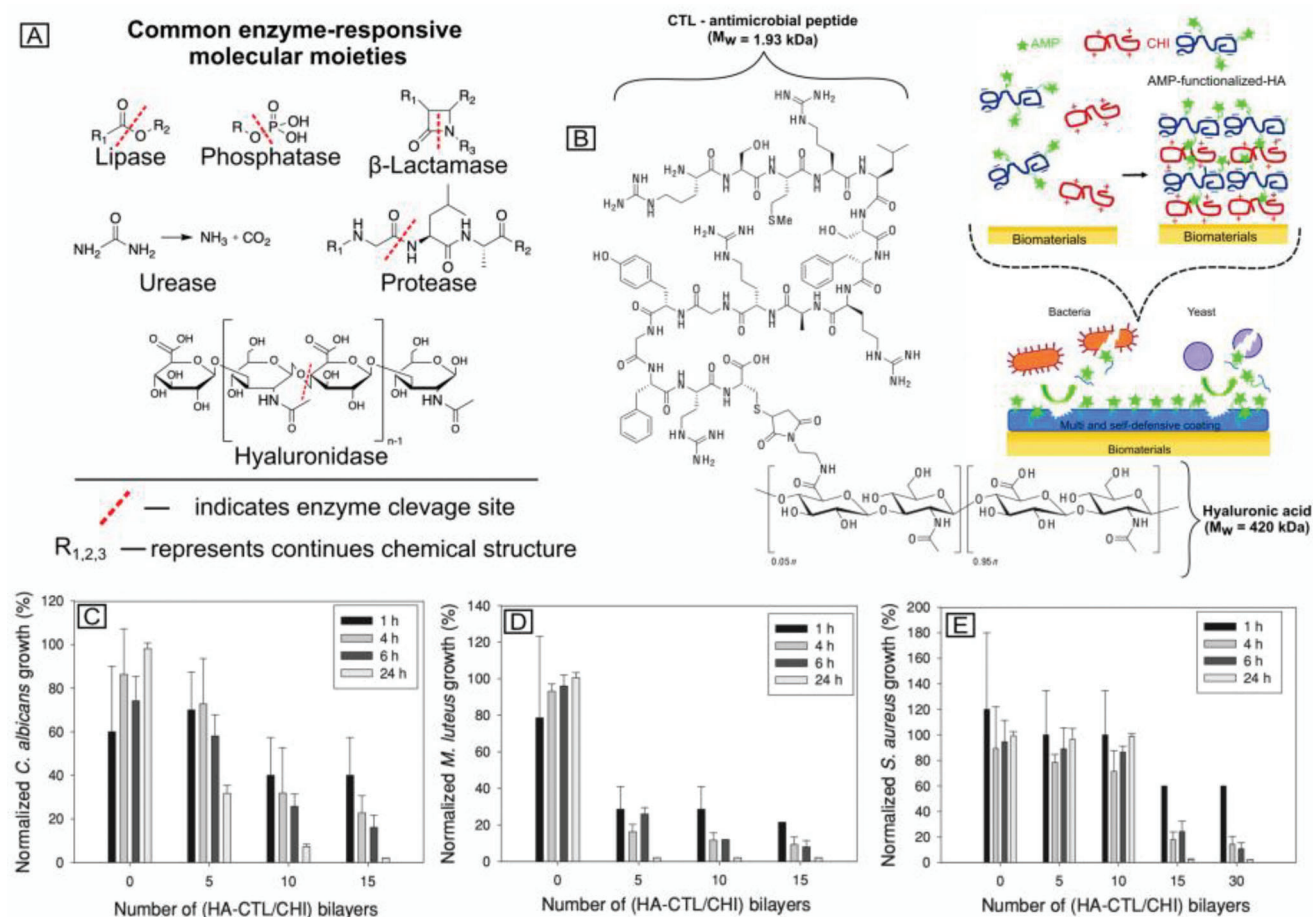


Figure 4. A) Schematic representation of enzyme-responsive molecular moieties with their corresponding enzymes used in the antimicrobial drug delivery systems. B) Schematic representation of cateslytin-modified CHI/HA multilayers. C–E) Antimicrobial activity of multi-layered films (HA-CTL/CHI) against *Candida albicans* (C), *Micrococcus luteus* (D), and *S. aureus* (E) after incubation for 1–24 h. B, C, D, E) Adapted with permission.^[66] Copyright 2013 Wiley–VCH, A) Adapted with permission under terms of the Creative Commons CC-BY 4.0 license.^[67] Copyright 2022, The Authors, published by Wiley–VCH.

the LasB-degradable peptides to facilitate electrostatic interactions with polyethyleneimine, while cysteine residues were incorporated to enable cross-linking within the system via disulfide formation (**Figure 5A**). In this system, the number of anionic and cysteine residues could be easily modified to optimize particle size and stability.^[76] These polyelectrolyte complex nanoparticles effectively shielded the cationic charge of polyethyleneimine, significantly reducing its toxicity and antimicrobial activity (**Figure 5B**, 2 h). Increasing the incubation time of the bacteria with these nanoparticles led to the secretion of increasing amounts of the LasB enzyme, consequently doubling the antimicrobial activity of the enzyme-responsive nanoparticles against *P. aeruginosa* (**Figure 5B**, 4 h, black bars). Furthermore, the particles displayed excellent selectivity—this increase in antimicrobial activity was not observed when the same experiment was performed with a *P. aeruginosa* strain that could not produce this protease (**Figure 5B**, 4 h, white bars). Similarly, these nanoparticles were not degraded by human leukocyte elastase (HLE) (**Figure 5C**, white bars), a protease secreted by our immune system in response to infection.^[77] Though this approach faces similar challenges to pH-responsive systems

when balancing stability and activity, this work demonstrates the potential of developing fully selective nano systems that release AMPs (and mimics) only in the presence of pathogenic bacteria.

Instead of using oppositely charged polyelectrolytes, Wang and co-workers developed chitosan–antimicrobial peptide (AMP) conjugates (chitosan–peptide conjugates, CPCs) to construct an enzyme-responsive AMP delivery system.^[78] These conjugates consisted of three covalently conjugated moieties: a chitosan backbone, an enzyme-cleavable peptide (GPL-GVRGC) coupled to PEG and KLAK,^[79] a cationic AMP that forms an amphipathic α -helix when bound to negatively charged lipid membranes (Figure 5D). In the absence of gelatinase, these CPCs self-assemble into nanoparticles. However, in the presence of gelatinases, the GPL-GVRGC peptide breaks down, leading to conformational changes that cause the nanoparticles to shift from spherical structures to nanofibers (Figure 5D). As this morphological change occurs, the AMP is exposed, resulting in multivalent electrostatic interactions with bacteria and an antimicrobial effect. As a result of these changes, the minimum inhibition concentration values of the enzyme-degradable system (Figure 5E, red bars) were considerably lower (i.e., stronger

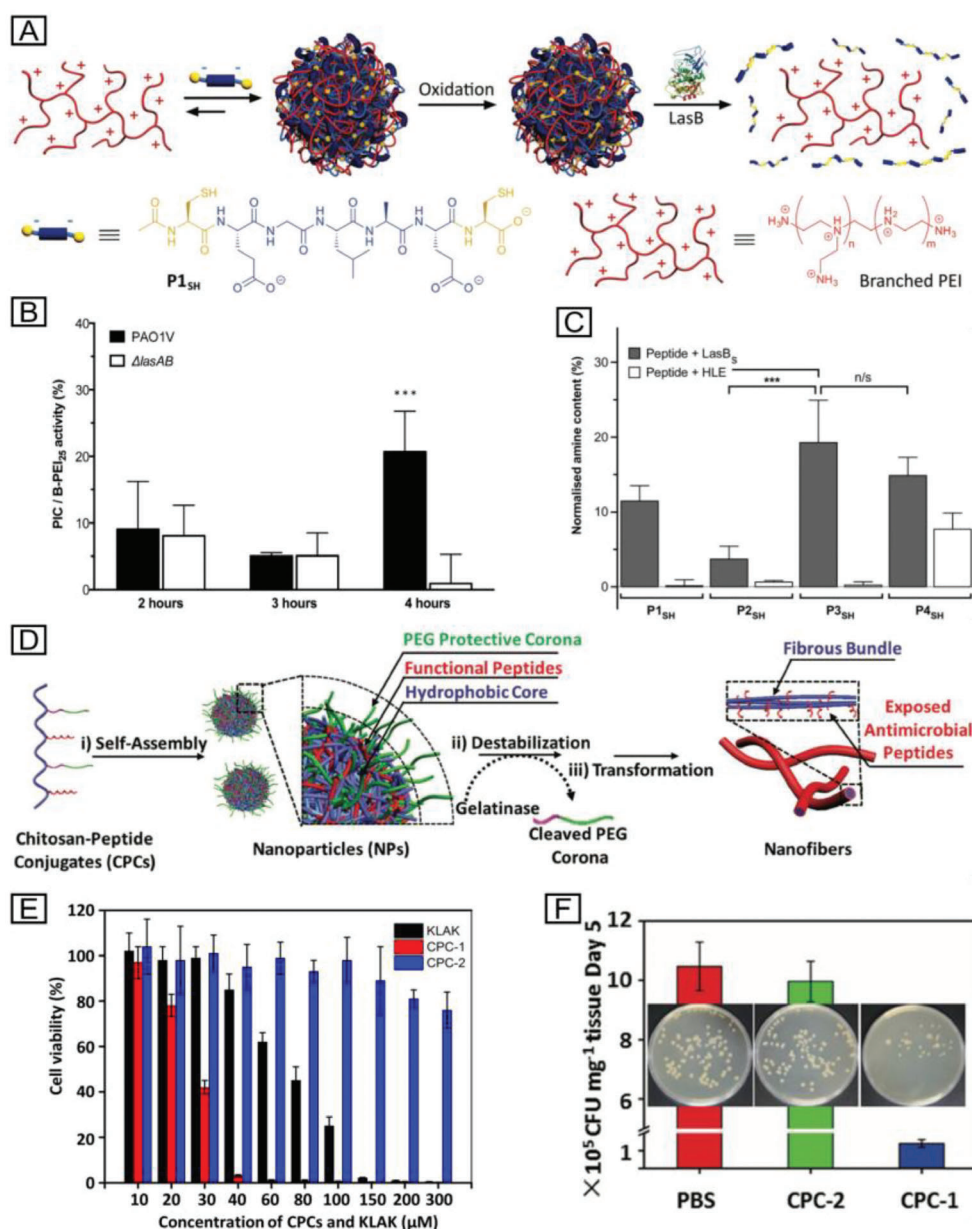


Figure 5. A) Assembly and oxidative cross-linking of antimicrobial polyelectrolyte complex nanoparticles constructed from LasB-degradable peptide and antimicrobial polymer branched poly(ethylene imine) (B-PEI). B) Normalized antimicrobial activity as a function of time of polyelectrolyte complex nanoparticles prepared at a N:COOH ratio of 1:0.3. The antimicrobial activity is normalized by dividing the relative antimicrobial activity of the polyelectrolyte complex nanoparticles by that of (B-PEI)₂₅ (Mw 25 KDa). *** $p < 0.001$ between pathogenic strain of *P. aeruginosa* (PAO1V) and a mutant strain (Δ lasAB) (CI = 99.9%) after 4 h; $n = 3$. C) Relative amine content in LasB-responsive anionic peptides following incubation with LasB or HLE. Data are shown as mean values \pm standard deviations ($n = 3$). One-way ANOVA, followed by Tukey's test (CI = 95%) was used to test for significance. n/s, not significant; *** $p < 0.001$. D) Illustration of the self-assembly of CPCs and the principle of enzyme-induced morphology transformation. (i) The CPCs self-assemble into nanoparticles with a PEGylated corona. (ii) The protective corona peels off upon cleavage of the peptide in the presence of gelatinase. (iii) Destabilization of the hydrophobic/hydrophilic balance spontaneously promotes reorganization of the self-assembled nanoparticle structures into fibrous structures via chain-chain hydrogen bonding interactions of chitosan. E) Viability of *S. aureus* in the absence and presence of CPC nanoparticles and KLAQ (0–300 μ M for KLAQ). Data are expressed as means \pm standard deviations ($n = 3$) and the experiments were repeated at least twice. F) Antibacterial properties evaluated in vivo. The survival of *S. aureus* in infected tissues was quantified on Day 5 by counting the number of colonies in infected tissues from mice injected with phosphate-buffered saline (PBS), enzyme-responsive (CPC-1), or non-responsive (CPC-2) nanoparticles. Data are shown as mean values \pm standard deviations ($n = 5$). A, B) Adapted with permission.^[75] Copyright 2016 The Royal Society of Chemistry, D–F) Adapted with permission.^[78] Copyright 2017 Wiley–VCH, C) Adapted with permission under terms of the Creative Commons CC-BY 4.0 license.^[76] Copyright 2018 The Authors, published by Wiley–VCH.

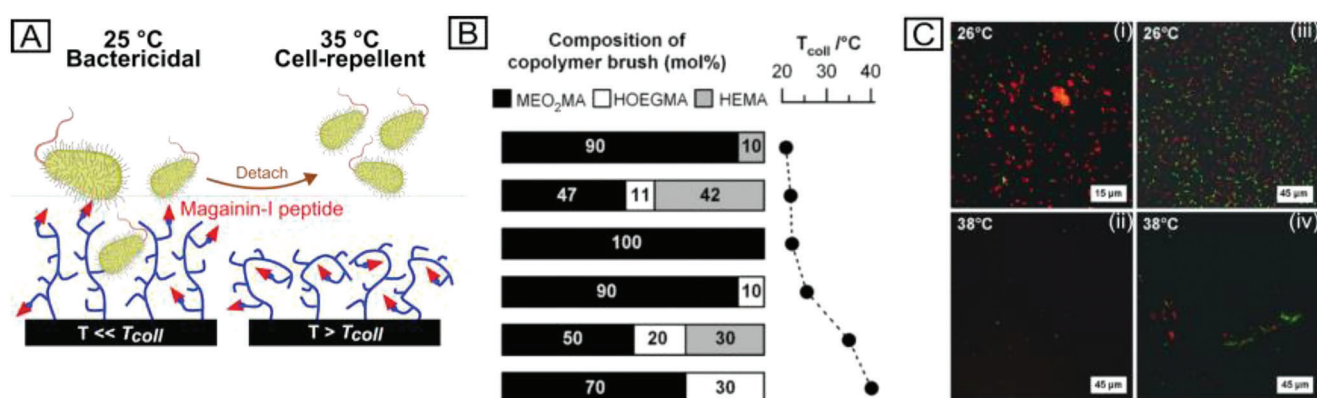


Figure 6. A) Schematic representation of the brush conformation below and above LCST of copolymer brushes derived from 2-(2-methoxyethoxy)ethyl and oligoethyl methacrylate. B) Collapse transition temperature (T_{coll}) of copolymer brushes depending on the composition of the monomer and (2-(2-methoxyethoxy)ethyl methacrylate, MEO₂MA; oligoethyl methacrylate, HOEGMA; hydroxyethyl methacrylate, HEMA). C) Colonization by *L. ivanovii* (i,ii) or *E. coli* (iii,iv) of surfaces coated with polymer brushes. Samples were incubated at 26 or 38 °C. A-C) Adapted with permission.^[86] Copyright 2010 Wiley-VCH.

antimicrobial effect) toward gelatinase positive *S. aureus* compared to the nondegradable system (Figure 5E, blue bars) and to the AMP (Figure 5E, black bars). Furthermore, in vivo studies using a mouse model confirmed the high antimicrobial efficacy of the enzyme-responsive particles (Figure 5F, blue bar), as shown by a 10× decrease in *S. aureus* colony counts compared to the nonresponsive control (Figure 5F, green bar) and to the negative control (Figure 5F, red bar).

4. Thermoresponsive AMP Delivery Systems

Although enzyme-responsive delivery of AMPs has the potential to be very specific, it may be limited to applications where the pathogenic agent is known. This strategy is often required in the treatment of resistant infections that do not respond to broad-spectrum antibiotics. Conversely, developing strategies that can target a broader range of bacteria has advantages as a first line of defense against infections. The presence of a pathogen within the human body induces an immune response that commonly leads to inflammation and an increase in tissue temperature.^[80–82] These changes in temperature can be localized (e.g., wounds) or systematic (e.g., fever). Local heating of a tissue can also be achieved externally (e.g., using microwave irradiation, infrared illumination, and ultrasound irradiation), which has been used extensively for the thermoresponsive release of anticancer drugs.^[83–85] To date, AMPs have been used primarily in thermoresponsive coatings and topical applications, wherein the difference between the internal temperature of the body (i.e., 37 °C) and the external environment is used as the main stimuli.^[66,86–89]

One of the most common thermoresponsive materials used for antimicrobial delivery is poly(*N*-isopropylacrylamide).^[90] This thermoresponsive polymer has a low critical solution temperature (LCST) of 32 °C, which is close to the typical human body temperature of 37 °C.^[90,91] Below the LCST (e.g., room temperature), poly(*N*-isopropylacrylamide) chains are hydrophilic, as the amide groups form hydrogen bonds with water that help solvate the polymer. Above the LCST (e.g., body temperature), hydrogen bonds with the solvent weaken, leading to the collapse of the poly(*N*-isopropylacrylamide) chains in aqueous solutions,

which become hydrophobic and potentially precipitate out of solution. Therefore, switchable antimicrobial systems can be produced with drugs attached to the hydrophilic or hydrophobic moieties of the poly(*N*-isopropylacrylamide) polymer.^[66,92] Although poly(*N*-isopropylacrylamide) has been used in various biomedical applications,^[93,94] some indications of polymer cytotoxicity have been reported under certain conditions.^[87]

Therefore, alternative polymer matrices with thermoresponsive properties are also being considered such as copolymer brushes derived from 2-(2-methoxyethoxy)ethyl and oligoethyl methacrylate, as developed by Glinel and collaborators (Figure 6A).^[86] The transition temperature of the polymer brushes could be fine-tuned by adjusting the content of oligoethyl methacrylate and the length of the oligoethyl methacrylate side chains, or by introducing a more hydrophilic monomer such as hydroxyethyl methacrylate.^[92,95] To achieve LCSTs similar to that of poly(*N*-isopropylacrylamide) (Figure 6B). To obtain antimicrobial properties, Glinel and co-workers grafted the AMP magainin-I^[63] onto the oligoethyl methacrylate moieties of a brush copolymer that had a transition temperature of 35 °C (Figure 6B). These polymer brushes were grown from silicon wafers to create surfaces with thermoresponsive antimicrobial activity.^[86] In a similar fashion to the pH-responsive coating developed by Yin and coworkers,^[44] the AMP was exposed to an environment below the LCST of the brush copolymer, successfully inhibiting the growth of pathogens *E. coli* and *Listeria ivanovii* (Figure 6C). However, at temperatures above the LCST of the brush copolymer, progressive collapse of the brushes occurred, which buried magainin-I within the polymer network and concurrently exposed the hydrophobic moieties of the brush copolymer, making the surface repellent to these bacteria. These polymer brushes represent the first example of antimicrobial coatings for biomedical devices that are bactericidal at room temperature (i.e., below the LCST) while inactive and cell-repellent under physiological conditions (i.e., above the LCST).

In the example presented above, the AMP was covalently immobilized onto the thermoresponsive polymers, which helped with drug retention on the surface and increased the lifetime of the antimicrobial coatings. Moreover, this covalent

attachment was critical to the mode of action of the antimicrobial coatings in preventing leaching from the surface and ensuring that the AMP would be shielded above the LCST. However, for systemic delivery and topical applications, self-assembled thermoresponsive polyelectrolyte complexes loaded with AMPs are expected to be better suited and warrant further investigations. To date, there are no examples of thermoresponsive polyelectrolyte complexes loaded with AMPs, although this strategy has been explored in other therapeutic areas.^[84,96,97] For instance, Möller and colleagues have developed promising thermoresponsive polyelectrolyte complex nanoparticles consisting of anionic poly(*N*-isopropylacrylamide-*co*-acrylic acid) and cationic EDA-modified cellulose, which were loaded with an anionic model drug zoledronate,^[98] which is used against osteoporosis.^[99] The LCST of the polyelectrolyte complex nanoparticles was considerably higher (41–48°C) than that of pure poly(*N*-isopropylacrylamide) solutions (33°C) possibly due to the introduction of hydrophilic moieties (e.g., acrylic acid) in the system.^[100,101] Therefore, the heat-dependent release of zoledronate was shifted toward higher temperatures, with only 40% of the drug released (within 24 h) at physiologically relevant temperature of 37°C. The release was thus gradual and sustained, starting from a low temperature of 25°C and progressing toward higher temperatures. This release profile was unexpected given that free poly(*N*-isopropylacrylamide) is known for its sharp phase-transition. However, such gradual release kinetics would be beneficial when a sustained delivery of therapeutic doses of AMP for a prolonged period of time is required.

The poly(*N*-isopropylacrylamide-*co*-acrylic acid)/EDA-modified cellulose polyelectrolyte complex also showed pH-responsive behavior, which resulted in significant changes in particle size. At pH 7.0, the particles were small and monodisperse, owing to the deprotonation of the acrylic acid moieties that strengthened the electrostatic interactions. In contrast, at pH 4, the particles became larger, thereby destabilizing the electrostatic interactions, which consequently facilitated drug release. This work, while not focused on the release of AMPs, exemplifies the potential of delivery systems based on polyelectrolyte complexes to exhibit multiple responses (in this case pH and temperature). This capacity to respond to multiple stimuli can potentially be used for more effective drug release at the site of infection, in response to both inflammation and pH acidification of the bacterial microenvironment.

5. Conclusion

We have provided a critical overview of the delivery of AMPs using stimuli-responsive polyelectrolyte complexes. These systems are ideally placed to producing new delivery systems for this family of antimicrobials in further unlocking their potential. The key features that make polyelectrolyte complexes particularly suitable for the stimuli-responsive delivery of AMPs are as follows:

- Most AMPs are cationic and can thus be encapsulated within polyelectrolyte complexes without requiring their chemical modification (e.g., via covalent conjugation). Preserving the chemical structure of the AMP should minimize any risks of compromising their mode of action and activity.

- Polyelectrolyte complexes are inherently sensitive to changes in pH and therefore can be used to target bacteria that affect the pH in their microenvironment. Moreover, this pH response can be used to target intracellular bacteria and promote the delivery of AMPs within cellular compartments such as the endosome.

The first part of the review has provided key examples that demonstrate the potential of polyelectrolyte complexes to deliver AMPs in response to changes in pH. Challenges faced in the development of these materials are discussed, in particular how to balance activity and stability. Furthermore, the highlighted examples demonstrate the ability of these systems to deliver a range of AMPs, including some that are in clinical use such as PolyB^[34,57] and colistin sulfate.^[102] Delivery from both surfaces and nanoparticulate systems have been developed, and these systems have been used to target a range of bacteria including some of the most virulent and antibiotic-resistant pathogens such as *S. aureus*^[102] and *P. aeruginosa*.^[75,76] The release of the AMP in many of these systems is triggered at low pH, as the anionic polyelectrolytes are neutralized at that pH, which results in weakened electrostatic interactions, which hold the polyelectrolyte complexes together. These materials may therefore be suitable for intracellular delivery of AMPs, targeting pathogens that commonly traffic through the endosomes such as *M. tuberculosis* and *Listeria monocytogenes*. A noteworthy class of systems is one that can switch their charge in response to pH such as the nanoparticles developed by Ji and co-workers (Figure 3F,G).^[61,62] The ability to reverse the charge should not only accelerate the release of the AMP, due to charge repulsion, but also provide additional antimicrobial properties by forming cationic polymers.

Bacterial infection is often accompanied by changes in parameters other than pH, which can also be exploited as alternative stimuli triggers. These changes include an imbalance in the concentration of enzymes^[103,104] or increases in temperature.^[80–82] The rest of the review showcases examples of AMP delivery in response to other stimuli, namely enzymes and changes in temperature. Enzyme-responsive delivery of AMPs from polyelectrolyte complexes is still in its infancy, with only a handful of examples reported in the literature. However, these examples highlight the potential of this strategy to develop systems that can target common enzymes^[103,104] that are expressed by a range of pathogens, such as the hyaluronidase-responsive surfaces developed by Boulmedais and collaborators (Figure 4B).^[67] and as such target a range of pathogens including bacteria and fungi. Alternatively, enzyme-responsive delivery can be used to target a single pathogenic species due to the specificity of the polyelectrolytes used (Figure 5A).^[75,76] This strategy may be ideal to treat resistant infections that do not respond to broad-spectrum antibiotics. Once the pathogenic agent is known, enzyme-responsive systems should restrict the release of the AMP to the microenvironment of the pathogen, minimizing the systemic delivery of the antimicrobial and thus, off-target effects including toxicity and the development of resistance in commensal bacteria. With regard to using temperature^[80–82] as a stimuli, there are currently no examples of specifically using thermoresponsive polyelectrolyte complexes to deliver AMPs. However, future studies are warranted given that infection often leads to local inflammation, and the associated increase in temperature^[80–82] provides a

localized stimuli to trigger AMP release. This review, therefore, includes a couple of examples that highlight some of the best features that this approach can offer. For example, temperature can be used to prepare switchable surfaces that, for instance, are bactericidal at room temperature while not active and cell-repellent under physiological conditions. This principle has been exemplified by Glinel and collaborators (Figure 6A) using an AMP covalently attached to a thermoresponsive polymer^[86] but is yet to be demonstrated for the development of polyelectrolyte complexes that incorporate AMPs. However, thermoresponsive polyelectrolyte complexes have been used to trigger the release of other therapeutic agents in response to increases in temperature. As the LCST of the polymers and polyelectrolytes used can be fine-tuned, we can anticipate the development of thermoresponsive polyelectrolyte complexes that trigger the release of AMPs > 37–38°C to respond to the increase in temperature^[80–82] associated with infections. Moreover, as polyelectrolyte complexes are intrinsically pH-responsive, the use of polyelectrolyte complexes in realizing dual-responsive delivery offers a viable avenue when compared to systems non-based on polyelectrolyte complexes, in achieving antimicrobial systems that can target the multifaceted aspects of microbial infection. Finally, although not included in this review, endogenous stimuli such as light or ultrasound could also be used to trigger the release of AMPs from polyelectrolyte complexes. These stimuli have been exploited to deliver other therapeutic agents, and they could be ideally suited to develop topical applications of AMPs where the location and penetration of the stimuli can be precisely controlled.^[105–110]

As mentioned previously, the main challenge when developing this type of delivery system is to balance the stability of the polyelectrolyte complexes with their antimicrobial activity. In a laboratory setting, the antimicrobial activity of the polyelectrolyte complexes is often smaller than that of the native AMP, as some of the antimicrobial remains encapsulated within the delivery vehicle. For conventional polyelectrolyte complexes maximizing stability will come at the expense of compromising activity. This limitation may be resolved during drug and clinical development by optimizing the concentration and dosing regime of the polyelectrolyte complex formulation so that therapeutic doses of the AMP can be reached without triggering any unwanted effects. Additionally, stimuli-responsive systems have the potential to address this limitation by reaching similar activities to those of the native AMP as long as they can accelerate particle decomposition once a stimulus is applied. Degradable polyelectrolytes should be particularly suited to achieve this acceleration, with enzyme-responsive materials the most likely candidates. However, as observed for some of the examples reported in Section 3, the activity of the enzyme-responsive system can remain below that of the native AMP. To accelerate degradation, some of these systems may need to be coupled with self-immolative materials with high decomposition rates due to a domino effect that triggers a self-programmed degradation in response to external stimuli. Self-immolative materials that respond to pH and enzymes have already been reported in the literature, and their application to develop stimuli-responsive polyelectrolyte complexes inspired by those reported above could address the current limitations observed when balancing stability and activity.^[111,112]

From a clinical perspective, developing stimuli-responsive polyelectrolyte complexes that can selectively deliver therapeutic

doses of AMPs at the site of infection has the potential to circumvent the off-target toxicity of many of these antimicrobials. This toxicity often prevents their translation to clinical use. As outlined above, the main challenge would be balancing antimicrobial efficacy and stability. Still, once this challenge is resolved, researchers would also have to consider overcoming the regulatory requirements needed to deliver a clinically viable product. As such, the best approach could be to focus on AMPs already approved for clinical use. For example, PolyB is approved for topical use to treat minor cuts, scrapes, or burns. As such, regulatory approval of a stimuli-responsive polyelectrolyte complex that delivers PolyB topically would focus on approving the new delivery vehicle, simplifying the translational pathway. This development may then set precedence and give a competitive advantage to develop a family of products that can deliver other non-approved AMPs with unique modes of action and antimicrobial activities.

Acknowledgements

P.F.-T. thanks the University of Birmingham for the John Evans Fellowship and the Spanish Ministerio de Educación, Cultura y Deporte for a Beatriz Galindo Award [BG20/00213]. F.C. acknowledges the National Health and Medical Research Council Leadership Investigator Research Fellowship (grant no. 2016732). This work was supported by the Priestley Joint Ph.D. Scholarship from the University of Birmingham (UK) and The University of Melbourne (Australia).

Conflict of Interest

The authors declare no conflict of interest.

Keywords

antimicrobial peptides, drug delivery, polyelectrolyte complexes, stimuli-responsive materials

Received: March 23, 2023

Revised: June 27, 2023

Published online:

- [1] A. R. Collaborators *Lancet* **2022**, 399, 629.
- [2] C. Årdal, M. Balasegaram, R. Laxminarayan, D. Mcadams, K. Outtersson, J. H. Rex, N. Sumpradit, *Nat. Rev. Microbiol.* **2020**, 18, 267.
- [3] WHO, "Antibacterial Products in Clinical Development for Priority Pathogens," <https://www.who.int/observatories/global-observatory-on-health-research-and-development/monitoring/antibacterial-products-in-clinical-development-for-priority-pathogens#what-you-see>, (accessed: March, 2023).
- [4] D. S. J. Ting, R. W. Beuerman, H. S. Dua, R. Lakshminarayanan, I. Mohammed, *Front. Immunol.* **2020**, 11, 983.
- [5] Y. Huan, Q. Kong, H. Mou, H. Yi, *Front. Cell. Infect. Microbiol.* **2020**, 11, 582779.
- [6] C. Wang, T. Hong, P. Cui, J. Wang, J. Xia, *Adv. Drug Delivery Rev.* **2021**, 175, 113818.
- [7] L. S. Bisworo, M. G. da Costa Sousa, T. M. B. Rezende, S. C. Dias, O. L. Franco, *Front. Microbiol.* **2018**, 9, 855.
- [8] H. B. Koo, J. Seo, *Pept. Sci.* **2019**, 111, 24122.

- [9] M. Magana, M. Pushpanathan, A. L. Santos, L. Leanse, M. Fernandez, A. Ioannidis, M. A. Giulianotti, Y. Apidianakis, S. Bradfute, A. L. Ferguson, A. Cherkasov, M. N. Seleem, C. Pinilla, C. De La Fuente-Nunez, T. Lazaridis, T. Dai, R. A. Houghten, R. E. W. Hancock, G. P. Tegos, *Lancet Infect. Dis.* **2020**, 20, e216.
- [10] P. Kumar, J. N. Kizhakkedathu, S. K. Straus, *Biomol* **2018**, 8, 4.
- [11] Y. Jiang, Y. Chen, Z. Song, Z. Tan, J. Cheng, *Adv. Drug Delivery Rev.* **2021**, 170, 261.
- [12] Z. Y. Ong, N. Wiradharma, Y. i Y. Yang, *Adv. Drug Delivery Rev.* **2014**, 78, 28.
- [13] W. Li, F. Separovic, N. M. O'brien-Simpson, J. D. Wade, *Chem. Soc. Rev.* **2021**, 50, 4932.
- [14] H. Sun, Y. Wang, J. Song, *Polymers* **2021**, 13, 2903.
- [15] X. Shen, Y. Zhang, Q. Mao, Z. Huang, T. Yan, T. Lin, W. Chen, Y. Wang, X. Cai, Y. Liang, *Int. J. Polym. Sci.* **2022**, 2022, 7610951.
- [16] A. R. P. Silva, M. S. Guimarães, J. Rabelo, L. H. Belén, C. J. Perecin, J. G. Farías, J. H. P. M. Santos, C. O. Rangel-Yagui, *J. Mater. Chem. B* **2022**, 10, 3587.
- [17] T. Matthyssen, W. Li, J. A. Holden, J. C. Lenzo, S. Hadjigol, N. M. O'Brien-Simpson, *Front. Chem.* **2022**, 9, 795433.
- [18] P. Tan, H. Fu, X. i Ma, *Nano Today* **2021**, 39, 101229.
- [19] R. L. Nation, J. Li, *Curr. Opin. Infect. Dis.* **2009**, 22, 535.
- [20] Y.-X. Fan, Y.-C. Chen, Y. Li, J.-C. Yu, X.-C. Bian, X. Li, W.-Z. Li, B.-N. Guo, H.-L. Wu, X.-F. Liu, Y. Wang, X.-Y. Xu, J.-L. Hu, J.-J. Wang, X.-J. Wu, G.-Y. Cao, J.-F. Wu, C.-J. Xue, J. Feng, Y.-Y. Zhang, J. Zhang, *Pharmaceut. Res.* **2021**, 38, 79.
- [21] M. Barnett, S. R. M. Bushby, S. Wilkinson, *Brit. J. Pharm. Chemoth.* **1964**, 23, 552.
- [22] J. Li, R. W. Milne, R. L. Nation, J. D. Turnidge, K. Coulthard, *Antimicrob. Agents Chemother.* **2003**, 47, 1364.
- [23] L. Zhao, M. Skwarczynski, I. Toth, *ACS Biomater. Sci. Eng.* **2019**, 5, 4937.
- [24] B. C. Borro, M. Malmsten, *Adv. Colloid. Interface* **2019**, 270, 251.
- [25] K. Smerkova, K. Dolezelikova, L. Bozdechova, Z. Heger, L. Zurek, V. Adam, *WIREs Nanomed. Nanobiotechnol.* **2020**, 12, 1636.
- [26] M. C. Teixeira, C. Carbone, M. C. Sousa, M. Espina, M. L. Garcia, E. Sanchez-Lopez, E. B. Souto, *Nanomaterials* **2020**, 10, 560.
- [27] Z. Tang, Q. Ma, X. Chen, T. Chen, Y. Ying, X. Xi, L. Wang, C. Ma, C. Shaw, M. Zhou, *Antibiotics* **2021**, 10, 990.
- [28] M. E. Van Gent, M. Ali, P. H. Nibbering, S. N. Klodzinska, *Pharmaceutics* **2021**, 13, 1840.
- [29] S. Gera, E. Kankuri, K. Kogermann, *Pharmacol. Therapeut.* **2021**, 232, 107990.
- [30] R. K. Thapa, D. B. Diep, H. H. Tønnesen, *J. Pharm. Invest.* **2021**, 51, 377.
- [31] J. Jampilek, K. Kralova, *Materials* **2022**, 15, 2388.
- [32] A. Escobar, N. Muzzio, S. E. Moya, *Pharm* **2020**, 13, 16.
- [33] I. Insua, A. Wilkinson, F. Fernandez-Trillo, *Eur. Polym. J.* **2016**, 81, 198.
- [34] I. Insua, S. Majok, A. F. A. Peacock, A. M. Krachler, F. Fernandez-Trillo, *Eur. Polym. J.* **2017**, 87, 478.
- [35] C. Wang, S. Feng, J. Qie, X. Wei, H. Yan, K. Liu, *Int. J. Pharm.* **2019**, 554, 284.
- [36] Y. Huang, L. Zou, J. Wang, Q. Jin, J. Ji, *Wiley Interdiscip. Rev.: Nanomed. Nanobiotechnol.* **2022**, 14, e1775.
- [37] O. Etienne, C. Picart, C. Taddei, Y. Haikel, J. L. Dimarcq, P. Schaaf, J. C. Voegel, J. A. Ogier, C. Egles, *Antimicrob. Agents Chemother.* **2004**, 48, 3662.
- [38] A. Shukla, K. E. Fleming, H. F. Chuang, T. M. Chau, C. R. Loose, G. N. Stephanopoulos, P. T. Hammond, *Biomaterials* **2010**, 31, 2348.
- [39] J. L. Webber, R. Namivandi-Zangeneh, S. Drozdek, K. A. Wilk, C. Boyer, E. H. H. Wong, B. H. Bradshaw-Hajek, M. Krasowska, D. A. Beattie, *Sci. Rep.* **2021**, 11, 1690.
- [40] C. Roupie, B. Labat, S. Morin-Grognet, P. Thébault, G. Ladam, *Colloids Surf., B* **2021**, 208, 112121.
- [41] S. Pavlukhina, Y. Lu, A. Patimetha, M. Libera, S. Sukhishvili, *Biomacromolecules* **2010**, 11, 3448.
- [42] ChemAxon, Calculations of Degree of Protonation were Done Using Marvin Protonation Plugin, Version 19.10.0, ChemAxon (<https://www.chemaxon.com>), (accessed: March 2023).
- [43] I. Zhuk, F. Jariwala, A. B. Attygalle, Y. Wu, M. R. Libera, S. A. Sukhishvili, *ACS Nano* **2014**, 8, 7733.
- [44] S. Yan, H. Shi, L. Song, X. Wang, L. Liu, S. Luan, Y. Yang, J. Yin, *ACS Appl. Mater. Interfaces* **2016**, 8, 24471.
- [45] H. Ejima, J. J. Richardson, K. Liang, J. P. Best, M. P. Van Koeverden, G. K. Such, J. Cui, F. Caruso, *Science* **2013**, 341, 154.
- [46] J. Zhou, Z. Lin, Y. i Ju, M. d. A. Rahim, J. J. Richardson, F. Caruso, *Acc. Chem. Res.* **2020**, 53, 1269.
- [47] J. Li, R. L. Nation, K. S. Kaye, Eds., in *Polymyxin Antibiotics: From Laboratory Bench to Bedside*, Springer, Cham **2019**.
- [48] R. N. Brogden, R. M. Pinder, P. R. Sawyer, T. M. Speight, G. S. Avery, *Drugs* **1976**, 12, 166.
- [49] C. Chen, Y. Chen, P. Wu, B. Chen, *J. Formos. Med. Assoc.* **2014**, 113, 72.
- [50] H. G. Boman, I. Faye, G. H. Gudmundsson, J.-Y. Lee, D.-A. Lidholm, *Eur. J. Biochem.* **1991**, 201, 23.
- [51] H. Suttman, M. Retz, F. Paulsen, J. Harder, U. Zwergel, J. Kamradt, B. Wullich, G. Unteregger, M. Stöckle, J. Lehmann, *BMC Urol* **2008**, 8, 5.
- [52] V. S. Meka, M. K. G. Sing, M. R. Pichika, S. R. Nali, V. R. M. Kolapalli, P. Kesharwani, *Drug Discovery Today* **2017**, 22, 1697.
- [53] A. Harada, K. Kataoka, *Polym. J.* **2018**, 50, 95.
- [54] V. A. Izumrudov, B. K. h. Mussabayeva, Z. S. Kassymova, A. N. Klivenko, L. K. Orazzhanova, *Russ. Chem. Rev.* **2019**, 88, 1046.
- [55] K. L. Niece, A. D. Vaughan, D. I. Devore, *J. Biomed. Mater. Res.* **2013**, 101A, 2548.
- [56] S. Y. Hong, J. E. Oh, M. i Y. Kwon, M. J. Choi, J. i H. Lee, B. L. Lee, H. M. o Moon, K. H. Lee, *Antimicrob. Agents Chemother.* **1998**, 42, 2534.
- [57] I. Insua, L. Zizmare, A. F. A. Peacock, A. M. Krachler, F. Fernandez-Trillo, *Sci. Rep.* **2017**, 7, 9396.
- [58] C. M. Perry, D. Ormrod, M. Hurst, S. V. Onrust, *Drugs* **2002**, 62, 169.
- [59] J. Song, C. Cortez-Jugo, S. J. Shirbin, Z. Lin, S. Pan, G. G. Qiao, F. Caruso, *Adv. Funct. Mater.* **2021**, 32, 2107341.
- [60] S. J. Lam, N. M. O'brien-Simpson, N. Pantarat, A. Sulistio, E. H. H. Wong, Y. u.-Y. Chen, J. C. Lenzo, J. A. Holden, A. Blencowe, E. C. Reynolds, G. G. Qiao, *Nat. Microbiol.* **2016**, 1, 16162.
- [61] S. Wang, Y. Yu, H. Li, Y. Huang, J. Wang, Q. Jin, J. Ji, *J. Polym. Sci.* **2022**, 60, 2289.
- [62] J.-Z. Du, H.-J. Li, J. Wang, *Acc. Chem. Res.* **2018**, 51, 2848.
- [63] M. Zasloff, *Proc. Natl. Acad. Sci.* **1987**, 84, 5449.
- [64] Q. Zhou, Z. Si, K. Wang, K. Li, W. Hong, Y. Zhang, P. Li, *J. Control Release* **2022**, 352, 507.
- [65] J. Y. Quek, E. Uroor, N. Goswami, K. Vasilev, *Mater. Today Chem* **2022**, 23, 100606.
- [66] X. Wang, M. Shan, S. Zhang, X. Chen, W. Liu, J. Chen, X. Liu, *Adv. Sci.* **2022**, 9, 2104843.
- [67] G. Cado, R. Aslam, L. Séon, T. Garnier, R. Fabre, A. Parat, A. Chassepot, J.-C. Voegel, B. Senger, F. Schneider, Y. Frère, L. Jierry, P. Schaaf, H. Kerdjoudj, M.-H. Metz-Boutigue, F. Boulmedais, *Adv. Funct. Mater.* **2013**, 23, 4801.
- [68] M. H. Metz-Boutigue, Y. Goumon, J. M. Strub, K. Lugardon, D. Aunis, *Ann. N. Y. Acad. Sci.* **2003**, 992, 168.
- [69] W. L. Hynes, S. L. Walton, *FEMS Microbiol. Lett.* **2000**, 183, 201.
- [70] D. R. Perinelli, L. Fagioli, R. Campana, J. K. W. Lam, W. Baffone, G. F. Palmieri, L. Casettari, G. Bonacucina, *Eur. J. Pharm. Sci.* **2018**, 117, 8.

- [71] G. Cavallaro, S. Micciulla, L. Chiappisi, G. Lazzara, *J. Mater. Chem. B* **2020**, 9, 594.
- [72] R. C. Goy, D. D.e Britto, O. B. G. Assis, *Polímeros* **2009**, 19, 241.
- [73] A. Alishahi, *J. Food Safety* **2014**, 34, 111.
- [74] G. Y. C. Cheung, J. S. Bae, M. Otto, *Virulence* **2021**, 12, 547.
- [75] I. Insua, E. Llamas, Z. Zhang, A. F. A. Peacock, A. M. Krachler, F. Fernandez-Trillo, *Polym. Chem.* **2016**, 7, 2684.
- [76] I. Insua, M. Petit, L. D. Blackman, R. Keogh, A. Pitto-Barry, R. K. O'reilly, A. F. A. Peacock, A. M. Krachler, F. Fernandez-Trillo, *Chem-NanoMat* **2018**, 4, 807.
- [77] B. Korkmaz, F. Gauthier, in *Handbook of Proteolytic Enzymes*, 3rd Ed., Academic Press, Cambridge, MA, USA **2013**.
- [78] G.-B. Qi, D.i Zhang, F.u-H. Liu, Z.-Y. Qiao, H. Wang, *Adv. Mater.* **2017**, 29, 1703461.
- [79] M. M. Javadvpour, M. M. Juban, W.-C. J. Lo, S. M. Bishop, J. B. Alberty, S. M. Cowell, C. L. Becker, M. L. Mclaughlin, *J. Med. Chem.* **1996**, 39, 3107.
- [80] R. Medzhitov, *Cell* **2010**, 140, 771.
- [81] R. Medzhitov, *Nature* **2008**, 454, 428.
- [82] O. Takeuchi, S. Akira, *Cell* **2010**, 140, 805.
- [83] C. M. Clavel, P. Nowak-Sliwinski, E. Paunescu, A. W. Griffioen, P. J. Dyson, *Chem. Sci.* **2015**, 6, 2795.
- [84] A. Bordat, T. Boissenot, J. Nicolas, N. Tsapis, *Adv. Drug Delivery Rev.* **2019**, 138, 167.
- [85] D. Rafael, M. M. R. Melendres, F. Andrade, S. Montero, F. Martinez-Trucharte, M. Vilar-Hernandez, E. F. Durán-Lara, S. Schwartz Jr, I. Abasolo, *Int. J. Pharmaceut.* **2021**, 606, 120954.
- [86] X. Laloyaux, E. Fautré, T. Blin, V. Purohit, J. Leprince, T. Jouenne, A. M. Jonas, K. Glinel, *Adv. Mater.* **2010**, 22, 5024.
- [87] Z. Guo, S. Li, C. Wang, J. Xu, B. Kirk, J. Wu, Z. Liu, W. Xue, *J. Bioact. Compat. Pol.* **2017**, 32, 17.
- [88] X. Wang, S. Yan, L. Song, H. Shi, H. Yang, S. Luan, Y. Huang, J. Yin, A. F. Khan, J. Zhao, *ACS Appl. Mater. Interfaces* **2017**, 9, 40930.
- [89] T. Feng, H. Wu, W. Ma, Z. Wang, C. Wang, Y. Wang, S. Wang, M. Zhang, L. Hao, *J. Mater. Chem. B* **2022**, 10, 6143.
- [90] A. Halperin, M. Kröger, F. M. Winnik, *Angew. Chem., Int. Ed.* **2015**, 54, 15342.
- [91] J.-F. Lutz, Ö. Akdemir, A. Hoth, *J. Am. Chem. Soc.* **2006**, 128, 13046.
- [92] S.-L. Qiao, M. Mamuti, H.-W. An, H. Wang, *Prog. Polym. Sci.* **2022**, 131, 101578.
- [93] S. Lanzalaco, E. Armelin, *Prog. Coll. Pol. Sci. S* **2017**, 3, 36.
- [94] Y. Hiruta, *Polym. J.* **2022**, 54, 1419.
- [95] J.-F. Lutz, *Adv. Mater.* **2011**, 23, 2237.
- [96] S. Chatterjee, P. C.-L. Hui, *Polymers* **2021**, 13, 2086.
- [97] W. H. Abuwatfa, N. S. Awad, W. G. Pitt, G. A. Hussein, *Polymers* **2022**, 14, 925.
- [98] I. R. Reid, J. R. Green, K. W. Lyles, D. M. Reid, U. Trechsel, D. J. Hosking, D. M. Black, S. R. Cummings, R. G. G. Russell, E. F. Eriksen, *Bone* **2020**, 137, 115390.
- [99] M. Müller, B. Urban, D. Vehlow, M. L. Möller, *Colloid Polym. Sci.* **2017**, 295, 1187.
- [100] M. K. Yoo, Y. K. Sung, S. C. Chong, M. L. Young, *Polymer* **1997**, 38, 2759.
- [101] Z. M. O. Rzaev, S. Dinçer, E. Piskin, *Prog. Polym. Sci.* **2007**, 32, 534.
- [102] S. A. Abouelmagd, N. H. Abd Ellah, O. Amen, A. Abdelmoez, N. G. Mohamed, *Int. J. Pharmaceut.* **2019**, 562, 76.
- [103] J. Y. Quek, E. Uroo, N. Goswami, K. Vasilev, *Mater Today Chem* **2022**, 23, 100606.
- [104] Q. Zhou, Z. Si, K. Wang, K. Li, W. Hong, Y. Zhang, P. Li, *J. Control Release* **2022**, 352, 507.
- [105] Y.u Tao, H. F. Chan, B. Shi, M. Li, K. W. Leong, *Adv. Funct. Mater.* **2020**, 30, 2005029.
- [106] T. Sun, A. Dasgupta, Z. Zhao, M.d Nurunnabi, S. Mitragotri, *Adv. Drug Delivery Rev.* **2020**, 158, 36.
- [107] Y. Chen, Y. Huang, Q. Jin, *Macromol. Chem. Phys.* **2022**, 223, 2100440.
- [108] C. S. Linsley, B. M. Wu, *Ther. Delivery* **2017**, 8, 89.
- [109] J. Sitta, C. M. Howard, *Int. J. Mol. Sci.* **2021**, 22, 11491.
- [110] C. Yang, Y. Li, M. Du, Z. Chen, *J. Drug Target* **2019**, 27, 33.
- [111] A. G. Gavriel, M. R. Sambrook, A. T. Russell, W. Hayes, *Polym. Chem.* **2022**, 13, 3188.
- [112] O. Shelef, S. Gnaim, D. Shabat, *J. Am. Chem. Soc.* **2021**, 143, 21177.



Alexander Antropenko holds an M.Sc Degree in Chemistry with Industrial experience from the University of Birmingham. Currently, Alexander is undertaking a Ph.D. under the supervision of Paco Fernandez-Trillo and Frank Caruso as part of the Joint Priestley Ph.D. Scholarships program. In his project he is looking into the development of controlled delivery systems for antimicrobial agents, combating the development of drug resistance in bacteria.



Frank Caruso is a Melbourne Laureate Professor and an NHMRC Leadership Investigator Fellow at The University of Melbourne. He received his Ph.D. in 1994 from The University of Melbourne and thereafter conducted postdoctoral research at the CSIRO Division of Chemicals and Polymers. From 1997 to 2002, he was a Humboldt Research Fellow and Group Leader at the Max Planck Institute of Colloids and Interfaces (Germany). Since 2003, he has been a professor at The University of Melbourne and has held ARC Federation and ARC Australian Laureate Fellowships. His research interests focus on developing advanced nano- and biomaterials for biotechnology and medicine.



Paco Fernandez-Trillo holds a Beatriz Galindo Award at Universidade da Coruña. After a Ph.D. in total synthesis and several post-docs developing polymeric materials for biomedical applications, Paco started his academic career in 2013 at the University of Birmingham. In 2021 he moved to Coruña, where he leads a research group working at the interface between Organic Chemistry, Polymer Science, and Life Sciences. In his group Organic Chemistry and Polymer Science are combined to develop nanomaterials for gene and drug delivery.

1.2 Scope of Thesis

In the published review (Chapter 1), the term "target" was sometimes used interchangeably with "specific," which is not always accurate. For instance, in the sentence, "Though these changes can be exploited to develop targeted systems, such as intracellular delivery as shown above, these changes can also lead to off-target effects, such as AMP release in the extracellular milieu," the phrase "targeted systems" should actually refer to bacteria-specific systems. Similarly, in the sentence, "These enzymes (Figure 4A) commonly degrade tissues and biomolecules, often targeting peptide sequences and biopolymers that are not targeted by host enzymes," the intended meaning is that "These enzymes commonly degrade specific tissues and biomolecules, which are not degraded by the host enzymes". AMP delivery systems reviewed in Chapter 1 exhibit specificity towards bacterial stimuli, wherein the drug release mechanism is activated in the presence of these stimuli. Therefore, the PECs systems discussed in the review do not "target" the pathogen directly; instead, they are sensitive to the stimuli generated by the bacteria.

As discussed in the literature review, the charged nature of AMPs makes them suitable for encapsulation within PECs without the need for chemical modification. PECs traditionally are formed as a result of electrostatic interactions between oppositely charged electrolytes, which makes them inherently pH-sensitive. Therefore, the majority of stimuli-responsive PECs rely primarily on the pH-sensitive nature of these systems, and only a few studies explored more specific delivery approaches targeting pathogen-released enzymes. There are a range of enzyme families, which has been effectively used as a stimuli for the controlled delivery systems. These include proteases, phospholipases, lipases, phospholipases, hyaluronidases and oxidoreductases.¹⁻³ Pathogens release extracellular and intracellular enzymes to promote their spread throughout the host body by either weakening the physical integrity of the host's tissue or deactivating antimicrobial agents. For example, phospholipases are known to hydrolyze ester and phosphodiester bonds of glycerophospholipids present in the membranes, enabling bacteria to penetrate niches in tissues where they are able to proliferate and distribute to other sites in the body.⁴ Therefore, to develop a phospholipase-responsive delivery system, the drug encapsulation components should incorporate phosphoester bonds susceptible to degradation.

In this Thesis, *P. aeruginosa* was selected as the target pathogen due to its notorious resistance mechanisms, contributing to high mortality rates (up to 61%) among patients.⁵ The bacterium is commonly associated with severe respiratory tract infections, particularly pneumonia and chronic bronchitis in patients with cystic fibrosis, acquired

immunodeficiency syndrome, severe burn wounds, gastrointestinal issues, osteomyelitis, as well as bone and joint infections.^{5,6} This high pathogenicity stems from the release of various virulence factors, including extracellular invasive enzymes.^{5,6} One such enzyme is **Elastase B from *Pseudomonas aeruginosa* (LasB)**, which has been demonstrated to degrade elastin (*i.e.*, specificity towards hydrophobic amino acid sequences), a major component of connective tissues, especially abundant in the lungs. The quantity of enzyme released by bacteria depends on various factors, including growth conditions, infection stage, and bacterial strains. For example, in a study of 30 clinical strains of *P. aeruginosa*, **LasB** concentrations in culture supernatants ranged from 0.009 to 0.80 mg/mL per strain. Considering the potential presence of multiple strains during infection, the total amount of released **LasB** could be significantly higher than 0.80 mg/mL and vary substantially among patients.^{7,8} What is also crucial to evaluate when selecting a target enzyme is its enzymatic activity, *i.e.*, the rate of hydrolysis.³ For example, it was reported that **LasB** can degrade 409 μmol of a peptide sequence -GLA- per min*mg enzymes, while for a peptide sequence -GLG- the rate was 31.0 $\mu\text{mol}/\text{min}*\text{mg}$ enzymes.⁹ Consequently, by incorporating the appropriate hydrophobic residues in the encapsulation components, **PECs** and other delivery systems can be designed to release the drug specifically in the presence of *P.aeruginosa*.¹⁰

The target application of enzyme-responsive **PECs** heavily relies on understanding the pathogenesis of the target bacteria. For instance, in the case of *P. aeruginosa*, it predominantly colonizes various anatomical sites such as the respiratory tract, burn and chronic wounds, bone, joints, and gastrointestinal tissues.^{5,6} Consequently, the envisioned application of these enzyme-responsive **PECs** would be in pulmonary delivery (*e.g.*, nebulization) and topical administration (*e.g.*, wound dressings for severe burn and chronic wounds). Enzyme-responsive **PECs** loaded with **AMP** are expected to reduce the systematic exposure of healthier cells towards the cationic drug. This reduction would not only minimize side effects but also prevent premature degradation of the peptide by human proteases widening the therapeutic window for the drug.^{11–16} Consequently, lower doses can be administered for the treatment of the same medical conditions, thereby improving the efficacy of antimicrobial therapy and even potentially reducing the risk of antimicrobial resistance development.^{12–14,17}

The potential mode of action of **PECs** designed to treat *P. aeruginosa* infections can be summarized as follows: Upon delivery to the target area (such as lungs or wounds), the particles initially remain primarily antimicrobially inactive. However, as the infected area becomes colonized with *P. aeruginosa*, **LasB** concentration would increase, inducing degradation of the encapsulation shell of **PECs**. Consequently, the particles would lose colloidal integrity, leading to the release of the **AMP** in the process. Release of

the sufficient amount of AMP would inhibit the growth of *P. aeruginosa*, preventing the development of the lung or wound infections.

Each delivery application necessitates distinct particle properties. For pulmonary delivery, such PECs must maintain stability during the drying or aerosolization process, with aerodynamic sizes ideally between 1 and 5 μm to facilitate deeper penetration into the lungs.^{18–20,20,21} Conversely, for topical application such as burn or chronic wounds, enzyme-responsive PECs should exhibit high proteolytic stability and pH stability, potentially integrating release mechanisms that enhance the penetration of the antimicrobial peptide through the stratum corneum skin layer.^{22–25}

Notably, no enzyme-responsive PECs have been published that use an FDA-approved antimicrobial peptide drug for delivery from a particle substrate, with the majority examples either focusing on the delivery from the surface or utilizing non-approved AMPs. This research gap is significant considering the urgent need for effective solutions against antimicrobial resistance in gram-negative pathogens such as *P. aeruginosa*, as the development of new antibiotic agents remains limited. To address this challenge, it is crucial to harness the potent properties of antimicrobial peptides while potentially improving biodistribution, reducing dosage requirements and possibly solving toxicity issues of AMPs.

Therefore, the primary focus of this Thesis was to explore the feasibility of creating an enzyme-responsive delivery system based on PECs for clinically approved antimicrobial peptides, with a focus on the synthesis of enzyme-responsive material and the enzyme-induced release from particle substrate. Consequently, the ideal target design characteristics of an enzyme-responsive AMP delivery system were set as follows:

- **Simplicity** - an FDA-approved antimicrobial peptide drug should be used in the delivery system without any chemical modifications.
- **Selectivity** - release of AMP should be triggered by the presence of an enzyme released by a target pathogen.
- **Efficacy** - the amount of AMP released should be sufficient to inhibit the growth of pathogens.
- **Stability** - the delivery system should be stable under physiological conditions.

The development of a drug delivery system can be divided into two distinct parts: the synthesis of the enzyme-responsive encapsulation material and the assembly of the drug delivery system with the chosen therapeutic. Therefore, Chapter 2 and 3 examine the synthesis of enzyme-degradable materials suitable for the encapsulation of AMPs

(i.e., part 1). Specifically, various synthetic methods and design modifications to enhance their enzyme-responsive drug-release properties are discussed. Subsequently, Chapter 4, focuses on the assembly of PECs using the enzyme-degradable material from Chapters 2/3 and the selected AMP (i.e., part 2). The assembly and selection process of an ideal formulation is discussed and the results of *in-vitro* release studies and antimicrobial efficacy tests are compared with the characteristics of a free drug.

1.3 References

- [1] Q. Hu, P. S. Katti, P. Katti and Z. Gu, *Nanoscale*, 2014.
- [2] J. Y. Quek, E. Uroro, N. Goswami and K. Vasilev, *Materials Today Chemistry*, 2022, **23**, 100606.
- [3] Q. Zhou, Z. Si, K. Wang, K. Li, W. Hong, Y. Zhang and P. Li, *Journal of Controlled Release*, 2022, **352**, 507–526.
- [4] J. W. Wilson, M. J. Schurr, C. L. LeBlanc, R. Ramamurthy, K. L. Buchanan and C. A. Nickerson, *Postgraduate Medical Journal*, 2002, **78**, 216.
- [5] J. Chadha, K. Harjai and S. Chhibber, *Environmental Microbiology*, 2022, **24**, 2630–2656.
- [6] S. Qin, W. Xiao, C. Zhou, Q. Pu, X. Deng, L. Lan, H. Liang, X. Song and M. Wu, *Signal Transduction and Targeted Therapy*, 2022, **7**, 199.
- [7] D. Coin, D. Louis, J. Bernillon, M. Guinand and J. Wallach, *FEMS Immunology & Medical Microbiology*, 1997, **18**, 175–184.
- [8] J. C. Olson and D. E. Ohman, *Journal of Bacteriology*, 1992, **174**, 4140–4147.
- [9] K. Morihara and T. Hiroshige, *Archives of Biochemistry and Biophysics*, 1971, **146**, 291–296.
- [10] I. Insua, E. Lamas, Z. Zhang, A. F. A. Peacock, A. M. Krachler and F. Fernandez-Trillo, *Polymer Chemistry*, 2016, **7**, 2684–2690.
- [11] M. Chai, Y. Gao, J. Liu, Y. Deng, D. Hu, Q. Jin and J. Ji, *Advanced Healthcare Materials*, 2020, **9**, 1901542.
- [12] T. Pham, P. Loupias, A. Dassonville-Klimpt and P. Sonnet, *Medicinal Research Reviews*, 2019, **39**, 2343–2396.
- [13] J. Aparicio-Blanco, N. Vishwakarma, C.-M. Lehr, C. A. Prestidge, N. Thomas, R. J. Roberts, C. R. Thorn and A. Melero, *Drug Delivery and Translational Research*, 2024, 1–10.
- [14] R. Lakshminarayanan, E. Ye, D. J. Young, Z. Li and X. J. Loh, *Advanced Healthcare Materials*, 2018, **7**, 1701400.
- [15] M. Kumar, A. Curtis and C. Hoskins, *Pharmaceutics*, 2018, **10**, 11.

- [16] J. Yao, P. Zou, Y. Cui, L. Quan, C. Gao, Z. Li, W. Gong and M. Yang, *Pharmaceutics*, 2023, **15**, 1188.
- [17] Z. Lei and A. karim, *Journal of Veterinary Pharmacology and Therapeutics*, 2021, **44**, 281–297.
- [18] J. Song, C. Cortez-Jugo, S. J. Shirbin, Z. Lin, S. Pan, G. G. Qiao and F. Caruso, *Advanced Functional Materials*, 2022, **32**, 2107341.
- [19] J. C. Sung, B. L. Pulliam and D. A. Edwards, *Trends in Biotechnology*, 2007, **25**, 563–570.
- [20] S. Azarmi, W. H. Roa and R. Löbenberg, *Advanced Drug Delivery Reviews*, 2008, **60**, 863–875.
- [21] J. S. Patton and P. R. Byron, *Nature Reviews Drug Discovery*, 2007, **6**, 67–74.
- [22] A. P. Raphael, G. Garrastazu, F. Sonvico and T. W. Prow, *Therapeutic Delivery*, 2015, **6**, 197–216.
- [23] T. Maver, S. Hribernik, T. Mohan, D. M. Smrke, U. Maver and K. Stana-Kleinschek, *RSC Advances*, 2015, **5**, 77873–77884.
- [24] R. K. Thapa, D. B. Diep and H. H. Tønnesen, *Acta Biomaterialia*, 2019, **103**, 52–67.
- [25] V. R. Krishnaswamy, D. Mintz and I. Sagi, *Biochimica et Biophysica Acta (BBA) - Molecular Cell Research*, 2017, **1864**, 2220–2227.

Chapter 2

Preparation and evaluation of enzyme-degradable polymers for encapsulation of AMPs

Contents

2.1	Aim	26
2.2	Introduction	26
2.3	Experimental Section	30
2.3.1	Materials	30
2.3.1.1	Peptide synthesis	30
2.3.1.2	Polymerization reactions	30
2.3.1.3	Enzyme degradation studies	30
2.3.2	Instrumentation	31
2.3.3	Solid-phase peptide synthesis of enzyme-degradable sequences	32
2.3.3.1	Characterization of the synthesized peptides	33
2.3.4	Synthesis of poly(methacrylamide) polymers with enzyme-degradable peptide side chain	34
2.3.4.1	Characterization of the enzyme-degradable polymers	35
2.3.5	Enzymatic degradation testing procedure	36
2.4	Results and discussion	38
2.4.1	Peptide synthesis	38
2.4.1.1	Coupling of methacrylate group	42
2.4.1.2	Further optimization of solid-phase peptide synthesis of P1/2 peptides	47
2.4.2	Synthesis of the polymers bearing enzyme-degradable side chains	48
2.4.3	Enzymatic degradation of poly(methacrylamides) with peptide side chain	55
2.5	Conclusions	59
2.6	Supporting Information	60
2.7	References	68

2.1 Aim

Chapter 2 explores the synthesis of an anionic enzyme-responsive polymer, designed to encapsulate clinically approved [AMP](#) within polyelectrolyte complexes ([PECs](#)). In addition, it evaluates the degradation properties of synthesized polymers towards the enzyme released by *P.aeruginosa*. The main challenges faced and the design choices made during its development are highlighted, which ultimately led to the creation of a complete enzyme-responsive [AMP](#) delivery system, discussed in later chapters.

2.2 Introduction

When designing stimuli-responsive delivery systems for antimicrobials, it is important to understand the pathogen that is being targeted, to incorporate specificity into the encapsulation system. For this study *P. aeruginosa* was selected as the target pathogen, a bacterium known for its formidable mechanisms of antimicrobial resistance.² It is one of the main pathogens responsible for hospital-acquired infections, which requires the urgent development of new antibiotics, as emphasized by [World Health Organization \(WHO\)](#).²

As part of colonization in the host organism *P. aeruginosa* secretes a variety of virulence factors, which contribute to successful infection and cause disease. One of such factors produced by *P. aeruginosa* is elastase B ([LasB](#)),^{2,3} which has selective elastolytic activity towards short hydrophobic domains (e.g., GLA, FGLA, ALA) in peptide sequences.^{3–5} Using [LasB](#) as a stimulus, Insua and co-workers developed a custom peptide sequence ($P4_{SH}$), which not only selectively degraded in the presence of secreted [LasB](#), but also due to the addition of anionic residues (e.g., glutamic acid) was able to encapsulate cationic polymer [Poly\(ethylene imine\) \(PEI\)](#) within the created [PECs](#) (Figure 2.1a).⁶ As a result of this, the toxicity of [PEI](#) was reduced in the encapsulated state and later recovered with enzyme degradation, which confirmed the potential of [PECs](#) to reduce the toxicity of antimicrobial polymers. Using a highly modular synthesis methodology (that is, solid-phase peptide synthesis), the stability of [PECs](#) was controlled by increasing the number of cross-linking (i.e., Cys) and anionic residues in the encapsulating peptide sequence (Figure 2.1a).¹ However, both drug release and antimicrobial efficacy of newly developed [LasB](#)-responsive [PECs](#) were not evaluated and highlighted as future work. Furthermore, [PEI](#) is not an approved drug, making [LasB](#)-responsive [PECs](#) clinically non-transferable at the current stage.

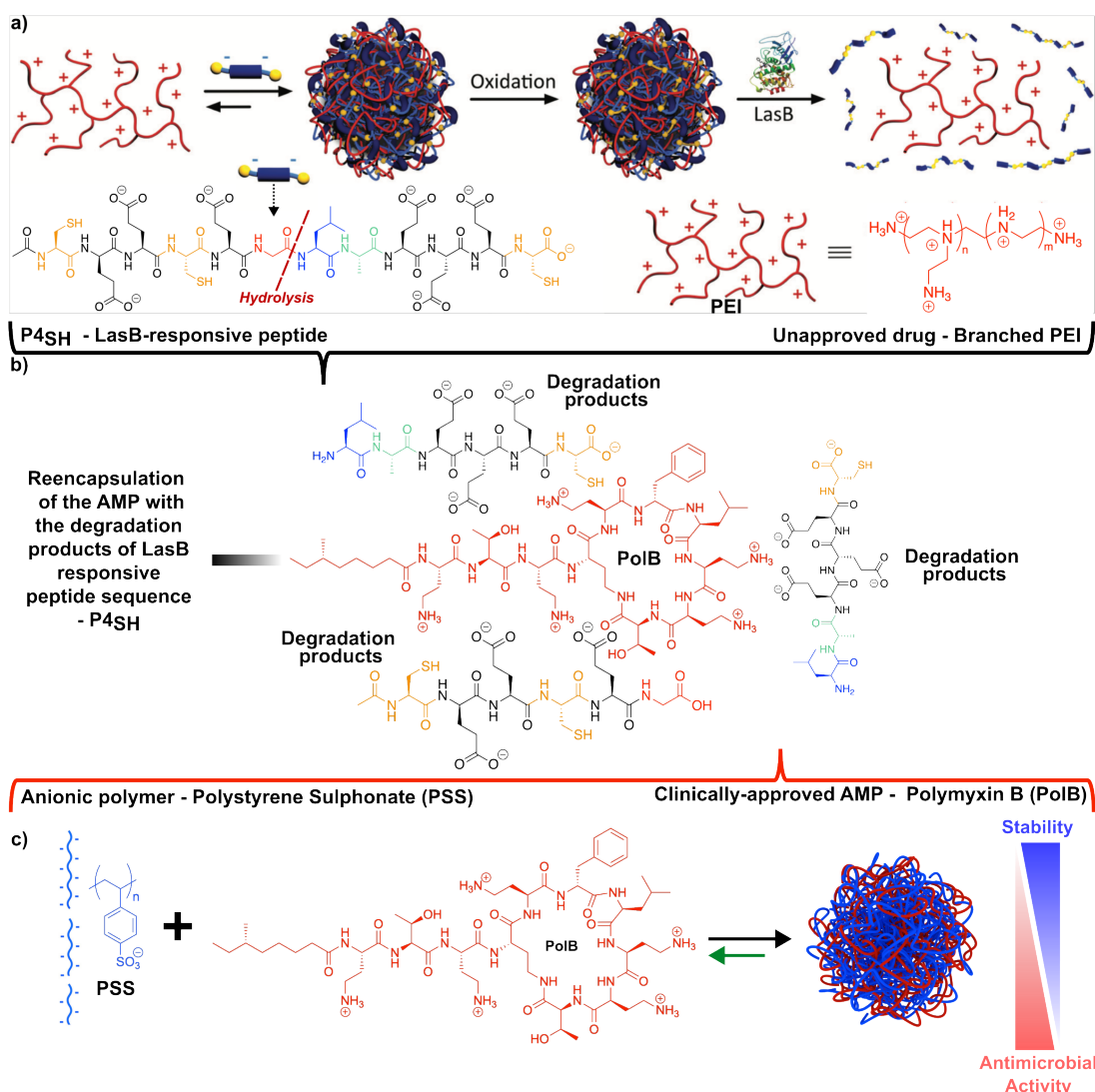


Figure 2.1 – a) Assembly and oxidative cross-linking of **PECs** nanoparticles from P4_{SH} (Ac-CEECE-GLA-EEEC-OH) and antimicrobial **B-PEI**. Degradation of **PECs** nanoparticles by **LasB** and subsequent **PEI** release, previously developed by Insua et al.¹ b) Enzyme degradation products of the **LasB**-degradable peptide sequence P4_{SH}. c) Assembly of non enzyme-responsive **PECs** nanoparticles using clinically-approved **AMP** - Polymyxin B. Indicating how the stability and antimicrobial efficacy of **PECs** can be tuned by changing the polyanion size.

In addition, the same research group successfully encapsulated a clinically approved **AMP**, **Polymyxin B (PoIB)**, within **PECs** using an anionic polymer, **Polystyrene sulfonate (PSS)** (Figure 2.1c).⁷ However, these **PECs** were not designed to be enzyme-degradable, and the drug was released passively through changes in pH and osmotic pressure. Most importantly, the study has shown that the stability and antimicrobial efficacy of a polyelectrolyte-based delivery system can be fine-tuned by changing the degree of polymerization of the anionic component, indicating the importance of using a macromolecule (*i.e.*, polymer) for effective encapsulation of an **FDA**-approved **AMP** such as Polymyxin B (Figure 2.1c).⁸

This new design is based on a brush-like polymer architecture, where anionic residues are located away from the main polymer backbone on the opposite side of the enzyme-cleavable bond (*i.e.*, bond between Gly and Leu). This ensures that after enzymatic degradation, the peptide sequence attached to the polymer backbone has a net positive charge (as seen in Figure 2.2b), which should repel cationic AMP, which facilitates the release of the drug. Toward this end, this chapter begins with the synthesis and further optimization of the enzyme-degradable peptide sequence. Subsequently, the polymerization of the selected peptide-containing monomers is explored. Lastly, the enzyme degradation characteristics of the chosen polymers are evaluated.

2.3 Experimental Section

2.3.1 Materials

2.3.1.1 Peptide synthesis

All Fmoc-protected-L-amino acids, Rink Amide MBHA resin (100-200 mesh) (0.51 mmol/g) were purchased from Merck Millipore. Alternative Rink Amide MBHA resin (100-200 mesh) (0.3 - 0.8 mmol/g) was purchased from FluroChem UK. Dimethylformamide (DMF), piperidine 20 % v/v in DMF were purchased from Merck®. N,N-diisopropylethylamine (DIPEA), Ethylenediaminetetraacetic acid (EDTA), Methacrylic acid, Methacrylic anhydride, N-methylmorpholine (NMM), Tetrakis (triphenylphosphine)palladium(0) (Pd[(C₆H₅)₃P]₄) and Formic Acid (FA), were bought from Sigma Aldrich® (UK). Trifluoroacetic acid (TFA) was purchased from Alfa Aesar®. N,N,N',N'-tetramethyl-O-(1H-benzotriazol-1-yl)uronium hexafluorophosphate (HBTU) was purchased from Carbosynth Ltd.

2.3.1.2 Polymerization reactions

Thermal initiator used - 4,4'-Azobis(4-cyanopentanoic acid) (V-501), (4-(2-hydroxyethyl)-1-piperazineethanesulfonic acid) (HEPES), were purchased from Sigma Aldrich® (UK). Dulbecco's Phosphate-Buffered Saline (DPBS) without Ca and Mg was purchased from Lonza (UK). Spectra/Por® 6 dialysis membranes (molecular weight cut off 3.5 and 1 KDa) were purchased from Spectrum® Laboratories. Ultrapure water (Milli-Q water) was obtained from Millipore Milli-Q plus 185 purification systems with electrical resistivity greater than 18.2 mΩ•cm (Millipore Corporation). Chain transfer agent used - 2-((Ethylthio)carbonothioyl)thio-2-methylpropanoic acid (CTA-1), was previously synthesized in the laboratory following the procedure from the literature.¹⁰

2.3.1.3 Enzyme degradation studies

Thermolysin from *Geobacillus stearothermophilus* and fluorescamine were purchased from Sigma Aldrich® (UK). Succinyl casein was previously produced in the laboratory using Ref.¹¹ A model degradation peptide **P3** (H₂N-LA-NH₂) was previously synthesized in our laboratory using the same solid-phase procedure as for **P1** and **P2** and previously reported in Ref.⁶

All other chemicals were purchased from Fisher Scientific® UK and VWR®, and were used without further purification. The pH values of the solutions were measured with a Mettler-Toledo MP220 pH meter.

2.3.2 Instrumentation

Nuclear magnetic resonance **NMR** data were acquired on a Bruker Avance Neo operating at 400 MHz and equipped with a 5 mm BBFO “smart” probe ($^1\text{H}/^{13}\text{C}$) as well as on Bruker AVIII operating at 300 MHz and equipped with a 5 mm BBFO probe. Chemical shifts were reported in ppm (units) referenced to the following solvent signals: dimethylsulfoxide (**DMSO**)- d_6 H at 2.50 ppm and C at 39.52 ppm. **MS** spectra were obtained on a Xevo® G2-XS ToF (Waters) from **Electrospray ionization (ESI)** and **Time-of-flight (TOF)** measurement in positive and negative ion modes. High-resolution **MS** data were calculated by comparing them with leucine-enkephalin as an internal standard. Solid phase **FTIR** spectroscopy analyses of products and starting materials were performed using a Bruker Tensor II **FTIR**.

Shimadzu Prominence LC-20A with an SPD20A **UV-Vis** detector was used to perform reverse phase HPLC analysis (**RP-HPLC**). Analyses were performed through a Kinetex®-C18-EVO column (Phenomenex®): 5 μm , 100 Å, 250 x 4.60 mm. A gradient of 5 to 60 % of (CH_3CN + 0.05 % **TFA**) in (H_2O + 0.05 % **TFA**) was used at 1 mL/min for 60 minutes. The column was kept at 25 °C and **UV-Vis** detection was set at 215 nm. 10 μL of sample was injected.

For purification purposes, Agilent 1260 Infinity II Preparative LC was used. Reverse phase preparative **HPLC** analysis was performed using a Kinetex® C18 (Phenomenex®): 5 μm , 100 Å, 250 x 21.20 mm. A gradient from 5 to 40 % of (CH_3CN + 0.05 % **TFA**) in (H_2O + 0.05 % **TFA**) was used with a flow rate of 10 mL/min for 60 minutes. Alternatively, Luna® C18 (Phenomenex®): 5 μm , 100 Å, 250 x 21.20 mm column was used. A gradient of 5 to 50 % of (CH_3CN + 0.1 % **FA**) in (H_2O + 0.1 % **FA**) was used, with a flow rate of 10 mL/min for 40 min.

Gel Permeation Chromatography (**GPC**) was run through two PL-aquagel 40:300 x 7.5 mm, 8 μm and PL-aquagel 30:300 x 7.5 mm, 8 μm **SEC** columns fitted with a PL-aquagel-OH guard column: 50 x 7.5 mm, 8 μm . As a solvent, Lonza **DPBS** buffer without Ca and Mg was used at 35 °C, and a flow rate of 1 mL/min. Molecular masses were calculated based on a standard calibration method using poly(ethylene glycol) standards. Shimadzu Prominence LC-20A equipped with a Thermo Fisher Refractomax 521 detector and an SPD20A **UV-Vis** detector were used as GPC detectors.

For the detection of enzymatic degradation monitored with the fluorescamine assay, a FLUOstar Omega (BMGLabtech GmbH) microplate reader was used. Readings were taken at 355 nm and 470 nm \pm 10 nm.

For the detection of enzymatic degradation using ζ -potentials, Zetasizer Nano-ZS instrument (Malvern Instrument, UK) was used. Standard operating procedure parameters for ζ -potentials measurements: enzyme degradation solutions were tested under the same conditions: temperature = 37 °C, solvent's viscosity = 0.6864, solvent's refractive index = 1.330, solvent's dielectric constant = 74.4, sample's [Refractive index \(RI\)](#) = 1.590, particles' absorption = 0.010, run duration = 10 s, automatic measurement duration, attenuation and voltage selection. 600 μ L of particle suspension was used to measure ζ -potentials. All measurements were made in triplicate (3 technical replicates). All ζ -potential data were presented as an average based on three technical replicates.

2.3.3 Solid-phase peptide synthesis of enzyme-degradable sequences

An exemplary procedure is presented for solid-phase peptide synthesis using 1000 mg of resin (0.51 mmol). For all peptides, commercial Rink Amide [MBHA](#) resin (100-200 mesh) (1000 mg, 0.51 mmol) was swollen in 10 mL of [DMF](#) for 30 minutes. Then, the [Fmoc](#) protecting group was removed from the Rink Amide [MBHA](#) resin with 10 mL of piperidine in [DMF](#) 20 % v/v for 10 minutes. A positive chloranil test confirmed the removal of the [Fmoc](#) group, which was followed by coupling of the first [Fmoc](#)-L-amino acid. Solutions of [Fmoc](#)-L-amino acid (3 eq), N,N,N',N'-tetramethyl-O-(1H-benzotriazol-1-yl)uronium hexafluorophosphate ([HBTU](#)) (2.8 eq) and [DIPEA](#) (2.8 eq) in [DMF](#) were added to a final volume of 10.25 mL (e.g., 5:5:0.25 mL). The reaction mixture was shaken for 45 - 90 min at room temperature, after which a negative chloranil test indicated that the reaction had reached completion. N-terminal [Fmoc](#) protecting group was removed with 10 mL of piperidine in [DMF](#) 20 % v/v for 10 minutes. A positive chloranil test confirmed the removal of the [Fmoc](#) group and the previous steps were repeated to couple all amino acids in the sequence. Following coupling of the first amino acid, the peptide sequence was capped with 4 mL of Ac₂O:DIPEA:DMF (1:1:3). Capping was also performed after the removal of the [Fmoc](#) group from the last amino acid in the sequence (e.g., Glu for **P1**). Only after the couplings of all amino acids were complete, while the peptide was still on a resin, [Alloc](#) deprotection of the Lys side chain was performed. For deprotection cocktail Pd[P(C₆H₅)₃]₄ (1 eq) dissolved in CHCl₃-AcOH-N-methylmorpholine ([NMM](#)) (37:2:1) (20 mL/g of resin) was used. The reaction was carried out under an inert atmosphere for 24 hours with light agitation. After [Alloc](#) deprotection, methacrylic acid was coupled using the same approach as for [Fmoc](#)-L-amino

acid. For the coupling of methacrylic anhydride, 4 mL of anhydride:DIPEA:DMF (1:1:3) solution was added and reacted for 1 hour.

After all couplings were completed, the resin was washed with Diethyl ether (Et_2O) and DCM and dried with air. For 1 g of resin, 10 mL of the 95 % aqueous solution of TFA was added to a dried resin and reacted for a minimum of 1 hour. The solutions obtained were concentrated under argon or air and precipitated in chilled Et_2O . Finally, these suspensions were centrifuged or filtered under vacuum and the pellets were freeze-dried from acidic water.

When the reaction scale was increased, the amounts and duration of the reaction were increased in relation to the amount of resin used, apart from the coupling with methacrylic anhydride, which was repeated twice with a new reaction mixture.

2.3.3.1 Characterization of the synthesized peptides

P1, Ac-EGLAK(COC(CH₃)C)-NH₂ (Crude 257 mg, 81 % yield), (Purified 109 mg, 34 % yield), ¹H-NMR δ_{H} (400 MHz, $\text{DMSO}-d_6$): 0.85 (6 H, dd, $J = 15.25, 6.51$ Hz, H^{δ} -Lue), 1.23 (5 H, dd, $J = 11.48, 6.57$ Hz, H^{β} -Ala, H^{γ} -Lue), 1.37 – 1.77 (8 H, m, $\text{H}^{\delta,\gamma,\beta}$ -Lys, $\text{H}^{\gamma,\beta}$ -Lue, H^{β} -Glu), 1.82 – 1.89 (6 H, Ac), 2.27 (2 H, t, $J = 7.92$ Hz, H^{γ} -Glu), 3.07 (2 H, q, $J = 6.77$ Hz, H^{ϵ} -Lys), 3.70 (2 H, d, $J = 5.72$ Hz, H^{α} -Gly), 4.07 – 4.34 (4 H, m, H^{α} -Ala, Lue, Lys, Glu), 5.30 (1 H, p, $J = 1.59$ Hz, $\text{CH}=\text{C}$), 5.62 (1 H, s, $\text{CH}=\text{C}$), 7.01 (1 H, s, NH), 7.21 – 7.27 (1 H, m, NH), 7.61 (1 H, d, $J = 7.96$ Hz, NHCO), 7.82 – 7.91 (2 H, m, NHCO), 8.09 (2 H, dd, $J = 20.74$ Hz, 7.173, NHCO), 8.22 (1 H, t, $J = 5.80$ Hz, NHCO) ppm. ¹³C-NMR δ_{C} (400 MHz, $\text{DMSO}-d_6$): 17.53 (C^{β} -Ala), 21.45 (Ac), 22.12 (C^{δ} -Leu), 22.48 (C^{γ} -Lys), 23.14 (C^{δ} -Leu), 24.04 (C^{γ} -Leu), 26.63 (C^{β} -Lys), 26.93 (C^{β} -Leu), 30.12 (C^{γ} -Glu), 31.37 (C^{δ} -Lys), 38.74 (C^{γ} -Glu), 40.56 (C^{ϵ} -Lys), 42.12 (C^{α} -Gly), 48.48 (C^{α} -Ala), 50.95 (C^{α} -Lys), 52.03 (C^{α} -Glu), 52.48 (C^{α} -Leu), 168.86 (NHCO), 169.92 (C-term), 171.89 (NHCO), 171.95 (NHCO), 172.02 (NHCO), 173.38 (NHCO), 173.92 (NHCO) ppm. MS (TOF, -eV): m/z 624.34 [M]⁻; 646.32 [$\text{M}-\text{H} + \text{Na}$]⁻. HR-MS (TOF, -eV): m/z 624.3357 (calculated for [$\text{M}-\text{H}$]⁻) 624.3371 (found). Purity (purified sample) by HPLC = 98 %.

P2, Ac-EEGLAK(COC(CH₃)C)-NH₂ (Crude 566 mg, 73 % yield), (Purified 229 mg, 30 % yield) ¹H-NMR δ_{H} (400 MHz, $\text{DMSO}-d_6$): 0.85 (6 H, dd, $J = 14.3, 6.5$ Hz, H^{δ} -Lue), 1.21 (4 H, d, $J = 7.1$ Hz, 3 H^{β} -Ala, 1 H^{γ} -Leu), 1.37 – 1.78 (17 H, m, 2 H^{β} -Lue, 2 H^{γ} -Lys, 2 H^{δ} -Lys, 4 H^{β} -Glu, 6 H-Ac), 2.19 – 2.30 (4 H, q, $J = 8.1$ Hz, H^{γ} -Glu), 2.98 – 3.13 (2 H, q, $J = 6.7$ Hz, H^{ϵ} -Lys), 3.61 – 3.82 (2 H, m, H^{α} -Gly), 4.05 – 4.37 (5 H, m, H^{α} -Ala, Lue, Lys, Glu), 5.29 and 5.62 (1 H, s, $\text{CH}=\text{C}$, $\text{C}=\text{CH}$), 7.01 and 7.25 (1 H, s, NH), 7.61 (1 H, d, $J = 8.0$ Hz, NHCO-Ala), 7.85 – 7.94 (2 H, m, NHCO-Lys, $\text{NH}^{\epsilon}\text{CO}$ -Lys), 8.03 (2 H, d,

$J = 7.6$ Hz, NHCO-Leu, NHCO-Glu), 8.12 (2 H, t, $J = 5.7$ Hz, NHCO-Glu, NHCO-Gly), 12.08 (2 H, s, COOH) ppm. $^{13}\text{C-NMR}$ δ_{C} (400 MHz, $\text{DMSO-}d_6$): 17.62 (C^β -Ala), 18.68 (Ac-C), 21.61 (Ac-C), 22.48 (C^δ -Lys), 22.66 (C^γ -Lys), 23.04 (C^δ -Leu), 24.06 (C^γ -Leu), 27.14 (C^β -Glu), 27.19 (C^β -Glu), 28.81 (C^δ -Lys), 30.02 (C^γ -Glu), 30.24 (C^γ -Glu), 31.8 (C^β -Lys), 38.75 (C^ϵ -Lys), 40.85 (C^β -Leu), 41.93 (C^α -Gly), 48.37 (C^α -Ala), 50.87 (C^α -Leu), 52.03 (C^α), 52.24 (C^α), 118.72 (C=C), 140.10 (C=C), 167.36 (NHCO-Leu), 168.54 (NHCO-Gly), 169.59 (NHCO-MA), 171.40 (NHCO), 171.48 (NHCO), 171.79 (171.79), 171.87 (NHCO), 173.44 (NHCO), 173.99 (NHCO), 174.03 (NHCO) ppm. **MS** (TOF, -eV): m/z 316.19 $[\text{M}-2\text{H}]^-$; 753.38 $[\text{M}-\text{H}]^-$; 776.36 $[\text{M}-\text{H} + \text{Na}]^-$; **HR-MS** (TOF, -eV): m/z 753.3783 (calculated for $[\text{M}-\text{H}]^-$) 753.3781 (found); Purity (purified sample) by **HPLC** $\geq 98\%$.

2.3.4 Synthesis of poly(methacrylamide) polymers with enzyme-degradable peptide side chain

Purified peptide sequences **P1** or **P2** were first dissolved in **Milli-Q** water with the support of added base (Na_2CO_3 or NaOH). Initiator **V-501** was dissolved in MeOH or EtOH. Both solutions were degassed with argon and mixed in an airtight vial.

For reversible addition-fragmentation chain transfer polymerizations (**RAFT**) purified **P2** (50 mg, 0.0664 mmol) was reacted with **CTA-1** (0.19 mg, 0.000678 mmol) and **V-501** (0.038 mg, 0.000136 mmol) in 0.4 or 0.3 mL of 50/50 % **Milli-Q**/MeOH solution with some addition of Na_2CO_3 for monomer solubilization. The mixtures were incubated under a fully inert atmosphere and stirred at 70 °C for a minimum of 20 h to produce functional polymers.

For **P1**. **P1** (172 mg, 0.275 mmol) was reacted with **V-501** (2.10 mg, 0.007493 mmol) to give 0.551 M monomer solution in 0.5 mL of 50/50 % **Milli-Q**/DMSO. The mixtures were incubated under a fully inert atmosphere and stirred at 70 °C for a minimum of 20 h to produce functional polymers.

For **P2**. Typically, this protocol involved the reaction of **P2** (50 mg, 0.0664 mmol) with **V-501** (0.4 mg, 0.00143 mmol) to give a 0.133 M monomer solution in 0.5 mL of 50/50 % **Milli-Q**/MeOH or EtOH for a minimum 20 hours. In the later stages of the project, MeOH and EtOH were substituted with water (*i.e.*, 50 % of the reaction volume) while the initiator was still dissolved in MeOH or EtOH before addition. The same protocol was used for the synthesis of larger batches of polymers using 100 mg of purified peptide sequence **P1** or **P2** keeping the same monomer/initiator ratios and concentrations. The list of conditions is shown in Table 2.1.

Table 2.1 – Summary of free-radical polymerization conditions and reactant concentrations, where **P2 (Ac-EEGLAK(COC(CH₃)CH₂)-NH₂)** is a monomer and **V-501** (4,4'-Azobis(4-cyanopentanoic acid) is a thermal initiator.

Pol-ID	Materials	mg	[M] ₀	[M] _f	Solvent (mL)	R (Molar)
Poly-P2-1	P2	50	0.0662	0.0662	1.00	100
	V-501	0.40	0.00143	0.00143	(50/50 % Milli-Q/MeOH + Na ₂ CO ₃)	2.15
Poly-P2-2	P2	50	0.0662	0.0884	0.750	100
	V-501	0.40	0.00143	0.00190	(50/50 % Milli-Q/MeOH + Na ₂ CO ₃)	2.15
Poly-P2-3	P2	50	0.0662	0.133	0.500	100
	V-501	0.40	0.00143	0.00285	(50/50 % Milli-Q/MeOH + Na ₂ CO ₃)	2.15
Poly-P2-4	P2	50	0.0662	0.133	0.500	100
	V-501	0.40	0.00143	0.00285	(50/50 % Milli-Q/MeOH + Na ₂ CO ₃)	2.15
Reacted for 20 hours at 70 °C.						

Subsequently, the crude polymer solutions were characterized by ¹H-NMR. Monomer conversions were calculated by reduction of an integration of the vinylic peaks between 5.1 to 5.7 ppm compared with the proton region of the H^δ-Lue at 0.85 ppm (6 H, dd, J = 14.3, 6.5 Hz, H^δ-Lue). Equation 2.1 was used to obtain % conversion, where *H_{ref}* corresponds to the integration of H^δ-Lue peaks at 0.85 ppm (6 H, dd, J = 14.3, 6.5 Hz), *H_m* and *H_p* correspond to the proton signals at 5.29 and 5.62 ppm of the C = C bond (1 H, s) in the monomer (*i.e.*, *H_m*) at the start of the reaction and in the polymer (*i.e.*, *H_p*) at the end of the polymerisation.

$$\text{Monomer Conversion} = \left(1 - \frac{\frac{H_p}{H_{ref}}}{\frac{H_m}{H_{ref}}}\right) \times 100\% \quad (2.1)$$

After the reaction was completed, the polymers underwent purification through dialysis in deionized water at room temperature for a minimum duration of 48 hours, employing a 3.5 kDa membrane. Subsequently, the polymer's molecular weight was assessed using Gel Permeation Chromatography (GPC).

2.3.4.1 Characterization of the enzyme-degradable polymers

Poly-P1, poly(Ac-EGLAK(COC(CH₃)CH₂)-NH₂) (86 mg after dialysis) ¹H-NMR δ_H (400 MHz, DMSO-*d*⁶): 0.63 – 0.96 (6 H, m, H^δ-Lue), 0.99 – 1.95 (17 H, m, H^β-Ala, H^γ-Leu, H^β-Lue, H^γ-Lys, H^δ-Lys, H^β-Glu, H-Ac), 2.25 (2 H, m, H^γ-Glu), 3.58 – 3.82 (2 H, m, H^ε-Lys, H^α-Gly), 3.95 - 4.50 (4 H, m, H^α-Ala, Lue, Lys, Glu), 6.85 - 8.40 (6 H, m, NHCO).

Poly-P2, poly(Ac-EEGLAK(COC(CH₃)CH₂)-NH₂) (63 mg after dialysis) ¹H-NMR δ_H (400 MHz, DMSO-*d*⁶): 0.66 – 0.95 (6 H, m, H ^{δ} -Lue), 1.05 - 2.01 (17 H, m, H ^{β} -Ala, H ^{γ} -Leu, H ^{β} -Lue, H ^{γ} -Lys, H ^{δ} -Lys, H ^{β} -Glu, H-Ac), 2.09 - 2.35 (4 H, m, H ^{γ} -Glu), 2.80 - 3.90 (10 H, m, H ^{ϵ} -Lys, H ^{α} -Gly, H ^{α} -Ala, Lue, Lys, Glu), 4.41 – 4.08 (4 H, m), 6.94 - 8.37 (7 H, m, NHCO).

For NMR spectra, HPLC chromatograms, and MS spectra, see the supporting information Section 2.6.

2.3.5 Enzymatic degradation testing procedure

Three buffer solutions were prepared: buffer (A) - 5mM HEPES at pH 7.45 buffer (B) - 20 mM CaCl₂ in buffer (A) and buffer (C) - 2.5 mM Na₂B₄O₇ at pH 8.0. Stock solutions of enzyme-degradable polymers (**Poly-P1** and **Poly-P2**) (1 mM), succinyl casein (SC) (0.5 mg/mL) and degradation peptide H₂N-LA-NH₂ (**P3**) were mixed with buffer (A) 12 hours before the experiment. Enzyme and substrate solutions alone were prepared as blanks. On the day of the test, all samples were mixed according to Table 2.2 in 1.5 mL Eppendorf tubes. In this experiment, 1.2 mg (0.100 mg/ μ L solution) of thermolysin per sample was used (Final enzyme concentration in reaction solution was 1.2 mg/mL). The temperature of the test tubes was controlled by a 55 °C water bath. At each time point, aliquots of 125 μ L were taken and mixed with 30 μ L of 0.1 M EDTA solution. Then each sample was mixed in a 1:1 volume with a 1 mM fluorescamine solution in methanol. Each sample was measured in triplicate (*i.e.*, 3 technical replicates). The microplate was incubated at 37 °C under orbital shaking for 30 minutes. After this time, fluorescence was measured excited at 355 nm and reading the emission at 460 \pm 10 nm.

The raw emission intensity data were then normalized to a degradation peptide (H₂N-LA-NH₂, referred to as **P3**) which was used as a positive control, representing 100 % degradation. The results were presented as a percentage of the relative amine content in the solutions.

For the detection of enzymatic degradation using ζ -potentials refer to Section 2.3.2. All measurements were made in triplicate (3 technical replicates).

Table 2.2 – Summary of the concentrations and conditions used in enzymatic degradation testing.

Samples	Buffer A	Buffer B	Buffer C	SC	Thermolysin	Poly-P solutions	Total Vol (μL)
Buffer	500	476	24	-	-	-	1000
Therm. (enzyme control)	500	488	-	-	12	-	1000
SC (succinyl casein)	-	476	24	500	-	-	1000
SC + Therm.	-	488	-	500	12	-	1000
P3 (+ve control)	-	488	-	-	12	500	1000
Poly-P1 control	-	500	-	-	-	500	1000
Poly-P2 control	-	500	-	-	-	500	1000
Poly-P1 + Therm.	-	488	-	-	12	500	1000
Poly-P2 + Therm.	-	488	-	-	12	500	1000

2.4 Results and discussion

2.4.1 Peptide synthesis

The first step in designing the [LasB](#)-responsive peptide sequence was to identify which hydrophobic amino acid residues should be used as the core of the enzyme-degradable material. Different combinations of hydrophobic amino acids were considered e.g, -FGLA-, -ALA- but were rejected due to the potential problems with the aqueous solubility of these sequences and the limited number of reports on their use in polyelectrolyte delivery systems. The only sequence that had proven enzyme degradation properties and was used in the assembly of [PECs](#) was -GLA-, previously reported by Insua and his co-workers.^{1,6} Consequently, the same core hydrophobic amino acid sequence (-GLA-) was used in all peptide sequences discussed in this Thesis. For the electrostatic complexation of positively charged [AMPs](#), anionic residues represented by glutamic acids (E) were selected.

Previous reports of successful encapsulation of cationic antimicrobials in [PECs](#) all used polymers (*i.e.*, large macromolecules) instead of monomers due to the superior multivalency of the former and its larger size.^{8,12} This is because a single polymer molecule is composed of multiple charged monomer units, which are linked together via a backbone chain. Moreover, in a polymer charged groups are structurally closer to each other due to being covalently linked, which increases the charge density of the material and strength of electrostatic interactions. More importantly, the formation of [PECs](#) is mainly driven by an increase in entropy, which is caused by the release of counterions during the self-assembly of particles in solution.^{13,14} The use of a polymer further increases the entropic change, as per each polymer chain, a larger number of counterions gets released. Consequently, the stability and antimicrobial efficacy of the [PECs](#) systems can be controlled by changing the size of the polyanionic component as well as its multivalency.^{8,15}

For example, in the case of the [LasB](#)-degradable sequence (P4_{SH}) reported by Insua and coworkers, the sulfide side chain in cysteine residues was used to crosslink individual peptides into a single macromolecule/polymer (Figure 2.3a, b).⁶ With increasing number of glutamic acids and cysteines in the peptide sequence, a larger number of colloiddally stable [PECs](#) formulations were obtained with improved stability in simulated physiological environment.¹ In P4_{SH} peptide glutamic acids were positioned on both sides of the enzyme-cleavable bond (-GLA-). When the amide bond between glycine and leucine in P4_{SH} is hydrolyzed by [LasB](#), both ends of the cleaved peptide sequence

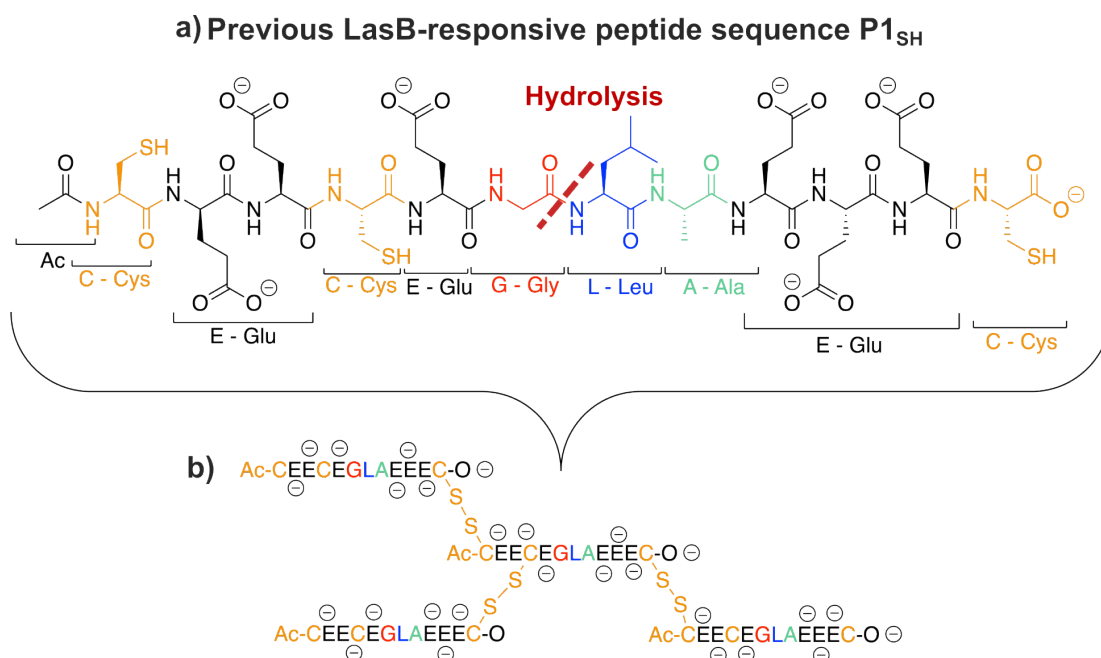


Figure 2.3 – a) Structure of previously developed LasB-degradable peptide (P4_{SH}), developed by Insua et al.¹ b) Schematic representation of disulfide cross-linking between the LasB-degradable peptide sequences, only for representation purposes.

remain anionic and are likely still attached to the drug (Figure 2.4a, b). This can potentially lead to poor drug release kinetics and significantly reduced antimicrobial activity, since the cationic groups of AMP would be partially shielded.

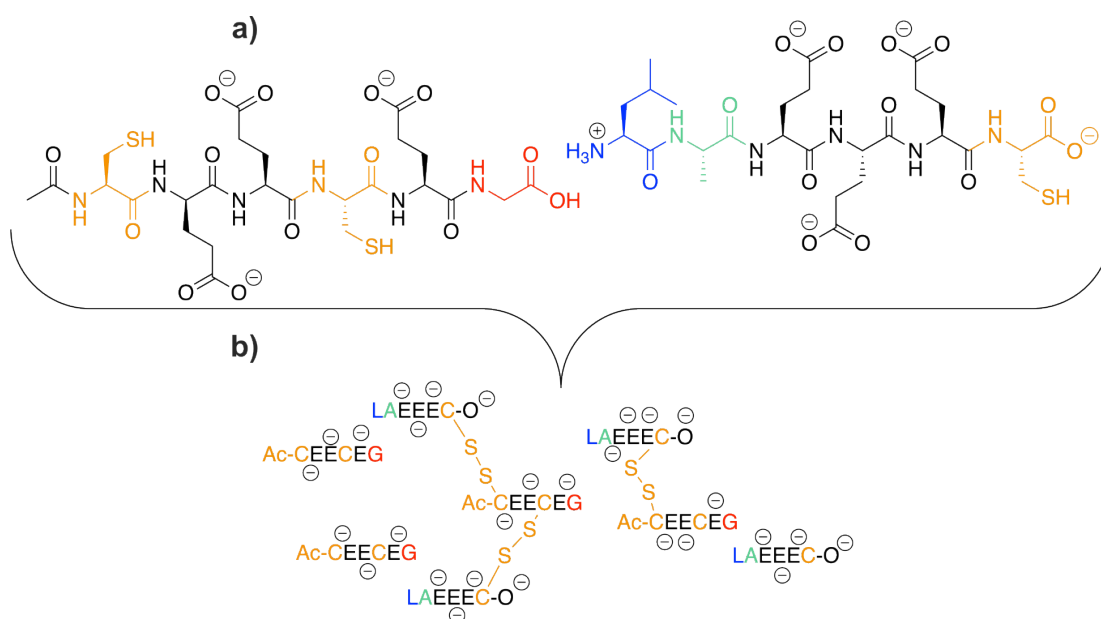


Figure 2.4 – a) Enzyme degradation products of the LasB-degradable peptide sequence (P4_{SH}) developed by Insua et al.¹ b) Schematic representation of the enzymatic degradation of cross-linked LasB-degradable peptide sequences, only for representation purposes.

Therefore, to minimize undesired shielding of the **AMP** during the breakdown of the polymer, the new design has a brush-like polymer structure (Figure 2.5a, b), with the **LasB**-degradable peptide sequence present as a side chain in the individual repeating units of the polymer. Most notably, glutamic acids were placed away from the main polymer backbone on the opposite side of the enzyme cleavable bond between glycine and leucine. The main purpose of this was to ensure that, after hydrolysis of the amide bond between leucine and glycine, the section of the peptide sequence attached to the polymer backbone had a net positive charge (labeled as **DP-2** in Figure 2.5c), repelling the cationic **AMP** and releasing the drug (Figure 2.5c, d). As a result of this design, a polymerizable group (*e.g.*, methacrylate) had to be attached to the peptide chain before alanine. To accomplish this in a traditional C to N solid-phase peptide synthesis, lysine (K) had to be the first amino acid coupled to the solid support resin, which was then followed by the rest of the sequence (Resin-K-A-L-G-E-E-Ac, Figure 2.5a).

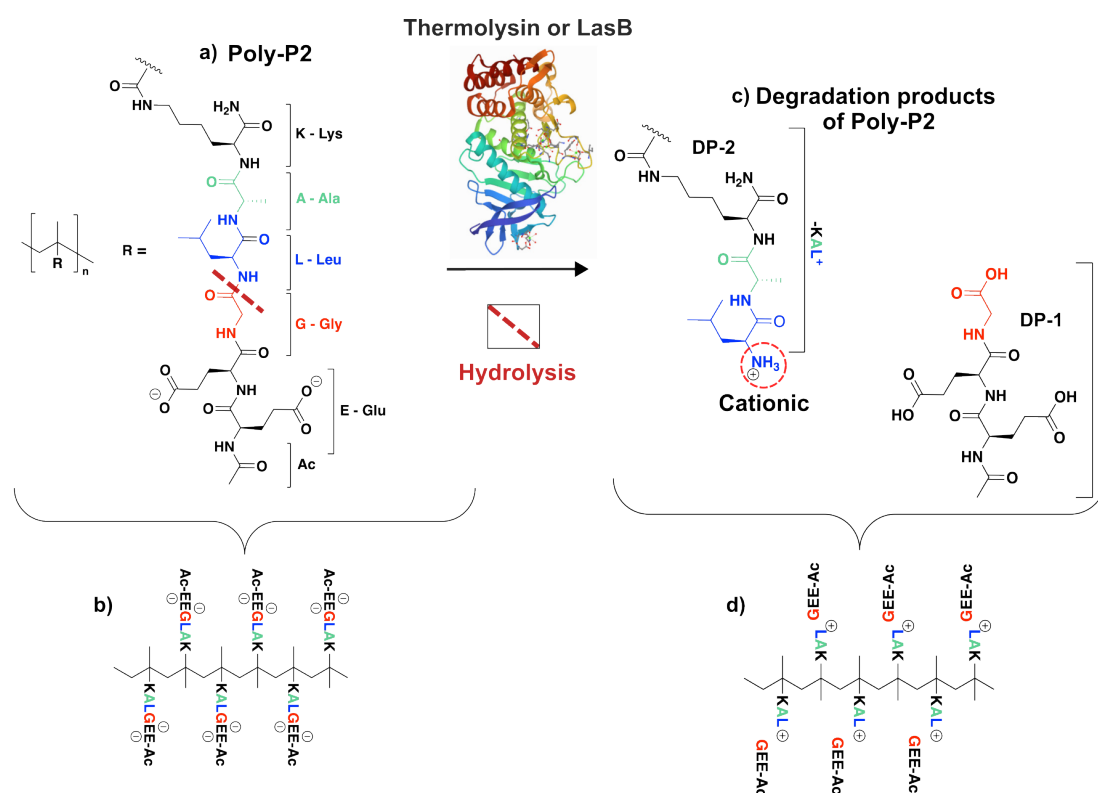


Figure 2.5 – a) The design (*i.e.*, chemical structure) of newly developed polymer with enzyme-degradable peptide side chain **Poly-P2**. b) Schematic representation of a **Poly-P2** structure with degree of polymerization (**Dp**) = 6. c) Enzyme degradation products of **Poly-P2**. d) Schematic representation of the enzymatic degradation of a **Poly-P2** structure with **Dp** = 6.

The main sequence was synthesized using **Fmoc**-protected amino acids using the **HBTU/DIPEA** coupling methodology. Therefore, to ensure that the lysine side chain

remained protected after all Fmoc-deprotection steps, lysine with an orthogonally protected side chain *i.e.*, Fmoc-Lys(Alloc)-OH was used. Therefore, after completion of the main peptide sequence (Resin-K-A-L-G-E-E-Ac), Alloc protection group was removed under mild conditions with a Tetrakis(triphenylphosphine)palladium(0) catalyst.¹⁶ Subsequently, to the deprotected lysine side chain, the methacrylate group was coupled, forming a methacrylamide moiety.

The methacrylate group was selected as the double bond source due to its extensive use in polymerization of various functional materials, including peptides.^{17–20} Furthermore, methacrylates can be reliably coupled (*i.e.*, forming methacrylamide moiety) through amide bond to the rest of the peptide sequence using identical conditions as for the coupling of Fmoc-protected amino acids. That meant that integration of methacrylate group coupling into the solid phase peptide synthesis procedure required no changes to the synthesis set-up. Additionally, our group possessed expertise in the polymerization of methacrylate-containing monomers, which proved to be valuable for troubleshooting unsuccessful reactions.^{21–23} Therefore, the finalized designs of LasB-responsive peptide sequences were **P1** and **P2** (Table 2.3), with single and double glutamic acids. Two peptide sequences, **P1** and **P2**, were created to investigate whether increasing the multivalence would have an impact on the enzyme degradation characteristics of related polymers.

Table 2.3 – Peptides and their structures evaluated in this Chapter in the deprotonated state.

I.D.	Sequence code	Structure
P1	Ac-EGLAK(COC(CH ₃)CH ₂)-NH ₂	
P2	Ac-EEGLAK(COC(CH ₃)CH ₂)-NH ₂	

Considering the complete structures of the polymerized forms of **P1** and **P2**, it is anticipated that the peptide side chain would undergo complete biodegradation in a biological system. While, the polymer backbone (*i.e.*, poly(methacrylamide)) would likely undergo partial degradation by proteases (*i.e.*, hydrolysis of amide bond), resulting in

the formation of anionic poly(methacrylic acid). Subsequently, poly(methacrylic acid) would either be cleared from the body or potentially taken up by immune cells. In the case of topical application, such as in wound dressings, non-degraded material can be removed with washing procedures, and it would not cause any retention associated toxicity. However, for pulmonary delivery a dedicated *in-vivo* testing in mouse models would be necessary to comprehend the cellular association and trafficking of these materials.^{24–26}

Solid-phase peptide synthesis of the peptide sequences -EGLAK- for **P1** and -EEGLAK- for **P2** was conducted using HBTU/DIPEA coupling methodology and proved to be reliable. However, the coupling of the methacrylate group with the lysine side chain posed the greatest difficulty in the monomer preparation workflow for both peptides **P1** and **P2**, resulting in a considerable loss of yields (as much as 45 %) of the purified peptide. For the sake of clarity, a more thorough examination of **P2** synthesis is presented, with the same observations and conclusions applicable to **P1**.

2.4.1.1 Coupling of methacrylate group

The methacrylate group was first coupled through the activation of methacrylic acid with HBTU and DIPEA, following the same procedure as for the rest of Fmoc-protected-L-amino acids in the sequence (Figure 2.6). In summary, methacrylic acid was first mixed with HBTU and DIPEA and then added to a solution containing a deprotected peptide chain bonded to the solid support. After completion of peptide synthesis, the purity of the crude product was verified with High performance liquid chromatography (HPLC), followed by structural analyses by Nuclear magnetic resonance (NMR) and Mass spectrometry (MS).

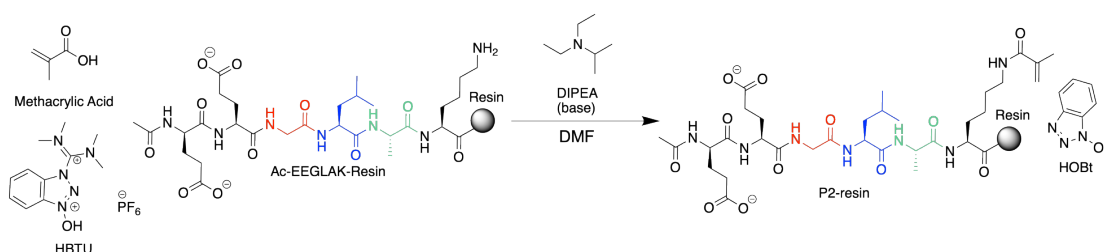


Figure 2.6 – Reaction scheme for coupling of methacrylic acid with **Ac-EEGLAK-Resin** to produce a final structure of **P2 (Ac-EEGLAK(COC(CH₃)CH₂)-NH₂)** sequence.

Early efforts to synthesize the **P2** monomer sequence resulted in a crude product that displayed a broad spectrum of peaks in the chromatogram (Figure 2.7a) between 5 and 35 minutes. This indicated that a range of different impurities and side-products were present at the end of the synthesis, leading to a low yield of the desired product

(55 %). To identify which of the peaks in the chromatogram corresponded to **P2** and which to the side-products, peaks with the highest intensities at 13.91 and 22.28 min were isolated with preparative HPLC and analyzed by analytical HPLC (Figure 2.7), NMR (Figure 2.8) and MS (Figure S2.24). The peak at 13.91 min (Figure 2.7a and b) produced an m/z value of 753.38 (Figure S2.24) in the negative ion mode, which was indicative of **P2** sequence. Furthermore, all $^1\text{H-NMR}$ peaks (Figure 2.8) were fully assigned to the corresponding proton environments present in **P2**, which further verified the identity of the peak at 13.91 min (Figure 2.7a and b). In particular, a successful coupling of the methacrylate group was indicated in $^1\text{H-NMR}$ by the presence of two protons in a vinylic environment between 5.25 - 5.75 ppm (Figure 2.8).

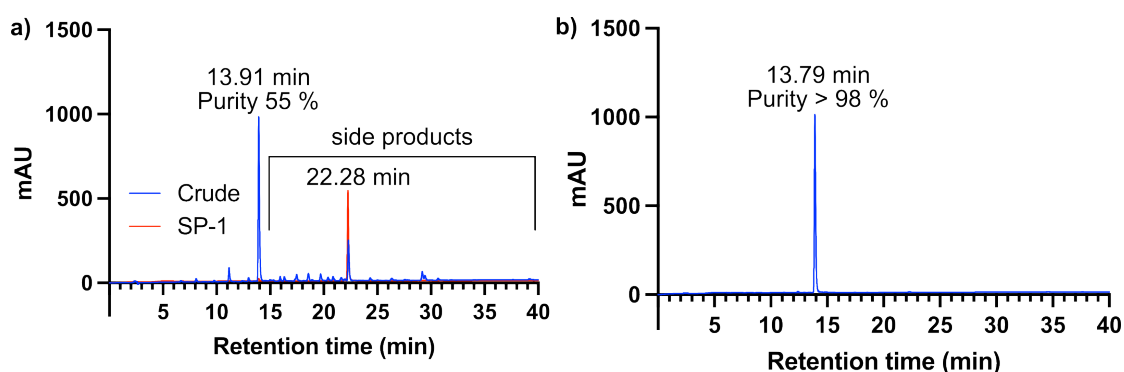


Figure 2.7 – a) RP-HPLC chromatogram of a) crude and b) purified **P2** (Ac-EEGLAK-(COC(CH₃)CH₂)-NH₂) sequence, where methacrylate group coupled with methacrylic acid.

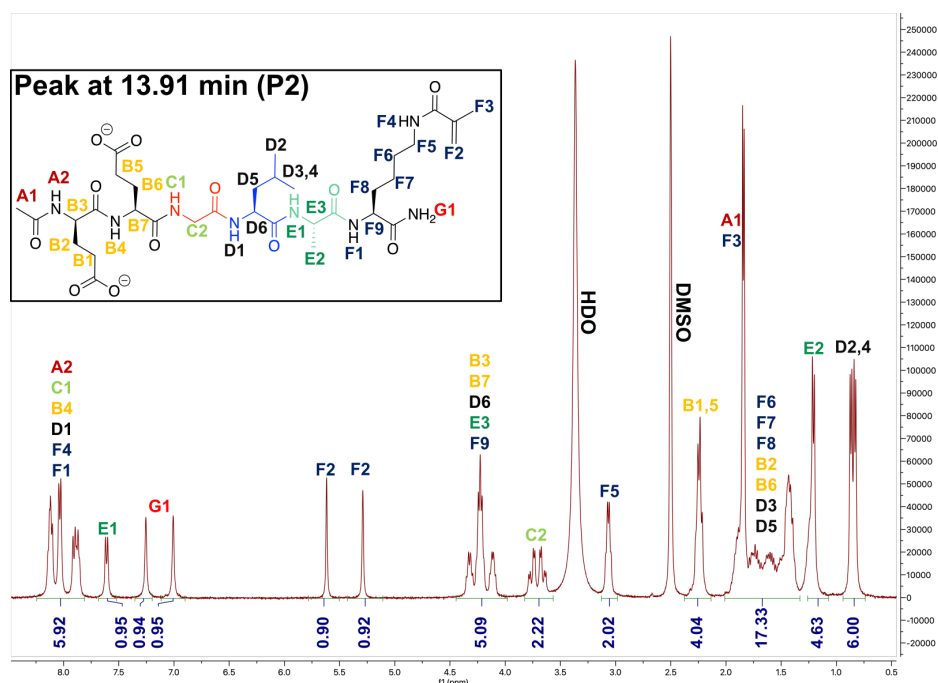


Figure 2.8 – Fully assigned $^1\text{H-NMR}$ (400 MHz, DMSO-*d*₆) spectrum of peak at 13.91 min (from Figure 2.7) - **P2** (Ac-EEGLAK(COC(CH₃)CH₂)-NH₂).

In the case of the second isolated peak (**SP-1**) at 22.28 min (Figure 2.7a), $^1\text{H-NMR}$ showed minimal presence of vinylic environments (5.25 - 5.75 ppm - Figure 2.9), indicating that the separated product did not contain vinylic groups and was highly likely cross-contaminated with other products during HPLC collection. Furthermore, new proton environments were found, which resulted in increased integration of multiplets between 3.6 - 3.8 ppm (integration increased by 2) and 1.1 - 2.0 (integration increased by 4). However, in general, most of the proton environments found in **P2** were present in $^1\text{H-NMR}$ of **SP-1** (Figure 2.9). It was concluded that the product collected at 22.28 minutes was formed during the coupling reaction involving methacrylic acid.

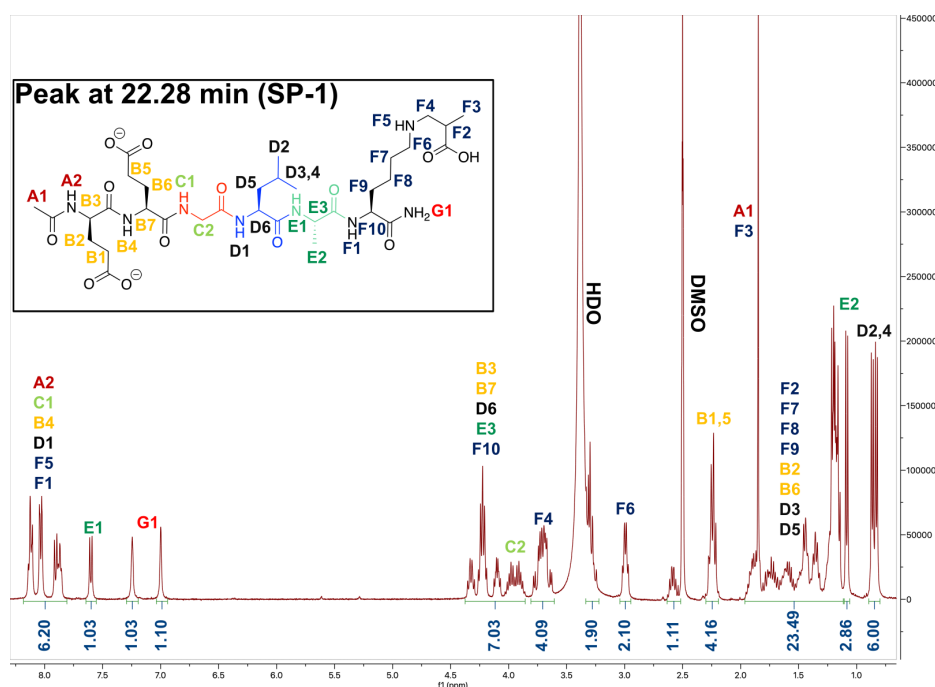


Figure 2.9 – Fully assigned $^1\text{H-NMR}$ (400 MHz, $\text{DMSO-}d_6$) spectrum of peak at 22.28 min (from Figure 2.7) **SP-1**- side product of 1,4-addition to the double bond of methacrylic acid.

Based on previous experience in coupling acrylate groups with primary amines, and the NMR data of **SP-1**, the chemical structure of **SP-1** side product was suggested, as illustrated in Figure 2.9. When the methacrylate group was coupled with the primary amine, the expected result of the 1,2-nucleophilic addition (to the carbonyl carbon of methacrylic acid-OBtu, Figure 2.10a) was accompanied by the formation of the competitive product of the 1,4-addition to C^β as indicated in Figure 2.10b.²⁷ This is because primary amines are weak nucleophiles and, as a result, can undergo 1,4-addition with other electrophilic sites of the molecule, such as C^β in the methacrylate group. For example, in the acrylate group, C^β is even more electron deficient due to the lack of the methyl group, which is electron-donating. As a result, under identical reaction conditions, coupling with acrylic acid would result in a higher yield of the 1,4-addition product.

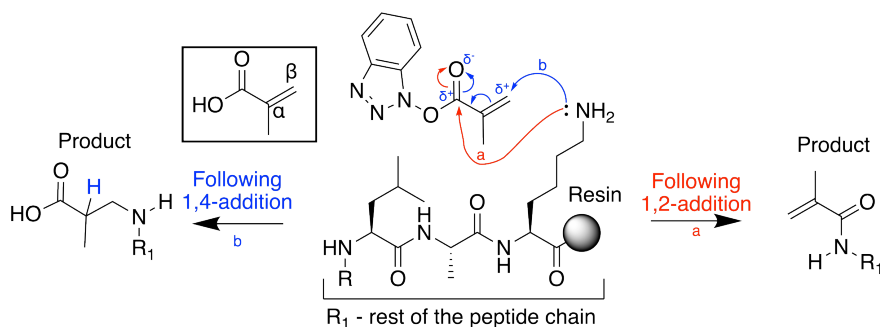


Figure 2.10 – Proposed mechanism of a) 1,2 and b) 1,4-addition during the methacrylic acid coupling to the lysine side chain.

To confirm our predictions about the side product, a mass analysis of **SP-1** sample (Figure 2.11) was carried out.

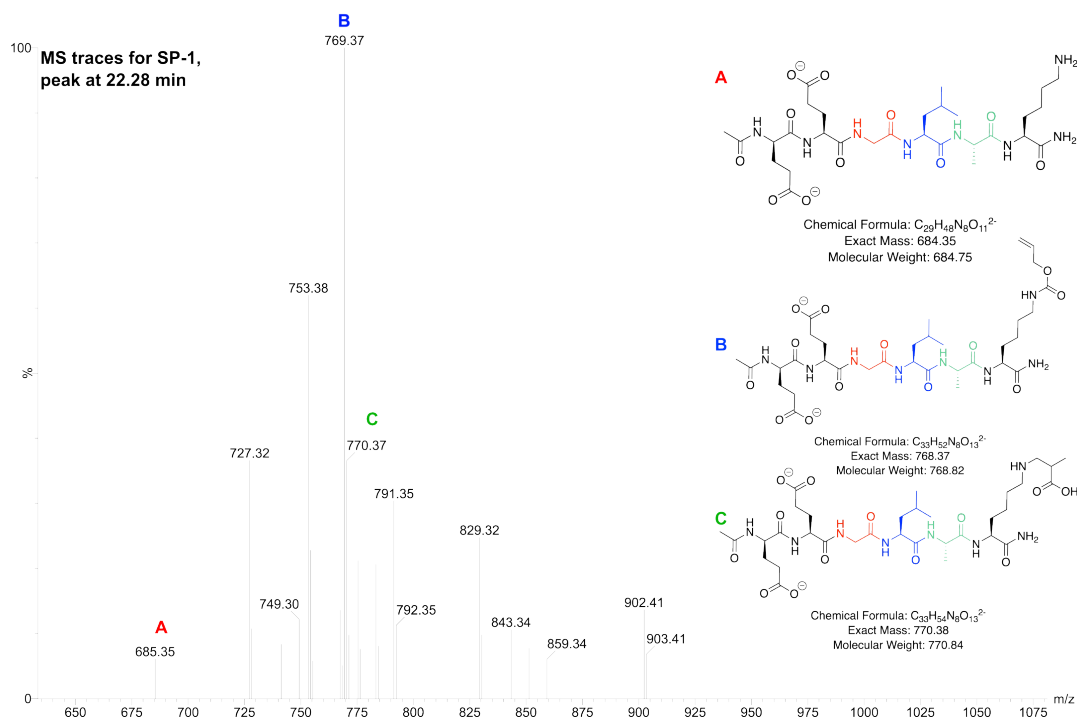


Figure 2.11 – MS traces for **SP-1** with proposed masses of different peptide adducts in negative ion mode. **SP-1** represents the unknown peak, which eluted at 22.28 min (Figure 2.7a) during the analytical HPLC of the crude sample of **P2**.

The MS results of **SP-1** revealed that the sample was composed of a variety of components, which was not fully evident from NMR since MS is a much more sensitive analytical technique. Most importantly, the mass peak corresponding to the side-product of 1,4-addition (**SP-1**) was found with m/z 770.37 (labeled **C** in Figure 2.11). In addition to **SP-1**, masses corresponding to **P2** with and without the methacrylate group (labeled **A** - m/z 685.35 in Figure 2.11) and with an Alloc protection group attached (labeled **B** -

m/z 769.37 in Figure 2.11) were also identified. This explained the presence of vinylic environments seen in $^1\text{H-NMR}$ of **SP-1** (Figure 2.9), which can be correlated with *Alloc*-protected -EEGLAK- sequence (m/z 769.37) or presence of **P2** sequence (m/z 753.38).

From these results, it was clear that using *HBTU* activation for coupling of methacrylic acid did not make carbonyl carbon sufficiently electrophilic to significantly suppress the production of **SP-1**. Therefore, the coupling of the methacrylate group had to be revised to improve the yields of a desired 1,2-addition product. Furthermore, the significant presence of impurities in the initial syntheses of **P2**, indicated that not only methacrylate, but all couplings and deprotection steps had to be closely monitored, eliminating the production of deprotected side-products, improving the purity of the synthesized peptide sequence.

The 1,4-addition pathway was hypothesized to be less favored than the 1,2-addition pathway when coupling the methacrylate group using methacrylic anhydride instead of methacrylic acid (*HBTU*/*DIPEA*). In acid anhydrides, the carbonyl carbon is more electrophilic than in carboxylic acids, as a result of higher electron delocalization, which makes carbonyl groups less electron-rich.²⁷ The coupling process involved mixing the methacrylic anhydride solution with *DIPEA* prior to adding it to the growing peptide chain still attached to the solid support, Figure 2.12.

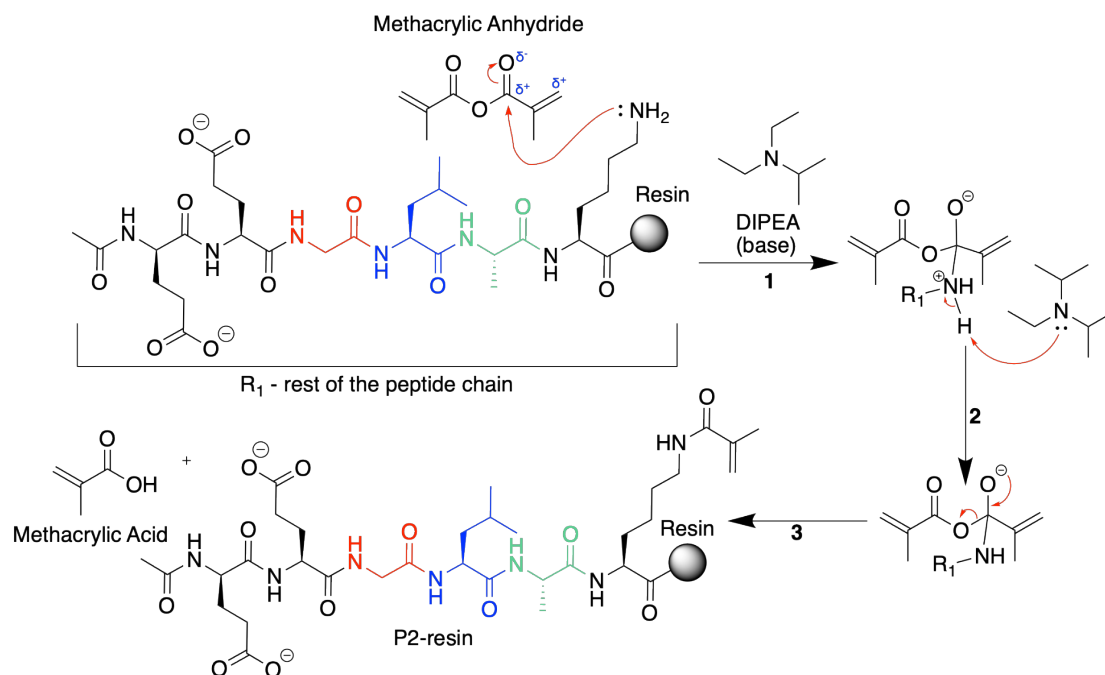


Figure 2.12 – Schematic representation of the coupling mechanism of the methacrylate group to the main peptide sequence (**Ac-EEGLAK-NH₂**) using methacrylic anhydride and *DIPEA*.

Once the peptide synthesis was completed, HPLC (Figure 2.13) was used to observe the production of any side products, particularly **SP-1**. This was possible as the position of the impurity peaks (**SP-1** eluted at 22.28 min) on the chromatograms was already known. HPLC analyses of newly synthesized **P2** sequences (Figure 2.13b and c) showed the absence of the **SP-1** peak at 22.28 min, indicating that the use of methacrylic anhydride improved the favorability of the 1,2-addition pathway. As a result of this, the crude purity of **P2** did rise from 55 to 63 %, thus increasing the amount of purified product, which can be collected with HPLC (Figure 2.13a, b).

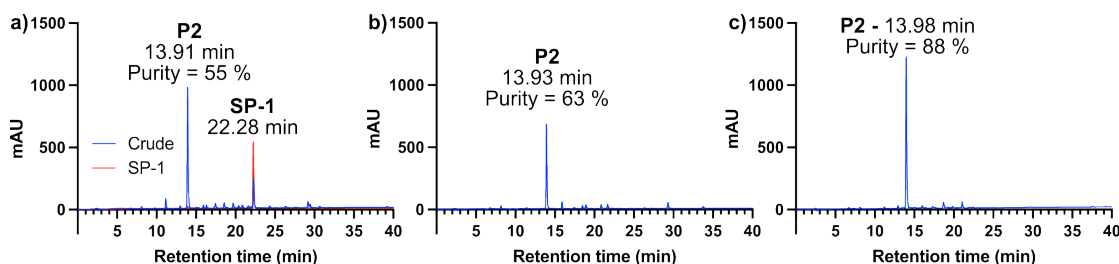


Figure 2.13 – RP-HPLC chromatograms a) to c) of crude **P2** (**Ac-EEGLAK-(COC(CH₃)CH₂)-NH₂**) with improving purities.

2.4.1.2 Further optimization of solid-phase peptide synthesis of P1/2 peptides

While the major side product (**SP-1**) was eliminated, there was still a range of small impurity peaks eluting between 14 to 35 min (Figure 2.14a), which together accounted for a substantial 37 % of the lost yield. Therefore, the goal was to increase the purity of the product peak with each peptide synthesis, primarily by improving manual handling techniques and engineering controls. This involved the use of double coupling for all residues, including methacrylic anhydride, and doubling of the reaction times. In addition to this, a filtration system was used instead of centrifugation to isolate the crude peptide solid after the resin cleavage step, which simplified the washing procedures.

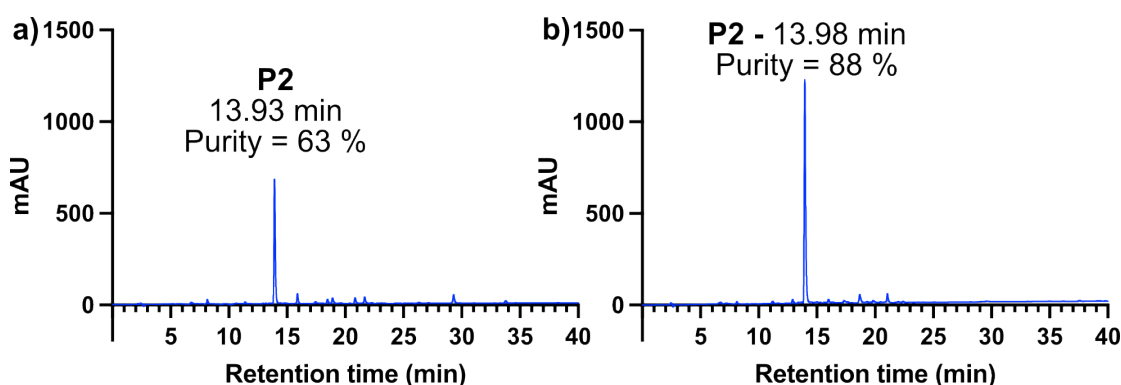


Figure 2.14 – RP-HPLC chromatograms a) to b) of crude **P2** (**Ac-EEGLAK-(COC(CH₃)CH₂)-NH₂**) with improving purities.

Together, these changes led to an increase in the crude purity from 63 to 88 % (Figure 2.14a compared to b), improving the amount of purified peptide that can be isolated.

However, all crude peptides still had to be purified before being used in polymerizations. This was crucial because consistent and comparable polymerization outcomes depended on the purity of the monomer used. For instance, the presence of DMF in the crude product of peptide synthesis led to poor water solubility of the monomer, which then required the use of a different solvent system for polymerization.

Initially, purifications were performed using a preparative HPLC system with manual fraction collection, which meant that occasional human errors led to partial losses of the collected products. For example, from the initially synthesized crude **P2** weighing 0.912 g (purity = 63 %), only 0.209 g of purified product was collected. On average, the synthesis and purification of the peptides **P1** and **P2** took at least 7 working days to complete. A total of 0.200 g of pure peptide monomer was enough to evaluate up to four different polymerization conditions (50 mg each). Unfortunately, this was not enough to identify the most suitable polymerization condition, so more material had to be synthesized. Consequently, in the later Chapters, an HPLC system with automatic fraction collection was used, which not only reduced the possibility of human error but also increased the purification throughput: 1.00 g of crude peptide per 2 days compared to the same amount per 3 - 4 days.

Therefore, by the end of all optimizations, an efficient workflow was established for the synthesis of LasB-responsive peptides **P1** and **P2**. This enabled the reliable production of a sufficient amount of material for the synthesis of enzyme-responsive polymers.

2.4.2 Synthesis of the polymers bearing enzyme-degradable side chains

Both **P1** and **P2** sequences have a methacrylamide group, which can be polymerized using a variety of polymerization techniques with control over the size of the polymer (e.g., reversible addition-fragmentation chain-transfer polymerization (RAFT),²⁸ atom transfer radical polymerization (ATRP)²⁹) and uncontrolled methods such as free radical polymerization (FRP).³⁰ In cases where the material's primary functions and properties depend on the polymer architecture (e.g., star, block, brush), size and chemical reactivity, controlled polymerization techniques are often preferred.^{31–34}

The goal of this project was to create enzyme-degradable PECs for the delivery of AMPs. The encapsulation component of these PECs had to meet two main criteria: enzyme-degradability and the ability to encapsulate AMPs. The enzyme degradation

properties were expected to depend on the peptide sequence specifically designed for this purpose, which formed the side chain of a polymer. The polymer backbone was thought to be a key structural element, which increased the multivalency and charge density of the material, facilitating the encapsulation of clinically approved AMP, e.g., Polymyxin B. Therefore, control over the polymer size was not the main focus. Instead, a reliable and straightforward polymerization approach was needed, which required minimal optimization, so that more time could be devoted to optimizing either the monomer composition or the particle assembly.

Additionally, it would be impractical to optimize the exact polymer size for a particular AMP because these agents are usually derived from bacteria as complex mixtures, with variations in component ratios from batch to batch. For example, Polymyxin B is extracted from cultures of various strains of *Bacillus polymyxa* as a combination of closely related peptides with different fatty acyl moieties and is commercially sold as a sulfate salt.^{35,36} The proportions of these peptide sequences in the purchased batches can vary, potentially requiring the use of a different polymer for effective encapsulation.^{35,36} Consequently, the search for the ideal polymerization conditions would need to be done again for each of the new batches of Polymyxin B.

Nevertheless, at an early stage of the project, a controlled radical polymerization in the form of RAFT was attempted (Figure 2.15, Table 2.4).

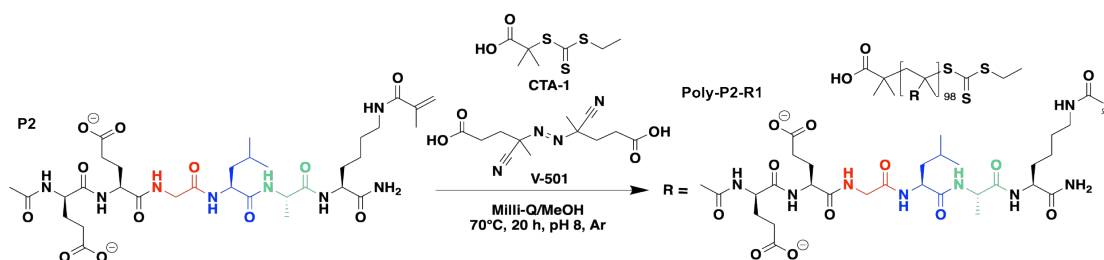


Figure 2.15 – Reaction scheme for RAFT polymerization of **P2** monomer, represents synthesis of **Poly-P2-R1** and **R2**.

As a chain transfer agent, **CTA-1** - (2-((Ethylthio)carbonothioyl)thio-2-methylpropanoic acid) was selected because it was not only suitable for the polymerization of methacrylamides ("more activated monomers"), but it was also commonly used in our laboratory for RAFT polymerizations (Figure 2.15, Table 2.4).^{28,37,38} Furthermore, owing to the limited solubility of the **P2** monomer in various organic solvents, water under basic pH conditions (*i.e.*, ≥ 8.0) was identified as the optimal medium for the polymerization reactions. Consequently, a water-soluble initiator, **V-501** (4,4'-Azobis(4-cyanopentanoic acid)) compatible with the **CTA-1** was used.

Table 2.4 – Summary of the concentrations and conditions of attempted RAFT polymerizations. **P2 (Ac-EEGLAK(COC(CH₃)CH₂)-NH₂)** used as a monomer, **CTA-1** (2-((Ethylthio)carbonothioyl)thio-2-methylpropanoic acid) as a chain transfer agent and **V-501** (4,4'-Azobis(4-cyanopentanoic acid)) as thermal initiator.

Pol-ID	Materials	mg	[M] ₀	[M] _f	Solvent (mL)	R (Molar)	Target DP	
Poly-P2-R-1	P2	50.0	0.0664	0.166	0.400 (50/50 % Milli-Q/MeOH + Na ₂ CO ₃)	100	78	
	CTA-1	0.190	0.000847	0.00212		1.28		
	V-501	0.0380	0.000136	0.000339		0.204		
Poly-P2-R-2	P2	50.0	0.0664	0.221	0.300 (50/50 % Milli-Q/MeOH + Na ₂ CO ₃)	100		
	CTA-1	0.190	0.000847	0.00282		1.28		
	V-501	0.0380	0.000136	0.000452		0.204		
Reacted for 20 hours at 70 °C.								

¹H-NMR was a primary technique used to monitor monomer conversion in all polymerizations discussed in this Chapter. Vinylic protons peaks in the methacrylate group (5.0 - 6.0 ppm) were carefully monitored, with a decrease in integrations, indicating the degree of conversion of **P2** into the polymeric form, **Poly-P2**. Equation 2.2 was used to obtain % conversion, where H_{ref} corresponds to the integration of the H^δ-Lue peaks at 0.85 ppm (6 H, dd, J = 14.3, 6.5 Hz), H_m and H_p correspond to the proton signals at 5.29 and 5.62 ppm of the C = C bond (1 H, s) in the monomer (*i.e.*, H_m) at the start of the reaction and in the polymer (*i.e.*, H_p) at the end of the polymerization.

$$Monomer\ Conversion = \left(1 - \frac{\frac{H_p}{H_{ref}}}{\frac{H_m}{H_{ref}}}\right) \times 100\% \quad (2.2)$$

None of the RAFT conditions (Table 2.4) attempted resulted in monomer conversion, as can be seen by the lack of any decrease in the integration of vinylic protons in the NMR analyses of **Poly-P2-R-1** and **Poly-P2-R-2** (Figure 2.16).

It was hypothesized that the main causes of the unsuccessful RAFT attempts were related to significantly diminished polymerization rate (*i.e.*, R_p) as well as the degradation of the RAFT agent at basic pH conditions. The dependence of R_p on the pH and solvent of the reaction was reported by Lacik, Buback and others in the context of aqueous polymerization of methacrylic acid.^{39–42} They reported that the propagation rate coefficient k_p for the polymerization of methacrylic acid decreased by a one order of magnitude upon ionization of the methacrylic acid due to lowering of the pre-exponential factor in the Arrhenious equation.³⁹ This reduction was associated with the hindrance of the internal rotational mobility of the transition state structure of the methacrylic acid

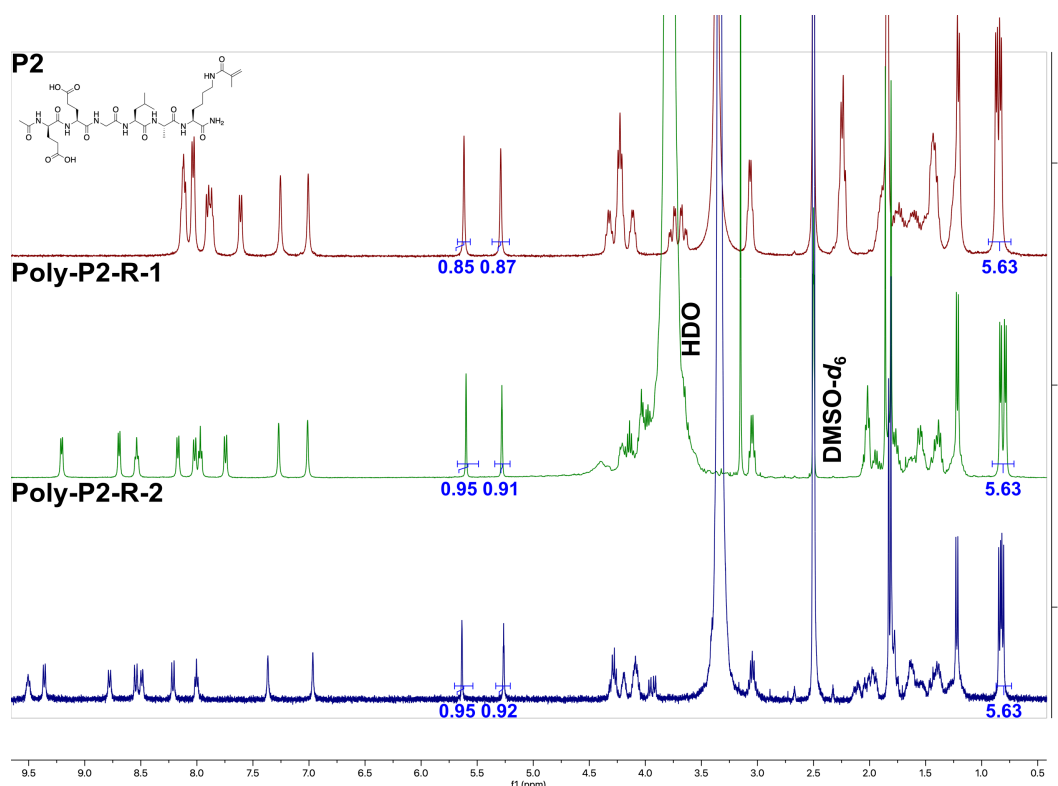


Figure 2.16 – Comparison of $^1\text{H-NMR}$ (400 MHz, $\text{DMSO-}d_6$) spectra of **P2** (**Ac-EEGLAK(COC(CH₃)CH₂)-NH₂)**) with **RAFT** polymerization reaction products **Poly-P2-R-1** and **Poly-P2-R-2**.

caused by strong intermolecular interactions such as H-bonding and electrostatics between the carboxylic groups.^{39,42}

In case of **P2** monomer, it contains a notably higher number of hydrogen bond donor (*i.e.*, eight amides and two carboxylic acids) and acceptor groups (*i.e.*, ten carbonyl groups) including additional carboxylic acid group compared to the methacrylic acid. Therefore, it is possible that strong secondary interactions between the transition state structures of **P2** significantly decreased the polymerization rate. Additionally, the use of basic pH ($\text{pH} \geq 8.0$) for solubilizing the peptide monomer could have caused hydrolysis of the **RAFT** agent, which in some cases can lead to creation of radical scavengers or retarders, inhibiting the polymerization completely.^{28,37,38} Therefore, it was clear that further optimization of the **RAFT** polymerisations were necessary, requiring a significant amount of purified peptide monomers to cover a wide range of different reaction conditions.

Given that precise control over polymer size was not prioritized, the decision was

made to use a free-radical polymerization technique that had previously proven successful in our laboratory for synthesizing elastin-like peptides. The same thermal initiator as for RAFT polymerisations was used in all of the FRP reactions, 4,4-Azobis(4-cyanovavric acid) (V-501) (see Figure 2.17).

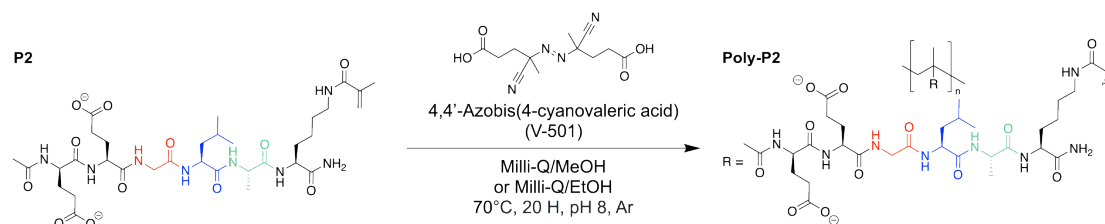


Figure 2.17 – Reaction scheme for the synthesis of **Poly-P2** (poly(Ac-EEGLAK(CO-C(CH₃)CH₂)-NH₂)). The same reaction scheme applies for **Poly-P1** (poly(Ac-EGLAK-COC(CH₃)CH₂)-NH₂)).

As a starting conditions for the FRP, molar ratios between the monomer and the initiator molecules were set at 100:2.15 (Table 2.5), similar to previously reported successful polymerizations of peptides.⁴³

Table 2.5 – Summary of free-radical polymerization conditions and reactant concentrations, where **P2** (Ac-EEGLAK(COC(CH₃)CH₂)-NH₂) is a monomer and **V-501** (4,4'-Azobis(4-cyanopentanoic acid)) is a thermal initiator.

Pol-ID	Materials	mg	[M] ₀	[M] _f	Solvent (mL)	R (Molar)
Poly-P2-1	P2	50	0.0662	0.0662	1.00	100
	V-501	0.40	0.00143	0.00143	(50/50 % Milli-Q/MeOH + Na ₂ CO ₃)	2.15
Poly-P2-2	P2	50	0.0662	0.0884	0.750	100
	V-501	0.40	0.00143	0.00190	(50/50 % Milli-Q/MeOH + Na ₂ CO ₃)	2.15
Poly-P2-3	P2	50	0.0662	0.133	0.500	100
	V-501	0.40	0.00143	0.00285	(50/50 % Milli-Q/MeOH + Na ₂ CO ₃)	2.15
Poly-P2-4	P2	50	0.0662	0.133	0.500	100
	V-501	0.40	0.00143	0.00285	(50/50 % Milli-Q/MeOH + Na ₂ CO ₃)	2.15
Reacted for 20 hours at 70 °C.						

During optimization of FRP, different conditions were investigated, mainly focusing on changing the reaction volume *i.e.*, increasing or decreasing the concentration ([M]_f in Table 2.5) of the components in the reaction while maintaining the same reaction time of 20 hours and temperature 70 °C (Table 2.5, Figure 2.17). For that purpose, **P2** sequence was chosen, as it was considered the most suitable candidate for the assembly of polyelectrolyte complexes with AMPs as a result of its higher multivalency. As with

RAFT polymerizations, NMR was used to confirm the degree of monomer conversion (Figure 2.18) with all **Poly-P2** samples showing close to 99 % conversion.

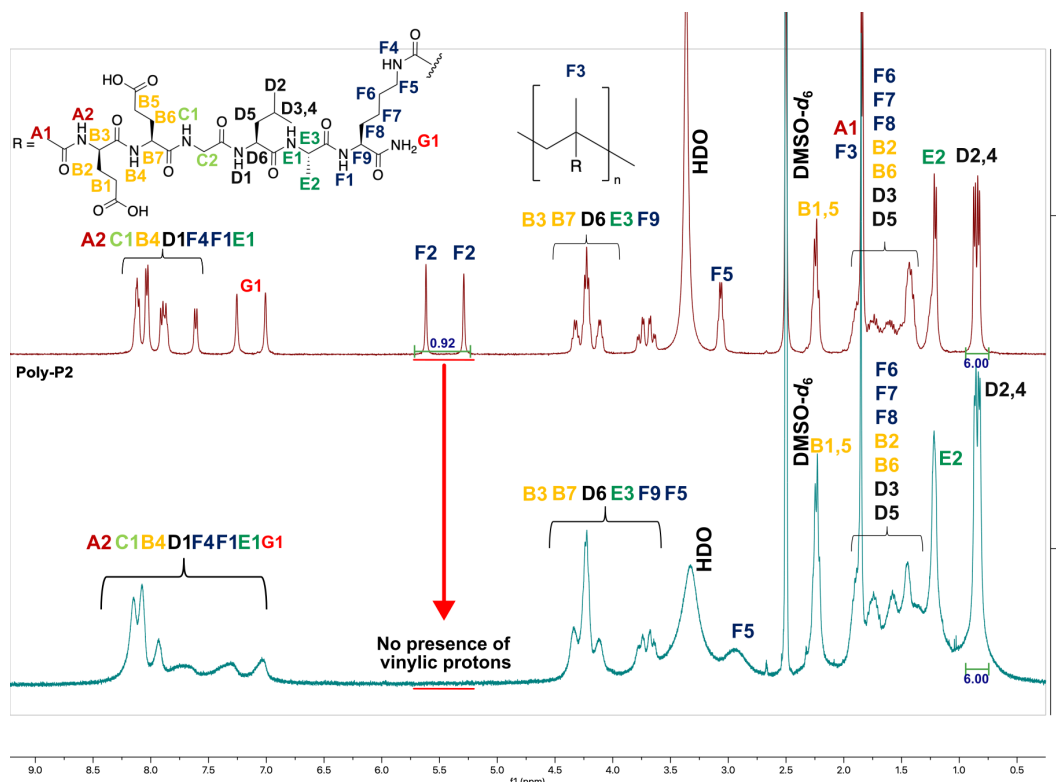


Figure 2.18 – Comparison of $^1\text{H-NMR}$ (400 MHz, DMSO-d_6) spectra of **P2** (**Ac-EEGLAK(COC(CH₃)CH₂)-NH₂**) with the polymerization reaction product **Poly-P2** (**poly(Ac-EEGLAK(COC(CH₃)CH₂)-NH₂)**).

More importantly, to understand how different reaction volumes affected polymer size, the GPC analyses of the **Poly-P2** samples were compared (Figure 2.19). As expected, FRP of **P2** at decreased concentrations (**Poly-P2-1** - 0.0662 M and **Poly-P2-2** - 0.0884 M) produced polymers with the lowest size dispersity (Đ) and degree of polymerizations (Dp) (Figure 2.19). By reducing the reaction volume by half, the degree of polymerization increased significantly from 22 and 16, to 56. However, the molecular weight distribution was bimodal, suggesting that the coupling reaction was occurring between the formed macromolecules, as polymerization was approaching 100 % conversion.³⁷ Furthermore, when working with reaction volumes less than 1 mL, the observed increase in the viscosity of the reaction mixture made it difficult to fully homogenize the components, which produced inconsistencies between batches under the same conditions as can be seen when comparing the size distributions of **Poly-P2-3** with **Poly-P2-4**. This engineering problem was quickly resolved using an improved homogenization setup, as well as substituting the rest of the organic solvent (*i.e.*, 50 %) with water (**V-501** initiator was still dissolved in MeOH or EtOH).

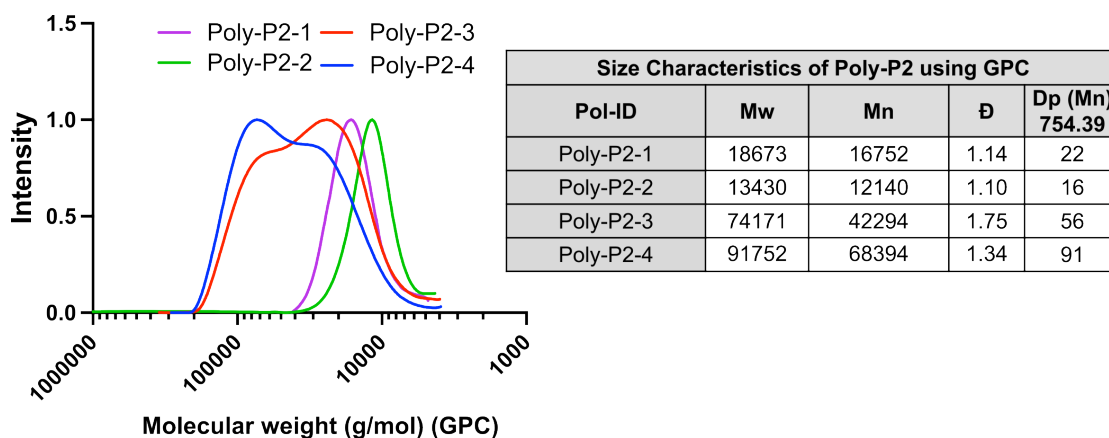


Figure 2.19 – GPC chromatograms of synthesized **Poly-P2** (**poly(Ac-EEGLAK(COC-(CH₃)CH₂)-NH₂)** polymers. Molecular masses were calculated based on a standard calibration method using poly(ethylene glycol) standards.

In general, the polymerization conditions used for the synthesis of **Poly-P2-4** produced the polymer with the highest **Dp** of 91, while still having a relatively low **Đ** of 1.34 (Figure 2.19). Furthermore, **Dp** was the key metric used to predict the likelihood of **PECs** formation since it reflects the degree of multivalency of the anionic polymer. For example, **Poly-P2-4** with **Dp** = 91 contains 182 (2 per each repeating unit) anionic groups, which is more than in the anionic polymer such as **PSS** with **Dp** = 141 *i.e.*, has 141 anionic groups, one per repeating unit. However, it is important to highlight that **GPC** analyses produces molecular weight data relative to the standards and solvents employed. In this work, poly(ethylene glycol) was used as a standard, which has significantly different molecular conformation compared to **Poly-P2** in aqueous environment. The presence of intermolecular interactions (*i.e.*, H-bonding, electrostatic, hydrophobic) between the **Poly-P2** repeating units could potentially induce the formation of secondary structures, resulting in polymers existing in different conformations depending on the **GPC** conditions (*i.e.*, solvent, temperature). This phenomenon is particularly notable in aqueous phase **GPC**, where the mobile phase, such as water, can interact with **Poly-P2** via H-bonding, leading to changes in polymer conformation (*e.g.*, polymer chains become more closely packed), thereby producing size information that may not accurately represent the actual polymer size. Consequently, the parameters obtained from the aqueous phase **GPC** analyses discussed in this Thesis have to be treated with caution, especially the dispersity (**Đ**), which is surprisingly low for **FRP** polymerisations. Nonetheless, at that time, aqueous **GPC** was the only suitable polymer size characterization technique, and there were no strict requirements for the molecular weights of the encapsulating polymer for design of the encapsulation material. Therefore, it was concluded that the reaction conditions for **Poly-P2-4** yielded optimal results, and as a result, they were utilized for the synthesis of subsequent **Poly-P2** polymers.

2.4.3 Enzymatic degradation of poly(methacrylamides) with peptide side chain

Before starting the assembly of the delivery system, the enzyme degradation properties of synthesized polymers **Poly-P1** and **Poly-P2** had to be evaluated using **LasB** as a stimulus. However, we were unable to find a supplier for **LasB** and instead used a different enzyme, thermolysin. Thermolysin has similar specificity as **LasB** *i.e.*, they both prefer to cleave hydrophobic residues (amino endopeptidases).^{5,44,45} Furthermore, thermolysin was readily available in sufficient quantities, making it ideal for performing a wide range of experiments.

In the -GLA- sequence present in all peptides discussed in this chapter, thermolysin would hydrolyze the bond between the Gly and Leu residues.^{5,44,45} Therefore, enzyme degradation of **Poly-P2** would result in the creation of two degradation products **DP-1** (with carboxylate terminus) and **DP-2** (with amine terminus) as presented in Figure 2.20. Consequently, a fluorogenic assay based on fluorescamine was used to detect the concentration of **DP-2** product in the enzyme degradation reaction solutions. This assay reacts with any of the available primary amine groups (primarily with **DP-2**), forming fluorescent conjugates that, when excited at 355 nm, emit a signal at 460 nm. Therefore, the intensities of the emission can be correlated with the degree of thermolysin-induced degradation of polymers **Poly-P1** and **Poly-P2** (experimental conditions can be found in Section 2.3.5 and Table 2.2).

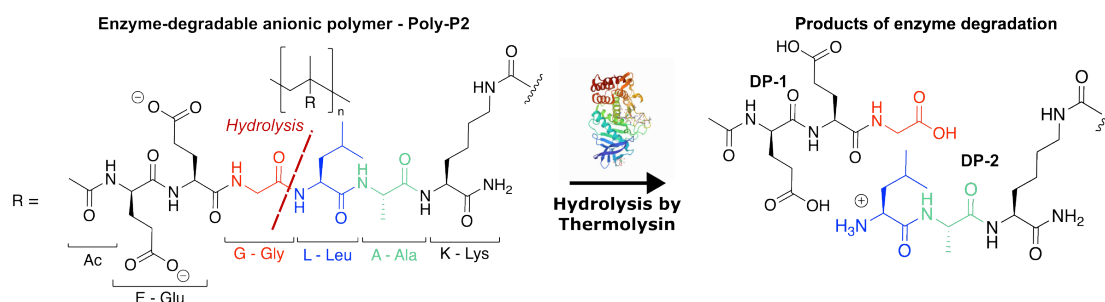


Figure 2.20 – Schematic representation of enzymatic degradation of **Poly-P2** which leads to the creation of degradation products **DP-1** and **DP-2**.

Sample aliquots were collected every hour for a total of five time points, which included relevant control samples (buffer, thermolysine, polymer controls **Poly-P1** and **Poly-P2**), including evaluation of thermolysin activity by monitoring succinyl casein degradation.¹¹ Subsequently, the emission intensities were normalized (Figure 2.21, for unnormalized emission intensities see Figure S2.29) to those produced by a model peptide **P3** ($\text{H}_2\text{N-LA-NH}_2$), which represented the simplified enzyme degradation product of the -GLA- peptide sequences.

Normalized emission intensities of fluorescamine conjugates

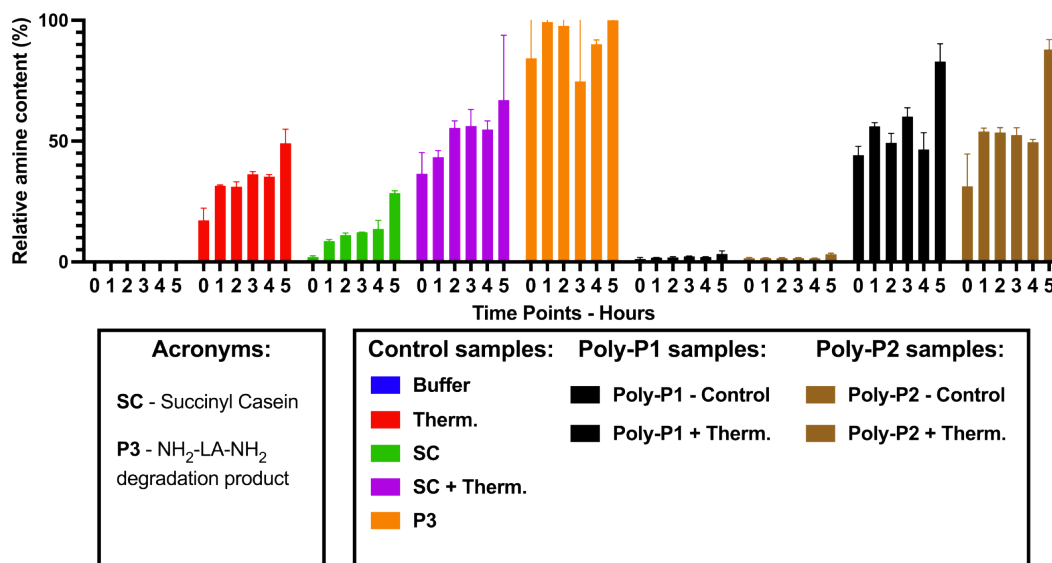


Figure 2.21 – Relative amine content (%) in samples of thermolysin-responsive polymers **Poly-P1** ($\text{poly}(\text{Ac-EG}(\text{LA}(\text{COC}(\text{CH}_3)\text{CH}_2)\text{-NH}_2))$) and **Poly-P2** ($\text{poly}(\text{Ac-EEGLAK}(\text{COC}(\text{CH}_3)\text{CH}_2)\text{-NH}_2))$) evaluated in this work. The relative amine content was calculated from fluorescamine conjugates formed after incubation with enzymes for 5 hours and normalized to the fluorescence observed with a model degradation peptide (**P3**). Emissions normalized for **Poly-P1** and **Poly-P2**, HEPES, CaCl_2 , $\text{Na}_2\text{B}_4\text{O}_7$ buffer (Buffer), Thermolysin as enzyme control (Therm.), succinyl casein (SC) as a control for enzymatic activity, degradation peptide $\text{H}_2\text{N-LA-NH}_2$ (**P3**) as a control to normalize fluorescence intensity. For unnormalized data, see Figure S2.29. Incubation time: 5 hours. $n = 3$.

Both non-enzyme treated samples of **Poly-P1** and **Poly-P2** (labeled **Poly-P1** - control and **Poly-P2** - control in Figure 2.21), showed a minimal increase in relative amine content (approaching 5%), which indicated no degradation. However, when thermolysin was added to **Poly-P1** and **Poly-P2**, a significant rise in amine content was observed with both polymers, reaching degradation of 80 % within 5 hours of an experiment (Figure 2.21). Interestingly, the degradation kinetics of these polymers were different, both showing distinct patterns. **Poly-P1** displayed a more fluctuating trend with a relative amine content that increased between T0 - T1, T2 - T3, T4 - T5 and decreased between T1 - T2 and T3 - T4. For example, in the first hour of an experiment, the relative amine content of **Poly-P1** increased from 44 to 56 % but then dropped to 49 %. In comparison, **Poly-P2** demonstrated burst-like degradation characteristics. The relative amine content of **Poly-P2** increased from 31 to 54 % within the initial hour, remaining relatively stable for the following 3 hours and then rapidly rising to 88 % at the 5-hour mark. However, in general, both polymers showed a significant increase in the relative amine content in the presence of thermolysin, which confirmed the enzyme sensitivity of the polymers.

To further investigate the differences in enzyme degradation characteristics, ζ -potential measurements were used. With the degradation of **Poly-P1** and **Poly-P2**, more positively charged groups should be produced in the form of protonated primary amines (Figure 2.20), leading to an increase in ζ -potentials (*i.e.*, become more positive) of any self-assembled peptide conjugates. In particular, this effect would be more extensive in the bacterial microenvironment as a result of the acidification that is typically caused by the release of anaerobic metabolites by pathogens.^{46,47}

Within the first hour of the experiment, ζ -potentials of **Poly-P2** rapidly increased from -5.80 to 1.25 mV (a difference of 7.05 mV) after which they remained constant (Figure 2.22), which confirmed that the polymer was being degraded by enzymes. The ζ -potentials of **Poly-P1** also became more positive, but the total charge change was only 3.66 mV. Notably, ζ -potentials data had similar characteristics to fluorescence - **Poly-P2** degraded in a burst and **Poly-P1** had a fluctuating pattern.

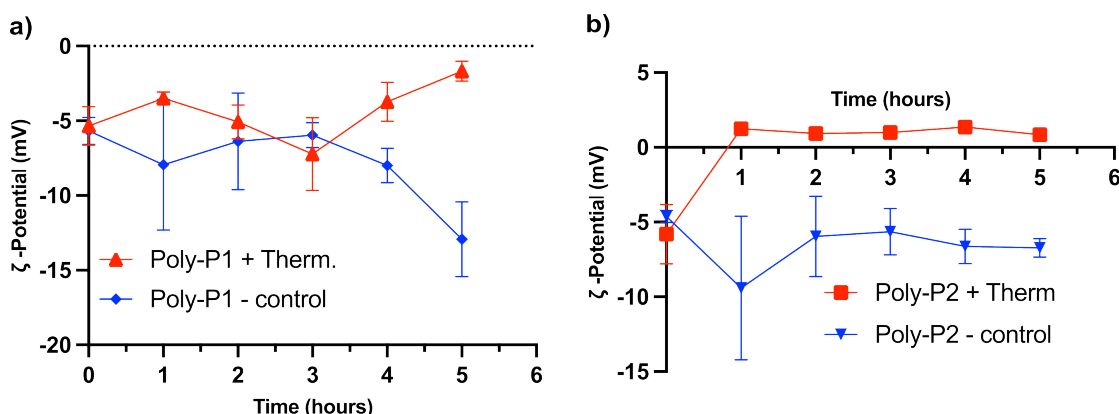


Figure 2.22 – Enzymatic degradation of a) **Poly-P1** (**poly(Ac-EGLAK(COC(CH₃)CH₂)-NH₂))** and b) **Poly-P2** (**poly(Ac-EEGLAK(COC(CH₃)CH₂)-NH₂))** monitored with ζ -potentials. Average data is presented from 3 technical replicates \pm standard deviation ($n = 3$). For enzyme degradation procedure, see Section 2.3.5.

The difference in the number of anionic residues present in the peptides (**P1** and **P2**) can explain the observed variations in the zeta potential between **Poly-P1** and **Poly-P2**. **Poly-P2** peptide side chain has one extra glutamic acid, which would be protonated under acidic conditions (Glu side chain pK_a = 4.25), resulting in a more pronounced change in zeta potentials of 7.05 mV, almost twice that of **Poly-P1** (3.66 mV). Moreover, thermolysin and LasB enzymes require zinc metal for their activity. Therefore, metal chelation groups, such as carboxylates in glutamic acids, would inhibit enzymatic activity.^{5,45} That is why the degradation of **Poly-P2** occurred rapidly in the initial hour of the experiment (*i.e.*, equilibration step) and then stayed stable for 3 hours while Zn metal was chelated by the side chains of the peptides. As degradation advanced, the pH of the environment became more acidic, resulting in the protonation of carboxylate

groups, which weakened the chelation effect. This allowed the enzyme activity to be restored, leading to an increase of 33 % in the relative amine content within an hour.

In summary, two polymers with different peptide side chains **Poly-P1** and **Poly-P2** degraded to a similar extent within 5 hours of an experiment, despite having different degradation profiles. The presence of extra glutamic acid in **Poly-P2** caused inhibition of enzyme activity for 3 hours, which was quickly restored in the last hour of the experiment. This behavior was attributed to the chelation effect of carboxylate groups. Nevertheless, in a particle system such as **PECs**, this effect should be significantly reduced, as carboxylate groups would be partially occupied by electrostatic interactions with cationic **AMP**.

2.5 Conclusions

The development of enzyme-responsive delivery systems, such as [PECs](#), can be divided into two parts: the design and synthesis of the encapsulation component with stimuli-responsive properties and the assembly of the delivery system with the desired drug. This Chapter described the synthesis of an enzyme-responsive polymer for the encapsulation of [AMP](#) inside polyelectrolyte nanoparticles.

As a target pathogen *P. aeruginosa* was selected due to being a difficult pathogen to treat with conventional antibiotics, as a result of its resistance mechanisms. Consequently, polymers had to be sensitive towards [LasB](#), an enzyme released by Gram-negative pathogen *P. aeruginosa* as well be able to encapsulate the cationic [AMP](#). Based on these requirements, two new enzyme-degradable polymers bearing enzyme-degradable side chains, **Poly-P1** and **Poly-P2**, were created. These polymers had a brush-like structure in which the peptides represented the side chain of the poly(methacrylamide) backbone. Peptide sequences **P1** (**Ac-EGLAK(COC(CH₃)CH₂)-NH₂)**) and **P2** (**Ac-EEGLAK(COC(CH₃)CH₂)-NH₂)**) specifically contained [LasB](#)-responsive sequence (-GLA-) as well anionic residues (E) with the polymer backbone attached to the Lys side chain through amide bond.

The workflow for the preparation of peptide monomers (solid-phase peptide synthesis and purification) was optimized to reduce the formation of by-products and to increase the yield of the purified product needed for polymerization reactions. Using purified peptide monomer **P1** and **P2**, optimal free-radical polymerization conditions were found for the reliable preparation of **Poly-P2** polymers with low $\bar{M}_n = 1.34$ and high $D_p = 91$.

Finally, the enzyme degradation properties of **Poly-P2** and **Poly-P1** were evaluated. Both polymers, **Poly-P1** and **Poly-P2** demonstrated mostly identical susceptibility to thermolysin degradation, which implies that they would also be sensitive to [LasB](#). Although the **Poly-P1** and **Poly-P2** were not specifically tested for degradation in the presence of elastase secreted by human leukocytes ([HLE](#)), it is worth noting that a similar [LasB](#)-degradable sequence (Ac-CE-GLA-EC-OH) demonstrated resistance to [HLE](#) degradation.⁶ Therefore, this chapter established that both **Poly-P1** and **Poly-P2** had suitable degradation properties for enzyme-responsive delivery of [AMPs](#) against *P. aeruginosa*. However, **Poly-P2** had greater multivalence than **Poly-P1**, suggesting that it could potentially lead to the formation of [PECs](#) with higher encapsulation efficiency and enhanced physiological stability. As a result, **Poly-P2** was selected as a candidate for the assembly of [PECs](#) with [AMPs](#), discussed in Chapter 4.

2.6 Supporting Information

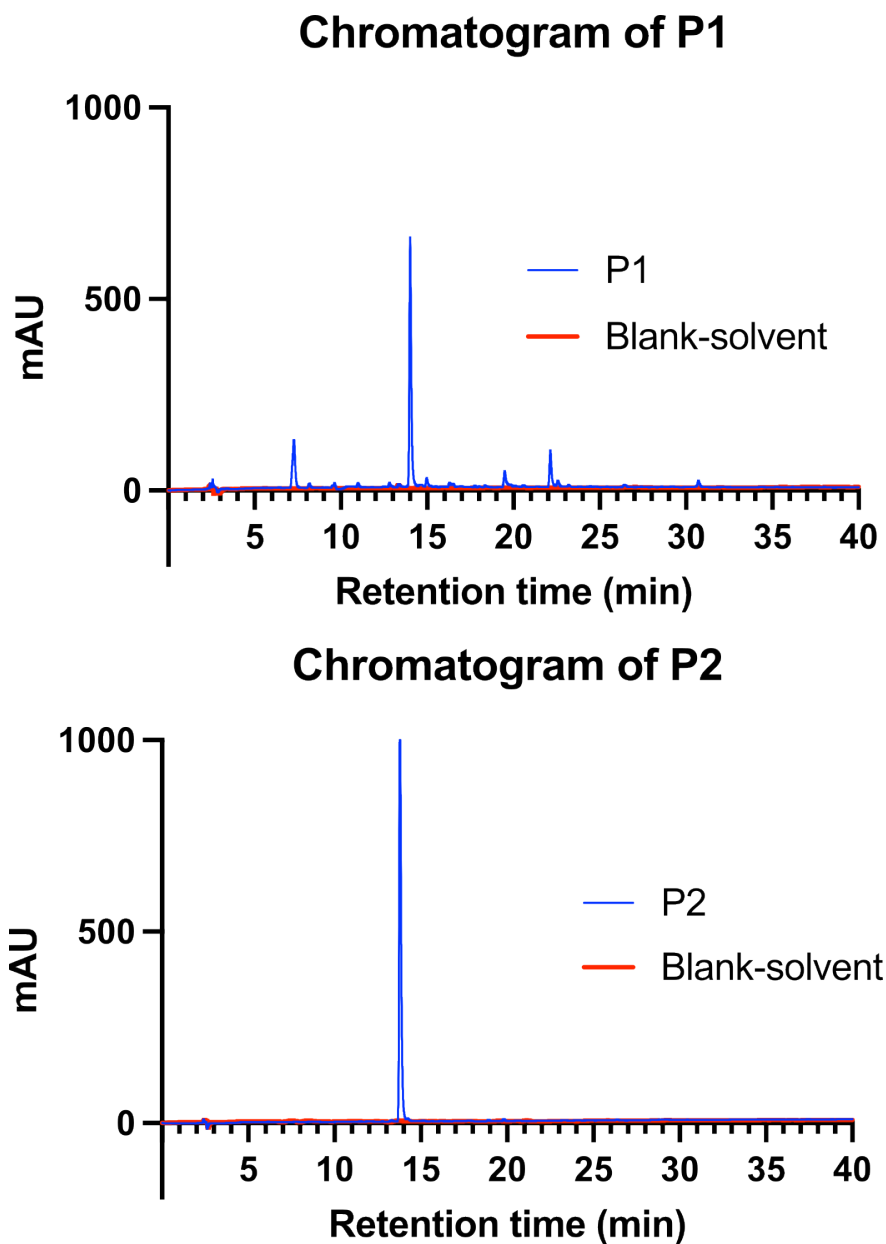


Figure S2.23 – Summary of RP-HPLC chromatograms of **P1** (Ac-EGLAK(COC(CH₃)CH₂)-NH₂) and **P2** (Ac-EEGLAK(COC(CH₃)CH₂)-NH₂).

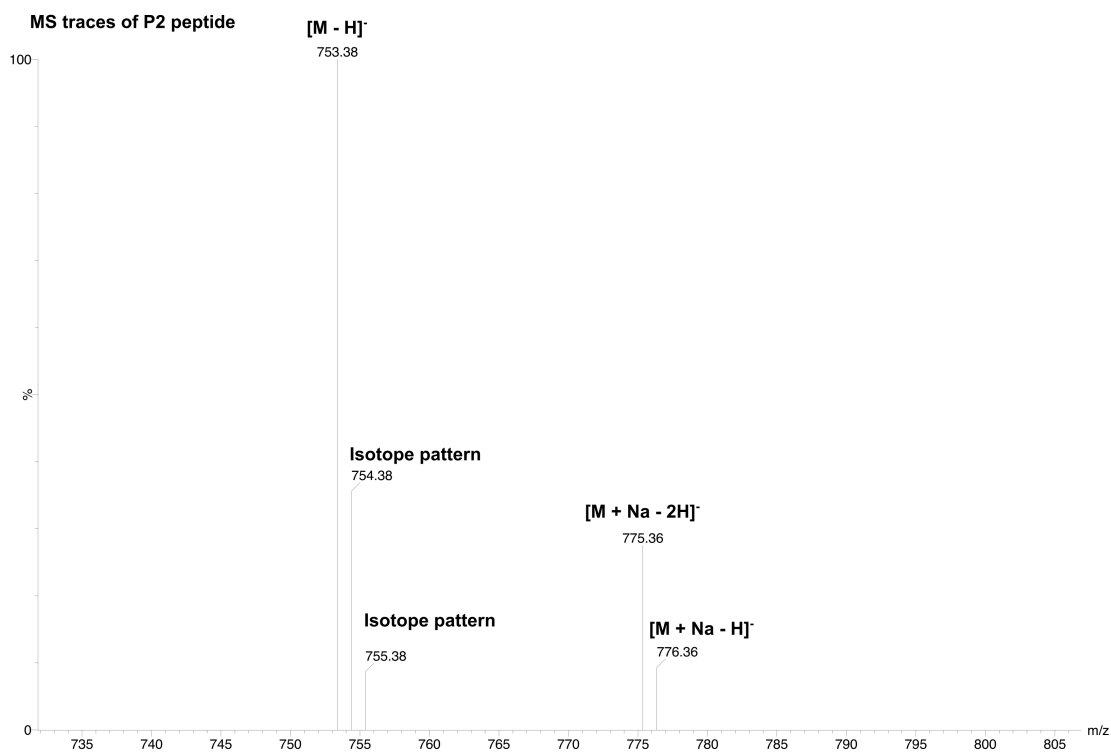
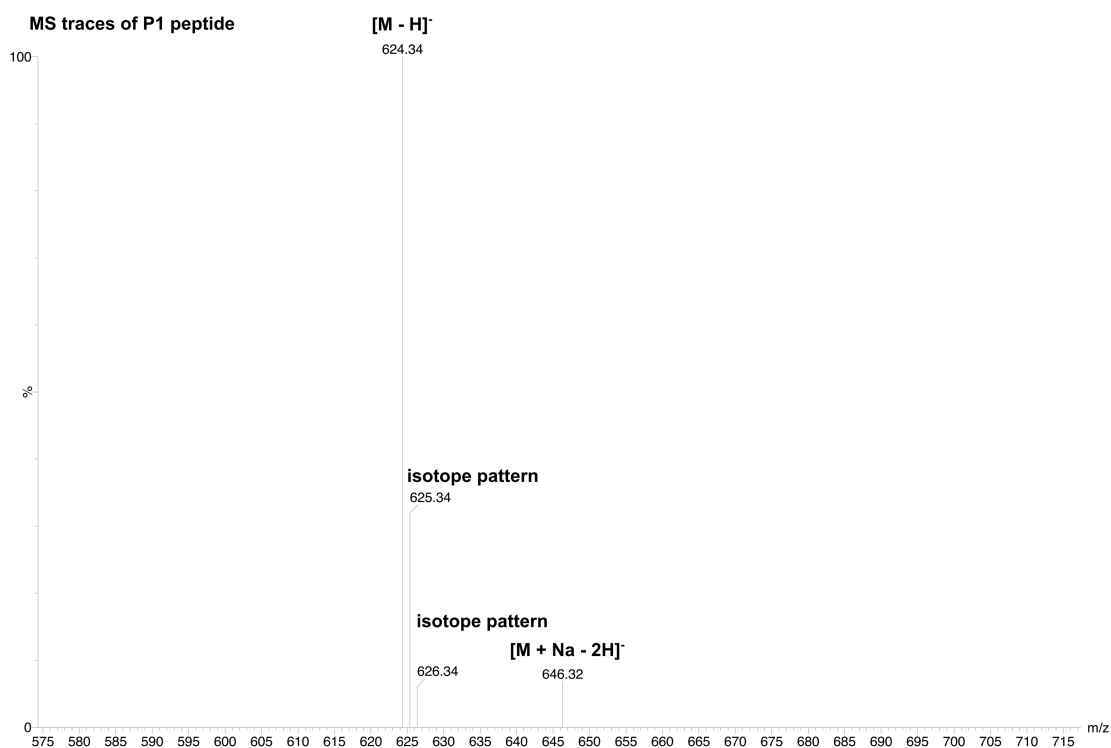


Figure S2.24 – MS traces for **P1** (Ac-EGLAK(COC(CH₃)CH₂)-NH₂) and **P2** (Ac-EEGLAK(COC(CH₃)CH₂)-NH₂) in negative ion mode.

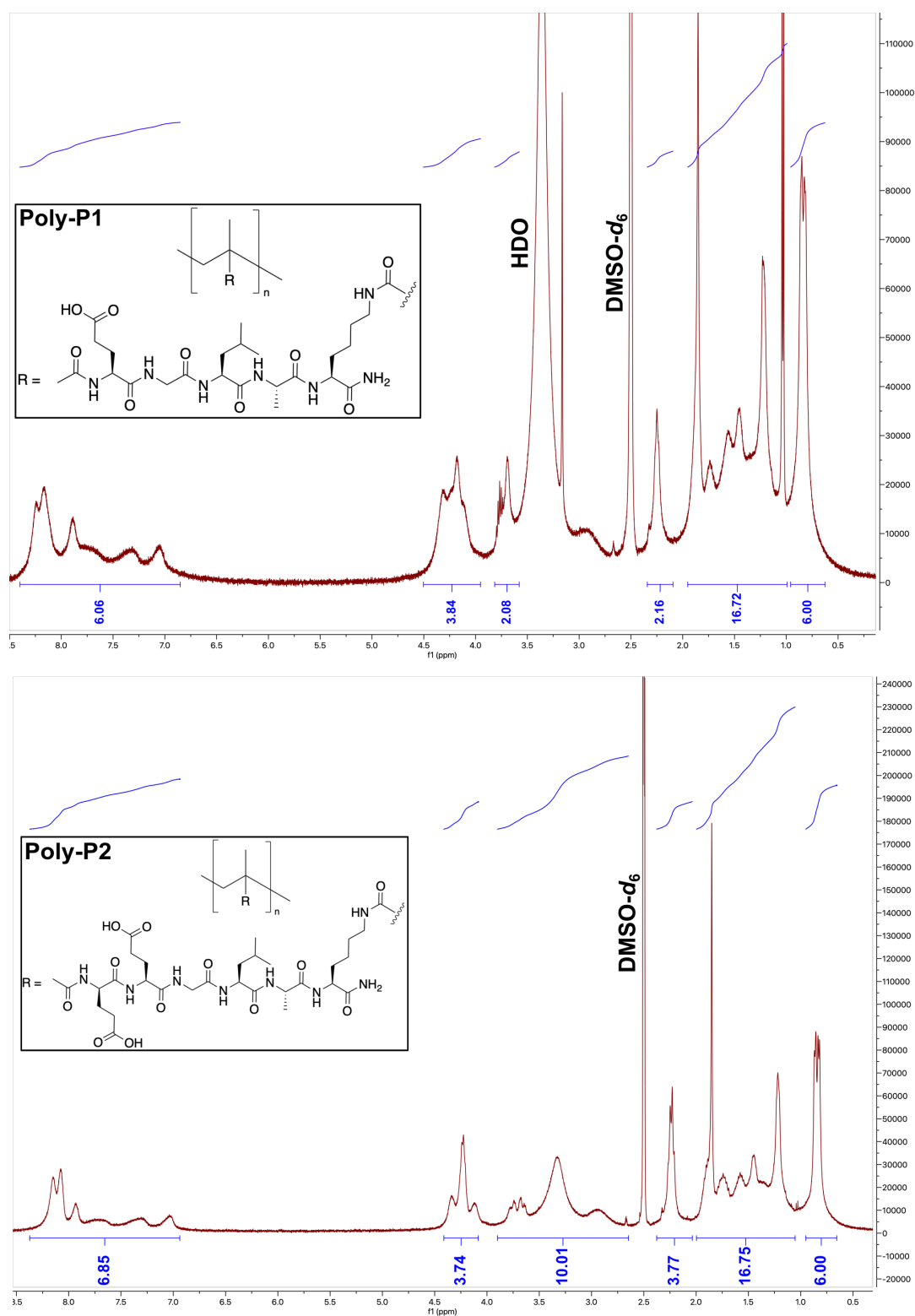
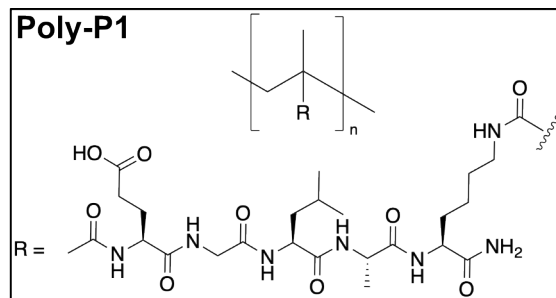
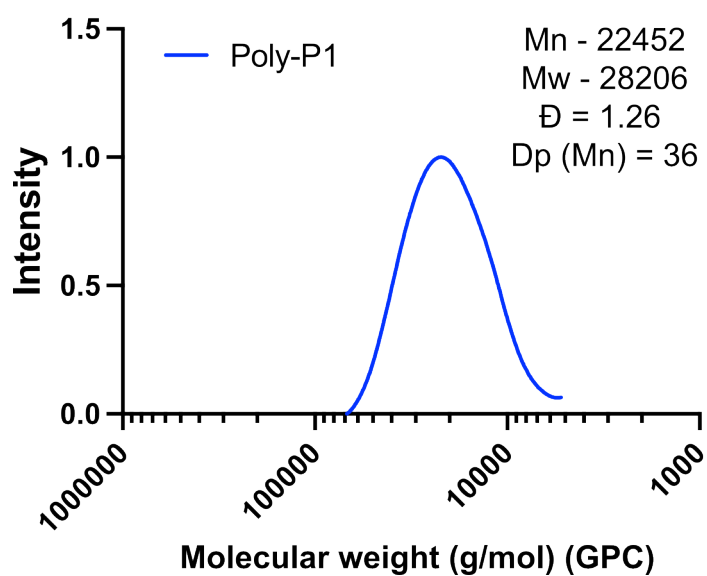


Figure S2.27 – $^1\text{H-NMR}$ (400 MHz, $\text{DMSO-}d_6$) (top) of **Poly-P1** ($\text{poly}(\text{Ac-EGLAK}(\text{COC}(\text{CH}_3)\text{CH}_2)\text{-NH}_2)$), $^1\text{H-NMR}$ (400 MHz, $\text{DMSO-}d_6$) (bottom) of **Poly-P2** ($\text{poly}(\text{Ac-EEGLAK}(\text{COC}(\text{CH}_3)\text{CH}_2)\text{-NH}_2)$).



Polymerisation conditions for FRP of P1	
Pol-ID	Poly-P1
mg	172/2.10 (V-501) Molar ratio of 100 to 2.15
[M] _r	0.551
Solvent (mL)	0.500
Reacted for 20 hours at 70 °C.	

Figure S2.28 – GPC chromatogram of **Poly-P1** (poly(Ac-EGLAK(COC(CH₃)CH₂)-NH₂)) with key polymerization reaction conditions.

Emission intensity of fluorescamine conjugates

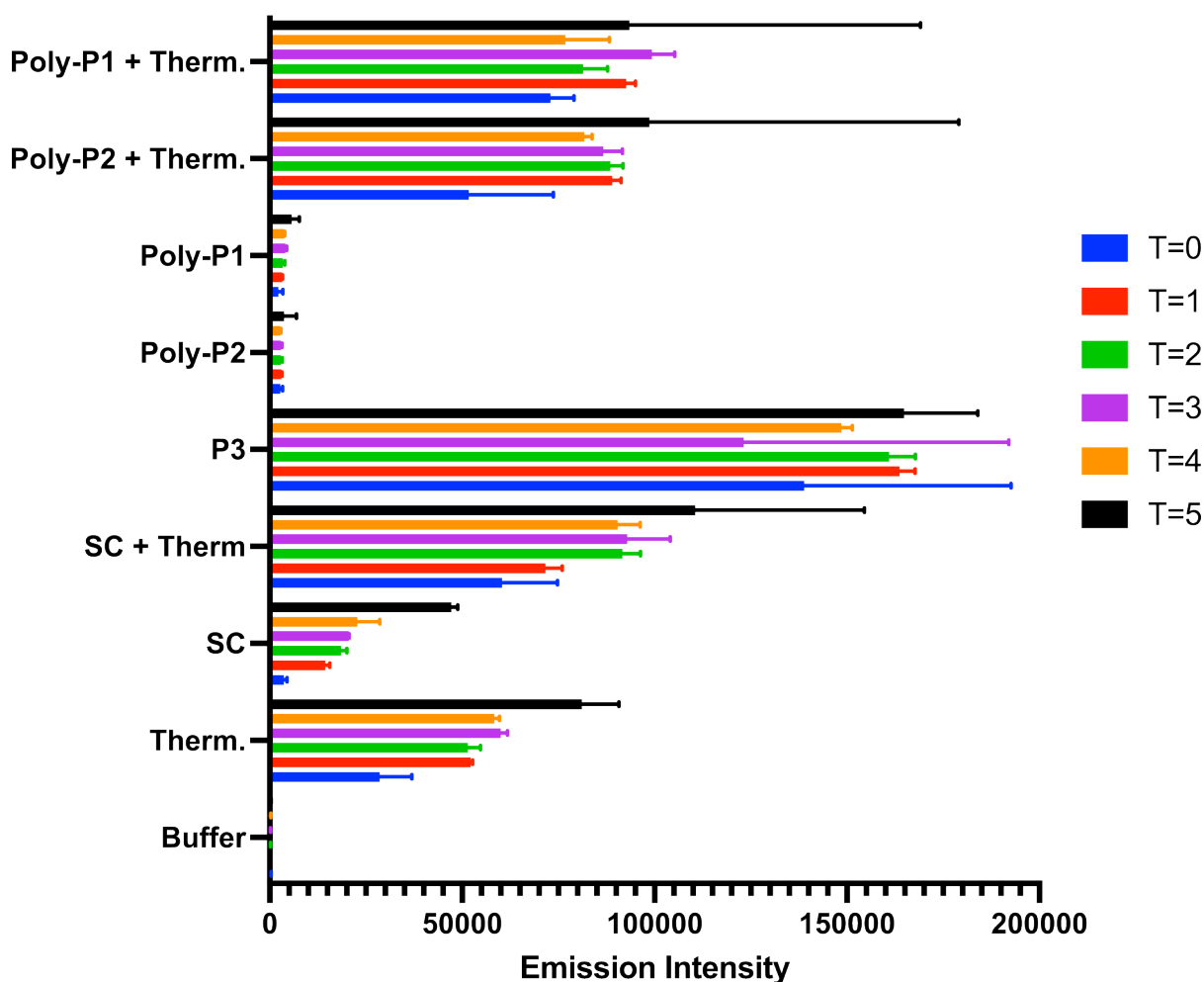


Figure S2.29 – Emissions intensity (λ_{exc} 355 nm, λ_{em} 470 nm) of fluorescamine conjugates for: HEPES, CaCl_2 , $\text{Na}_2\text{B}_4\text{O}_7$ buffer (Buffer), thermolysin as enzyme control (Therm.), succinyl casein (SC) as a control for enzymatic activity, degradation peptide **P3**($\text{H}_2\text{N-LA-NH}_2$) as a control to normalize fluorescence intensity, thermolysin-responsive polymers **Poly-P1** ($\text{poly}(\text{Ac-EG}(\text{LA}(\text{COC}(\text{CH}_3)\text{CH}_2)\text{-NH}_2))$) and **Poly-P2** ($\text{poly}(\text{Ac-EEGLAK}(\text{COC}(\text{CH}_3)\text{CH}_2)\text{-NH}_2)$). All substrates were evaluated in the absence and presence of thermolysin. Incubation time: 5 hours. $n = 3$.

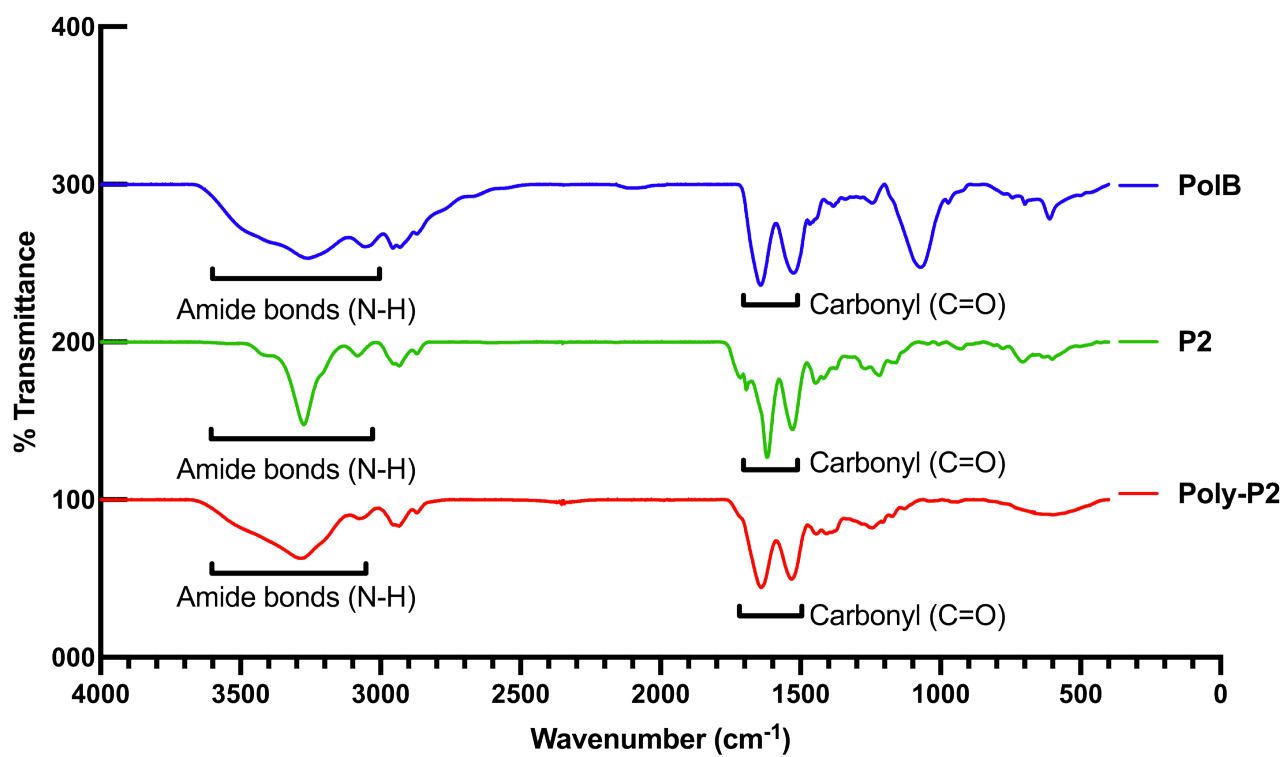


Figure S2.30 – Solid phase FTIR spectra of the antibiotic Polymyxin B (**PolB**), **P2** peptide and its polymer **Poly-P2**. $n = 1$

2.7 References

- [1] I. Insua, M. Petit, L. D. Blackman, R. Keogh, A. Pitto-Barry, R. K. O'Reilly, A. F. A. Peacock, A. M. Krachler and F. Fernandez-Trillo, *ChemNanoMat : chemistry of nanomaterials for energy, biology and more*, 2018, **4**, 807–814.
- [2] S. Qin, W. Xiao, C. Zhou, Q. Pu, X. Deng, L. Lan, H. Liang, X. Song and M. Wu, *Signal Transduction and Targeted Therapy*, 2022, **7**, 199.
- [3] B. Wretling and O. R. Pavlovskis, *Clinical Infectious Diseases*, 1983, **5**, S998–S1004.
- [4] J. M. SAULNIER, A. M. RAYSSIGUIE, M. C. DUCLOS and J. M. WALLACH, *Biochemical Society Transactions*, 1990, **18**, 900–901.
- [5] K. Morihara and T. Hiroshige, *Archives of Biochemistry and Biophysics*, 1971, **146**, 291–296.
- [6] I. Insua, E. Lamas, Z. Zhang, A. F. A. Peacock, A. M. Krachler and F. Fernandez-Trillo, *Polymer Chemistry*, 2016, **7**, 2684–2690.
- [7] I. Insua, S. Majok, A. F. A. Peacock, A. M. Krachler and F. Fernandez-Trillo, *European Polymer Journal*, 2017, **87**, 478–486.
- [8] I. Insua, L. Zismare, A. F. A. Peacock, A. M. Krachler and F. Fernandez-Trillo, *Scientific Reports*, 2017, **7**, 9396.
- [9] I. Insua, *Ph.D. thesis*, University of Birmingham, 2017.
- [10] J. Skey and R. K. O'Reilly, *Chemical Communications*, 2008, 4183–4185.
- [11] T. Hatakeyama, H. Kohzaki and N. Yamasaki, *Analytical Biochemistry*, 1992, **204**, 181–184.
- [12] I. Insua, A. Wilkinson and F. Fernandez-Trillo, *European Polymer Journal*, 2016, **81**, 198–215.
- [13] C. B. Bucur, Z. Sui and J. B. Schlenoff, *Journal of the American Chemical Society*, 2006, **128**, 13690–13691.
- [14] J. Fu and J. B. Schlenoff, *Journal of the American Chemical Society*, 2016, **138**, 980–990.

- [15] S. A. Abouelmagd, N. H. A. Ellah, O. Amen, A. Abdelmoez and N. G. Mohamed, *International Journal of Pharmaceutics*, 2019, **562**, 76–85.
- [16] F. Guibé, *Tetrahedron*, 1998, **54**, 2967–3042.
- [17] F. Fernández-Trillo, A. Duréault, J. P. M. Bayley, J. C. M. van Hest, J. C. Thies, T. Michon, R. Weberskirch and N. R. Cameron, *Macromolecules*, 2007, **40**, 6094–6099.
- [18] D. J. Keddie, *Chemical Society Reviews*, 2013, **43**, 496–505.
- [19] J.-F. Lutz, W. Jakubowski and K. Matyjaszewski, *Macromolecular Rapid Communications*, 2004, **25**, 486–492.
- [20] M. Teodorescu and K. Matyjaszewski, *Macromolecules*, 1999, **32**, 4826–4831.
- [21] O. Creese, P. Adoni, G. Su, A. Romanyuk and P. Fernandez-Trillo, *Polymer Chemistry*, 2019, **10**, 5645–5651.
- [22] J. M. do O, R. Foralosso, G. Yilmaz, F. Mastrotto, P. J. S. King, R. M. Xerri, Y. He, C. F. van der Walle, F. Fernandez-Trillo, C. A. Laughton, I. Styliari, S. Stolnik and G. Mantovani, *Nanoscale*, 2019, **11**, 21155–21166.
- [23] E. P. Magennis, N. Francini, F. Mastrotto, R. Catania, M. Redhead, F. Fernandez-Trillo, D. Bradshaw, D. Churchley, K. Winzer, C. Alexander and G. Mantovani, *PLOS ONE*, 2017, **12**, e0180087.
- [24] J. Cui, J. J. Richardson, M. Björnmalm, M. Faria and F. Caruso, *Accounts of chemical research*, 2016, **49**, 1139–1148.
- [25] R. Duncan, *Nature Reviews Drug Discovery*, 2003, **2**, 347–360.
- [26] A. Salvati, C. Åberg, T. d. Santos, J. Varela, P. Pinto, I. Lynch and K. A. Dawson, *Nanomedicine: Nanotechnology, Biology and Medicine*, 2011, **7**, 818–826.
- [27] J. Clayden, N. Greeves and S. Warren, *Organic Chemistry*, Oxford University Press, 2012, vol. 1.
- [28] S. Perrier, *Macromolecules*, 2017, **50**, 7433–7447.
- [29] Z. Li, J. Lyu, Y. Li, B. Qiu, M. Johnson, H. Tai and W. Wang, *Macromolecules*, 2023, **56**, 5111–5116.
- [30] V. F. Gromov, *Russian Chemical Reviews*, 1995, **64**, 87.
- [31] A. Blencowe, J. F. Tan, T. K. Goh and G. G. Qiao, *Polymer*, 2009, **50**, 5–32.

- [32] A. J. Limer, A. K. Rullay, V. S. Miguel, C. Peinado, S. Keely, E. Fitzpatrick, S. D. Carrington, D. Brayden and D. M. Haddleton, *Reactive and Functional Polymers*, 2006, **66**, 51–64.
- [33] N. Corrigan, K. Jung, G. Moad, C. J. Hawker, K. Matyjaszewski and C. Boyer, *Progress in Polymer Science*, 2020, **111**, 101311.
- [34] W. A. Braunecker and K. Matyjaszewski, *Progress in Polymer Science*, 2007, **32**, 93–146.
- [35] J. A. Orwa, A. V. Gerven, E. Roets and J. Hoogmartens, *Journal of Chromatography A*, 2000, **870**, 237–243.
- [36] *Polymyxin Antibiotics: From Laboratory Bench to Bedside*, ed. J. Li, R. L. Nation and K. S. Kaye, Springer Cham, 2019, vol. 1145.
- [37] L. Albertin, M. H. Stenzel, C. Barner-Kowollik and T. P. Davis, *Polymer*, 2006, **47**, 1011–1019.
- [38] J. Chiefari and E. Rizzardo, in *Handbook of Radical Polymerization*, John Wiley & Sons, Ltd, 2002, pp. 629–690.
- [39] I. Lacík, L. Učňová, S. Kukučková, M. Buback, P. Hesse and S. Beuermann, *Macromolecules*, 2009, **42**, 7753–7761.
- [40] S. Beuermann, M. Buback, P. Hesse and I. Lacík, *Macromolecules*, 2006, **39**, 184–193.
- [41] S. Beuermann, M. Buback, P. Hesse, F.-D. Kuchta, I. Lacík and A. M. v. Herk, *Pure and Applied Chemistry*, 2007, **79**, 1463–1469.
- [42] I. Chaduc, M. Lansalot, F. D’Agosto and B. Charleux, *Macromolecules*, 2012, **45**, 1241–1247.
- [43] N. M. O’Brien-Simpson, N. J. Ede, L. E. Brown, J. Swan and D. C. Jackson, *Journal of the American Chemical Society*, 1997, **119**, 1183–1188.
- [44] K. Morihara, H. Tsuzuki and T. Oka, *Biochimica et Biophysica Acta (BBA) - Enzymology*, 1973, **309**, 414–429.
- [45] M. A. Durá and B. Franzetti, 2013, 1638–1645.
- [46] Y. Huang, L. Zou, J. Wang, Q. Jin and J. Ji, *Wiley Interdisciplinary Reviews: Nanomedicine and Nanobiotechnology*, 2022, **14**, e1775.
- [47] J. Y. Quek, E. Uroro, N. Goswami and K. Vasilev, *Materials Today Chemistry*, 2022, **23**, 100606.

Chapter 3

Synthesis of stimuli-responsive helical polymers

Contents

3.1	Aim	73
3.2	Introduction	73
3.3	Experimental Section	77
3.3.1	Materials	77
3.3.1.1	Peptide synthesis	77
3.3.1.2	Polymerization reactions	77
3.3.2	Instrumentation	77
3.3.3	Solid-phase peptide synthesis of acetylene-containing peptides	78
3.3.3.1	Specific for synthesis of P4	79
3.3.3.2	Specific for synthesis of P5	79
3.3.3.3	Specific for synthesis of P6	79
3.3.3.4	Specific for synthesis of P7	80
3.3.4	Characterization of the synthesized peptides	80
3.3.5	Synthesis of poly(acetylene) polymers with enzyme-degradable peptide side chain	82
3.3.5.1	Characterization of the poly(acetylene) polymers	82
3.4	Results and discussion	84
3.4.1	Synthesis of an anionic acetylene-containing peptide (P4) from previous design of P1	84
3.4.2	Polymerization of P4 peptide	88
3.4.3	Synthesis of phenylacetylene-containing peptide P5	94
3.4.4	Polymerization of P5 peptide	96
3.4.5	Synthesis of propargyl containing peptides P6 and P7	98
3.4.6	Polymerization of P6 and P7 peptides	104
3.5	Conclusions	110
3.6	Supporting information	112
3.7	References	122

3.1 Aim

Chapter 2 discussed the synthesis of two enzyme-degradable methacrylamide polymers, **Poly-P1** (**poly(Ac-EGLAK(COC(CH₃)CH₂)-NH₂)**) and **Poly-P2** (**poly(Ac-EEGLAK(COC(CH₃)CH₂)-NH₂)**). The enzyme degradation properties of these two polymers were largely dependent on the sequence of the peptide side chain, with the polymer backbone providing a structural role. To explore new ways of improving the efficacy of stimuli-responsive release of **AMPs**, it was necessary to make the backbone itself responsive to stimuli. Therefore, this Chapter seeks to combine the enzyme-degradable peptide sequence from Chapter 2 with the dynamic helical properties of poly(acetylene) backbones, in order to create a fully stimuli-responsive polymer with potentially improved drug release capabilities.

3.2 Introduction

The designs of **Poly-P1** and **Poly-P2** were specifically tailored for electrostatic encapsulation of **AMPs** and subsequent enzyme-induced drug release towards *P. aeruginosa*. Enzyme-responsive properties were achieved by incorporating a peptide sequence that is degradable by *P. aeruginosa*'s protease (Figure 3.1a). The encapsulation properties were expected to depend on the polymeric nature of **Poly-P1** and **Poly-P2**. This is because the formation of polyelectrolyte complexes is driven by an increase in entropy due to the release of counterions during the self-assembly of particles in solution.^{1,2} Furthermore, compared to a single peptide sequence with anionic residues, polyanions such as **Poly-P1** and **Poly-P2**, have a much greater multivalency and size, which have been demonstrated to be essential for the stability of polyelectrolyte complexes.^{3,4} For example, Insua and colleagues found that **PECs** assembled with a larger anionic polymer (larger **Dp**) had better physiological stability than **PECs** that used a smaller polymer.^{3,5} Therefore, poly(methacrylamide) backbone (Figure 3.1a) was used primarily for connecting the enzyme-degradable peptide side chains (**P1** or **P2**) into a single large macromolecule (forming **Poly-P1** and **Poly-P2**), thus increasing multivalency of the encapsulation component.

Poly(methacrylamide) backbones do not possess stimuli-responsive properties on their own and typically require fictionalization with stimuli-responsive side chains⁶ During enzymatic degradation of **Poly-P2** (or **Poly-P1**), one of the degradation products, denoted as **DP-2** and illustrated in Figure 3.1b, remains attached to the methacrylamide polymer backbone. **DP-2** was intentionally designed to be cationic under enzymatic

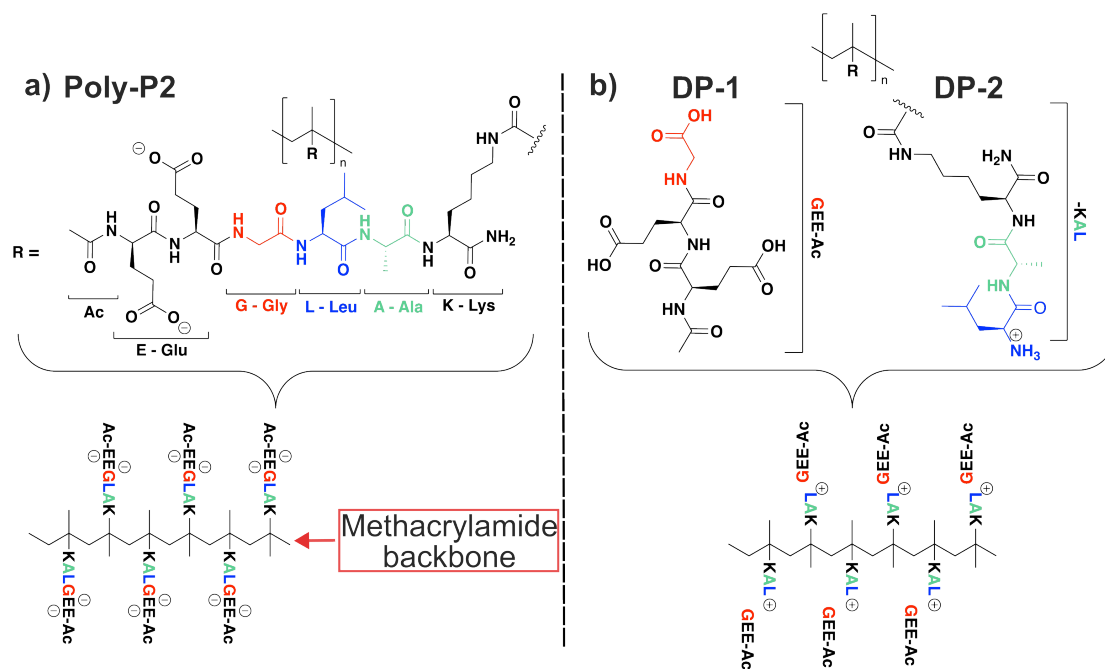


Figure 3.1 – a) Chemical structure of methacrylamide polymer **Poly-P2** (poly(Ac-EEGLAK(COC(CH₃)CH₂)-NH₂)). b) Chemical structures of **DP-1** and **DP-2** - an enzyme degradation products of **Poly-P2**.

degradation, which should repel cationic **AMP** and accelerate the release rate. However, there is still the possibility of **DP-2** sterically blocking the **AMP** due to its size slowing down Polymyxin B release. Therefore, we hypothesized that by incorporating stimuli-responsive and degradation properties into the polymer backbone, the effectiveness of drug release could be enhanced, with potentially different release mechanisms being investigated. To this end, it was decided to attempt a different polymer architecture, moving from a brush-like design of methacrylamides to a helical structure, which has recently been explored in our group.

In particular, the focus was changed to poly(acetylenes), a type of dynamic helical polymers that can alter their helical characteristics (such as helical sense and pitch) in response to stimuli (Figure 3.2).⁷ Poly(acetylenes) are created by the polymerization of substituted alkynes, forming a backbone of conjugated double bonds. Due to the deviation from planarity in conjugated bonds, four stereoisomers can be formed, depending on the type of double bonds (*cis* or *trans*) and the connecting single bonds (cisoid or transoid) (as shown in Figure 3.2). Most importantly, the stereochemistry and molecular conformation (*i.e.*, change in the helical sense and pitch) of poly(acetylenes) can be altered after the polymer has formed through the application of external stimuli, such as temperature, pH and redox.⁷ These changes occur as a result of stimuli-induced isomerization around the double bond. In particular, under acidic conditions, close to that of the bacterial microenvironment, induced isomerization was observed to degrade the

polymer backbone.⁸ Interestingly, poly(acetylenes) are unique among responsive helical polymers in that they can maintain their helical structure even when the environment changes. This can be advantageous in situations where the side chain functionality must remain intact after the application of stimuli. Additionally, some poly(acetylenes), such as phenylacetylenes, have been demonstrated to self-assemble into stimuli-responsive nanoparticles, due to extensive pi-stacking between phenolic groups, which was used to encapsulate the anti-inflammatory drug naproxen.

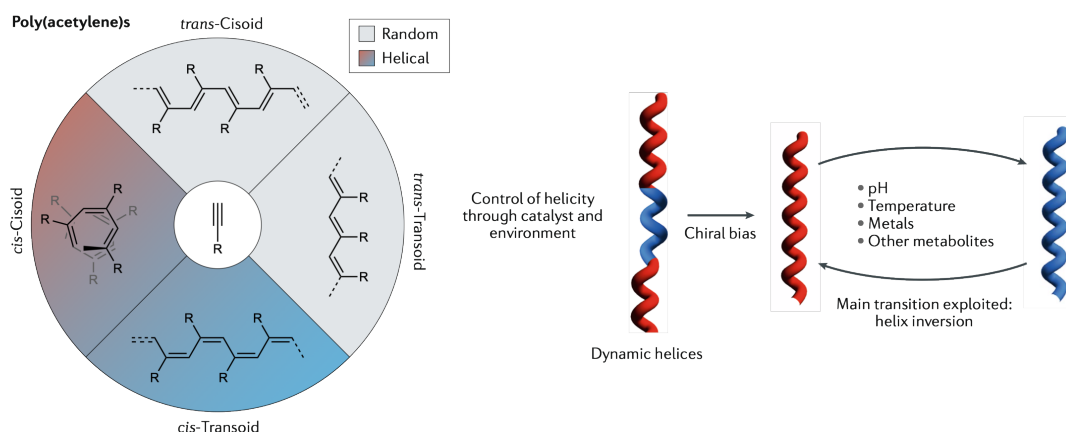


Figure 3.2 – Representation of different stereoisomers of poly(acetylenes), which arise from polymerization of substituted acetylenes. The dynamic helical properties of poly(acetylenes) are presented, allowing the helical chirality (P versus M) to change via stimuli post-polymerization. Adapted with permission.⁷ Copyright © 2020, Springer Nature Limited.

In comparison to methacrylamide backbones, poly(acetylenes) are inherently stimuli-responsive, which makes them more suitable for stimuli-responsive drug release applications. Therefore, it was suggested that helical enzyme-degradable polymers could be produced by combining a LasB-responsive -GLA- sequence with a poly(acetylene) backbone (Figure 3.3a). This would lead to the formation of a novel polymer that, when exposed to bacterial stimuli such as enzymes and acidic pH, would cause the degradation of a peptide side chain and the conformational change of the helical backbone due to acid-induced isomerization (Figure 3.3b). If used in a particle system such as PECs, the stability of these nanoparticles would be significantly reduced in the presence of bacteria, as two stimuli (*i.e.*, enzyme and pH) would cause the degradation or destabilization of the encapsulating polymer. Moreover, the use of poly(acetylene) backbones in the encapsulating polymer can open up the possibility of exploring novel stimuli-responsive properties, which can then be used for the delivery of AMPs.⁷

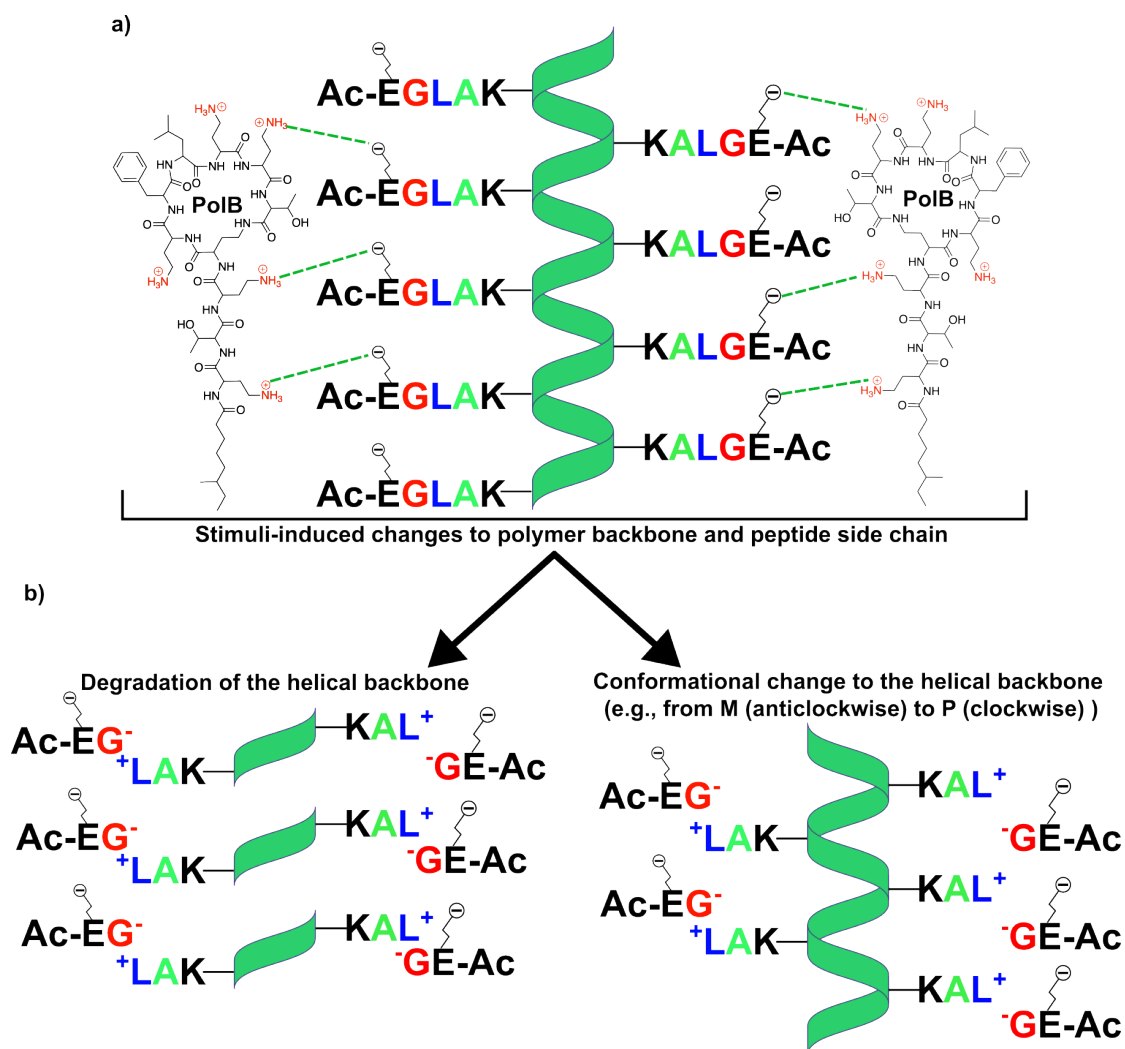


Figure 3.3 – a) Schematic illustration of the **LasB**-degradable helical polymers. b) Schematic illustration of the potential pathways of degradation of helical polymers derived from the **P1** peptide.

3.3 Experimental Section

3.3.1 Materials

3.3.1.1 Peptide synthesis

All Fmoc-protected-L-amino acids, Rink Amide MBHA resin (100-200 mesh) (0.51 mmol/g), were purchased from Merck Millipore. Alternative Rink Amide MBHA resin (100-200 mesh) (0.3 - 0.8 mmol/g) was purchased from FluroChem UK. H-Ala-2-CITrt resin (0.72 mmol/g), Dimethylformamide (DMF), piperidine 20 % v/v in DMF were purchased from Merk®. N,N-diisopropylethyl amine (DIPEA), Ethylenediaminetetraacetic acid (EDTA), N-methylmorpholine (NMM), Tetrakis (triphenylphosphine)palladium(0) (Pd-[(C₆H₅)₃P]₄), propargyl chloroformate, 4-ethynylbenzoic acid, propargyl amine were bought from Sigma Aldrich® (UK). Trifluoroacetic acid (TFA), 1,1'-Carbonyldiimidazole (CDI) were purchased from Alfa Aesar®. N,N,N',N'-tetramethyl-O-(1H-benzotriazol-1-yl)uronium hexafluorophosphate (HBTU) was purchased from Carbosynth Ltd.

3.3.1.2 Polymerization reactions

Catalysts used for the polymerizations of acetylene-containing peptides: **Cat.1** - Bicyclo[2.2.1]hepta-2,5-diene-rhodium(I) chloride dimer was purchased from Sigma Aldrich® (UK) and **Cat.2** - 2,5-norbornadienerhodium(I) tetraphenylborate was prepared according to Ref.⁹ Spectra/Por® 6 dialysis membranes (molecular weight cut off 3.5 and 1 KDa) were purchased from Spectrum® Laboratories.

All other chemicals were purchased from Fisher Scientific® UK and VWR®. and were used without further purification. The pH values of the solutions were measured with a Mettler-Toledo MP220 pH meter.

3.3.2 Instrumentation

Nuclear magnetic resonance (NMR) data were acquired on a Bruker Avance Neo operating at 400 MHz and equipped with a 5 mm BBFO "smart" probe (¹H/¹³C) as well as on a Bruker AVIII operating at 300 MHz and equipped with a 5 mm BBFO probe. Chemical shifts were reported in ppm (units) referenced to the following solvent signals: dimethylsulfoxide (DMSO)-d₆ at 2.50 ppm and C at 39.52 ppm. Mass spectrometry (MS) spectra were obtained on a Xevo® G2-XS ToF (Waters) from ESI and TOF

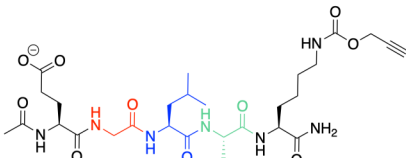
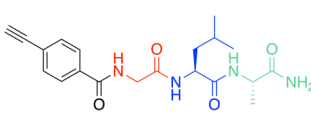
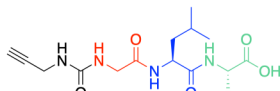
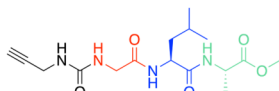
measurement in positive and negative ion modes. High-resolution **MS** data were calculated by comparing with leucine-enkephalin as an internal standard. Fourier transform infrared spectroscopy (**FTIR**) spectroscopy analysis was performed using a Tensor II **FTIR** analyses were acquired from Bruker spectrometer of solid and liquid samples.

Shimadzu Prominence LC-20A with an SPD20A **UV-Vis** detector was used to perform reverse phase HPLC analysis (**RP-HPLC**). Analyses were performed through a Kinetex[®]-C18-EVO column (Phenomenex[®]): 5 μ m, 100 Å, 250 x 4.60 mm. A gradient of 5 to 60 % of (CH₃CN + 0.05 % **TFA**) in (H₂O + 0.05 % **TFA**) was used at 1 mL/min for 60 minutes. The column was kept at 25 °C and **UV-Vis** detection was set at 215 nm. 10 μ L of sample was injected.

For purification purposes, Agilent 1260 Infinity II Preparative LC was used. Reverse phase preparative **HPLC** analysis was performed using a Kinetex[®] C18 (Phenomenex[®]): 5 μ m, 100 Å, 250 x 21.20 mm. A gradient of 5 to 40 % of (CH₃CN + 0.05 % **TFA**) in (H₂O + 0.05 % **TFA**) was used with a flow rate of 10 mL/min for 60 minutes.

3.3.3 Solid-phase peptide synthesis of acetylene-containing peptides

Table 3.1 – Chemical structures the acetylene-containing peptides, synthesized in this Chapter.

I.D.	Structure	I.D.	Structure
P4		P5	
P6		P7	

An exemplary procedure is presented for solid-phase peptide synthesis using 1000 mg of resin (0.51 mmol). For peptides **P4** and **P5** (Table 3.1), commercial Rink Amide **MBHA** resin (100-200 mesh) (1000 mg, 0.51 mmol) was swollen in 10 mL of **DMF** for 30 minutes. For peptides **P6** and **P7** (Table 3.1), commercial H-Ala-2-CITrt resin (0.72 mmol/g) was swollen in 10 mL of **DMF** for 30 minutes. Then, the **Fmoc** protecting group was removed from the Rink Amide **MBHA** or from Ala of H-Ala-2-CITrt resin with 10 mL of piperidine in **DMF** 20 % v/v for 10 minutes. A positive chloranil test confirmed the removal of the **Fmoc** group, which was followed by coupling of the first **Fmoc**-L-amino acid. Solutions of **Fmoc**-L-amino acid (3 eq), N,N,N',N'-tetramethyl-O-(1H-benzotriazol-1-yl)uronium hexafluorophosphate (**HBTU**) (2.8 eq) and **DIPEA** (2.8 eq) in **DMF** were

added to a final volume of 10.25 mL (e.g., 5:5:0.25 mL). The reaction mixture was shaken for 45 - 90 min at room temperature, after which a negative chloranil test indicated that the reaction had reached completion. N-terminal **Fmoc** protecting group was removed with 10 mL of piperidine in **DMF** 20 % v/v for 10 minutes. A positive chloranil test confirmed the removal of the **Fmoc** group and the previous steps were repeated to couple all amino acids in the sequence. Following the coupling of the first amino acid, the peptide sequence was capped with 4 mL of Ac₂O:DIPEA:DMF (1:1:3).

3.3.3.1 Specific for synthesis of P4

Capping was also performed for **P4** after the removal of the **Fmoc** group from the last amino acid in the sequence (Glu). Only after the couplings of all amino acids were completed, while the peptide was still on a resin, **Alloc** deprotection of the Lys side chain was performed. For deprotection cocktail Pd[P(C₆H₅)₃]₄ (1 eq) dissolved in CHCl₃-AcOH-N-methylmorpholine (**NMM**) (37:2:1) (20 mL/g of resin) was used. The reaction was carried out under an inert atmosphere for 24 hours with light agitation. After **Alloc** deprotection, a solution of propargyl chloroformate (3 eq) and **DIPEA** (9 eq) in **DMF** was added to a final volume of 10.0 mL and reacted for 45 minutes (e.g., 0.300:0.750:8.95 mL). After 45 minutes, the coupling was repeated using a fresh propargyl chloroformate coupling solution (3 eq), followed by a negative chloranil test indicating that the reaction had reached completion.

3.3.3.2 Specific for synthesis of P5

Following the coupling of Fmoc-Gly-OH, **Fmoc** group was removed, confirmed by a positive chloranil test. 4-ethynylbenzoic acid was coupled using the same procedure as for any other **Fmoc**-L-amino acid *i.e.*, 4-ethynylbenzoic acid (3 eq), N,N,N',N'-tetramethyl-O-(1H-benzotriazol-1-yl)uronium hexafluorophosphate (**HBTU**) (2.8 eq) and **DIPEA** (2.8 eq) in **DMF** were added to a final volume of 10.25 mL (e.g., 5:5:0.25 mL) and reacted for 45 min, followed by a negative chloranil test indicating that the reaction had reached completion.

3.3.3.3 Specific for synthesis of P6

Following the coupling of Fmoc-Gly-OH, **Fmoc** group was removed, confirmed by a positive chloranil test. Following deprotection, 5 ml of cold **CDI** (2.80 eq) was added on ice, while the resin was lightly vortexed. **CDI** solution was mixed with the resin for

1 hour, after which the coupling was repeated. Following the coupling procedures, the resin was thoroughly washed with DMF, DCM and DMF again. The completion of the reaction was confirmed by a negative chloranil test, which was followed by the addition of 5 ml of propargyl amine solution (3.0 eq) and left to react for 12 hours. A Chloranil test was performed following propargyl amine coupling and after washing with DMF in order to double-check the absence of unreacted amines.

After all couplings were completed, the resin was washed with Et₂O and DCM and dried with air. For cleavage of **P4** and **P5** peptide sequences per 1 g of resin, 10 mL of 95 % aqueous solution of TFA was added to a dried resin and reacted for a minimum of 1 hour. For cleavage of **P6** and **P7** peptide sequences per 1 g of resin, 10 mL of 2 % solution of TFA in DCM was added to a dried resin and reacted for a minimum of 1 hour. The solutions obtained were concentrated under argon or air and precipitated in chilled Et₂O. Finally, these suspensions were centrifuged or filtered under vacuum, and the pellets were freeze-dried from acidic water.

3.3.3.4 Specific for synthesis of P7

For the preparation of **P7**, first **P6** was synthesized and cleaved from the resin following the procedure described in Section 3.3.3.3. Synthesis of **P7** began by slowly adding the crude product **P6** to (CH₃)SiCl (3.0 eq) and purging it with argon. Subsequently, MeOH (2.50 eq, 1 mL per 100 mg of monomer) was added under stirring. The reaction mixture was then degassed before being left to react for 24 hours.

3.3.4 Characterization of the synthesized peptides

P4, (Ac-EGLAK(COOCH₂CCH)-NH₂) (Crude 380 mg, 58 % yield) (Purified 0.104 mg, 16 % yield) ¹H-NMR δ_H (400 MHz, DMSO-*d*₆): 0.85 (6 H, dd, J = 15.0, 6.5 Hz, H^δ-Lue), 1.15 – 2.00 (17 H, m, 3H^β-Ala, 6H^{δ,γ,β}-Lys, 3H^{γ,β}-Lue, 2H^β-Glu, 3H-Ac), 2.16 – 2.35 (2 H, m, H^γ-Glu), 2.94 (2 H, q, J = 7.2 Hz, H^ε-Lys), 3.45 (1 H, t, J = 2.5 Hz, CH-Alkyne), 3.69 (2 H, d, J = 5.9 Hz, H^α-Gly), 4.03 – 4.34 (6 H, m, H^α-Ala, Lue, Lys, Glu, HDO), 4.58 (2 H, d, J = 2.5 Hz, H^α-Propargyl), 6.94 – 7.06 (1 H, m, NH), 7.18 – 7.27 (1 H, m, NH), 7.30 (1 H, d, J = 5.7 Hz, NHCO-propargyl formate), 7.59 (1 H, d, J = 8.0 Hz, NHCO-Ala), 7.84 (1 H, d, J = 8.2 Hz, NHCO-Lue), 8.08 (2 H, dd, J = 15.0, 7.2 Hz, NHCO-Lys, Glu), 8.15 – 8.28 (1 H, m, NHCO-Gly) ppm. ¹³C-NMR (400 MHz, DMSO-*d*₆) 17.60 (C^β-Ala), 21.50 (Ac), 22.46 (C^δ-Leu), 22.48 (C^γ-Lys), 22.83, 23.11 (C^δ-Leu), 24.05 (C^γ-Leu), 27.01 (C^β-Leu), 29.07 (C^β-Glu), 30.11 (C^γ-Glu), 31.75 (C^β-Lys), 40.27 (C^ε-Lys), 40.69 (CH₂-Propargyl), 42.03 (C^α-Gly), 48.32 (C^α), 50.88 (C^α),

51.33 (CH-Alkyne), 52.23 (C^α), 52.31 (C^α), 76.98 (C-Alkyne), 155.21 (NHCO), 168.69 (NHCO), 169.72 (NHCO), 171.76 (NHCO), 171.83 (NHCO), 171.89 (NHCO), 173.40 (NHCO), 173.92 (NHCO) ppm. Purity (purified sample) by **HPLC** = 84%.

P5, (CHC₆H₄-GLA-NH₂) (Crude 380 mg, 58 % yield) (Purified 104 mg, 16 % yield) **¹H-NMR** δ_H (400 MHz, **DMSO-d₆**): 0.86 (6 H, dd, J = 14.7, 6.5 Hz, H^δ-Leu), 1.23 (3 H, d, J = 7.2 Hz, H^β-Ala), 1.43 – 1.54 (2 H, m, H^β-Lue), 1.63 (1 H, dt, J = 13.3, 6.6 Hz, H^β-Lue), 3.82 – 3.96 (2 H, m, H^α-Gly), 4.15 (1 H, p, J = 7.1 Hz, H^α-Ala), 4.28 (1 H, q, J = 7.8 Hz, H^α-Lue), 4.38 (1 H, s, CH-Alkyne), 6.90 – 7.00 (1 H, m, NH), 7.07 (1 H, s, NH), 7.53 – 7.63 (2 H, m, H-Phenyl), 7.82 – 7.92 (3 H, m, H-Phenyl, NHCO), 8.17 (1 H, d, J 7.9, NHCO), 8.91 (1 H, t, J 5.8, NHCO-Gly) ppm. **¹³C-NMR** (400 MHz, **DMSO-d₆**): 18.03 (C^β-Ala), 21.50 (C^δ-Leu), 23.17 (C^δ-Leu), 24.16 (C^γ-Leu), 35.82 (CH-Alkyne), 40.58 (C^β-Leu), 42.87 (C^α-Gly), 48.14 (C^α), 51.25 (C^α), 82.99 (C-Alkyne), 124.64 (C-Phenyl), 127.65 (CH-Phenyl), 131.70 (CH-Phenyl), 133.94 (C-Phenyl), 165.96 (NHCO), 169.21 (NHCO), 171.58 (NHCO), 174.15 (NHCO) ppm. **MS** (ESI-TOF, -eV): m/z 385.19 [M - H]⁻; 431.19 [M + 2Na]⁻; **HR-MS** (ESI-TOF, -eV): m/z 385.1876 (calculated for [M - H]⁻) 385.1878 (found); Purity (purified sample) by **HPLC** = 95%.

P6, (CHCCH₂NHCO-GLA-OH) (Pure 109 mg, 45% yield) **¹H-NMR** δ_H (400 MHz, **DMSO-d₆**): 0.86 (6 H, dd, J = 3.3, 6.5 Hz, H^δ-Leu), 1.27 (3 H, d, J = 7.3 Hz, H^β-Ala), 1.34 – 1.52 (2 H, m, H^β-Lue), 1.59 (1 H, ddt, J = 14.7, 12.8, 6.4 Hz, H^β-Lue), 3.04 (1 H, t, J = 2.5 Hz, CH-Alkyne), 3.66 (2 H, d, J = 1.8 Hz, H^α-Gly), 3.78 (2 H, s, H^α-Propargyl), 4.16 (1 H, p, J = 7.3 Hz, H^α-Ala), 4.36 (1 H, td, J = 9.2, 5.2 Hz, H^α-Lue), 6.20 (1 H, s, NHCO-Gly), 6.49 (1 H, s, NHCO-Propargyl), 7.91 (1 H, d, J = Hz 8.5, NHCO-Ala), 8.24 (1 H, d, J = 7.2 Hz, NHCO-Gly) ppm. **¹³C-NMR** (400 MHz, **DMSO-d₆**): 16.93 (C^β-Ala), 21.66 (C^δ-Leu), 23.12 (C^δ-Leu), 24.02 (C^γ-Lue), 28.80 (CH₂-propargyl), 41.09 (C^β-Leu), 42.75 (C^α-Gly), 47.44 (C^α), 50.42 (C^α), 72.62 (CH-Alkyne), 82.33 (C-Alkyne), 157.43 (NHCO), 169.46 (NHCO), 171.75 (NHCO), 173.93 (NHCO) ppm. **MS** (ESI-TOF, -eV): m/z 339.17 [M - H]⁻; **HR-MS** (ESI-TOF, -eV): m/z 339.1668 (calculated for [M - H]⁻) 339.1669 (found); Purity (purified sample) by **HPLC** ≥ 98%.

P7, (CHCCH₂NHCO-GLA-OCH₃) (Pure 196 mg, 38% yield) **¹H-NMR** δ_H (400 MHz, **DMSO-d₆**): 0.86 (6 H, dd, J = 14.8, 6.6 Hz, H^δ-Leu), 1.28 (3 H, d, J = 7.3 Hz, H^β-Ala), 1.34 – 1.52 (2 H, m, H^β-Lue), 1.59 (1 H, ddt, J = 14.6, 12.7, 6.5, H^β-Lue), 3.04 (1 H, t, J = 2.5, 2.4, Hz CH-Alkyne), 3.60 (3 H, s, CH₃), 3.65 (2 H, dd, J = 5.4, 2.2 Hz, H^α-Gly), 3.78 (2 H, dd, J = 5.7, 2.5 Hz, H^α-Propargyl), 4.24 (1 H, p, J = 7.2 Hz, H^α-Ala), 4.29 – 4.43 (1 H, m, H^α-Lue), 6.20 (1 H, t, J = 5.5, 1.8 Hz, NHCO-Gly), 6.49 (1 H, t, J = 5.7 Hz, NHCO-Propargyl), 7.93 (1 H, d, J = 8.5 Hz, NHCO-Ala), 8.38 (1 H, d, J = 6.9 Hz, NHCO-Leu) ppm. **¹³C-NMR** (400 MHz, **DMSO-d₆**): 16.70 (C^β-Ala), 21.12 (C^δ-Leu), 23.02 (C^δ-Leu), 24.02 (C^γ-Lue), 27.96 (CH₂-propargyl), 41.04 (C^β-Leu), 42.75

(C^α-Gly), 47.52 (C^α), 50.38 (C^α), 51.79 (CH₃), 71.24 (CH-Alkyne), 80.07 (C-Alkyne), 157.44 (NHCO), 167.63 (NHCO), 171.92 (NHCO), 173.58 (NHCO) ppm. **MS** (ESI-TOF, +eV): m/z 354.20 [M + H]⁺; m/z 388.18 [M + Na + H]⁺ **HR-MS** (ESI-TOF, +eV): m/z 377.1801 (calculated for [M + Na + H]⁺) 377.1809 (found); Purity (purified sample) by **HPLC** ≥ 88%.

For **NMR** spectra, **HPLC** chromatograms, and **MS** spectra, see the supporting information Section 3.6.

3.3.5 Synthesis of poly(acetylene) polymers with enzyme-degradable peptide side chain

Polymerizations of acetylene-containing peptide monomers were attempted using two catalysts: **Cat.1** - Bicyclo[2.2.1]hepta-2,5-diene-rhodium(I) chloride dimer and **Cat.2** - 2,5-norbornadienerhodium(I) tetraphenylborate. The molar ratio of the monomer to the catalyst was the same for all conditions attempted - 100:1.00. The concentrations of the monomers used ranged from 0.10 M to 0.15 M. Three solvents were used **THF**, **DMF** and **ACN**. The solutions were degassed with argon before polymerization and reacted under an inert atmosphere. All attempted polymerization conditions are summarized in Table 3.2.

An exemplary procedure is presented. First, the monomers were dissolved in 50% volume of the solvent. In some cases, the product became viscous at room temperature and, as a result, the monomer solutions were heated to 55°C to decrease the viscosity. Subsequently, triethylamine was added in 0.01 ratio to the monomer (Only used with **Cat.1** - Bicyclo[2.2.1]hepta-2,5-diene-rhodium(I) chloride dimer), with the catalyst solution added as a last step. The reactions were left to react for 24, 48 and 72 hours under 30°C or 50°C. At 24 hours, the heating was stopped and the ¹H-NMR of the polymerization mixture was recorded to investigate monomer conversions. As none of the polymerizations were successful, **GPC** analysis was not performed.

3.3.5.1 Characterization of the poly(acetylene) polymers

¹H-NMR was used to calculate monomer conversions. Monomer conversions were calculated by reduction of an integration of the acetylenic peak at 3.45 ppm for **P4**, at 4.38 ppm for **P5** and at 3.04 ppm for **P6**, **P7** compared with the proton region of the H^δ-Lue at 0.85 ppm (6 H, dd, J = 14.3, 6.5 Hz) for **P4**, **P5** and compared with the proton region of H^β-Ala at 1.23 ppm (3 H, d, J = 7.3 Hz) for **P6**, **P7**. Equation 3.1 was used to obtain % conversion, where H_{ref} corresponds to either integration of H^δ-Lue at 0.85

ppm or H^β-Ala at 1.23 ppm, H_m and H_p correspond to the signals of the acetylenic protons in C triple bond C environment in the monomer (*i.e.*, H_m) at the start of the reaction and in the polymer (*i.e.*, H_p) at the end of the polymerization.

$$\text{Monomer Conversion} = \left(1 - \frac{\frac{H_p}{H_{ref}}}{\frac{H_m}{H_{ref}}}\right) \times 100\% \quad (3.1)$$

Table 3.2 – Summary of polymerization conditions and reactant concentrations for the reaction of acetylene-containing peptide sequences **P4** - **P7**.

Pol-ID	Materials	mg	[M] _f	Solvent (mL)	R (Molar)
Poly-P4-1	P4	50.0	0.157	0.50 - DMF	100
	Cat.1	0.361	0.00157		1.00
Poly-P4-2	P4	50.0	0.157		100
	Cat.2	0.403	0.00157		1.00
Poly-P5-1	P5	45.0	0.116	0.50 - ACN	100
	Cat.1	0.537	0.00116		1.00
Poly-P5-2	P5	45.0	0.116	0.50 - THF	100
	Cat.1	0.537	0.00116		1.00
Poly-P6-1	P6	35.0	0.103	1.00 - THF	100:1.0
	Cat.1	0.474	0.00103		
Poly-P6-2	P6	35.0	0.103		
	Cat.2	0.529	0.00103		
Poly-P7-1	P7	17.5	0.100	0.50 - THF	100:1.0
	Cat.1	0.228	0.00100		
Poly-P7-2	P7	17.5	0.100		
	Cat.2	0.254	0.00100		
Poly-P7-3	P7	40.0	0.226		
	Cat.1	0.520	0.00226		
Poly-P7-4	P7	40.0	0.226		
	Cat.2	0.580	0.00226		

3.4 Results and discussion

3.4.1 Synthesis of an anionic acetylene-containing peptide (P4) from previous design of P1

The first step in the creation of stimuli-responsive poly(acetylenes) is the synthesis of the peptide monomer with the acetylene component. To preserve the enzyme degradation properties of **P1** (or **P2**) peptides, a peptide sequence resembling **P1** but lacking the acrylate group (referred to as **P1_{der}** in Figure 3.4), was used as a starting point. The solid-phase peptide synthesis of **P1** and **P2** sequences was extensively discussed in Chapter 2 (Sections 2.3.3 and 2.4.1.1). With the deprotected lysine side chain, coupling of the acetylene functional group had to be done through the amide bond. For this purpose, propargyl chloroformate was chosen, as the coupling procedure was similar to the coupling of methacrylic anhydride *i.e.*, without using activation agents such as **HBTU** as a result of the already high electrophilicity of carbonyl carbon (Figure 3.4). It should be noted that during the coupling of propargyl chloroformate, hydrochloric acid vapors were produced, which were carefully vented between mixing. As with all other peptides discussed in this Thesis, the coupling of the propargyl chloroformate group was followed by global deprotection and acid cleavage (*i.e.*, 95 % **TFA**) from the resin, producing **P4** (**Ac-EGLAK(COOCH₂CCH)-NH₂**) (Figure 3.4).

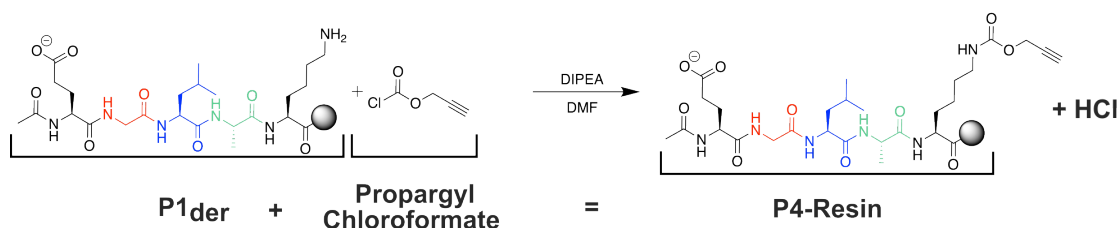


Figure 3.4 – Reaction scheme for coupling propargyl chloroformate to the lysine side chain, producing **P4** (**Ac-EGLAK(COOCH₂CCH)-NH₂**).

To assess purity levels and any potential coupling issues that may have arisen during the synthesis, **HPLC** analysis was performed on the crude mixture of **P4** that was produced (Figure 3.5). **HPLC** chromatograms contained a large number of peaks with different intensities, indicating a significant presence of impurities and side products, which developed during the synthesis of **P4**. To identify which peaks corresponded to the peptide sequence **P4**, two peaks with the largest areas at 15.62 and 19.53 min were collected with preparative **HPLC** and analyzed by **NMR** (Figure 3.6).

This time, the assignment of the **NMR** peaks to the corresponding chemical structure of **P4** was easier as most of the proton environments in **P4** were identical to **P1**

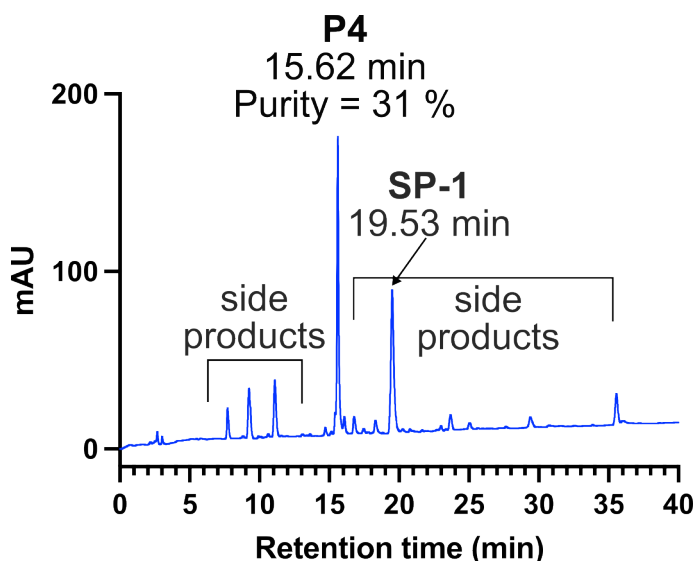
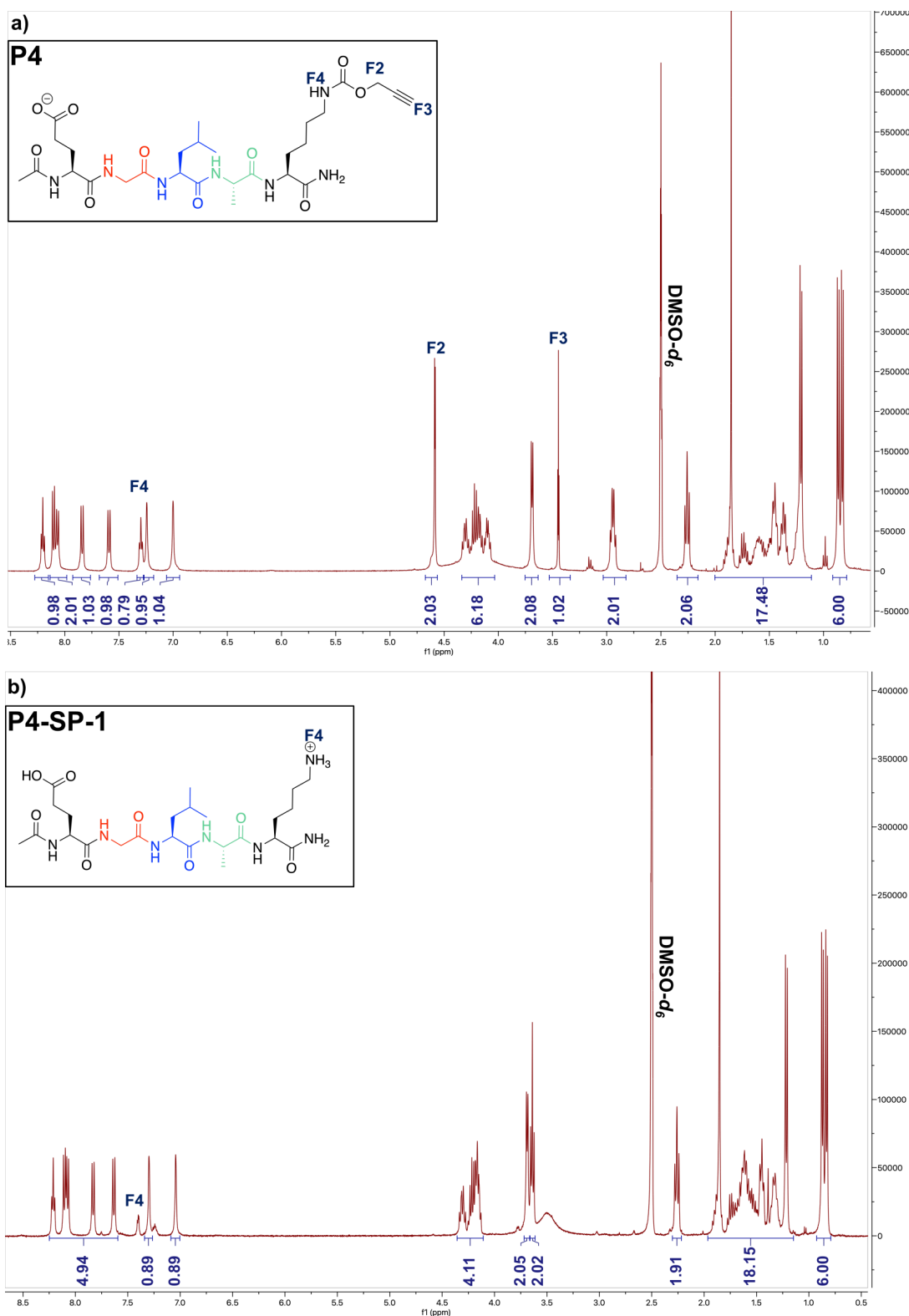


Figure 3.5 – RP-HPLC chromatogram of crude **P4** (Ac-EGLAK(COOCH₂CCH)-NH₂) sequence.

peptide, which was thoroughly analyzed in Chapter 2 (Section 2.4.1.1). The key difference between **P4** and **P1** structures is the presence of a propargyl (C triple bond C-H) instead of methacrylate group. The environment of the terminal proton (labeled as **F3** in Figure 3.6a) of the acetylene group was identified as a triplet peak at 3.44 ppm with integration 1.02, split by two protons across the triple bond. It is common for alkynes to experience long-range coupling of protons and, as a result, to produce spin-spin coupling separated by three carbons.¹⁰ Using 2D-COSY analysis (Figure S3.28), a corresponding neighboring environment (labeled as **F2** in Figure 3.6a) was identified as a doublet at 4.58 ppm with integration 2.03. With all remaining proton environments fully assigned, it was concluded that the highest peak at 15.62 min (Figure 3.5a) represented the **P4** peptide. After the identification of the primary product peak (**P4**), the identity of the secondary peak eluted at 19.53 min was also checked via NMR.

¹H-NMR analysis of **P4-SP-1** (Figure 3.6b) revealed the presence of most of the environments corresponding to Ac-EGLAK-NH₂ sequence but did not have any peaks that represented protons of the propargyl formate group (*i.e.*, **F2** at 4.80 ppm and **F3** in Figure 3.6a at 3.40 ppm). These results suggested that the peak at 19.53 min represented the **P4** sequence but without the propargyl formate group, which meant that the protons on the primary amine side chain of the lysine residue should be present in the ¹H-NMR spectrum. Indeed, a low-intensity peak at 7.39 ppm (primary amine region) was identified and attributed to the primary amine side chain of lysine (Figure 3.6b).

This reduction in intensities could be related to a significantly decreased dipole moment of amine protons when present as an ammonium salt, which formed as a result of protonation caused by reaction with acid chloride (*i.e.*, propargyl chloroformate).



Therefore, the main side product of the propargyl chloroformate coupling was identified as **P4-SP-1**, an ammonium chloride salt. This was attributed to the use of an excessive amount of propargyl chloroformate reagent (3 equivalents to the peptide sequence), which resulted in the production of HCl. This HCl protonated the primary amine of the lysine side chain, creating an ammonium chloride salt. In the protonated state, the amine group loses its nucleophilicity since nitrogen does not have any pairs of electrons left to form a bond with the electrophilic carbon of the carbonyl group, limiting the production of a desired product, **P4**. A potential solution to this problem could involve substitution of **DIPEA** with a stronger non-nucleophilic base, such as Lithium diisopropylamide. This would neutralize any HCl present in the reaction, thus avoiding the protonation of amines and the production of ammonium salt.

After the location of the product peak of **P4** determined, analytical **HPLC** was performed on the collected sample to verify the final purity of the product obtained (Figure 3.7). Compared to the crude chromatogram of **P4**, the purity of the peak of the product increased from 31 to 84 % (Figure 3.5b and 3.7). However, the "purified" sample still contained some impurity peaks at 4.31, 15.98, and 16.66 min, which meant that the purification efficacy was not high (Figure 3.7). In particular, it was found that the separation of closely eluting peaks at 15.98 and 16.66 min was challenging using equipment and the existing preparative **HPLC** method. Ideally, a different preparative **HPLC** column with an automated fraction collection system would have made a significant improvement in purification efficacy. Unfortunately, these were not available at the time of synthesis of acetylene-containing peptide monomers.

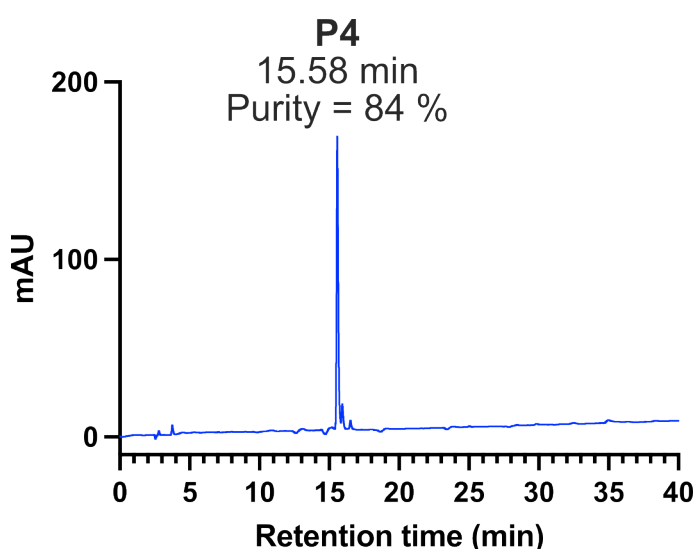


Figure 3.7 – **RP-HPLC** chromatogram of purified **P4** (**Ac-EGLAK(COOCH₂CCH**)-NH₂) sequence.

Therefore, to minimize the peak co-elution, smaller injection volumes with a more

accurate sample collection technique were used for the subsequent syntheses. Before synthesizing more of the **P4** sequence, it was necessary to evaluate its polymerization abilities. Consequently, a sample of **P4** with 84 % purity was used in polymerization reactions.

3.4.2 Polymerization of P4 peptide

To polymerize acetylenes, drastically different conditions and reactants were required compared to radical polymerization of methacrylamide-containing peptides **P1** and **P2** due to the different polymerization mechanisms involved. Acetylenes are most commonly polymerized with the use of transition metal catalysts (e.g., Rh, W, Ti, Ta, Fe) through two mechanisms, metathesis and insertion, which are dictated by the metal catalyst used in the reaction.^{11,12} For example, when W, Mo, and Ta catalysts are used, the polymerization reaction is carried out through the metathesis mechanism.^{11,12} On the other hand, polymerization involving Rh, Fe, and Ti catalysts is carried out through an insertion mechanism. The typical polymerization procedure for substituted acetylenes is generally straightforward, involving the mixing of an acetylene monomer with a metal catalyst in an organic solvent, such as THF. The control of which stereoisomer (i.e., *cis-transoid*, *cis-cisoid*, *trans-transoid*, *trans-cisoid*) is synthesized depends on the type of metal catalyst (e.g., Rh, W, Ti, Ta, Fe) used in the polymerization reaction. For example, rhodium-based catalysts (e.g. rhodium norbornadiene chloride dimer, $[\text{Rh}(\text{nbd})\text{Cl}]_2$ + triethylamine (Et_3N) base) produce *cis-transoid* polymers and work best with monosubstituted alkynes (e.g., propargyl) under mild conditions. Furthermore, the selection of the metal catalyst is based on the polarity of the monomers. Polar monosubstituted acetylenes are usually only polymerized with the Rh catalyst, while Mo and W catalysts can handle sterically crowded monomers.^{11,12}

Therefore, considering **P4** being a polar monomer with a monosubstituted acetylene group, a Rh-based catalyst was selected. The two most widely used Rh catalysts for the polymerization of polar monomers including amides are **Cat.1** - $[\text{Rh}(\text{nbd})\text{Cl}]_2$ and **Cat.2** - $\text{Rh}(\text{nbd})(\text{nPh-BPh}_3)$ (Figure 3.8a). **Cat.1** requires the use of a tertiary amine base such as triethylamine (TEA) for the formation of an active catalytic species, $2[\text{Rh}(\text{nbd})(\text{TEA})(\text{Cl})]$, whereas **Cat.2** does not require any activation and was used as is in polymerization reactions (Figure 3.8a). Depending on the catalyst employed, the stereoregularity of the resulting polymer was determined. In the case of Rh catalysts, conjugated double bonds of poly(acetylene) polymer (i.e., **Poly-P4**) would adopt a *cis-transoid* conformation, as depicted in Figure 3.8b.^{7,11,12}

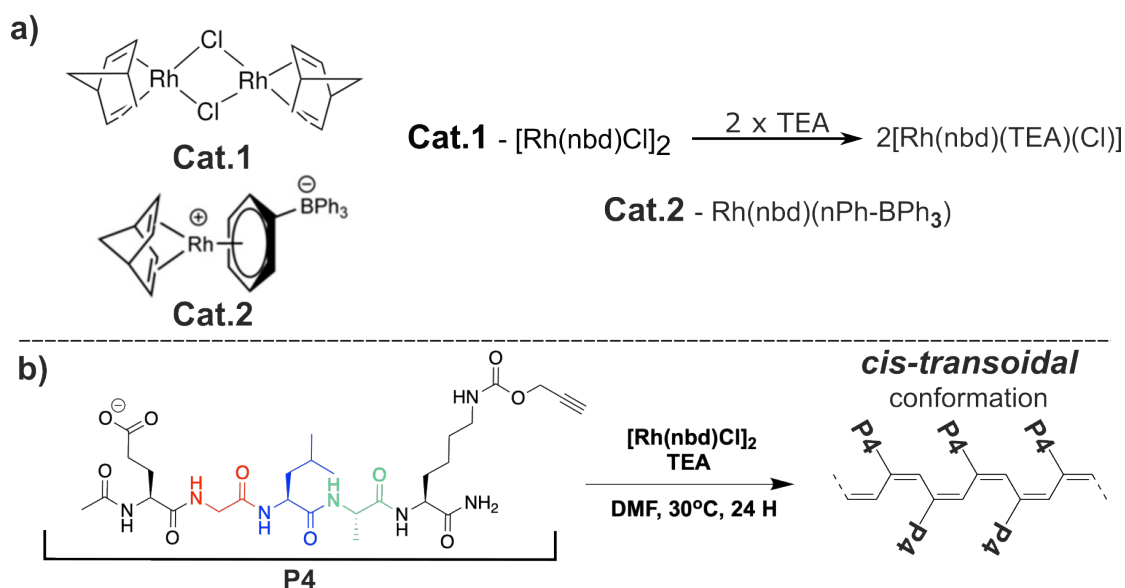


Figure 3.8 – a) Chemical structures of two Rh catalysts used in polymerizations of acetylene-containing peptides. **Cat.1** - $[\text{Rh}(\text{nbd})\text{Cl}]_2$, its activation using a triethylamine (TEA) base. **Cat.2** - $\text{Rh}(\text{nbd})(\text{nPh-BPh}_3)$, no activation required. b) Reaction scheme of polymerization **P4** (**Ac-EGLAK(COOCH₂CCH)-NH₂**) peptide sequence using **Cat.1**. The same reaction scheme applies for polymerization with **Cat.2** but without the addition of TEA.

Two polymerization conditions were attempted, **Poly-P4-1** and **Poly-P4-2** with the only difference in the catalyst used (Table 3.3). Solutions of the monomer and catalyst were degassed and left to react for 24 hours. According to previously reported polymerization conditions for monosubstituted polar acetylene monomers^{13,14} and the experience of our laboratory, the ratio of monomer to catalyst was chosen 100:1.00. The choice of a solvent plays an important role in stabilizing the formation of the helical

Table 3.3 – Summary of polymerization conditions and reactant concentrations for the reaction of **P4** with **Cat.1** - $[\text{Rh}(\text{nbd})\text{Cl}]_2$ and **Cat.2** - $\text{Rh}(\text{nbd})(\text{nPh-BPh}_3)$.

Pol-ID	Materials	mg	[M] _f	Solvent (mL)	R (Molar)
Poly-P4-1	P4	50.0	0.157	0.50 - DMF	100:1.00
	Cat.1	0.400	0.00157		
Poly-P4-2	P4	50.0	0.157		
	Cat.2	0.400	0.00190		
Reacted for 24 hours at room temperature ~ 20 °C.					

structure.¹¹ Ideally, the monomer chains should maintain their secondary interactions (e.g., pi-stacking, H-bonding) during the formation of the polymer backbone, so solvents that disrupt these interactions should be avoided. For instance, H₂O and alcohols would

disrupt the hydrogen bonding between the peptide strands of **P4**, which then could inhibit the formation of a helical backbone. For that reason, DMF and especially THF are widely used in polymerization of monosubstituted acetylenes (Table 3.3). Moreover, as with the polymerization of acrylates (**P1** and **P2**), the concentration of monomers in solution should be kept as high as possible (taking into account their solubility). The reason for this is that a higher concentration increases the probability of the formation of covalent bonds between monomer molecules (*i.e.*, higher chance for monomers to meet each other), potentially leading to better monomer conversions. Considering that only 100 mg of "purified" **P4** was obtained, only two polymerizations were performed involving 50 mg of monomer (Table 3.3).

To monitor the conversion of acetylene monomer **P4**, ¹H-NMR was used. As acetylene monomer is consumed to produce the polymer, C = C bonds are formed, which should be indicated by the presence of proton peaks between 5.0 - 6.0 ppm in the ¹H-NMR spectrum. At the same time, the integration of the proton peak corresponding to the terminal alkyne environment (labeled as **F3** in Figure 3.9) at 3.44 ppm should decrease as the conversion progresses. Equation 3.2 was used to obtain % conversion, where H_{ref} corresponds to either integration of H^δ-Lue at 0.85 ppm (6 H, dd, J = 14.3, 6.5 Hz) or H^β-Ala at 1.23 ppm (3 H, d, J = 7.3 Hz), H_m and H_p correspond to the signals of the acetylenic protons in C triple bond C environment in the monomer (*i.e.*, H_m) at the start of the reaction and in the polymer (*i.e.*, H_p) at the end of the polymerization.

$$Monomer\ Conversion = \left(1 - \frac{\frac{H_p}{H_{ref}}}{\frac{H_m}{H_{ref}}}\right) \times 100\% \quad (3.2)$$

The ¹H-NMR spectra of **Poly-P4-1** and **Poly-P4-2** showed no evidence of vinyl proton environments in the range of 5.0 - 6.5 ppm. In addition, the integration of the terminal H (labeled as **F3** in Figure 3.9) at 3.44 ppm of the propargyl group did not decrease, but increased due to overlap with the HDO peak. On examination of the rest of the NMR spectrum, the same environments as those of the monomer **P4** were identified. The presence of DMF solvent peaks (including satellite peaks at 2.55/3.06 ppm and 7.71/8.20) added significant broadening to the peaks between 2.67 - 2.97 ppm and 7.87 - 8.05 ppm. The terminal amide peaks observed at 7.01 and 7.25 ppm appeared to be broader in **Poly-P4-1** and **Poly-P4-2**, which can be attributed to the self-assembly of **P4** in DMF, likely due to the H-bonding between the peptide chains. Furthermore, the presence of small amine peaks at 7.03 ppm could be related to the side product derived from **P4** with similar primary amide terminal groups. These could be shorter versions of **P4** sequence, created as a result of the degradation of the main chain. Nevertheless, no evidence of clear monomer conversion was observed, suggesting that no polymerization occurred.

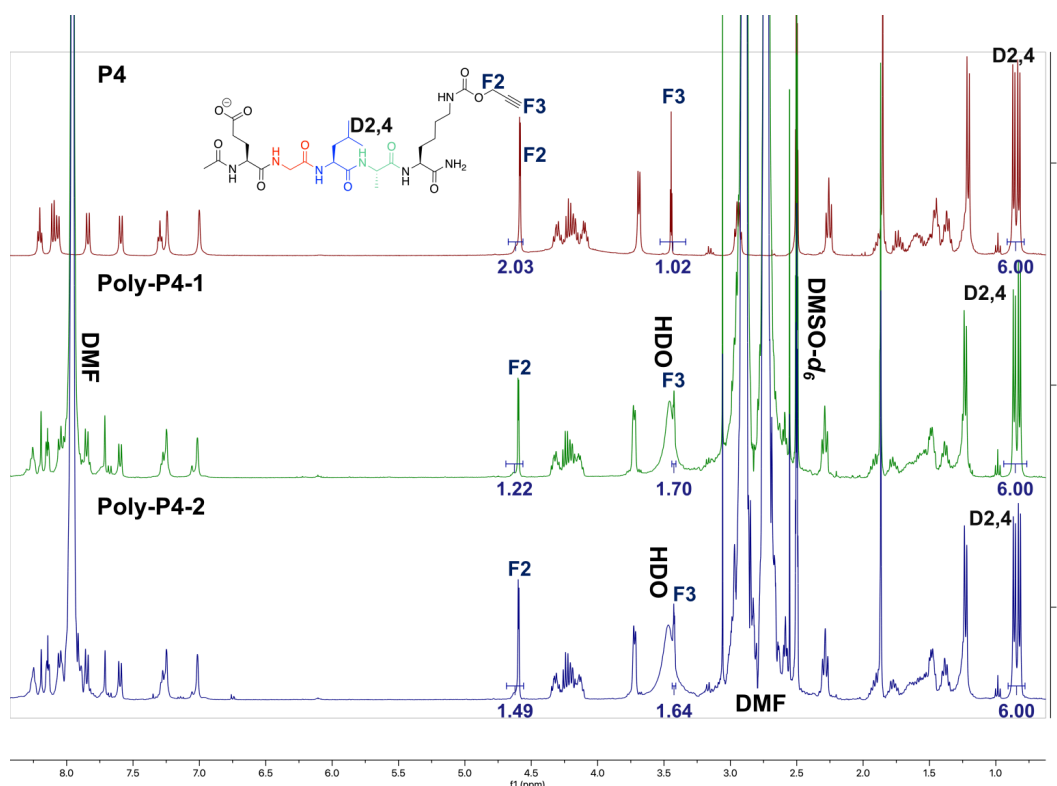


Figure 3.9 – Comparison of ^1H -NMR (400 MHz, $\text{DMSO}-d_6$) spectra of **P4** (Ac-EGLAK(COOCH_2CCH)- NH_2) with products of polymerization reactions **Poly-P4-1** and **Poly-P4-2**.

On the basis of these initial results, several reasons for unsuccessful polymerization were proposed. First, metal catalysts are sensitive to impurities, especially those that contain nucleophilic groups, such as amines.¹¹ Amines can coordinate with the metal center instead of the propargyl group, which inhibits polymerization. With **P4** having 84 % purity, unknown impurities could have caused catalyst deactivation, preventing monomer polymerization. Second, carboxylate-containing monomers (*i.e.*, COOH of glutamic acid in **P4**) are known to terminate Rh-catalyzed polymerization, due to the same coordination issue as with nucleophilic groups.¹¹ Therefore, to solve the limitations mentioned above, the efficacy of purification had to be improved, while carboxylate groups of glutamic acid had to be protected for the duration of the polymerization reaction.

The glutamic acid used in the synthesis of **P4** has an acid-labile tert-butyl ester group, which protects the COOH side chain. It is deprotected during acidic cleavage (95 % TFA) of the peptide sequence of the rink amide resin. To keep glutamic acid protected during the final cleavage step, 2-Chlorotriyl chloride resin can be used instead of rink amide as it only requires weak acidic conditions (1 % TFA) to be cleaved. This way, the tert-butyl group would remain intact and can be removed after polymerization under harsher acidic conditions. However, synthesis with 2-Chlorotriyl chloride resin yields

peptide sequences with a carboxylate terminus that are much more effective at binding to metal centers compared to the amides produced from rink amide resin. Consequently, it becomes essential to protect the carboxylate terminus if the 2-Chlorotrityl chloride resin is used in the synthesis of the peptides.

Before attempting the synthesis of **P4** using 2-Chlorotrityl chloride resin and subsequent protection of its carboxylate terminus, preliminary synthesis and polymerization experiments were performed using shorter peptide sequences as a proof of concept. As a result, various acetylene groups that could be connected to the -GLA- sequence were taken into account. The first requirement for selecting the alkyne group was that it could be linked through an amide bond to the -GLA- sequence, which is attached to the solid support. Therefore, considering that -GLA- is synthesized from the C to N terminus (*i.e.*, from COOH to NH₂), the acetylene group had to have an electrophilic group (*e.g.*, carboxylate).

The second requirement was related to the ability of the acetylene-containing monomer to stabilize the helical structure, which contributes to the formation and stability of the polymeric backbone. The helical structure can be stabilized by a range of secondary interactions such as H-bonding, pi-stacking, and hydrophobic. These secondary interactions pre-organize acetylene monomers (*i.e.*, steric alignment), guiding the formation of the helical backbone.

For example, phenylacetylenes are often used for the formation of poly(acetylene) polymers (poly(phenylacetylenes) - **PPAs**) because of their ability to form a helix with the help of Pi stacking, allowing the development of a variety of supramolecular structures with helicity. Most notably, a thermoresponsive polymer was formed by the successful polymerization of poly(phenylacetylene) with an elastin-based side chain (-VPGVG-sequence) using a rhodium-based catalyst.¹⁴ The polymer obtained had a remarkably different temperature response compared to the majority of elastin-based polymers. Instead of the usual decrease in solubility when heated (**LCST**), elastin-based poly(phenylacetylenes) showed an increase in solubility, exhibiting an upper critical solution temperature (**UCST**).¹⁴ Differences in behavior upon heating were attributed to the helical structure induced by poly(phenylacetylene) groups. This structure caused the terminal amino acids of the -VPGVG- sequence to be oriented outward, making the polymer more soluble in water.¹⁴ The phenylacetylene moiety was represented by 4-ethynylbenzoic acid and was coupled to the protected C-terminal sequence -VPGVG- with the help of uronium activation agents (**HATU**, **HOBt** and **DMAP**).¹⁴ These conditions were not too different from those used for the synthesis of enzyme-responsive peptide sequences (**P1** and **P2**) discussed in Chapter 2 of this Thesis, making the incorporation

of 4-ethynylbenzoic acid into the solid-phase peptide synthesis of the -GLA- sequence relatively straightforward.

H-bonding interactions can also contribute to the stability of helices, particularly of peptide sequences, where each amide bond is an H-bond donor and carbonyl oxygen is an H-bond acceptor. As a result of H-bonding between peptide strands, secondary structures such as α -helices and β -sheets can be formed. Moretto's group used the formation of parallel β -sheets to promote the polymerization of acetylene-containing peptides.¹⁵ To do this, they synthesized a variety of peptides (Figure 3.10, PA-1 to PA-4) from β -sheet promoter amino acid residues such as Val, Leu, Phe and Cys(Me).¹⁶ These amino acids have a high degree of hydrophobicity, comparable to the core enzyme-responsive sequence used in this project -GLA-.

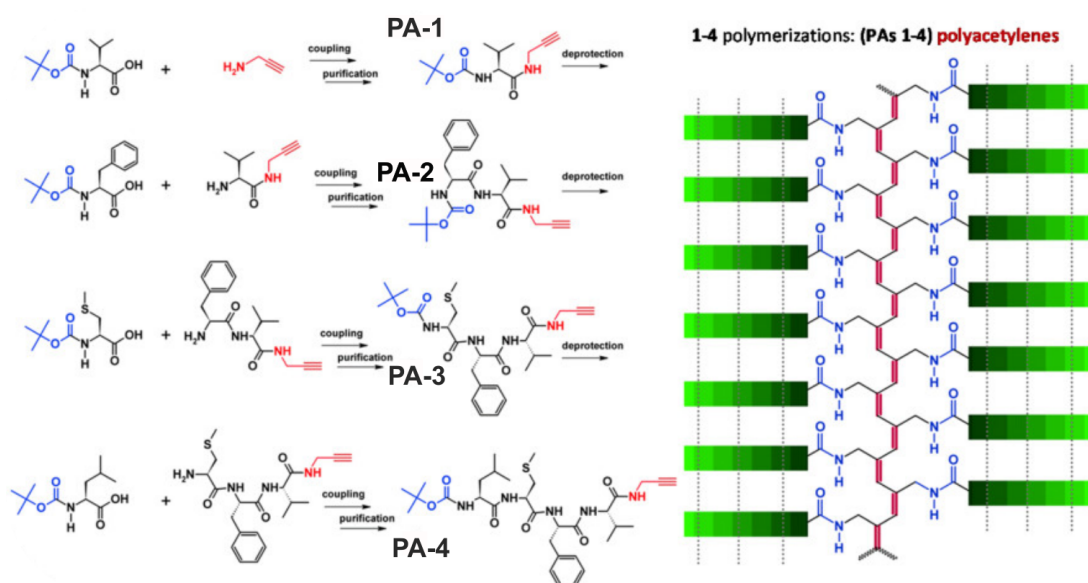


Figure 3.10 – Left: Syntheses and chemical structures of PA-1- 4. Right: Schematic representations of poly(acetylene) polymers. Highlighted in red are the novel, unsaturated and conjugated, polymeric backbones. Reused with permission.¹⁵ Copyright©, 2018 Wiley Periodicals, Inc.

As anticipated, the longest peptides (*i.e.*, PA-3 and PA-4 in Figure 3.10) had a greater tendency to pre-organize into β -sheet structures due to the larger number of amide groups that could form H-bonds. This propensity for pre-organization caused the self-aggregation of these peptides, forming viscous solutions in less polar solvents, such as tetrahydrofuran (THF), with the longest peptides needing the least amount of concentration to do so. Subsequently, Moretto's team conducted polymerization reactions above the critical self-assembly concentration of these peptides, using the same catalyst (**Cat.1**), solvent (THF), and monomer concentration (0.100 M) as those used for the polymerization of **P4** peptides discussed in this Chapter.¹⁵ Of the four peptides, three of them underwent polymerization, while the longest peptide (PA-4, Figure 3.10)

with four amino acid residues (5 amide bonds) did not.¹⁵ This was attributed to the highly stable molecular arrangement (*i.e.*, self-assembly) and the steric hindrance of the peptide sequence (Figure 3.10), which made the formation of the poly(acetylene) backbone energetically unfavorable.

The examples discussed showed that acetylene-containing peptides can stabilize the formation of poly(acetylene) backbones, thus promoting the conversion of peptide monomers into polymers. Therefore, we hypothesized that, by using pre-organization strategies such as π -stacking and β -sheet formation, we could successfully polymerize -GLA- peptides with an acetylene moiety. To test this, two new peptide sequences were created, each consisting of three hydrophobic residues -GLA- (*i.e.*, LasB-responsive segment) and different acetylene functional groups (Table 3.4). **P5** was designed to stabilize the helical structure via π -stacking of the phenyl(acetylene) groups, while **P6** and **P7** had an increased number of H-bond donor groups for the formation of β -sheets. First, the synthesis and polymerization of **P5** is discussed.

Table 3.4 – Chemical structures of the acetylene-containing peptide monomers, evaluated in this Chapter.

I.D.	Structure	I.D.	Structure
P4		P5	
P6		P7	

3.4.3 Synthesis of phenylacetylene-containing peptide **P5**

For the source of phenylacetylene functionality, 4-ethynylbenzoic acid was chosen as it was successfully used before for the polymerization of elastin-like peptides.¹⁴ 4-ethynylbenzoic acid was coupled with the deprotected amine of the Gly residue using **HBTU** and **DIPEA**, following the same solid-phase peptide synthesis procedure as for **P1**-type peptides (Figure 3.11). In the case of **P5** peptide, rink amide resin was used, which produces peptides with a primary amide terminus *e.g.*, **P4**. It is important to note that primary amides are weaker Lewis bases than carboxylates and primary amines, as the lone pair of electrons is more delocalized, making nitrogen less electron rich. As a result, amides are less likely to form metal coordination bonds, which could deactivate the metal catalyst.

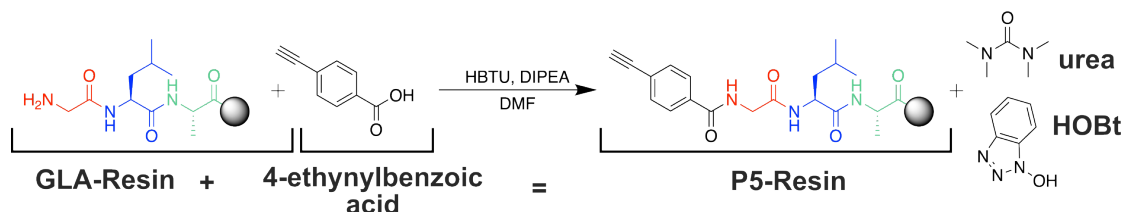


Figure 3.11 – Reaction scheme for coupling 4-ethynylbenzoic acid to -GLA-Resin sequence producing **P5** ($\text{CHC}_6\text{H}_4\text{-GLA-NH}_2$).

HPLC was used to verify the purity of the products obtained (Figure 3.12a, b). This time the chromatogram of the crude mixture from the synthesis of **P5** had a considerably smaller number of peaks compared to **P4** (Figure 3.5), indicating an improved purity (62 %) with the highest peak eluting at 20.69 min. The peak at 20.69 min was then collected with preparative HPLC and analyzed by NMR.

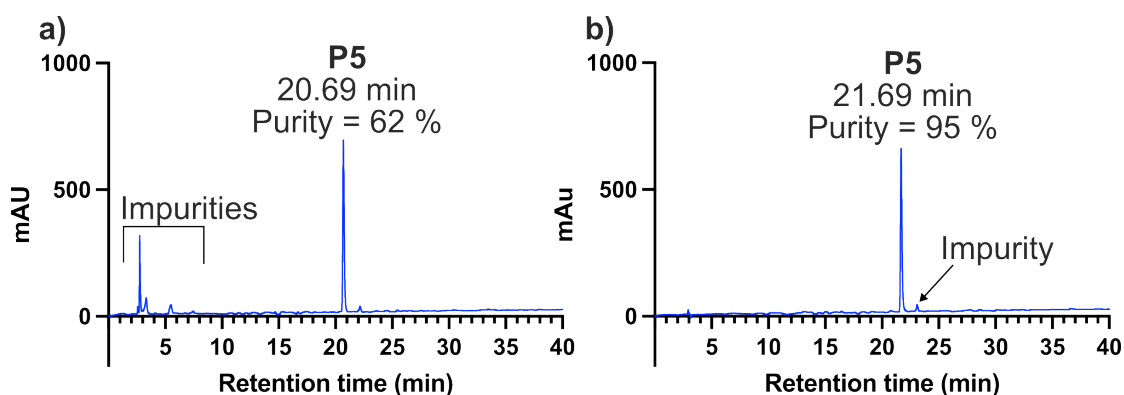


Figure 3.12 – RP-HPLC chromatogram of a) crude and b) purified **P5** ($\text{CHC}_6\text{H}_4\text{-GLA-NH}_2$) sequence.

$^1\text{H-NMR}$ environments of the collected peak at 20.69 min, were perfectly assigned to **P5** chemical structure (Figure 3.13 and fully assigned in Figure S3.34). In this case, the successful coupling of 4-ethynylbenzoic acid was indicated by the presence of aromatic proton environments at 7.58 and 7.87 ppm labeled as **A2** and **A3** in Figure 3.13. The presence of an acetylene group was confirmed by a singlet peak at 4.37 ppm with integration 0.91 (≈ 1) (labeled as **A1** in Figure 3.13). Furthermore, MS was performed on a purified sample of **P5**, where peak with m/z 385.19 (negative ion mode, Figure S3.30) was identified, indicative of **P5** calculated mass 386.20 ($[\text{M} - \text{H}]^- = 385.20$). As before, the crude product of **P5** synthesis had to be purified before being polymerized. The purification process of **P5** peptide was more straightforward compared to the purification of **P4** due to the reduced number of impurity peaks present. Consequently, the purity of the separated product peak **P5** was 95 %, considerably higher than that of **P4** (*i.e.*, 84 %). Following purification, the polymerizations of **P5** were investigated.

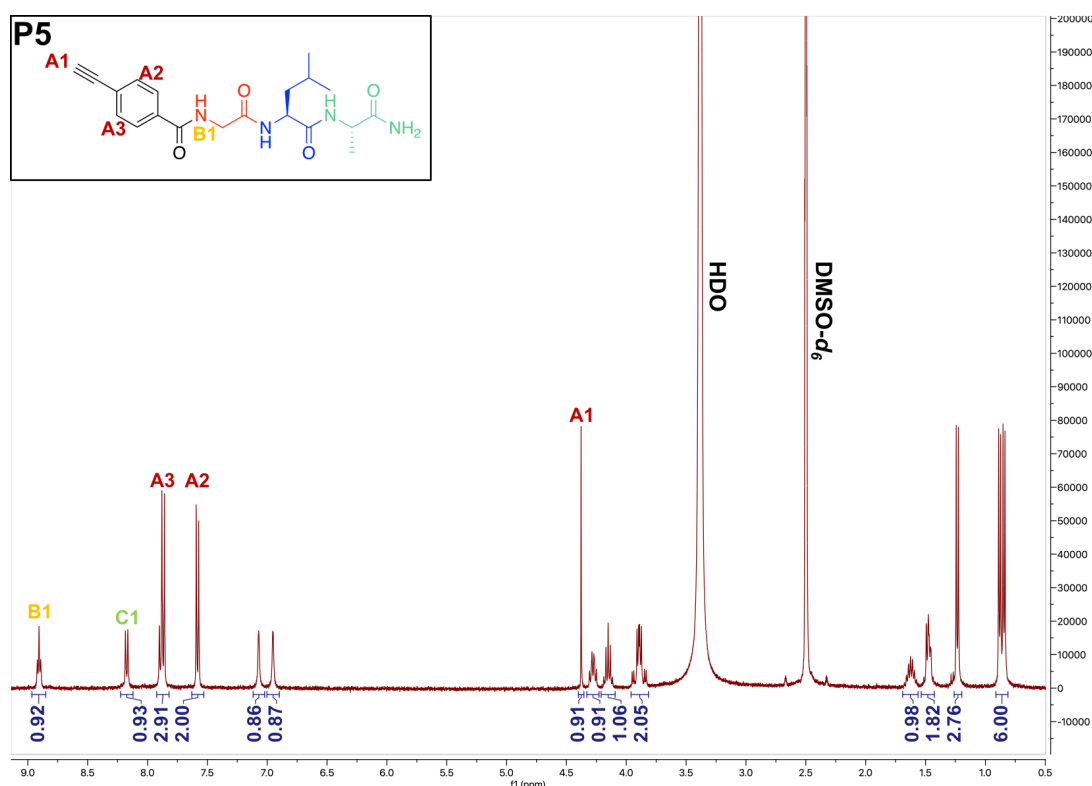


Figure 3.13 – ^1H -NMR(400 MHz, $\text{DMSO}-d_6$) spectrum of the peak at 20.69 min (Figure 3.12) - **P5** ($\text{CHC}_6\text{H}_4\text{-GLA-NH}_2$). For fully assigned NMR spectra see S3.34.

3.4.4 Polymerization of **P5** peptide

With only 90 mg of **P5** monomer recovered, only two polymerization conditions were attempted (Table 3.5), which were similar to those used to polymerize **P4** (Table 3.3).

Table 3.5 – Summary of polymerization conditions and reactant concentrations for the reaction of **P5** with **Cat.1** - $[\text{Rh}(\text{nbd})\text{Cl}]_2$ using acetonitrile (**ACN**) and tetrahydrofuran (**THF**) solvents.

Pol-ID	Materials	mg	[M] _f	Solvent (mL)	R (Molar)
Poly-P5-1	P5	45.0	0.116	0.50 - ACN	100:1.00
	Cat.1	0.537	0.00116		
Poly-P5-2	P5	45.0	0.116	0.50 - THF	
	Cat.1	0.537	0.00116		
Reacted for 24 hours at room temperature ~ 20 °C.					

This time, the effect of solvent polarity on monomer conversion was explored by trying two different solvents: acetonitrile (**ACN**), a more polar solvent, and tetrahydrofuran

(THF) as a less polar solvent, while using the same catalyst, **Cat.1** (Figure 3.14). The monomer and catalyst solutions were reacted for 24 hours, followed by $^1\text{H-NMR}$ analyses to monitor monomer conversion, where decrease in the integration of the acetylinic peaks was monitored. The method for calculating monomer conversions was discussed in Section 3.3.5.1.

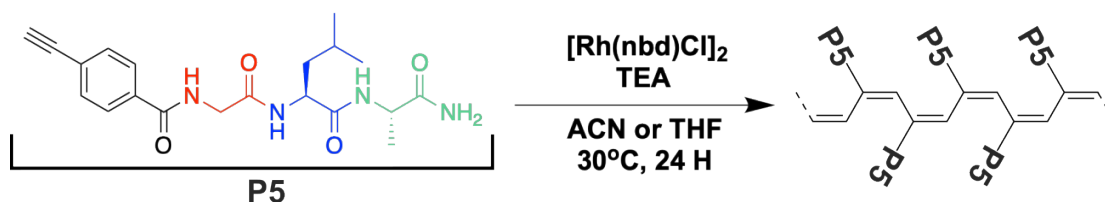


Figure 3.14 – Reaction scheme of polymerization **P5** ($\text{CHC}_6\text{H}_4\text{-GLA-NH}_2$) peptide sequence using **Cat.1**.

By comparing the $^1\text{H-NMR}$ of the monomer with the products of the polymerizations **Poly-P5-1** and **Poly-P5-2**, no broadening of the peaks was observed that would indicate a polymeric structure (Figure 3.15). As in the **P4** polymerizations, all peaks of the **P5**

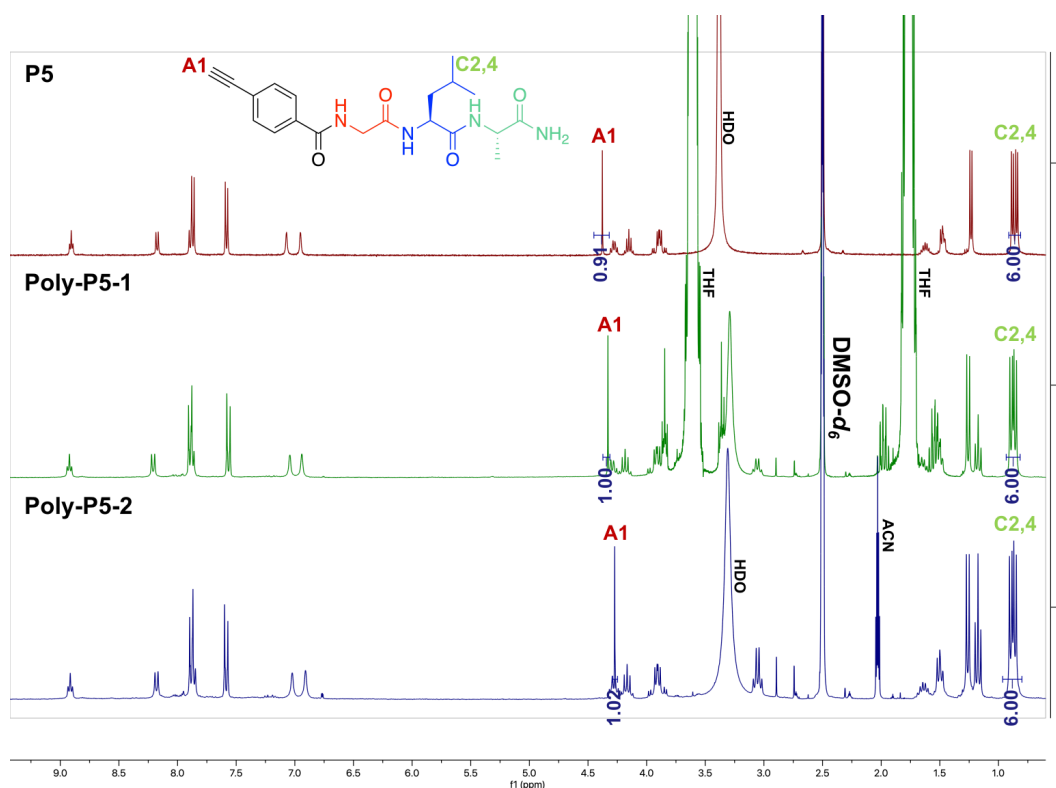


Figure 3.15 – Comparison of $^1\text{H-NMR}$ (400 MHz, $\text{DMSO-}d_6$) spectra of **P5** ($\text{CHC}_6\text{H}_4\text{-GLA-NH}_2$) with products of polymerization reactions **Poly-P5-1** and **Poly-P5-2**.

monomer were present in the crude sample of the polymerization solutions. Additionally, there were no peaks in the range of 5.0 - 6.5 ppm that would represent protons in the $\text{C}=\text{C}$ bond, and the integration of the terminal acetylene proton peak at 4.37 ppm (labeled

as **A1** in Figure 3.15) remained relatively unchanged (Figure 3.15 integrations of **A1** peak: 0.91, 1.00 and 1.02). At 8.0 ppm a group of small multiple peaks was seen in the NMR spectra of **Poly-P5-1** and **Poly-P5-2** (Figure 3.15). These peaks were linked to the environment of the C = C bond in the 2,5-norbornadiene group of **Cat.1** - [Rh(nbd)Cl]₂, which shifted slightly downfield as a result of the Rh atom pulling the electron density from the bond, deshielding the protons (*i.e.*, experiences a stronger magnetic field). Overall, these results clearly indicated that polymerization did not occur.

Although only a few polymerization conditions were attempted for **P5**, it is possible to deduce why the attempts were unsuccessful. The chromatogram of a purified sample of **P5** contained an impurity peak, which eluted after the product peak (21.69 min) at 23.64 min (Figure 3.12). This longer retention time indicated that the polarity of the impurity was lower than that of the product, suggesting that it could be the -GLA- sequence that did not react with 4-ethynylbenzoic acid. The presence of peptide sequences with deprotected primary amine groups could lead to deactivation of the metal catalyst as a result of amines' ability to chelate metal centers.

Another key factor contributing to the unsuccessful polymerization can be attributed to the low monomer concentration used in the reaction (0.116 M, **P5**). When the monomer concentration is low, the metal catalyst does not interact with an adequate amount of **P5** chains before it undergoes degradation, which prevents the formation of a poly(acetylene) backbone, ultimately resulting in insufficient monomer conversion. To illustrate, Arias and colleagues used a monomer concentration of 0.300 M for the polymerization of phenylacetylene-containing peptides, which is three times higher than that used for **P5**.¹⁴ With only 90 mg of pure **P5** available, the decision was made to attempt polymerizations under different solvents rather than using all of the available purified peptide for a single polymerization condition. At that time, it was not possible to synthesize more **P5** due to difficulties in obtaining 4-ethynylbenzoic acid in sufficient quantities. Furthermore, with the **P5** sequences containing hydrophobic groups (*i.e.*, phenolic, -GLA-) solubility of **P5** monomer even in polar solvents would be an additional barrier to obtaining high monomer concentrations. Therefore, the development of **P5** poly(acetylene) polymer was put on hold and the focus shifted to other acetylene-containing peptides **P6** and **P7**, which used a more readily available propargyl amine group as a source of acetylene functionality.

3.4.5 Synthesis of propargyl containing peptides **P6** and **P7**

Our aim with peptides **P6/P7** was to investigate if the pre-organization of the acetylene-containing monomers into secondary structures such as β -sheets can facilitate the

formation of the helical backbone with enzyme-degradable peptide side chain. The key to the formation of the β -sheet lies in the ability of the peptides to align next to each other, allowing H-bonds to form between the strands, stabilizing the structure. Therefore, the easiest way to increase the H-bonding capacity of the -GLA- sequence was to add more amide groups (e.g., more amino acid residues) while simultaneously coupling propargyl amine.

For the peptides presented in this Thesis, synthesis occurred in the direction C to N, which meant that to couple the propargyl amine to the Gly residue, the primary amine had to be converted into or coupled to an electrophilic group such as carboxylate. Furthermore, the addition of an extra amino acid residue to increase the number of amide groups was not considered because this could result in changes to the enzyme degradation properties of the sequence. At that time, our laboratory frequently employed the reactivity of 1,1'-Carbonyldiimidazole (CDI) for nucleophilic addition reactions, particularly for coupling propargyl amine with various nucleophilic groups. Consequently, a similar strategy was adopted for the synthesis of **P6** and **P7**.

To start, CDI was reacted with the amine of the deprotected Gly residue, forming the intermediate acyl imidazole-peptide (labeled as **CI-GLA-Resin** in Figure 3.16). In the intermediate form, the imidazole group pulls the electron density from the carbonyl bond, making carbonyl carbon electrophilic enough for propargyl amine to attack it. Consequently, propargyl amine was coupled, producing peptide **P6**, which was then cleaved from the solid support (Table 3.6).

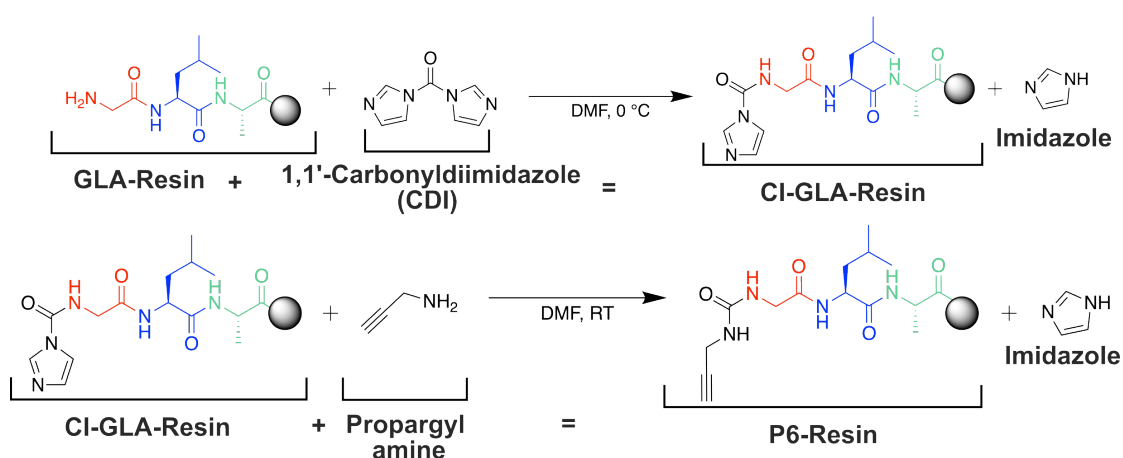


Figure 3.16 – Reaction scheme for coupling propargyl amine to -GLA-Resin sequence through imidazole-peptide intermediate, forming **P6** and **P7** peptide.

The coupling of Gly with propargyl amine was made possible by the formation of a urea bond. This resulted in peptides derived from **P6** having four amide groups, which

Table 3.6 – Chemical structures of the **P6** and **P7** peptides.

I.D.	Structure	I.D.	Structure
P6		P7	

were hypothesized to stabilize the formation of β -sheets by H-bonding between neighboring peptide sequences. Two β -sheet configurations were theoretically possible: parallel (Figure 3.17 a) and anti-parallel (Figure 3.17 b). In the anti-parallel arrangement of β -sheets (Figure 3.17b), the acetylene groups would be arranged in an alternating pattern, which could inhibit the formation of the poly(acetylene) backbone and result in low monomer conversions. On the other hand, in the parallel arrangement (Figure 3.17a), the acetylene groups would be on the same side, which should make it easier to form a helical backbone.

a) Theoretical parallel β -sheets for P6 **b) Theoretical anti-parallel β -sheets for P6**

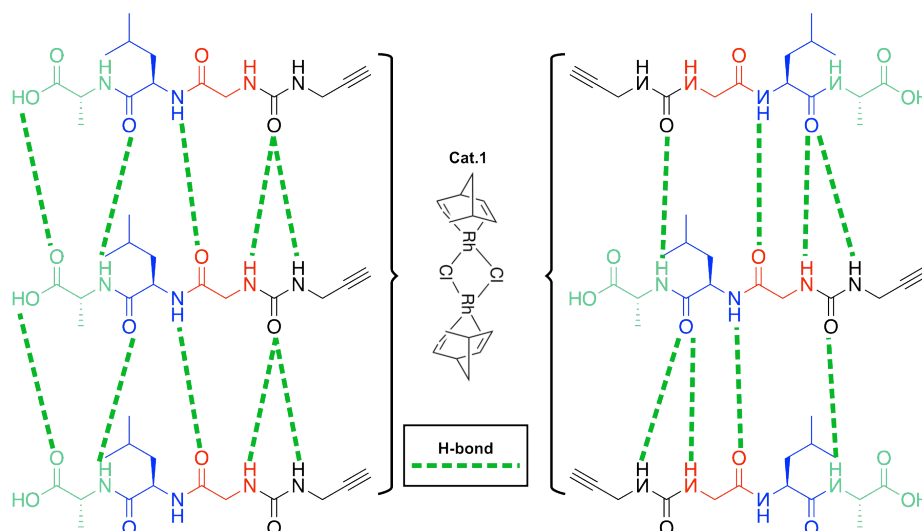


Figure 3.17 – Schematic representation of a) parallel and b) anti-parallel β -sheet formation between the monomers of **P6**.

The peptide sequence **P6** was synthesized using the standard **SPPS** methodology (as described in Section 3.3.3.3). However, compared to other sequences (e.g., **P4**, **P5**), 2-Chlorotrityl chloride resin was used to explore new synthesis conditions that could be applied to the future synthesis of **P4**-derived acetylene-containing peptides (Table 3.6). Additionally, the effect of protecting the peptide terminus on monomer conversion was also studied in polymerization reactions. This is because cleavage from the 2-Chlorotrityl chloride resin produced peptide **P6** with a carboxylate terminus, which

has the potential to chelate metal centers and deactivate the Rh catalyst in the polymerization reaction, leading to low monomer conversion. Therefore, in addition to the **P6** peptide, a terminus-protected version **P7** was also synthesized (Table 3.6). To protect the carboxylate terminus, a methylation reaction was performed using $(\text{CH}_3)\text{SiCl}$ and MeOH on the cleaved **P6** sequence.¹⁷ For more details, see Section 3.3.3.4.

As with other peptides discussed in this thesis, the crude product of peptide synthesis contained some impurities, as seen from the HPLC chromatograms (Figure 3.18).

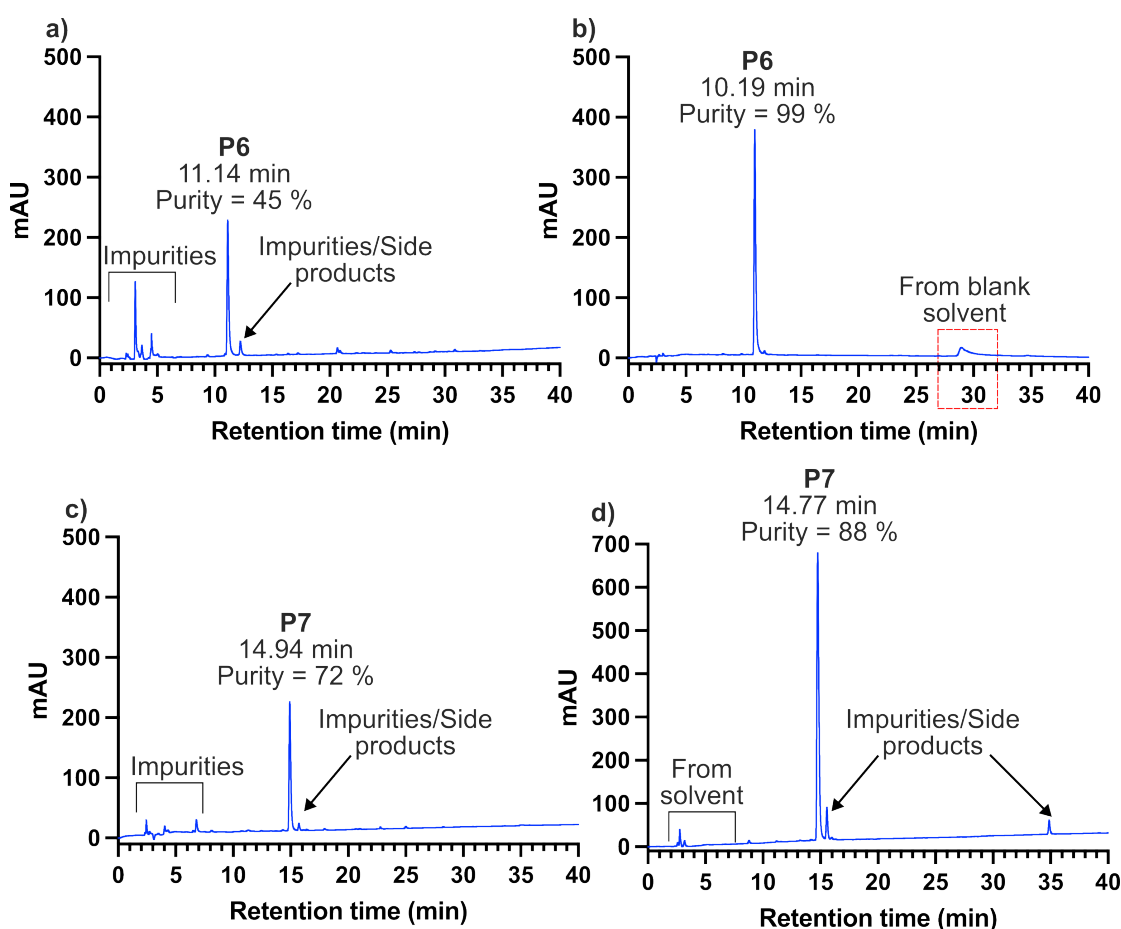


Figure 3.18 – RP-HPLC chromatogram of a) crude and b) purified **P6** ($\text{CHCCH}_2\text{NHCO-GLA-OH}$) sequences. b) RP-HPLC chromatogram of c) crude and d) purified **P7** ($\text{CHCCH}_2\text{NHCO-GLA-OCH}_3$).

The product peak of **P6** eluted earlier than **P7** (11.14 min compared to 14.94 min) due to the higher polarity of the former as a result of the deprotected carboxylate terminus. In both cases **P6** and **P7** product peaks were separated by preparative HPLC. Despite using the same experimental procedure, purification of **P7** was not as successful as **P6**, with a purity of only 88% (Figure 3.18d). This was attributed to poor peak separation caused by injection of a larger volume of the analyte, resulting in column overload.

Interestingly, the chromatograms of **P6** and **P7** had an extra peak that eluted later than the product peaks (at 12.33 min for **P6** and 15.61 min for **P7**). This peak could be attributed to the presence of unreacted -GLA-OH and -GLA-OMe sequences, which may have been created due to an incomplete coupling of CDI + Propargyl amine. After the product peaks of **P6** and **P7** were collected, the samples were characterized by NMR.

NMR analyses of purified samples of **P6** and **P7** indicated the presence of all environments related to their chemical structures (Figures 3.19 and 3.20). Peaks corresponding to the propargyl group were present in both NMRs of the analyzed peptides: triplet peak at 3.00 ppm (labeled as **A1**), multiplet representing the CH₂ group (labeled as **A3**), and triplet amide peak at 6.50 ppm (labeled as **A2**) as illustrated in Figure 3.19 and 3.20. ¹H-NMR spectra of **P7** did have an additional singlet peak at 3.59 ppm (labeled as **D4** in Figure 3.20) with integration 3.06, which was assigned to the methyl group at the C-terminus of the peptide sequence.

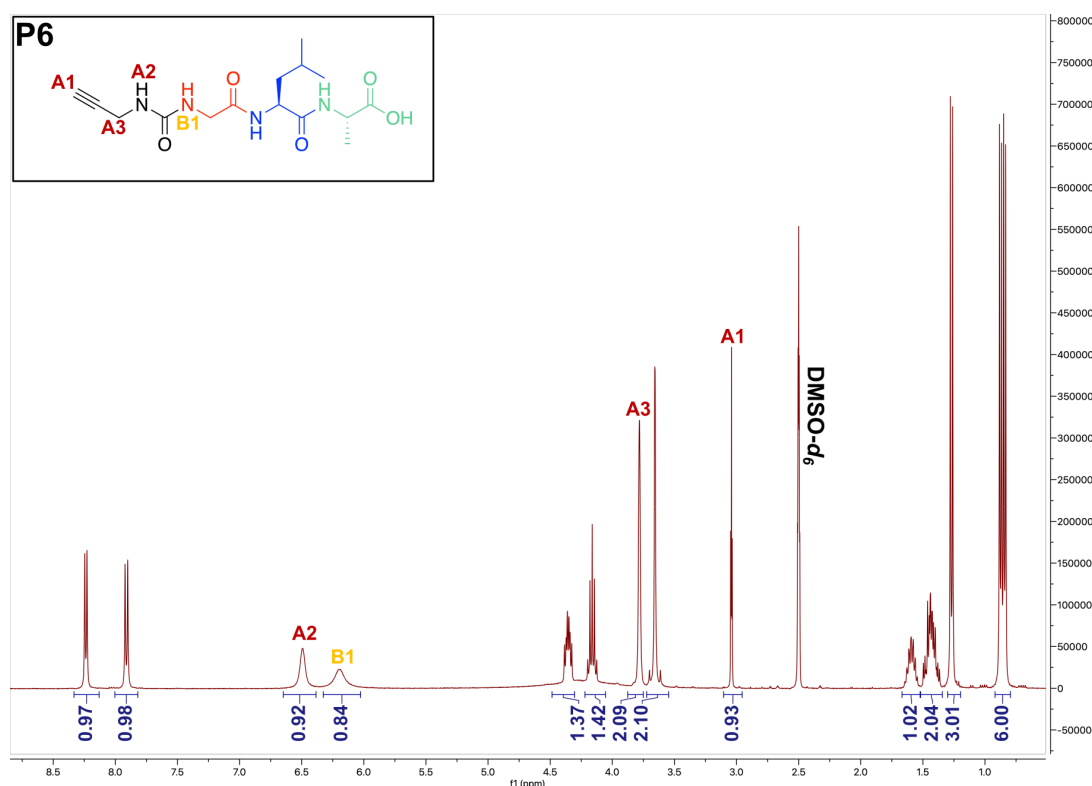
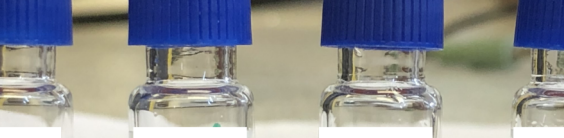
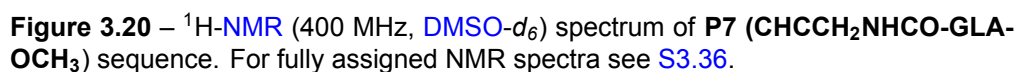


Figure 3.19 – ¹H-NMR (400 MHz, DMSO-*d*₆) spectrum of **P6** (CHCCH₂NHCO-GLA-OH) sequence. For fully assigned NMR spectra see S3.35.

Interestingly, triplet peaks representing propargyl-glycine linkage (urea bond, labeled as **A2** and **B1** in Figure 3.19) amide environments had poor resolution and were considerably broader in the ¹H-NMR spectra of **P6**. This broadening of the peaks could be attributed to the pre-organization of the **P6** monomers into β sheets induced by the



Four glass vials with blue caps are shown, each containing a solution of increasing concentration. The solutions become progressively more turbid from left to right. The concentrations are labeled on white labels in front of each vial.

Concentration
0.0147 M
0.0294 M
0.0588 M
0.118 M

Figure 3.21 – Turbidity changes of **P6** samples under different monomer concentration in THF.

Starting from a concentration of 0.0588 M and above a viscous white self-standing **P6** samples were obtained, indicating that the critical self-assembly concentration was achieved between 0.0294 and 0.0588 M (Figure 3.21). These results confirmed that **P6** sequence self-assembles in non-polar solutions, similar to the peptides reported by Marafon et al.¹⁵ However, without using circular dichroism (CD) to analyze the self-assembled sample of **P6**, it is difficult to conclude which conformation was formed when self-assembly occurs, but based on previous research and the relatively small size of **P6**, the secondary structure is probably composed of β -sheets.¹⁵ The critical concentration of self-assembly for **P7** was not determined. However, as **P7** contained fewer H-bond donor groups (*i.e.*, carboxylate terminus is protected), the critical self-assembly concentration would be slightly higher than that of **P6**.

3.4.6 Polymerization of P6 and P7 peptides

After determining the critical concentration required for the self-assembly of **P6** monomers, attempts were made to polymerize them (Figure 3.22). To ensure that the peptide monomers were in a pre-organized state (*i.e.*, self-assembled), all polymerizations were carried out at concentrations higher than the critical concentration of 0.100 M in a low-polarity solvent such as THF (Table 3.7). Notably, both **P7** and **P6** formed viscous solutions at 0.100 M concentrations, suggesting the presence of pre-organization. In addition, to investigate the influence of concentration on monomer conversion, a higher concentration of 0.226 M was used for **Poly-P7-3** and **Poly-P7-4** polymerizations. For both peptide monomers (**P6** and **P7**), **Cat.1** and **Cat.2** were used.^{14,15} The temperature of the reaction for the polymerization of **P6** and **P7** monomers was maintained at 50 °C to ensure that the self-assembled structures were present in a mobile state, which should improve the kinetics of the polymerization. As with all other polymerizations of acetylene-containing peptides, the reaction was conducted for 24 hours with ¹H-NMR used to track monomer conversions, where decrease in the integration of the acetylinic peaks was monitored. The method for calculating monomer conversions was discussed in Section 3.3.5.1.

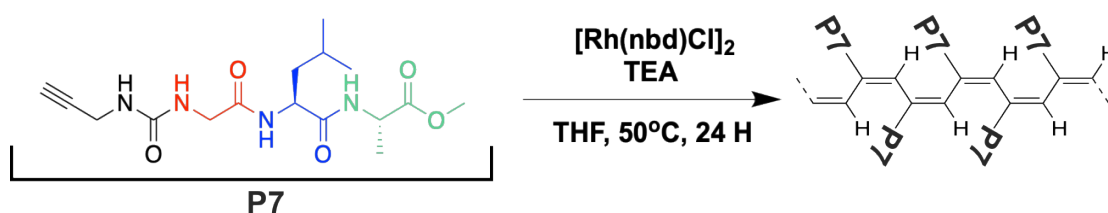


Figure 3.22 – Reaction scheme of polymerization **P7** (**CHCCH₂NHCO-GLA-OCH₃**) peptide sequence using **Cat.1**. The same scheme can be applied for polymerization of **P6** (**CHCCH₂NHCO-GLA-OH**).

Table 3.7 – Summary of polymerization conditions and reactant concentrations for the reaction of **P6** and **P7** monomers with **Cat.1** - [Rh(nbd)Cl]₂ and **Cat.2**, Rh(nbd)(nPh-BPh₃) using tetrahydrofuran (THF) solvent.

Pol-ID	Materials	mg	[M] _f	Solvent (mL)	R (Molar)
Poly-P6-1	P6	35.0	0.103	1.00 - THF	100:1.0
	Cat.1	0.474	0.00103		
Poly-P6-2	P6	35.0	0.103		
	Cat.2	0.529	0.00103		
Poly-P7-1	P7	17.5	0.100	0.50 - THF	100:1.0
	Cat.1	0.228	0.00100		
Poly-P7-2	P7	17.5	0.100		
	Cat.2	0.254	0.00100		
Poly-P7-3	P7	40.0	0.226		
	Cat.1	0.520	0.00226		
Poly-P7-4	P7	40.0	0.226		
	Cat.2	0.580	0.00226		
Reacted for 24 hours at 50 °C.					

The **Poly-P6-1** and **Poly-P6-2** NMR spectra revealed a slight decrease in acetylene protons integration at 3.00 ppm from 0.93 in a monomer to 0.71 in **Poly-P6-1** and 0.86 in **Poly-P6-2** (labeled as **A1** in Figure 3.23). Initially, these results suggested that polymerizations occurred, but with very low conversion, specifically 24 % for **Poly-P6-1** and 8 % for **Poly-P6-2**. Given that **Poly-P6-1** exhibited a conversion of 24 %, one could expect a more significant broadening in its spectra compared to the **Poly-P6-2** sample. However, both samples **Poly-P6-1** and **Poly-P6-2** had identical levels of peak broadening, particularly evident in the amide region (8.25 - 8.50 ppm). Consequently, this led to the hypothesis that side reactions involving the acetylene group occurred instead of the desired polymerization, which led to a decrease in integrations. Before further investigation of this concept, the results of **P7** polymerizations were examined using NMR (Figure 3.24).

Polymerization's **Poly-P7-1** and **Poly-P7-2** yielded results similar to the ¹H-NMR of **P7** monomer (Figure 3.24). The acetylene proton peak at 2.98 - 3.00 ppm (labeled as **A1** in Figure 3.24) had integration values (0.96 for **Poly-P7-1** and 0.97 for **Poly-P7-2**) close to the original value of 0.92 (Figure 3.24). However, for polymerizations at higher monomer concentrations **Poly-P7-3** and **Poly-P7-4**, the integrations of the peak corresponding to the acetylene proton decreased from 0.92 in the monomer to 0.86

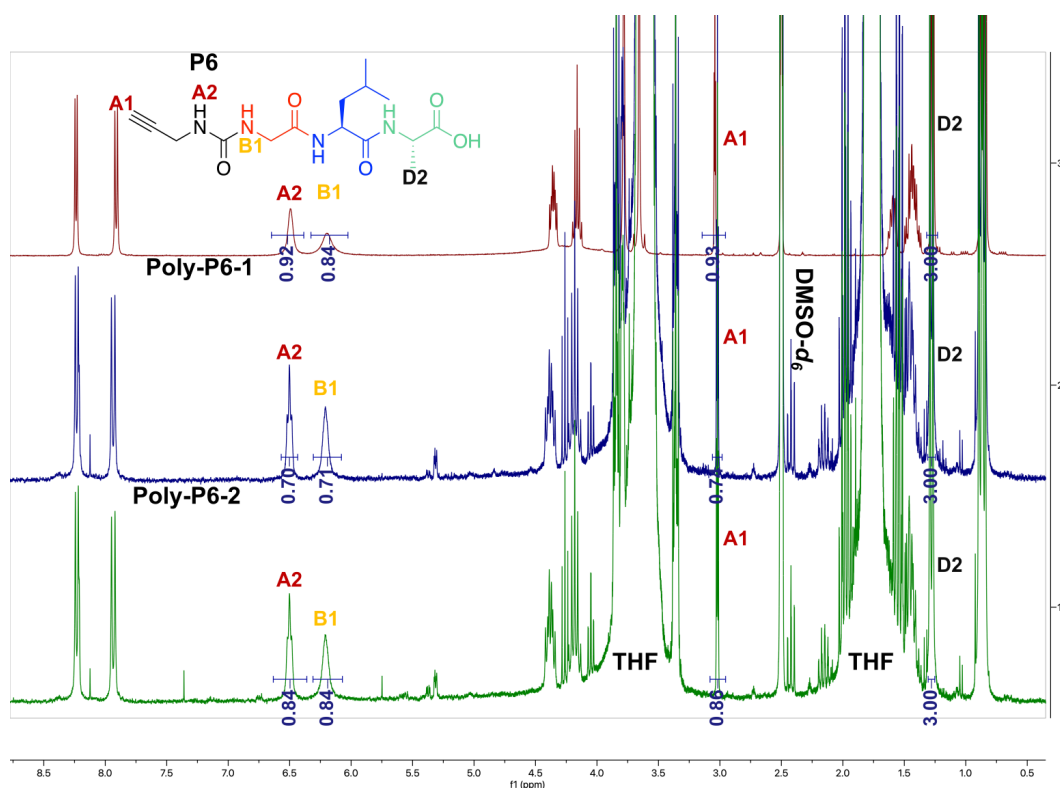


Figure 3.23 – Comparison of $^1\text{H-NMR}$ (400 MHz, $\text{DMSO-}d_6$) spectra of **P6** ($\text{CHCCH}_2\text{NHCO-GLA-OH}$) with the product of polymerizations **Poly-P6-1** and **Poly-P6-2**.

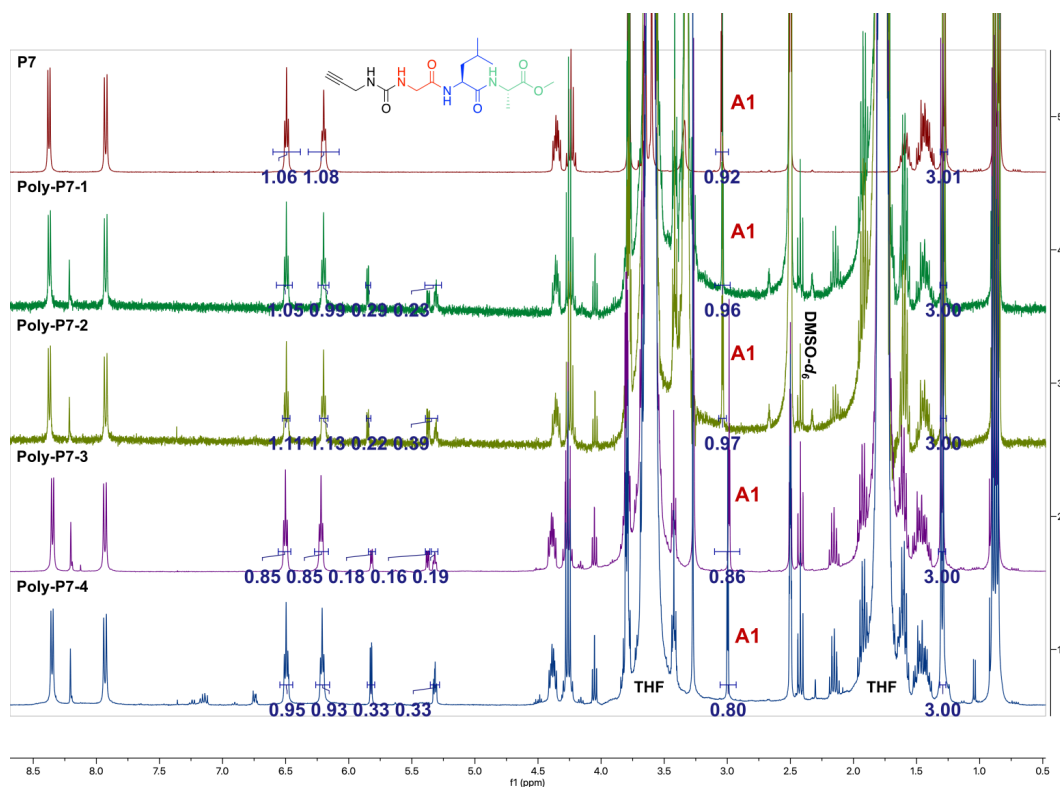


Figure 3.24 – Comparison of $^1\text{H-NMR}$ (400 MHz, $\text{DMSO-}d_6$) spectra of **P7** ($\text{CHCCH}_2\text{NHCO-GLA-OCH}_3$) with product of polymerizations **Poly-P7-1** to **Poly-P7-4**.

and 0.80, indicating that the $C \equiv C$ bond reacted. Furthermore, a set of multiplet peaks appeared between 5.20 and 5.85 ppm for all **Poly-P7** conditions. The first multiplet at 5.32 ppm was identified as a triplet of doublets (td), the second multiplet at 5.38 ppm was a doublet of doublets (dd), and another doublet of doublets at 5.82 ppm (Figure 3.24). It was noticed that **Poly-P6-1** and **Poly-P6-2** had similar multiple peaks at 5.31 ppm, implying that similar side reactions were occurring for **P6** and **P7**, which were more noticeable when the monomer concentration was higher, such as in **Poly-P7-3** and **Poly-P7-4**.

In the event of a successful polymerization of **P7** or **P6**, a polymer with *cis-trans*oidal conformation would have been produced, as illustrated in Figure 3.25. In this conformation, the single proton located within the $C = C$ bond would not exhibit spin-spin coupling with neighboring protons due to being separated by two-carbon atoms (Figure 3.25). This would have resulted in a singlet peak in the 1H -NMR spectrum between 5.0 - 6.0 ppm, which was not observed for either **P6** or **P7**. Therefore, the multiple peaks seen between 5.20 and 5.80 ppm (Figure 3.24) did not correspond to the poly(acetylene) backbone.

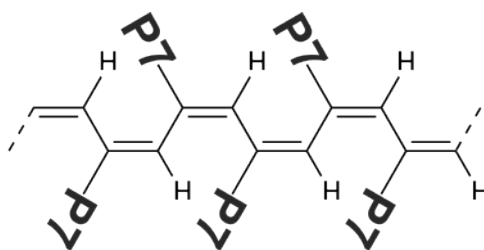


Figure 3.25 – Proposed chemical structure of *cis-trans*oidal conformation of **Poly-P7**.

Upon considering the potential products of side reactions involving the acetylene group in **P6** and **P7**, the formation of a dimer structure was proposed, as illustrated in Figure 3.26. The approximate chemical structure of **P7**-dimer was predicted from the 1H -NMR based on the multiplet peaks between 5.20 and 5.80 ppm and a peak at 8.20 ppm. In the proposed **P7**-dimer one of the protons in the $C = C$ bond, labeled as **H1** in Figure 3.26 would be split by the two protons of a CH_2 in the propargyl group, as well as by its vicinal neighbor, labeled as **H2** in Figure 3.26, resulting in a triplet of doublets splitting (Figure 3.26), which was observed for the peak at 5.32 ppm (td, $J = 4.8, 4.7, 1.6$ Hz). However, a coupling constant of 1.6 Hz, is too small for a vicinal 3J coupling (e.g., 5 - 14 Hz) and more accurately represents the coupling to geminal protons. The second proton of the $C = C$ bond (labeled as **H2** in Figure 3.26) would form a doublet of doublets from the spin-spin coupling with the amide proton, as well as its neighbor $C = C$ proton **H1**. A doublet of doublets peak at 5.38 ppm (dd, $J = 6.0, 2.1$ Hz) was found in NMR of **Poly-P7-3** (Figure 3.26). Although, similarly to **H1**, the coupling constant of

2.1 Hz is considerably low for 3J coupling. The protons in CH_2 of the propargyl group would also form a doublet of doublets as they would be split by the amide of the Gly residue and **H1** (Figure 3.26), which was assigned to the peak at 5.82 ppm (dd, $J = 4.6, 0.9$ Hz). Furthermore, in all **Poly-P7** spectra, a new single doublet-shaped peak appeared at 8.20 ppm (d, $J = 4.6$ Hz), which can be related to the environment of **H3** (Figure 3.26), since it is split by a single proton of the $\text{C} = \text{C}$ bond labeled as **H2** in Figure 3.26. The proposed **P7**-dimer chemical structure had clear inconsistencies with the coupling constants of the NMR spectrum. This discrepancy underscores the necessity for additional characterization of **Poly-P7-3** such as MS as well as further analysis with Nuclear Overhauser Effect Spectroscopy NMR to identify the chemical structure of the side-product

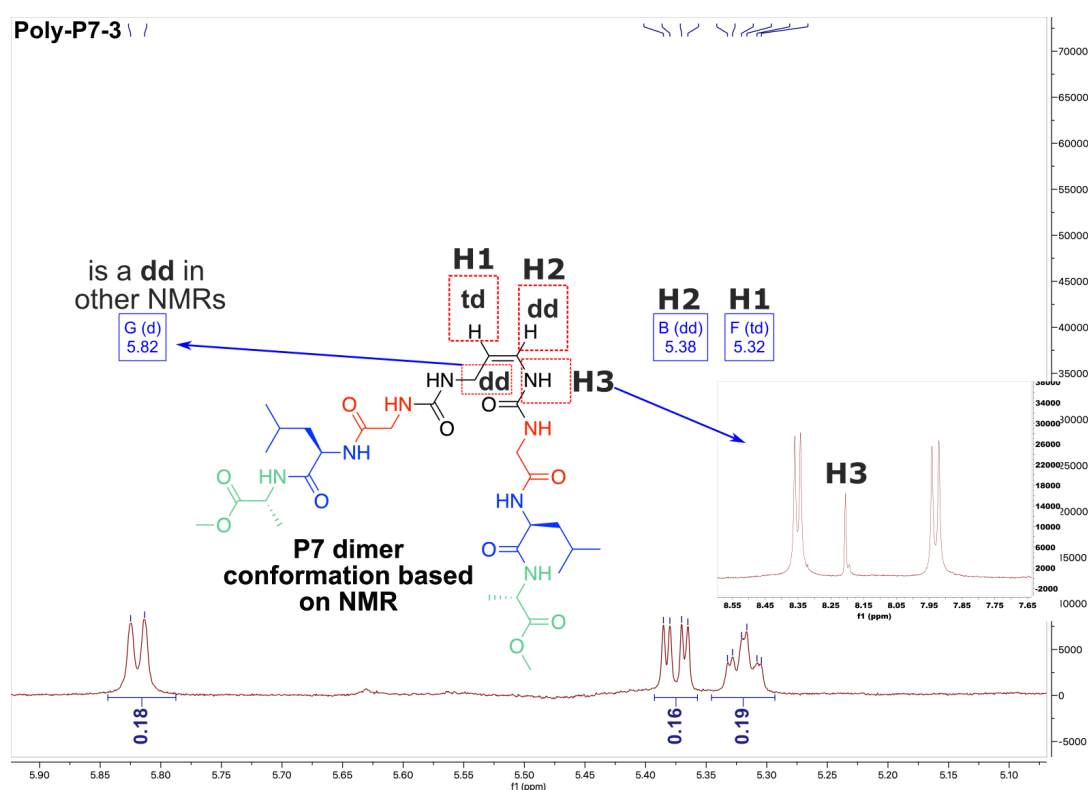


Figure 3.26 – Zoomed in ^1H -NMR (400 MHz, $\text{DMSO}-d_6$) spectrum of **Poly-P7-3**.

In summary, based on the NMR analysis of **Poly-P7** samples, none of the conditions resulted in the formation of a polymer. It was proposed that the primary cause of the unsuccessful polymerizations of **P6** and **P7** was their high stability when pre-organized into β -sheets, particularly in the case of an anti-parallel arrangement, which makes the formation of conjugated bonds thermodynamically unfavorable. The formation of secondary structures was directly associated with the number of H-Bond donor and acceptor groups. As propargyl amine was coupled through the carbonylimidazole intermediate, an additional amide bond was formed, forming a total of 4 amide groups

in **P6** and **P7** sequence. Furthermore, in urea bond amides are located closer to each other (only one carbon away) compared to amino acid residues (two carbons away), which should result in overall stronger affinities of the neighboring peptide sequences. Therefore, to further optimize the polymerization conditions of **P6/7** peptides, different approaches that focus on reducing the strength of secondary interaction but not completely eliminating them should be attempted. An example of one of the approaches could be to use a polar protic solvents for the polymerization *e.g.*, MeOH, which would compete for H-bonding with the peptide monomers, reducing the strength of secondary interactions.

3.5 Conclusions

In this chapter, we shifted our focus from the enzyme-responsive poly(methacrylamides) discussed in Chapter 2 to explore the potential of poly(acetylenes) as promising candidates to encapsulate and facilitate the enzyme-responsive delivery of AMPs. The distinctive feature of poly(acetylenes) lies in their dynamic helical backbones, which can alter their structural conformation in response to external stimuli, such as changes in pH, temperature, and oxidation stress. In comparison, the methacrylamide backbones often lack this responsiveness and are primarily used to connect stimuli-responsive side chains to larger macromolecules for improved drug encapsulation efficacy.

Therefore, this Chapter investigated the possibility of combining the stimuli-responsive properties of poly(acetylenes) with the anionic enzyme-degradable peptide sequence (-EGLA-). The goal was to develop a novel encapsulating polymer that can release AMP more effectively in response to stimuli when incorporated into the nanoparticle. First, the acetylene-containing group had to be coupled to the -EGLA- sequence. To achieve this, propargyl chloroformate was used to couple the functional group of acetylene to the Lys side chain, successfully producing **P4**. For the polymerization reaction, two Rh catalysts were used (**Cat.1** - $[\text{Rh}(\text{nbd})\text{Cl}]_2$, **Cat.2** - $\text{Rh}(\text{nbd})(\text{nPh-BPh}_3)$), which are known to produce poly(acetylenes) backbones with *cis-transoidal* conformation. However, none of the conditions led to monomer conversion, which was linked to the deprotected carboxylate side chain of glutamic acid in **P4**, which could coordinate to the metal center, deactivating the catalyst. Thus, the choice was made to first test the polymerization of shorter peptide sequences (**P5**, **P6** and **P7**) with only three core residues (-GLA-) as a demonstration of the concept. Moreover, to promote the formation of a helical backbone, different stabilizing interactions of acetylene-containing groups were studied. For example, in **P5** acetylene group was coupled to -GLA- through the phenolic ring, which is known to stabilize the poly(acetylenes) backbones via pi-stacking interactions. For **P6** and **P7**, propargyl amine was used as a source of acetylene functionality, which was coupled to the Gly residue through the formation of an intermediate acyl imidazole peptide. This coupling created a urea bond between propargyl amine and Gly residue, introducing two additional H-bonding groups for the stabilization of the poly(acetylene) backbone.

The coupling techniques used produced the desired acetylene-containing peptides, which were later purified, resulting in sequences with different purities ranging from 84 to 99 %. Two of the four synthesized peptides, **P6** and **P7**, self-assembled in non-polar solvents such as THF, forming a viscous, off-white, self-standing sample. This was related to the extensive H-bonding network, facilitated by the urea bond between the

Gly and propargyl amine groups. We hypothesized that pre-organization of **P6** and **P7** could be beneficial for the formation of the helical polymer backbone, as the monomer sequence would be closer together, improving the efficacy of polymerization. However, despite the intention of enhancing the stability of the poly(acetylene) backbone with peptides **P5**, **P6**, and **P7**, none of the attempted polymerization conditions yielded polymerization products. Taking into account all efforts to polymerize acetylene-containing peptides (**P4** - **P7**), potential explanations for the absence of polymerization include:

- The presence of impurities in (e.g., **P4**) with metal coordinating groups (e.g., NH_2 and COOH), resulting in deactivation of the Rh catalyst.
- Use of insufficient monomer concentrations, particularly with **P5** peptide.
- Self-assembly of the monomers into highly stable secondary structures prevented the formation of the helical backbone, as was the case for the **P6** and **P7** peptides.

In conclusion, none of the peptides with acetylene groups could be polymerized, as a result, they were not suitable for the creation of an enzyme-responsive delivery system for **AMPs**. As a result poly(acrylamide) polymers (*i.e.*, **Poly-P1** and **Poly-P2**) from Chapter 2 which had previously demonstrated the desired enzyme-responsive properties, were selected for the assembly of polyelectrolyte complexes with **AMP**.

3.6 Supporting information

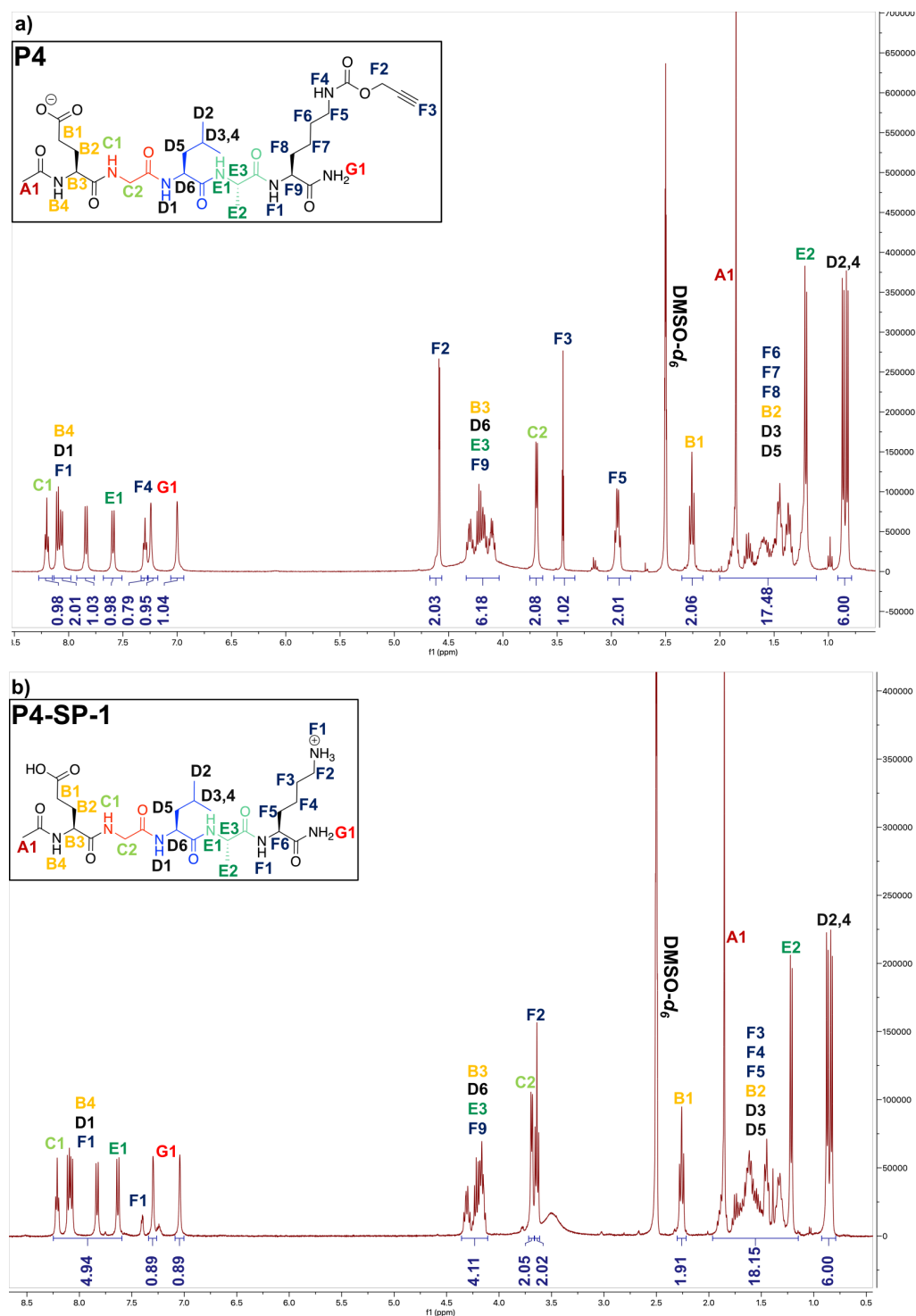


Figure S3.27 – a) Fully assigned ¹H-NMR (400 MHz, DMSO-*d*₆) spectra of the peak at 15.62 min - **P4** (Ac-EGLAK(COOCH₂CCH)-NH₂). b) Fully assigned ¹H-NMR (400 MHz, DMSO-*d*₆) spectra of peak at 19.53 min **P4-SP-1** (Ac-EGLAK-NH₂).

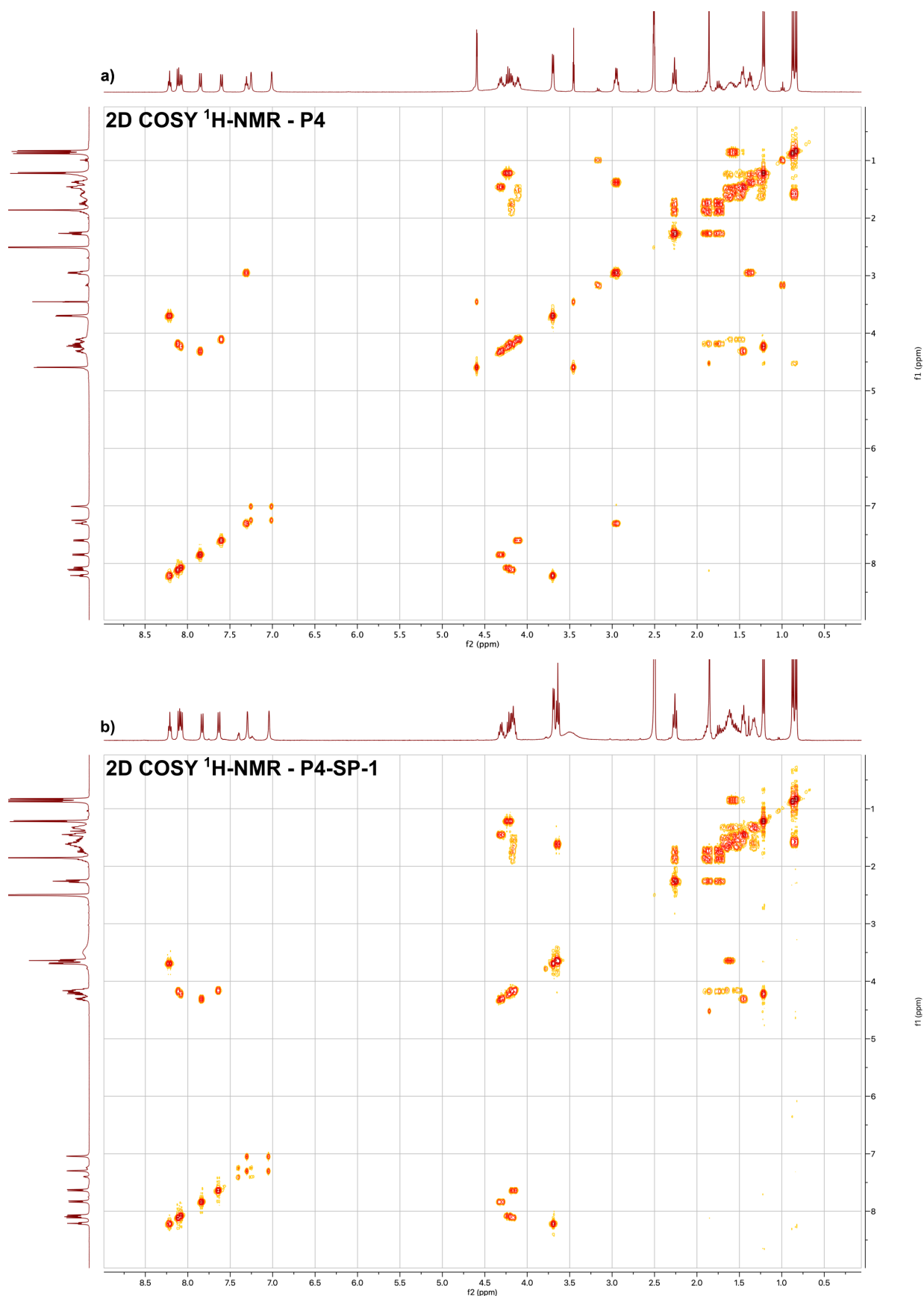


Figure S3.28 – 2D-COSY ^1H -NMR (400 MHz, $\text{DMSO}-d_6$) spectra of **P4** ($\text{Ac-EGLAK}(\text{COOCH}_2\text{CCH})\text{-NH}_2$) and of a side product **P4-SP-1** (Ac-EGLAK-NH_2).

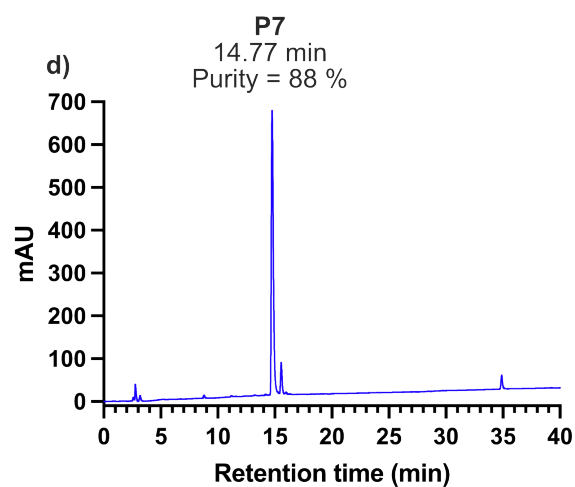
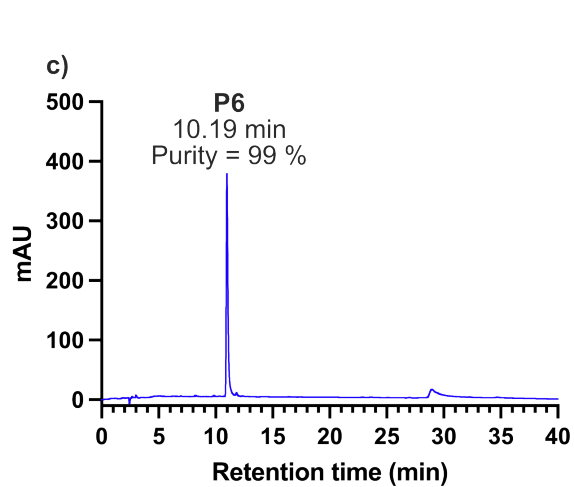
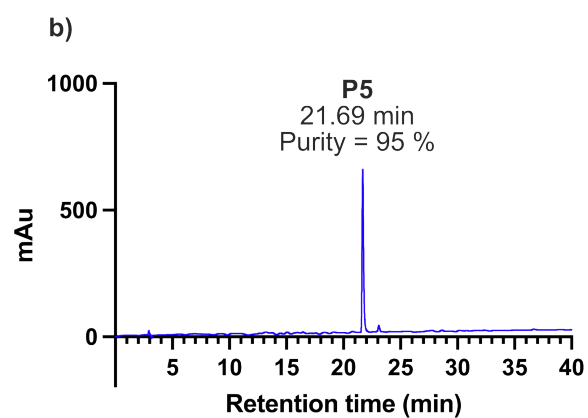
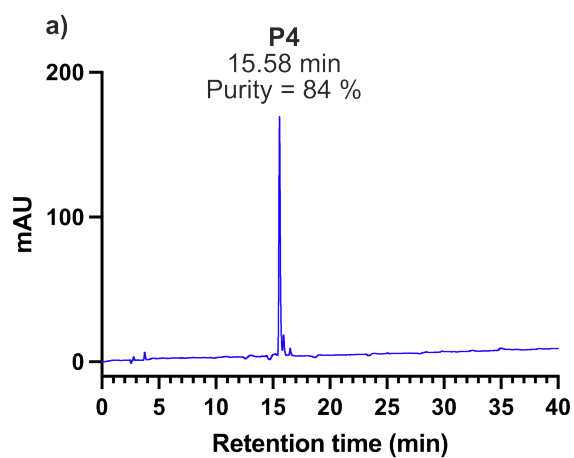


Figure S3.29 – Summary of RP-HPLC chromatograms of a) **P4**, b) **P5**, c) **P6**, d) **P7**.

MS traces of P5 peptide

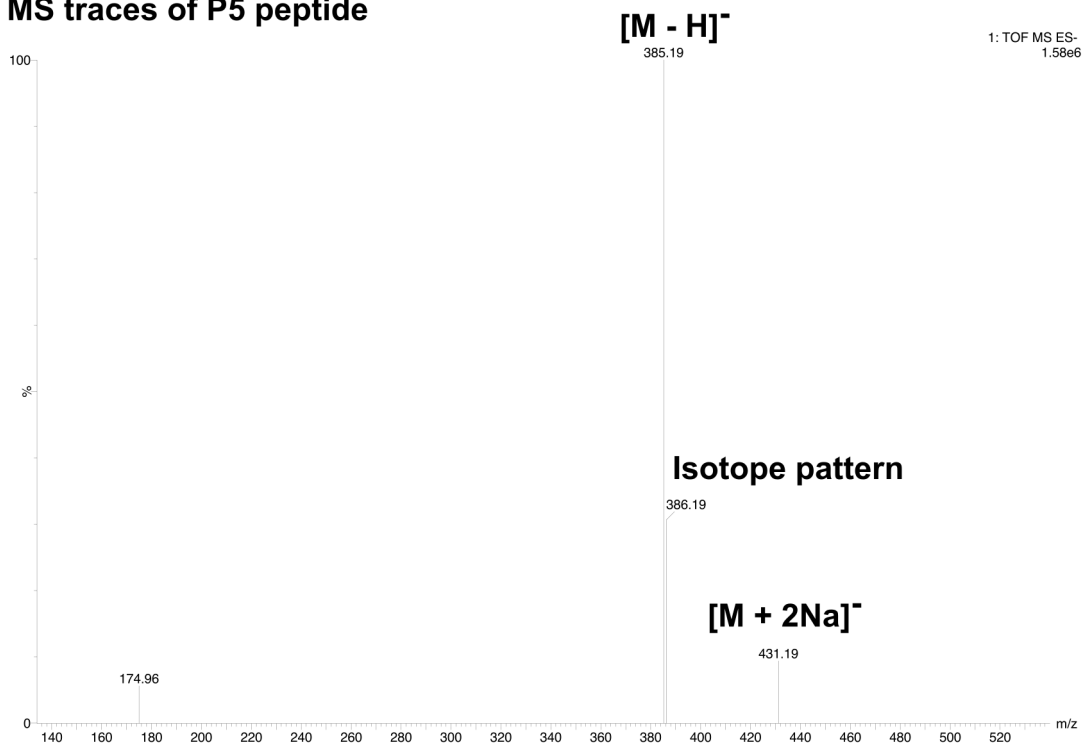


Figure S3.30 – MS traces for P5 (CHC₆H₄-GLA-NH₂) in negative ion mode.

MS traces of P6 peptide

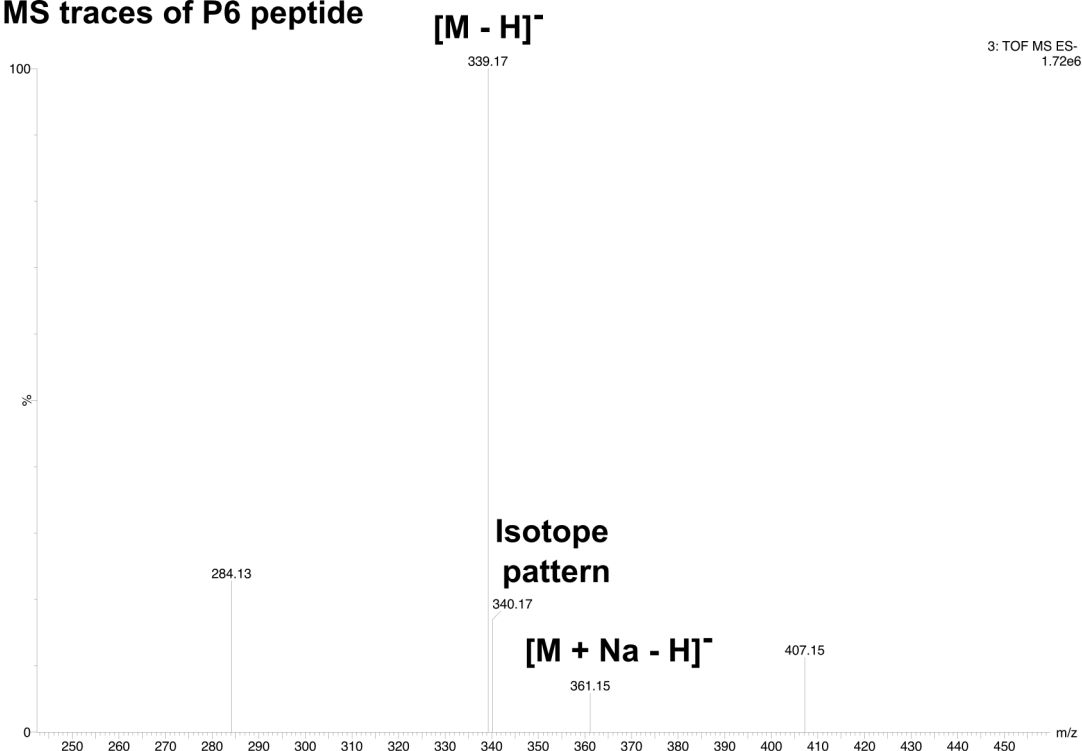


Figure S3.31 – MS traces for P6 (CHCCH₂NHCO-GLA-OH) in negative ion mode.

MS traces of P7 peptide

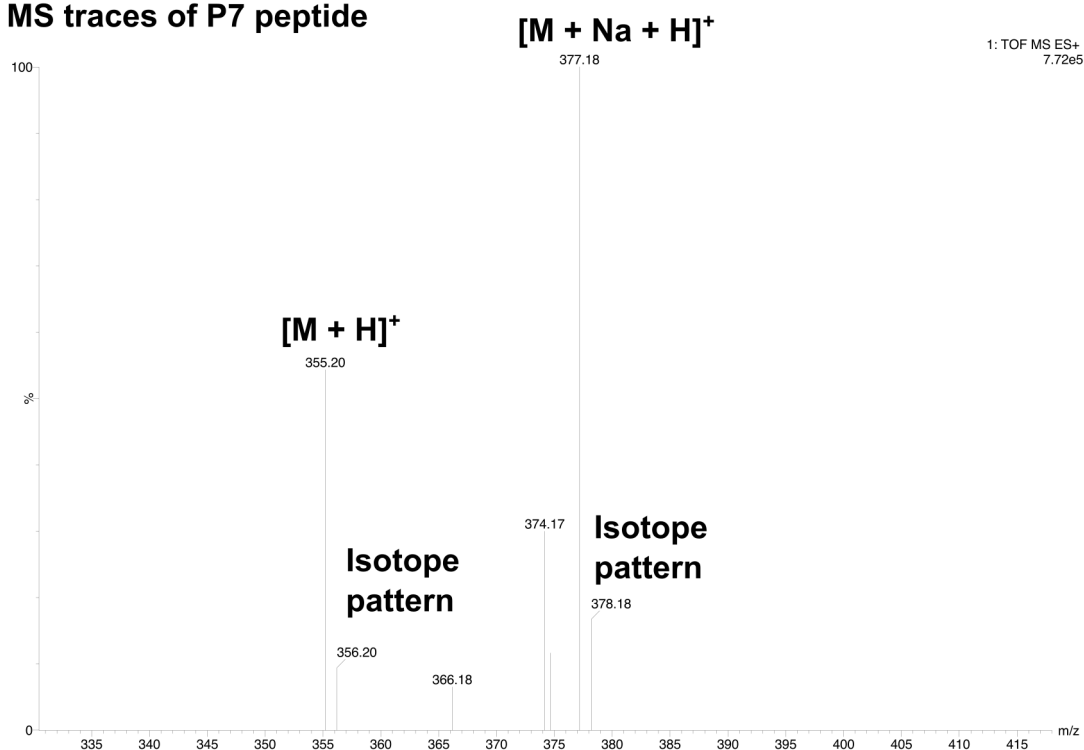


Figure S3.32 – MS traces for P7 ($\text{CHCCH}_2\text{NHCO-GLA-OCH}_3$) in positive ion mode.

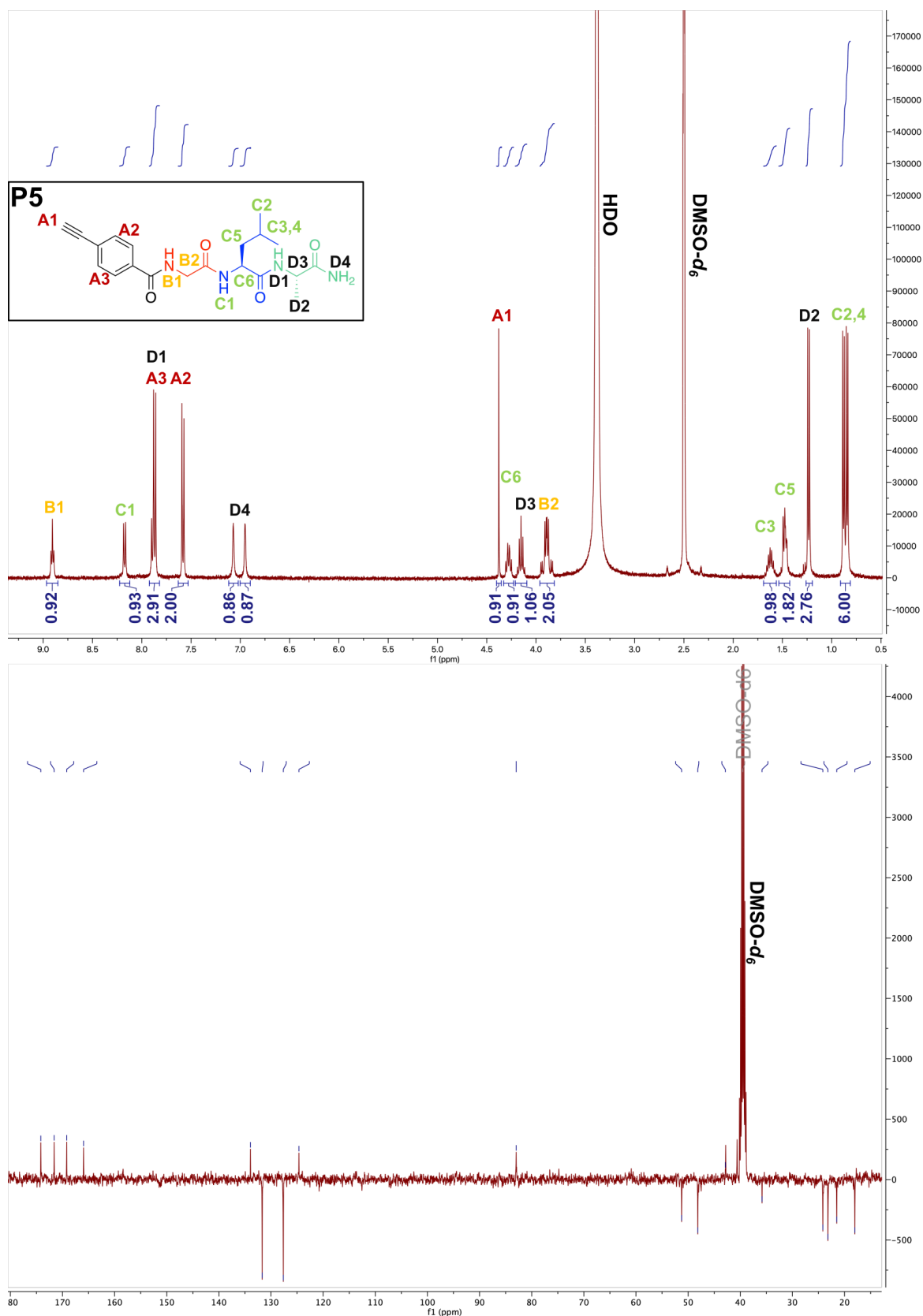


Figure S3.34 – ¹H-NMR (top) and ¹³C (bottom) NMR (400 MHz, DMSO-*d*₆) spectra of P5 (CHC₆H₄-GLA-NH₂).

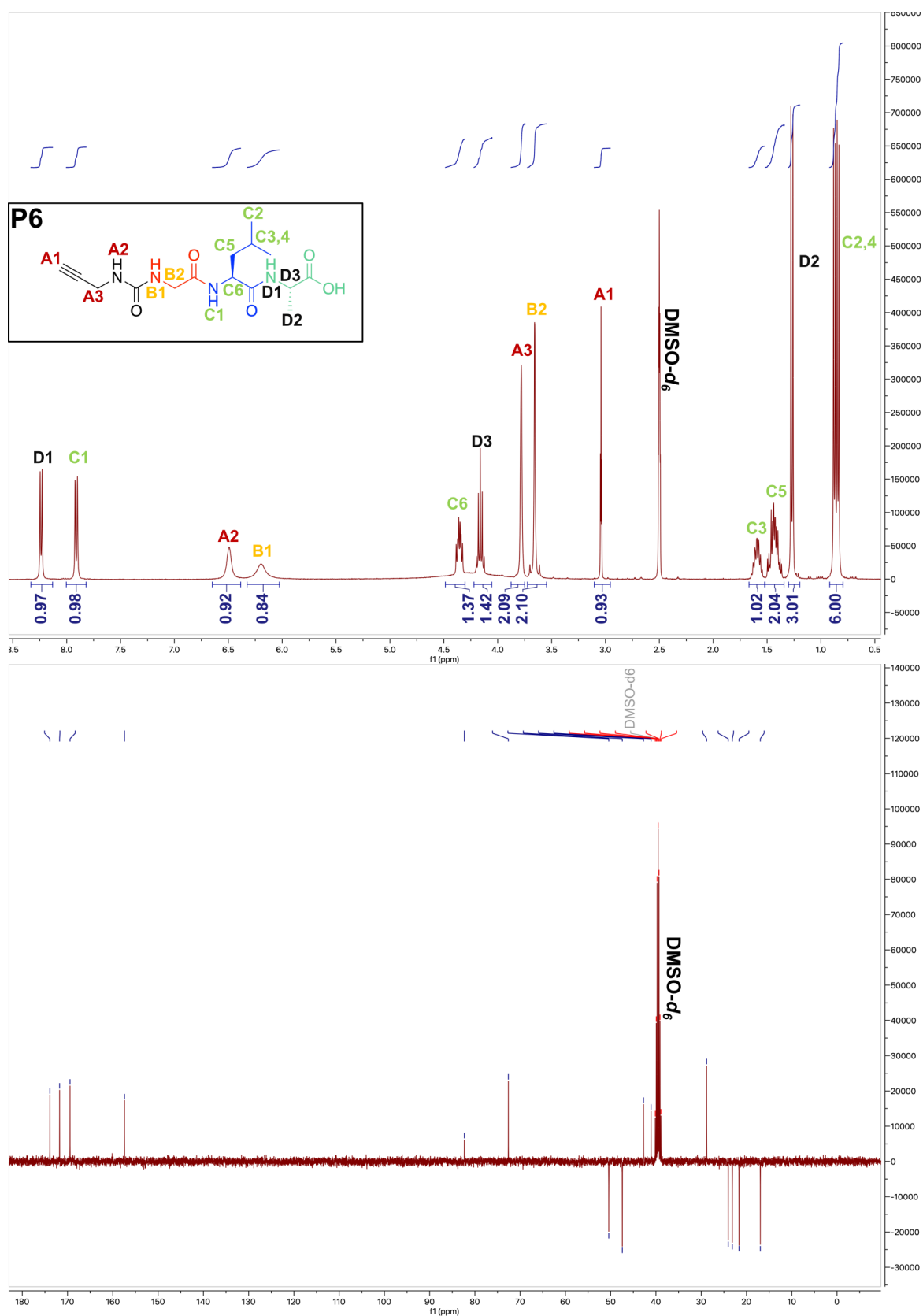


Figure S3.35 – ¹H-NMR (top) and ¹³C (bottom) NMR (400 MHz, DMSO-*d*₆) spectra of P6 (CHCCH₂NHCO-GLA-OH).

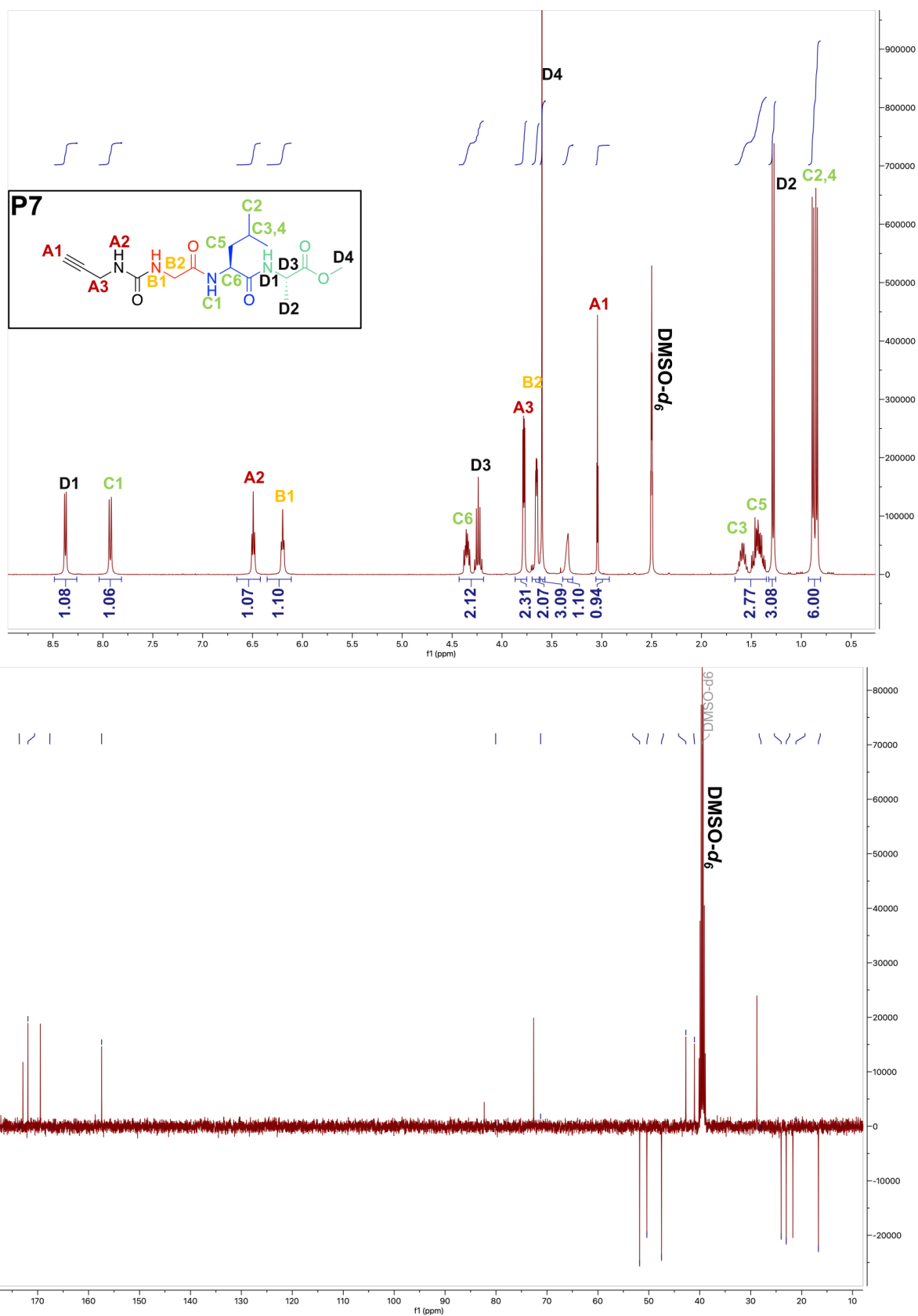


Figure S3.36 – ¹H-NMR (top) and ¹³C (bottom) NMR (400 MHz, DMSO-*d*₆) spectra of P7 (CHCCH₂NHCO-GLA-OCH₃).

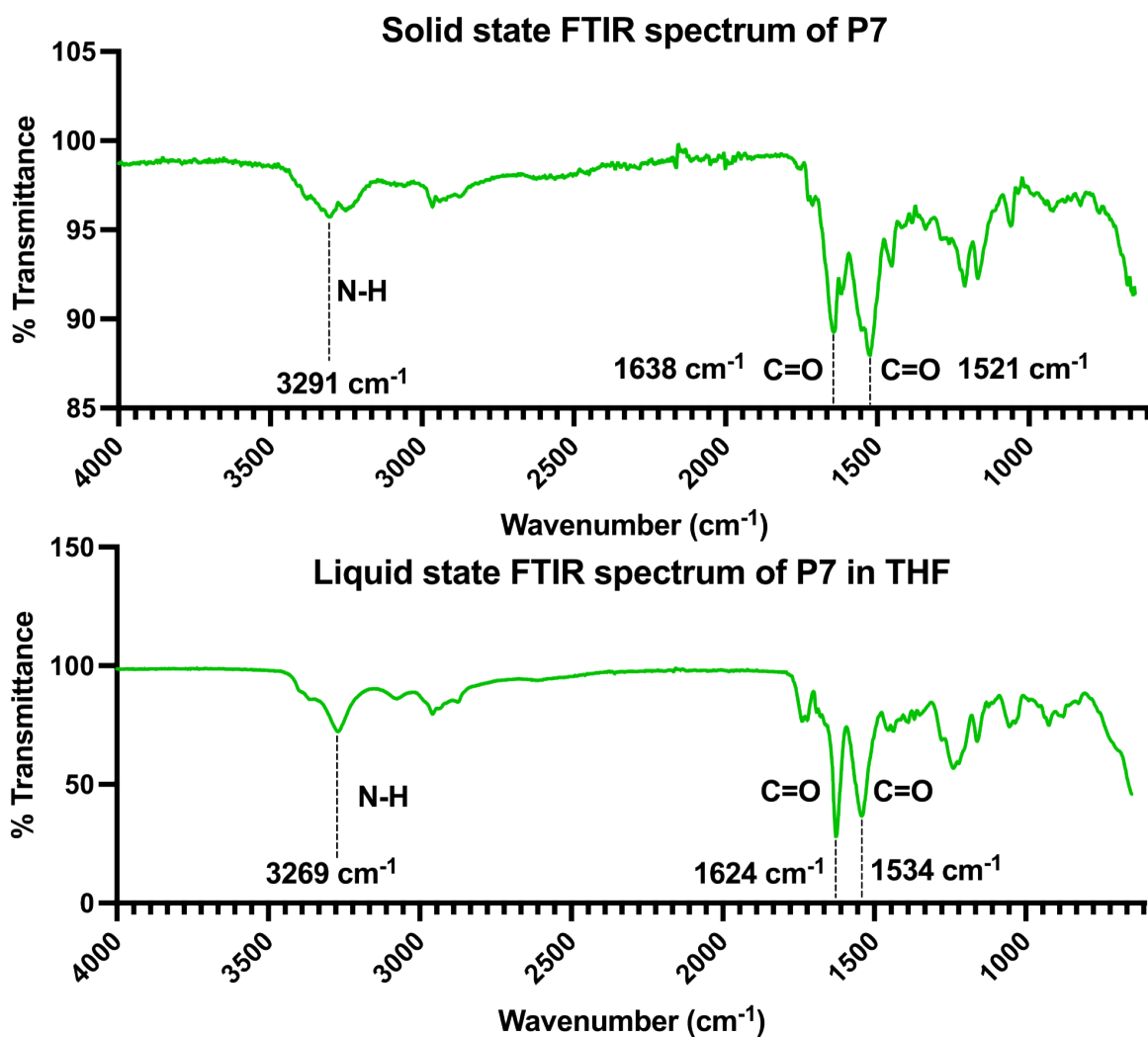


Figure S3.37 – FTIR spectra of P7 ($\text{CHCCH}_2\text{NHCO-GLA-OCH}_3$) in solid state (top) and in liquid state in THF (bottom). $n = 1$.

3.7 References

- [1] C. B. Bucur, Z. Sui and J. B. Schlenoff, *Journal of the American Chemical Society*, 2006, **128**, 13690–13691.
- [2] J. Fu and J. B. Schlenoff, *Journal of the American Chemical Society*, 2016, **138**, 980–990.
- [3] I. Insua, L. Zizmare, A. F. A. Peacock, A. M. Krachler and F. Fernandez-Trillo, *Scientific Reports*, 2017, **7**, 9396.
- [4] I. Insua, A. Wilkinson and F. Fernandez-Trillo, *European Polymer Journal*, 2016, **81**, 198–215.
- [5] I. Insua, M. Petit, L. D. Blackman, R. Keogh, A. Pitto-Barry, R. K. O'Reilly, A. F. A. Peacock, A. M. Krachler and F. Fernandez-Trillo, *ChemNanoMat : chemistry of nanomaterials for energy, biology and more*, 2018, **4**, 807–814.
- [6] M. Wei, Y. Gao, X. Li and M. J. Serpe, *Polymer Chemistry*, 2016, **8**, 127–143.
- [7] T. Leigh and P. Fernandez-Trillo, *Nature Reviews Chemistry*, 2020, **4**, 1–20.
- [8] T. Masuda, H. Izumikawa, Y. Misumi and T. Higashimura, *Macromolecules*, 1996, **29**, 1167–1171.
- [9] R. R. Schrock and J. A. Osborn, *Inorganic Chemistry*, 1970, **9**, 2339–2343.
- [10] J. Clayden, N. Greeves and S. Warren, *Organic Chemistry*, Oxford University Press, 2012, vol. 1.
- [11] T. Masuda, in *Encyclopedia of Polymeric Nanomaterials*, ed. S. Kobayashi and K. Müllen, Springer, Berlin, Heidelberg, 2021, pp. 1–11.
- [12] J. Liu, J. W. Y. Lam and B. Z. Tang, *Chemical Reviews*, 2009, **109**, 5799–5867.
- [13] J. Bergueiro, F. Freire, E. P. Wendler, J. M. Seco, E. Quiñoá and R. Riguera, *Chemical Science*, 2014, **5**, 2170–2176.
- [14] S. Arias, F. Freire, M. Calderón and J. Bergueiro, *Angewandte Chemie (International ed. in English)*, 2017, **56**, 11420–11425.
- [15] G. Marafon, M. Crisma and A. Moretto, *Angewandte Chemie International Edition*, 2018, **57**, 10217–10220.

- [16] K. Fujiwara, H. Toda and M. Ikeguchi, *BMC Structural Biology*, 2012, **12**, 18.
- [17] J. Li and Y. Sha, *Molecules (Basel, Switzerland)*, 2008, **13**, 1111–1119.

Chapter 4

Polyelectrolyte complexes for enzyme-responsive delivery of AMPs

Contents

4.1	Aim	127
4.2	Introduction	127
4.3	Experimental Section	130
4.3.1	Materials	130
4.3.1.1	Assembly of PECs nanoparticles	130
4.3.1.2	Enzymatic degradation studies	130
4.3.1.3	Evaluation of antimicrobial activity of PECs	130
4.3.2	Instrumentation	131
4.3.3	Assembly of PECs nanoparticles	131
4.3.4	Characterization of PECs nanoparticles.	132
4.3.4.1	Dynamic Light Scattering (DLS) ¹⁶	132
4.3.4.2	Standard operating procedure parameters for DLS measurements	133
4.3.4.3	Standard operating procedure parameters for ζ -potential measurements	133
4.3.4.4	TEM imaging of PECs particles	134
4.3.5	PECs particles disassembly and physiological stability assays	134
4.3.6	Estimation of encapsulation efficacy of Polymyxin B in PECs	134
4.3.7	Enzymatic degradation testing procedure	135
4.3.8	<i>In-vitro</i> release of Polymyxin B from PECs in presence of thermolysin	136
4.3.9	<i>In-vitro</i> evaluation of antimicrobial activity PECs against <i>P. aeruginosa</i>	136
4.4	Results and discussions	138
4.4.1	Assembly and characterization of PECs nanoparticles loaded with AMP	138
4.4.2	Estimation of encapsulation efficacy of Polymyxin B in PECs	147
4.4.3	Investigating physiological stability and dominant interactions in selected PECs	149
4.4.3.1	Enhancing physiological stability of PolB:Poly-P2 PECs nanoparticles	152

4.4.4	Evaluation of enzyme degradation properties of PolB: Poly-P2 PECs nanoparticles	156
4.4.5	<i>In-vitro</i> release of Polymyxin B from PolB: Poly-P2 PECs nanoparticles	161
4.4.6	Antimicrobial activity of PolB: Poly-P2 PECs nanoparticles against <i>P. aeruginosa</i>	168
4.5	Conclusions	172
4.6	Supporting information	174
4.7	References	185

4.1 Aim

In the previous two Chapters, the synthesis of enzyme-degradable polymers was discussed. Among all the materials synthesized only **Poly-P1**, (**Ac-EGLAK(COC(CH₃)C-H₂)-NH₂**) and **Poly-P2**, (**Ac-EEGLAK(COC(CH₃)CH₂)-NH₂**) proved to be degradable by thermolysin, an enzyme with similar selectivity toward hydrophobic residues as *P. aeruginosa* protease **LasB**. **Poly-P2** was selected over **Poly-P1** as a result of a higher multivalence (*i.e.*, had extra negative charge per monomer unit from the Glu residue) of the former, which should result in a stronger electrostatic encapsulation of the selected **AMP**. Consequently, the aim of this Chapter is to investigate the assembly, stability, drug release, and antimicrobial activity of enzyme-responsive polyelectrolyte complexes formed from **Poly-P2** and selected clinically-approved **AMP**.

4.2 Introduction

Polyelectrolyte complexes (**PECs**) have been shown to be a simple and attractive solution for the encapsulation of **AMPs**.¹ The positively charged nature of the majority of **AMPs** means that they can be encapsulated in **PECs** without the need for chemical modification, which should reduce the possibility of affecting their mode of action. For this work, a clinically-approved antimicrobial peptide, Polymyxin B sulfate (**PolB**), was selected as the antibiotic of choice.² The amphipathic nature of **PolB**, derived from its combination of lipophilic and hydrophobic groups, contributes to its membrane permeabilizing action and therefore its high potency against antimicrobial resistant Gram-negative pathogens such as *P. aeruginosa* (**MIC** \leq 1-2 mg/L), *Klebsiella pneumoniae* (**MIC** \leq 1-2 mg/L) and *Acinetobacter species* (**MIC** \leq 1-8 mg/L).^{2,3} However, amphipathicity and cationic charge of Polymyxin B are associated with nephrotoxicity in patients, which is why it is commonly used as a last resort antimicrobial agent.^{2,4,5} Moreover, Polymyxins are polyamino acids, meaning they are highly susceptible to degradation by proteases in biological environments. This degradation significantly reduces the peptides' bioavailability in biological systems, necessitating higher dosing in patients.²

Attempts have been made to improve the stability of Polymyxins in physiological environments by encapsulating them with anionic polyelectrolytes within **PECs** (Figure 4.1a).⁶⁻⁸ However, these systems had to make compromises between formulation stability and antimicrobial efficacy, as the release mechanisms were passive and reversible. An example of such a system is **PECs** developed by Insua et al., where Polymyxin B was encapsulated within anionic polymer poly(styrene sulphonate) (**PSS**).⁸ The drug was released passively with a weakening of attractive electrostatic interactions

between polyelectrolytes caused by a decrease in pH and the presence of salts. Therefore, when using a larger (*i.e.*, higher degree of polymerization (**DP**)) **PSS** polymer, it formed stronger electrostatic interactions with Polymyxin B, significantly increasing **PECs** stability (Figure 4.1a). However, this increased stability also reduced the rate and extent of particle disassembly, thus decreasing the antimicrobial activity of the delivery system (Figure 4.1a).

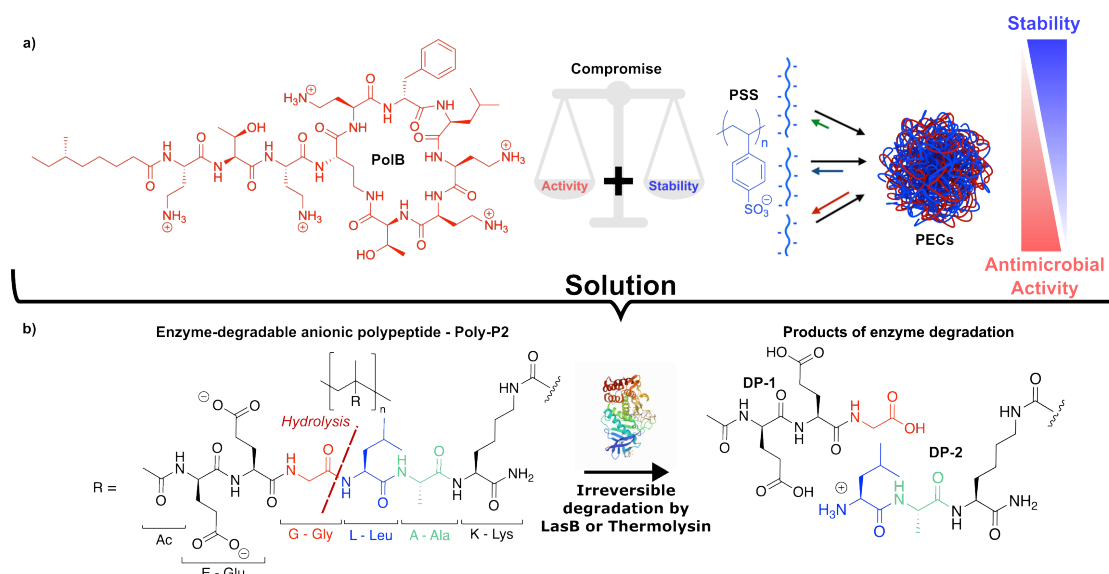


Figure 4.1 – a) Schematic representation of the formation of **PECs** nanoparticles by self-assembly of cationic Polymyxin B (**PolB**) with poly(styrene sulphonate) (**PSS**) and effect of the different multivalency of anionic polymer on physiological stability and antimicrobial activity. b) Schematic representation of anionic polymer bearing enzyme-degradable side chain **Poly-P2**, **poly(Ac-EEGLAK(COC(CH₃)CH₂)-NH₂)**, represented as a key component in an active delivery system, solution to passive drug delivery.

An active delivery system, such as when the encapsulation material is degraded, can lead to irreversible drug release (Figure 4.1b), minimizing the potential for reencapsulation, improving antimicrobial efficacy while maintaining stability in the inactive state. Consequently, Chapter 2 of the Thesis discussed the synthesis of a new enzyme-degradable polymer sequence - **Poly-P2**, **poly(Ac-EEGLAK(COC(CH₃)CH₂)-NH₂)**, which was designed to form polyelectrolyte complexes with **AMPs** such as Polymyxin B (Figure 4.1b). Additionally, **Poly-P2** was created to expel cationic **AMP** through electrostatic repulsion due to enzymatic breakdown of the peptide sequence (Figure 4.1b). This functionality was integrated into the design of the peptide side chain (**P2**) by placing anionic residues away from the polymer backbone across the cleavable bond between the Gly and Leu residues (Figure 4.1b). Therefore, as the **Poly-P2** peptide sequence is hydrolyzed, positively charged degradation products (labeled **DP-2** in Figure 4.1b) are created that repel positively charged Polymyxin B, releasing the drug.

This chapter investigates the assembly of enzyme-responsive **PECs** using a polymer with enzyme-degradable peptide side chain, **Poly-P2** for encapsulation and subsequent release of a **FDA**-approved **AMP**, Polymyxin B (Figure 4.2). An optimized formulation was determined based on the size and efficacy of the encapsulation, followed by the examination of *in-vitro* enzyme-induced drug release from the selected particles. Finally, the antimicrobial activity of the selected formulations of **PECs** was examined.

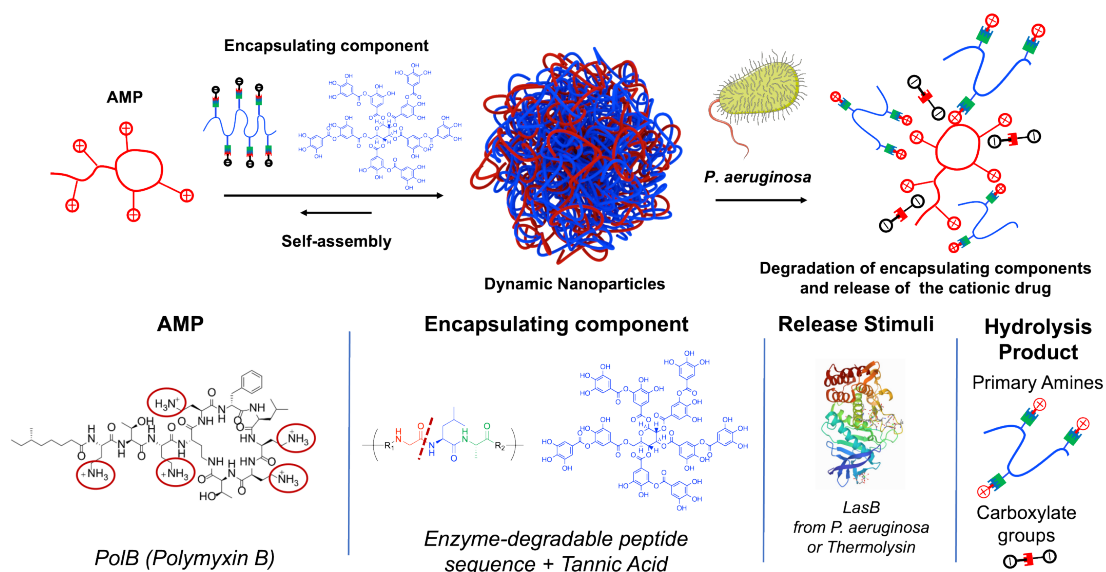


Figure 4.2 – Schematic representation of enzyme-responsive **PECs**-based delivery system.

The proposed application of these **PECs** would potentially involve treating *P. aeruginosa* infections in lungs as well as in chronic wounds scenarios. Encapsulation of **PolB** within the anionic polymer **Poly-P2** is expected to reduce the degradation of the drug caused by proteases released at the site of the bacterial infection, thereby increasing the therapeutic window for **AMP** therapeutics and reducing the dosing requirements. As a result, there is a possibility of reducing toxicity and other off-target effects linked with **AMPs**, which could even lead to a decline in the development of bacterial resistance.^{9–13}

4.3 Experimental Section

4.3.1 Materials

4.3.1.1 Assembly of PECs nanoparticles

PECs discussed in this work were assembled using an anionic polymer with enzyme-degradable peptide side chain **Poly-P2**. Its synthesis and degradation properties were thoroughly described in Chapter 2, Sections 2.3.3, 2.4.3. For a complete characterization of the **P2** monomer and their corresponding polymers **Poly-P2**, see Sections 2.3.3.1 and 2.3.4.1.

Tannic Acid (TA), Polymyxin B sulfate (PoIB), Polysorbate 20 (Tween 20), NaCl, Urea, (4-(2-hydroxyethyl)-1-piperazineethanesulfonic acid) (HEPES) were purchased from Sigma Aldrich® (Australia). Carbon Support Film 5 - 6 nm on Square 200 mesh Cu TEM Grids were purchased from Electron Microscopy Sciences. Spectra/por Float-A-Lyzer G2 Dialysis Devices with weight cut off 100 kDa, 5 mL were purchased from Spectrum® Laboratories. Ultrapure water (Milli-Q water) was obtained from Millipore Milli-Q plus 185 purification systems with electrical resistivity greater than 18.2 mΩ·cm (Millipore Corporation).

4.3.1.2 Enzymatic degradation studies

Thermolysin from *Geobacillus stearothermophilus* and fluorescamine were purchased from Sigma Aldrich® (Australia). Succinyl casein was previously produced in the lab using Ref. ¹⁴ A model degradation peptide **P3** (H₂N-LA-NH₂) was synthesized using the same solid-phase procedure as for **P1** and **P2** and previously reported in Ref. ¹⁵

4.3.1.3 Evaluation of antimicrobial activity of PECs

Luria–Bertani broth (LB) contained 1 % wt/vol bacto tryptone, 1 % wt/vol NaCl, 0.5 % wt/vol Oxoid yeast extract. Tryptone, and Bacto™ Agar were purchased from BD Biosciences. Mueller-Hintin broth (MHB) (Ca⁺) and Yeast Extract were purchased from Oxoid™ (Australia). All broths were sterilized prior to use.

All other chemicals were purchased from Sigma Aldrich® (Australia) and used without further purification. The pH values of the solutions were measured with a Mettler-Toledo MP220 pH meter.

4.3.2 Instrumentation

ζ -potentials, intensity size distributions and polydispersity index (PDI) of Nanoparticleless (NPs) were measured in solution (either Milli-Q water or buffer solution) using Zetasizer Nano-ZS instrument (Malvern Instrument, UK). The morphology of the NPs was analyzed by Transmission electron microscopy (TEM) on an FEI Tecnai TF20 instrument at an operation voltage of 200 kV. The size of the PECs nanoparticle was measured from TEM micrographs using ImageJ software (1.53 v) and measured each nanoparticle twice: both in their longest and shortest diameters. UV-Vis absorption spectra of particle solutions and starting material were recorded on a Varian Cary 4000 UV-Vis spectrophotometer. Solid-state Fourier transform infrared (FTIR) spectroscopy analysis was performed on freeze-dried samples of PECs using Bruker Tensor II FTIR spectrometer.

For identification of Polymyxin B content, Shimadzu Prominence LC-20A with an SPD20A UV-Vis detector was used to perform reverse phase HPLC analysis (RP-HPLC). Tests were run through Kinetex®C18-XB column (Phenomenex®): 5 μ m, 100 Å, 150 x 4.60 mm. The isocratic gradient in 50:23:22:5 mixture of 50 mM Na₂SO₄ in H₂O:H₂O:ACN:5 % (v/v) dilution of 85 % H₃PO₄ was used with a flow rate of 1 mL/min, maintaining the column at 30 °C with a detection set at 215 nm.

Fluorescence measurements (enzymatic degradation) were performed using an infinite M200 microplate reader (Tecan, Switzerland). For the detection of enzymatic degradation readings were taken at 365 nm and 470 nm \pm 10 nm. For the detection of enzymatic degradation using ζ -potentials, Zetasizer Nano-ZS instrument (Malvern Instrument, UK) was used.

Optical densities were measured using a BioTek 800 TS, Agilent plate reader at 630 nm.

4.3.3 Assembly of PECs nanoparticles

For PECs preparation, stock solutions of Polymyxin B sulfate (0.5 mM) and Poly-P2 (1.0 mM) in 10 or 15 mM 4-HEPES buffer at pH 7.45 were prepared. All solutions including buffer were filtered using 0.45 μ m syringe filter and mixed drop-wise under stirring. PECs nanoparticles prepared at different N:COOH ratios - $[n^+/n^-]$ (defined as the molar ratio between amines in Polymyxin B (5 amines) and carboxylic acids in the polymer Poly-P2 (2 acids) accounting for the valency of both polyelectrolytes) were obtained only by changing the amount of added Polymyxin B solution substituted by additional HEPES buffer, keeping the total reaction volume to 4 mL. For example, for

the preparation of PECs-F3 ($[n^+/n^-] = 0.750$ ratio), 1.20 mL (0.600 μmol) of Polymyxin B solution (0.5 mM) were mixed with 2.00 mL (2.00 μmol) of **Poly-P2** (1.0 mM) solution and 0.80 mL of additional HEPES buffer, ensuring that the total volume of the assembly is 4 mL. For PECs formulations with $[n^+/n^-]$ ratio less than 0, the components were added in the following order: buffer, **Poly-P2** solution, and Polymyxin B solution. For PECs formulations with $[n^+/n^-]$ ratios > 0 , the components were added in the following order: buffer, Polymyxin B solution, and **Poly-P2** solution. The reaction mixture was stirred for 24 hours at room temperature and pressure. All reaction tubes were sealed for the entire assembly duration. After 24 hours, the samples were analyzed neat by DLS and ζ -potentials without prior filtration. The DLS technique gave a quick indication of the assembly that took place by analyzing the colloidal size distributions in solutions.

4.3.4 Characterization of PECs nanoparticles.

4.3.4.1 Dynamic Light Scattering (DLS)¹⁶

DLS measures fluctuations in the intensities of scattered light arising from the continuous motion (Brownian motion) of particles in colloidal dispersion. These intensity fluctuations are then correlated over short decay intervals (τ) with the diffusion coefficient (D) of the particles, producing an Autocorrelation function (ACF). Following the creation of ACF, DLS software uses deconvolution algorithms to obtain diffusion coefficient (D) values. The most commonly used algorithms are Cumulant and non-negative least squares (NNLS). Both algorithms can be selected for data interpretation in Malvern's Zetasizer software, used in this Thesis. Consequently, diffusion coefficients (D) are then transformed into hydrodynamic diameter values (D_H) using the Stokes-Einstein equation 4.1; where K_B - Boltzmann's constant, T is the absolute temperature and η is the viscosity of the solution:

$$D = \frac{K_B T}{3\pi\eta D_H} \quad (4.1)$$

All nanoparticles described in this Thesis were analyzed using Malvern's Zetasizer software and plotted using GraphPad Prism software. Z-Average and intensity-weighted mean size, calculated by Cumulants and NNLS General Purpose algorithms, were recorded for all samples (see Supporting information 4.6). In some cases where the samples showed multimodal size distributions, for example, during enzyme degradation, the use of a Cumulant algorithm to determine the size *i.e.*, Z-average size is inappropriate as it does not provide any information about the modality of the size distribution.¹⁶ Therefore, for consistency purposes, only intensity-weighted mean size data were discussed in the main section of Chapter 4. Furthermore, the polydispersity index (PDI), which is reported in Chapter 4 for different PECs, does not correspond to that

obtained by Cumulants algorithm, which is reported along the Z-average value, but was calculated using equation 4.2:

$$Pdi = \left(\frac{SD}{Mean} \right)^2 \quad (4.2)$$

4.3.4.2 Standard operating procedure parameters for DLS measurements

Most particle solutions were tested under the same conditions: temperature = 25 °C, solvent's viscosity = 0.8872, solvent's refractive index = 1.330, particles' RI = 1.450, particles' absorption = 0.001, measuring angle = 173 °(non-invasive backscatter), run duration = 10 s, with automatic measurement position and attenuation.

To test the behavior of the size distributions at different temperatures: 37, 40, 50 °C solvent viscosity was adjusted accordingly. For 37 °C solvent's viscosity = 0.6864; for 40 °C solvent's viscosity = 0.6490 and for 50 °C solvent's viscosity = 0.5482.

For particle disassembly and physiological stability experiments, NaCl, Tween 20, EDTA, and Urea were added to the nanoparticle solution, which should lead to an increase in the viscosity of the aqueous medium. This alteration was not taken into account when performing the DLS analysis, as the focus of the experiment was on trends rather than absolute changes in size. All samples were tested under the same conditions, making sure that the data sets were comparable. According to the Stokes-Einstein equation (Equation 4.1), there is an inverse relationship between viscosity and D_H . Therefore, the actual D_H values measured in the presence of NaCl, Tween 20, EDTA, and Urea would be lower than those reported in this Thesis.

4.3.4.3 Standard operating procedure parameters for ζ -potential measurements

All particle solutions were tested under the same conditions: temperature = 25 °C, solvent's viscosity = 0.8872, solvent's refractive index = 1.330, solvent's dielectric constant = 78.5, particles' RI = 1.450, particles' absorption = 0.001, run duration = 10 s with automatic measurement duration, attenuation, and voltage selection.

To measure size distributions using DLS, 50 μ L of particle suspension was used, while 600 μ L of particle suspension was used to measure ζ -potentials. All DLS and ζ -potential data were presented as an average based on 3 technical replicates.

4.3.4.4 TEM imaging of PECs particles

For TEM analysis, 10 μL of a suspension of PECs nanoparticles was deposited on the surface of the TEM grid and left to dry at ambient temperature covered from dust. No staining was performed on the samples of PECs used for TEM imaging.

4.3.5 PECs particles disassembly and physiological stability assays

To investigate the stability of selected PECs at physiological osmolality (154 mM NaCl),¹⁷ 0.5 mL of freshly prepared PECs were diluted with 91 μL of 1 M NaCl solution in Milli-Q water to produce the final NaCl concentration of 154 mM. When mixed, the samples were incubated at 37 °C with light agitation for up to 4 hours. A control sample of PECs with added Milli-Q water (0.5 mL) instead of NaCl solutions was also added to the test. 100 μL aliquots were collected and analyzed by DLS at each 1-hour time point. The ACF and intensity distributions of these samples were compared with those of a control in the absence of NaCl.

To evaluate the dominant interactions between Polymyxin B and anionic enzyme-degradable polymer in the selected PECs, 100 μL of freshly prepared PECs were diluted with 100 μL 100 mM solutions of Urea, Tween 20, NaCl and EDTA and incubated for 24 hours at 37 °C. 50 μL aliquots were collected and analyzed by DLS at 24-hour time point. ACFs, intensity distributions were compared with those of a control sample of PECs.

4.3.6 Estimation of encapsulation efficacy of Polymyxin B in PECs

The encapsulation efficiency of Polymyxin B in PECs nanoparticles was calculated according to the percentage of encapsulated (*i.e.*, available) Polymyxin B in PECs samples that reacted with fluorescamine dye. First, the standard curve of PolB-fluorescamine conjugates was established (Figure S4.31) by reacting 0.125 mL of Polymyxin B solution at different concentrations (dissolved in 5mM HEPES) with 0.125 mL of fluorescamine dye (2 mM) (dissolved in methanol) for 30 minutes and measuring fluorescence at 365 nm (excitation) and 470 ± 10 nm (emission). HEPES buffer was used as a blank reagent.¹⁸ 3 technical replicates were recorded for each sample. Based on the emission intensities, seven data points were selected that represent the concentration range of PolB in PECs formulations. A linear regression was plotted based on seven Polymyxin B concentrations. Having established the standard curve of Polymyxin B, selected PECs samples were analyzed following the same procedure (Figure S4.31).

Using the standard curve equation, the concentration of available Polymyxin B was calculated in terms of mg/mL. From this, the encapsulation efficiency (%) was estimated using equation 4.3:

$$\frac{[mg \times mL^{-1}]_{total PolB} - [mg \times mL^{-1}]_{available PolB}}{[mg \times mL^{-1}]_{total PolB}} \times 100 \quad (4.3)$$

4.3.7 Enzymatic degradation testing procedure

Three buffer solutions were prepared: buffer (A) - 5.00 mM HEPES at pH 7.45 buffer (B) - 20.0 mM CaCl₂ in buffer (A) and buffer (C) - 2.50 mM Na₂B₄O₇ at pH 8.0. Stock solutions of PECs (1.00 mM) at different [n⁺/n⁻] ratios were used fresh, directly after assembly. Succinyl casein (SC) (0.500 mg/mL), degradation peptide H₂N-LA-NH₂ (P3) (1.00 mM), Tannic Acid (0.0235 mM) were mixed with buffer (A) 12 hours before the experiment. On the day of the test, all samples were mixed according to Table 4.1 in 1.5 mL Eppendorf tubes. In this experiment, 1.2 mg (0.100 mg/μL solution) of thermolysin was used per sample (Final enzyme concentration in reaction solution was 1.2 mg/mL). The temperature of the test tubes was controlled by a 55 °C water bath. At each time point, aliquots of 125 μL were taken and mixed with 30 μL of 0.1 M ethylenediaminetetraacetic acid (EDTA) solution. Then each sample was mixed in a 1:1 volume with a 1 mM fluorescamine solution in methanol. Each sample was prepared in triplicate. The microplate was incubated at 37 °C under orbital shaking for 30 minutes. After this time, fluorescence was measured, excited at 365 nm and emission collected at 470 ± 10 nm. The raw emission intensity data was then normalized to a degradation peptide P3

Table 4.1 – Summary of the concentrations and conditions used in enzymatic degradation testing.

Samples	Buffer A	Buffer B	Buffer C	SC	Thermolysin	TA	PECs solutions	Total Vol (μL)
Buffer	500	476	24	-	-	-	-	1000
Therm. (enzyme control)	500	488	-	-	12	-	-	1000
SC (succinyl casein)	-	476	24	500	-	-	-	1000
SC + Therm.	-	488	-	500	12	-	-	1000
TA control	495	500	-	-	-	5	-	1000
P3 (+ve control)	-	488	-	-	12	-	500	1000
PECs control	-	500	-	-	-	-	500	1000
PECs + Therm.	-	488	-	-	12	-	500	1000

(H₂N-LA-NH₂) which was used as a positive control, representing 100 % degradation. Results were presented as a percentage of the relative amine content.

For the detection of enzymatic degradation using ζ -potentials, see Section 4.3.2. All measurements were made in triplicate (3 technical replicates).

4.3.8 *In-vitro* release of Polymyxin B from PECs in presence of thermolysin

2.5 mL of PECs nanoparticles and Polymyxin B with equivalent total drug loading of tested PECs (e.g., 0.209 mg/mL for PECs-F3 [n^+/n^-] = 0.750 ratio) were added to the dialysis membrane (M.W. cut off 100 kDa) respectively. Subsequently, 0.15 mL of thermolysin solution (1 mg/mL) prepared in HEPES (5 mM) buffer was transferred to dialysis membranes containing PECs nanoparticles. They were dialyzed against 14 mL HEPES buffer supplemented with NaCl to obtain a final NaCl concentration of 100 mM for 24 h. The dialysis systems were heated to 40 °C, mimicking hypothermia caused by a bacterial infection in the human body.^{19–21} At predetermined time intervals, 1 mL of dialysate was collected and replaced with 1 mL of fresh HEPES (with NaCl) solution, making sure that the total volume of dialysate was constant throughout the experiment. To identify the concentration of Polymyxin B content in the collected dialysate, a fluorescamine assay was used as previously described in Section 4.3.7. Measured fluorescence of the mixture was normalized to the fluorescence of fluorescamine-PolB (0.0373 mg/mL = amount of Polymyxin B in membrane(g)/14 mL), which represented the total concentration of Polymyxin B that was presumed to pass, assuming 100% encapsulation efficacy. An increase in emission intensity caused by the presence of thermolysin-fluorescamine adducts was also taken into account when calculating cumulative Polymyxin B release from the primary amine content data. From 1 mL of collected dialysate samples, 0.7 mL was analyzed by HPLC to determine the content of Polymyxin B in the dialysate. HPLC method is described in Section 4.3.2, adapted from ref.^{8,22} Lastly, from the dialysis membranes containing enzyme-treated or non-enzyme treated PECs nanoparticles, 0.5 mL of nanoparticle solution was analyzed by DLS at different time points and placed back into the dialysis membrane. Results for the DLS measurements are presented in Figure S4.34.

4.3.9 *In-vitro* evaluation of antimicrobial activity PECs against *P. aeruginosa*

The antimicrobial activity of PECs was assessed using a broth microdilution methodology following the previously reported procedure.²³ For a detailed procedure on cell

culture preparation, see ref.²³ To allow bacteria growth to proceed *P. aeruginosa* (American Type Culture Collection (ATCC-47085) was incubated overnight in LB broth at 37 °C with aeration and without agitation. Multidrug-resistant strain (FADDI-PA067) was cultured overnight in LB broth at 37 °C with aeration and agitation (150 rpm). The next day, the bacteria cultures were further diluted with LB broth (20 mL), and incubated for 3 - 4 h at 37 °C with aeration and shaking (150 rpm) before use. The bacteria (which gave an optical density (OD) reading of ≈ 1.07 for ATCC-47085 and ≈ 0.8 for FADDI-PA067) were then dispersed in MHBca+ to achieve a concentration of 2.5×10^6 cells mL⁻¹, after which the *P. aeruginosa* suspensions (100 μ L) were added to a 96-well microplate. Then 100 μ L of serial two-fold dilutions of free Polymyxin B solution (200 - 0.200 μ g/mL) or PECs-F1 (160 - 0.200 μ g/mL), PECs-F3 (105 - 0.100 μ g/mL) suspensions at pH 7.4 were added to the microplate, resulting in a mixture (200 μ L) of bacteria and PECs. The microplate was incubated at 37 °C under orbital shaking (180 rpm) on a microplate reader (BioTek 800 TS, Agilent), and the optical density (OD) readings of each well at 630 nm were measured every 10 min for 14 hours. Negative controls containing cells alone were incorporated. The OD₆₃₀ of the samples at the time when the exponential growth of bacterial (only cells) was complete (*i.e.*, late exponential phase) was normalized to the OD₆₃₀ of the negative control (100%), expressed as relative bacterial growth (%). The relative bacterial growth (%) was plotted against the concentration of Polymyxin B in each of the samples (*i.e.*, each dilution). Linear regression analysis was used to determine the minimum inhibitory concentration (MIC). The MIC was determined as the concentration corresponding to 10% relative bacterial growth in the linear regression and was reported as MIC₉₀. Two sample replicates were used in each experiment for each bacterium and concentration. Data are expressed as mean \pm s.d. of the replicates.

4.4 Results and discussions

4.4.1 Assembly and characterization of PECs nanoparticles loaded with AMP

The assembly of **PECs** was carried out following a slightly modified self-assembly method, previously reported by our group.¹⁵ The formation of particles involved the mixing of the two oppositely charged polyelectrolytes (e.g., **PolB** with **Poly-P2**) at different ratios, keeping the reaction volume constant. The most notable advantage of the self-assembly methodology was its relatively straightforward setup, which requires the use of commonly accessible laboratory apparatus, such as stirring plates and pipettes (Figure 4.3). The main downside of this method is that it does not provide as much control over particle size or reproducibility as a template-based assembly (e.g., silica or calcium carbonate), where the size is determined by the template itself.^{24,25} For example, for the same formulation of **PECs** prepared with a charge ratio of 0.750, the average size distributions measured with **DLS** ranged from 196 to 415 nm. Considering that the main mode of action of **AMPs** is membrane disruption, intracellular delivery of these particles was not a design requirement.^{26,27} However, in certain target treatment scenarios, such as pulmonary delivery, poor size control could potentially be a limiting factor for achieving high drug distribution inside the lungs, reducing the therapeutic efficacy of such drug delivery systems.^{28,29}

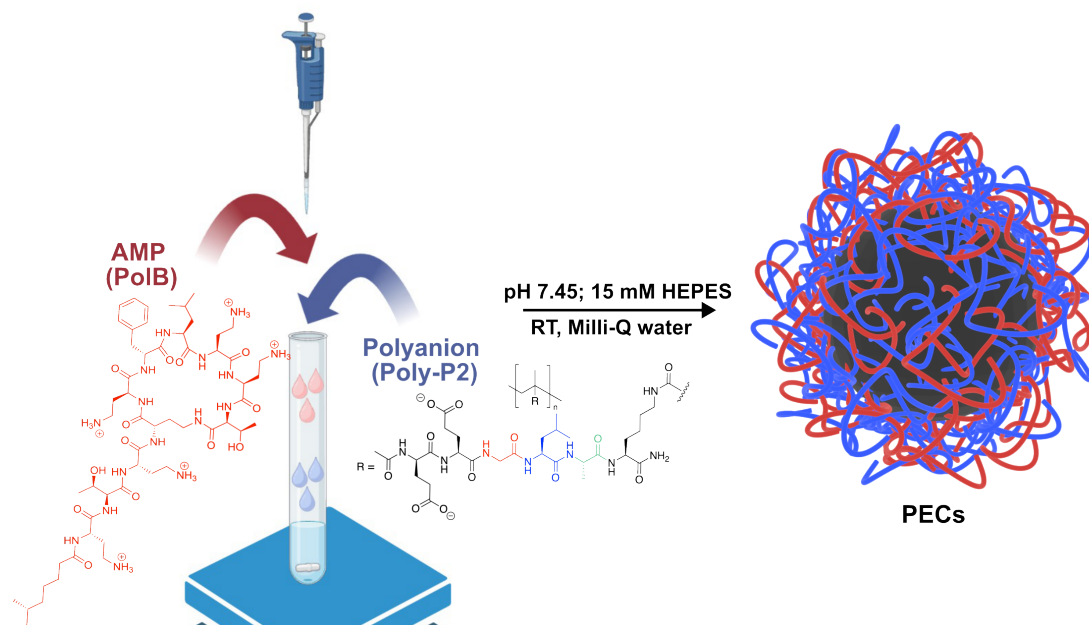


Figure 4.3 – Schematic representation of the laboratory method for preparation of **PECs** particles.

In this study, the core components of **PECs** were Polymyxin B (**PolB**) as a polycation and **Poly-P2** as an enzyme-degradable polyanion (Figure 4.3). The pH of the reaction was kept close to physiological (pH 7.45), so amines in **PolB** (from diaminobutyric acid (Dab), producing +5 charge)³⁰ are protonated and carboxylates in **Poly-P2** (from glutamic acids, -2 charge for a single monomer unit) are deprotonated, promoting electrostatic attraction between the components.

To identify which ratio of **PolB** to **Poly-P2** would lead to the formation of colloidal nanoparticles (**PECs**), eight different formulations (Table 4.2) with varying ratios of **PolB** to **Poly-P2** (*i.e.*, different $[n^+/n^-]$ ratios) were prepared. The concentration of **Poly-P2** was kept constant (0.5 mM), while the concentration of **PolB** was reduced from F1 (0.227 mM) to F8 (0.0253 mM), to determine the maximum amount of **PolB** that can be encapsulated by the anionic polymer (**Poly-P2**). Ideally, an optimal formulation of **PECs** would have the highest colloidal stability with the highest achievable drug loading. To reduce the toxicity effects of **PolB**, the amphipathic and cationic nature of the agent had to be shielded in the inactive state of the delivery system (Figure 4.2), forming an anionic corona surrounding the drug. Therefore, six of the eight formulations had an excess anionic component with $[n^+/n^-]$ ratio < 0.

Table 4.2 – Summary of **DLS** data for the formulations of **PECs** evaluated in this work. For **ACFs**, see Figure 4.4 and for size-intensity plots, see Figure 4.5.

DLS data for PECs-N1						
PECs-N1	I.D.	$[n^+/n^-]$ ratio	$D_H \pm SD$ (nm)	Pdi	ζ -Potential $\pm SD$ (mV)	[PolB] (mM)
	F1	1.13	259 \pm 32.9	0.0161	-9.09 \pm 3.34	0.227
	F2	1.00	216 \pm 40.6	0.0353	-12.4 \pm 3.20	0.202
	F3	0.750	222 \pm 108	0.237	-17.6 \pm 4.49	0.15
	F4	0.606	283 \pm 194	0.472	-7.52 \pm 12.6	0.123
	F5	0.500	281 \pm 158	0.318	-17.6 \pm 8.53	0.101
	F6	0.438	98.3 \pm 48.4	0.243	-16.3 \pm 6.83	0.0884
	F7	0.375	286 \pm 179	0.391	-15.2 \pm 8.28	0.0758
	F8	0.125	302 \pm 121	0.159	-17.4 \pm 11.0	0.0253

To scientifically evaluate the differences between nanoparticle formulations, the **DLS** technique was used because it provides a rapid, controlled, and non-destructive analysis methodology to approximate particle size in solution. **DLS** measures fluctuations in the intensities of scattered light arising from the continuous motion (Brownian motion) of particles in colloidal dispersion.¹⁶ These intensity fluctuations are then correlated over short decay intervals (τ) with the diffusion coefficient (D) of the particles, producing an autocorrelation function (**ACF**), *e.g.*, Figure 4.4. For larger particles, their Brownian motion is slower, meaning that intensity fluctuations will occur less often, producing the **ACF** curve with slower decay, whereas for smaller particles an opposite

result is observed. At short decay intervals (τ), the correlation coefficient is high (between 0.8 - 0.9) because the particles do not have the opportunity to move to a great extent from the initial state in which they were. However, if the starting correlation coefficient decreases (below 0.8), it indicates that the sample analyzed potentially has a reduced concentration of colloidal particles, *i.e.*, the light gets scattered by the starting material used to assemble the particles *e.g.*, polymers, which considerably smaller in size. Therefore, ACF can be used as an initial evaluation point for the examination of nanoparticle formation. Subsequently, ACFs were used to calculate the hydrodynamic diameters (D_H) correlated with intensity fluctuations. These data were presented as size intensity histograms, which were used to identify the average D_H , polydispersity index (PDI) and used to evaluate the formation of multimodal size distributions (Table 4.2). In addition to this, ζ -potentials of the assembled PECs were measured, representing the surface charge of colloidal particles in solution (Table 4.2). Hence, the effectiveness of **Poly-P2** in masking the cationic charge of Polymyxin B was evaluated using ζ -potentials.

It is important to emphasize that DLS measurements are highly susceptible to presence of dust and aggregates, which will scatter the light together with the desired particles. Such contaminants can lead to either noisy or inaccurate signals, thereby resulting in a false representation of particle size, dispersity and especially of the particle concentration. For example, when there is a precipitate in the sampled particle solution, the DLS signal will be primarily influenced by the larger-sized particles from the precipitate. Consequently, this signal may not be representative of all the particles present in the solution. That is why the data obtained from DLS was carefully monitored and used primarily for conforming the assembly of nanoparticles and their estimated hydrodynamic radii in solution.

All eight formulations of PECs (Table 4.2) produced size distributions with relatively similar hydrodynamic radii (D_H) from 302 to 216 nm (*i.e.*, within the standard deviation), with only one F6 being an outlier for this trend with a size of 98 nm (Table 4.2). However, from F4 ($[n^+/n^-] = 0.750$) the maximum correlation coefficient decreased from 0.83 to 0.28 (Figure 4.4), indicating that the PECs suspensions colloidal content decreased (*i.e.*, high signal to noise ratio) with the excess of smaller non-colloidal components such as **Poly-P2** dominating the signal. These observations correlate well with the amount of added PolB, which decreased from F1 to F8 while **Poly-P2** concentration stayed constant.

For formulations with a charge ratio of ≥ 0 (F1 and F2), a sharp increase in the correlation coefficient between 10^3 and $10^5 \mu s$ (Figure 4.4) indicated the formation of

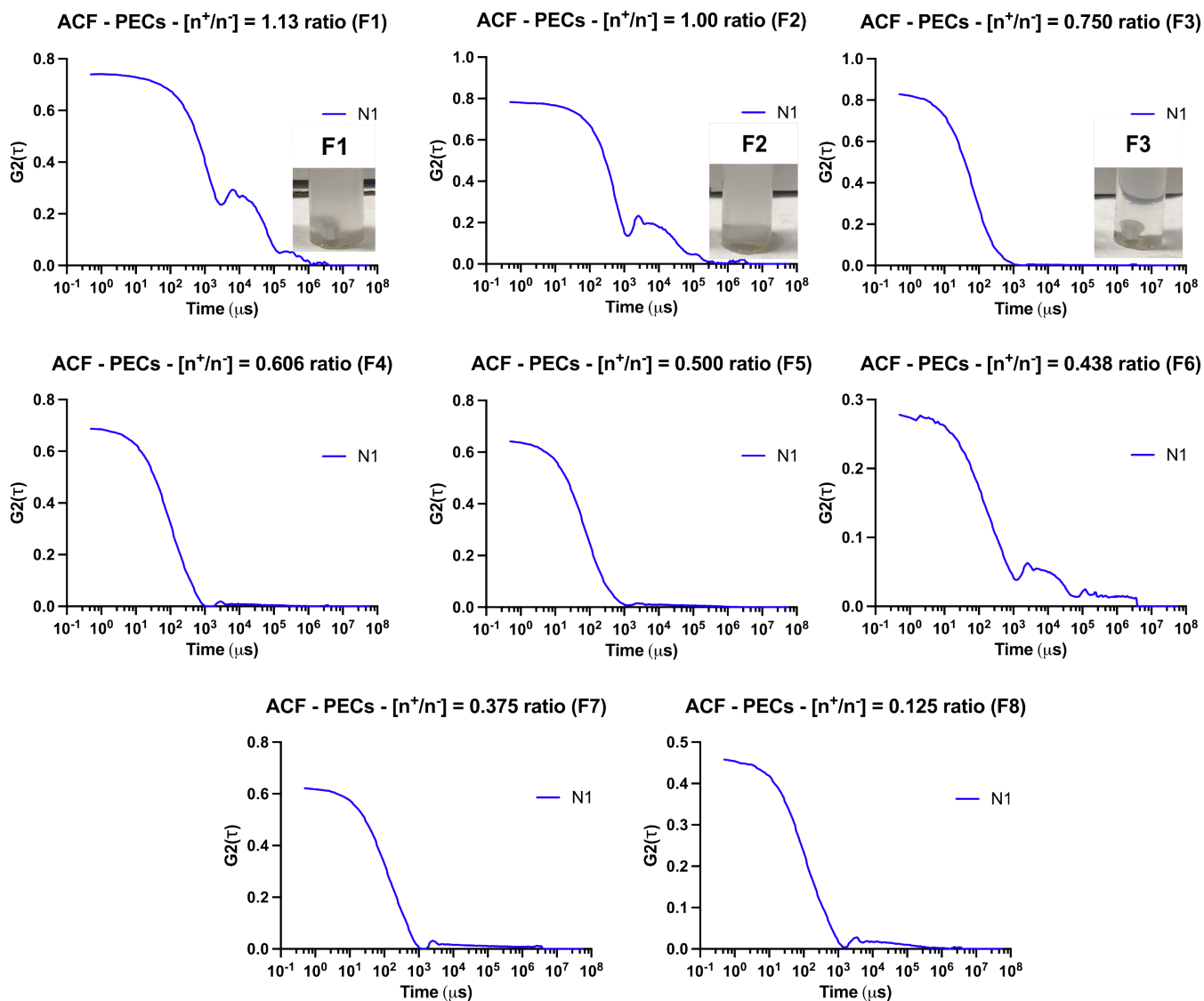


Figure 4.4 – Summary of DLS autocorrelation function (ACF) curves of PECs nanoparticles prepared with Poly-P2 and PolB at $[n^+/n^-]$ ratios of 1.13, 1.00, 0.750, 0.606, 0.500, 0.438, 0.375, 0.125. **N1** - ACF curves directly after 24 hours of mixing. The results are presented as an average of 3 technical replicates for each sample.

aggregates with sizes outside the instrumental range during assembly. Particle aggregation was visually evident in the case of PECs-F1 and F2 samples, causing them to form excessively cloudy solutions, as illustrated in Figure 4.4. Furthermore, on standing particle suspensions PECs-F1 and F2 formed white precipitate at the bottom of the vials, which only further confirmed formation of heavier, poorly dispersed particles *i.e.*, aggregates. These results suggest that at $[n^+/n^-]$ ratio = 0, complete neutralization of negatively charged Poly-P2 occurs, leading to the formation of neutral PECs particles, which are not stable in solution, resulting in phase separation. For formulations with a charge ratio greater than 0 ($[n^+/n^-] > 0$), the same neutral PECs are initially formed, which flocculate. Thus, as more PolB is added to neutral aggregates, it does not have

an effect on the state of the particles, while the formation of more PECs is restricted due to the absence of uncomplexed polyanion molecules. The results of formulations with fewer PolB, such as F3 - F8, were different from others, as they did not flocculate and instead formed dispersed solutions (e.g., F3, Figure 4.4) with no evidence of precipitation, even on prolonged standing (*i.e.*, samples kept in the fridge at 3 - 5 °C for 3 months). This is in line with previous studies on the formation of PECs particles from charged polymers, suggesting that stable colloidal particles are generally formed when an excess of anionic components is used.^{7,31–33} It should be noted that, based on the size-intensity DLS data (Figure 4.5), the formulations F3, 4, 5, 6, 7, and 8 of PECs generated multimodal size distributions. This can be attributed to the formation of aggregates

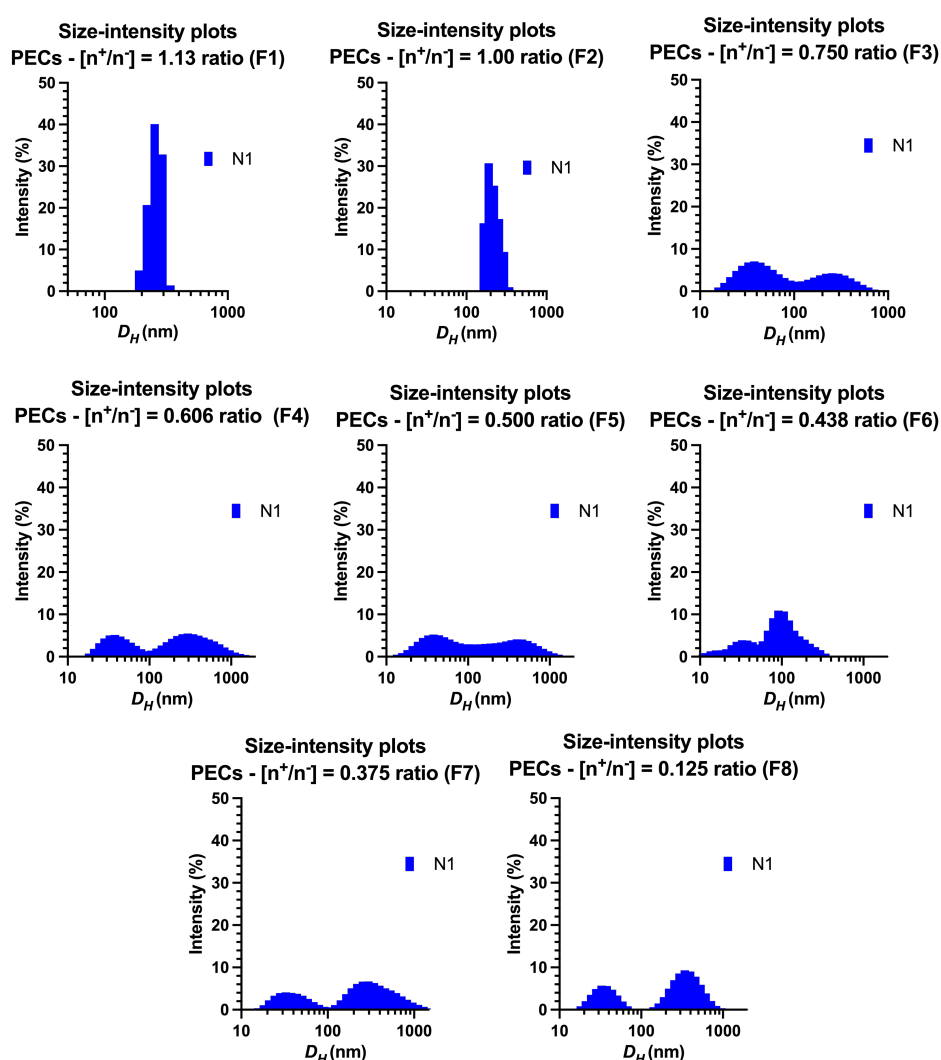


Figure 4.5 – Summary of DLS size-intensity plots of PECs nanoparticles prepared with Poly-P2 and PolB at $[n^+/n^-]$ ratios of 1.13, 1.00, 0.750, 0.606, 0.500, 0.438, 0.375, 0.125. N1 - size-intensity plots directly after 24 hours of mixing. The results are presented as an average of 3 technical replicates for each sample.

for $D_H > 500$, and even possibly incomplete assembly for $D_H < 50$ nm. However, the

degree of aggregation was not as significant as in PECs-F1 and F2, since the particle dispersions of PECs-F3 to PECs-F8 did not flocculate or precipitate. Notably, PECs-F3 had the smoothest ACF curve with a starting correlation coefficient greater than 0.80, indicating the presence of a high concentration of colloidal particles.

The ζ -potential data revealed that all PECs had a negatively charged surface, even when the charge ratio was greater than zero (F1 = $-9.09 \text{ mV} \pm 3.34$, Figure 4.6). This was expected, as the average ζ -potential of a PolB control solution in HEPES was also slightly negative = $-2.99 \text{ mV} \pm 4.01 \text{ mV}$. As the charge ratios decreased from F1 to F8 (i.e., less PolB was added), the ζ -potentials followed the same trend (Figure 4.6), reaching $-17.4 \pm 11.0 \text{ mV}$ in F8 (Table 4.6), which was close to the charge of Poly-P2 control solution in HEPES ($-13.9 \pm 12.6 \text{ mV}$). These data indicated that all formulations of PECs had a negatively charged surface, which should help reduce the cytotoxicity of the system towards healthy cells.

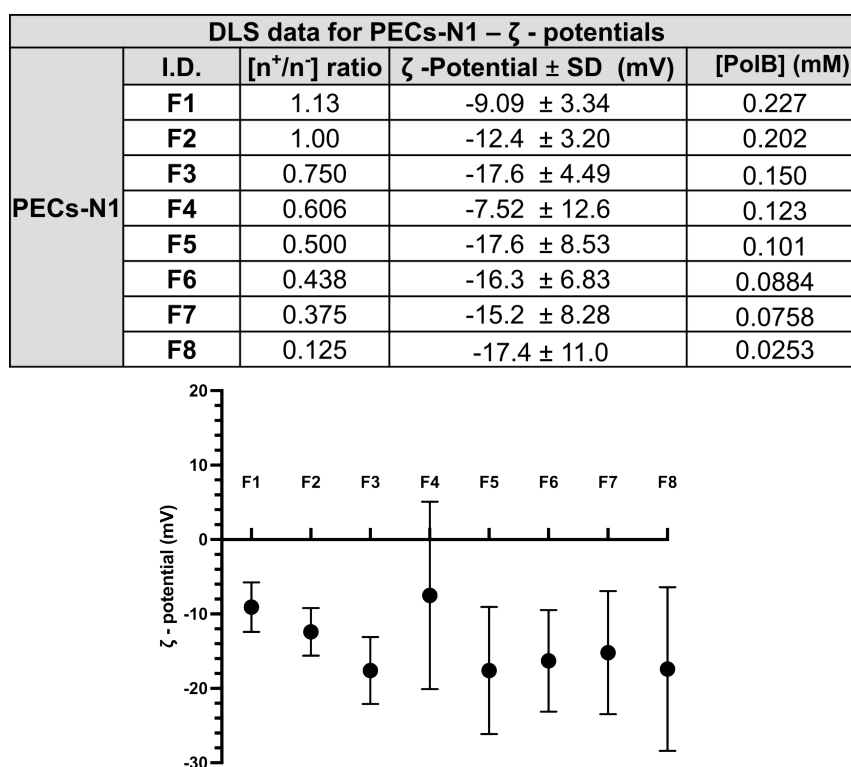


Figure 4.6 – ζ -potential values for all of the formulations of PECs-N1, presented as a table and as a graph. Results are shown as means \pm standard deviation ($n = 3$).

It is crucial to highlight that the ζ -potentials of PolB and Poly-P2 samples had a high standard deviation (i.e., high error), due to the fact that ζ -potential measurements depend on the formation of colloidal particles in the solution, which is not fully applicable to the solutions of PolB and Poly-P2 on their own. Therefore, the ζ potential data for PolB and Poly-P2 were used only as a reference.

The initial DLS analysis of PECs revealed that formulation F3 with a $[n^+/n^-] = 0.750$ produced the least aggregated particles. However, the presence of size distribution < 100 nm (Figure 4.5) suggested that the assembly was incomplete. To test this hypothesis, extending the mixing time was considered a potential solution. Unfortunately, this was not a feasible option as the mixing time was already quite long (24 hours) and would not have solved the aggregation issues. Consequently, a different approach was taken, which included the use of a higher shear mixing (*i.e.* a smaller stirrer bar with a faster rotation speed) and a slower addition of PolB to the solution of Poly-P2 (Figure 4.3). To evaluate the modified preparation method, 4 different batches of PECs-F3 ($[n^+/n^-] = 0.750$) were prepared and analyzed with DLS (Figure 4.7). As expected, the reproducibility of the PECs self-assembly method was not high with D_H ranging from 196 to 415 nm. However, the quality of the size distributions was excellent: low polydispersity index (PDI) < 0.1 , without signs of aggregation, producing particles with average $D_H = 294$ nm in HEPES (pH 7.45), based on batches B1 - B4, Figure 4.7. The bimodal size distribution that had previously been observed (as seen in Figure 4.5-F3) was not present, which confirmed the benefit of using an improved assembly methodology. Consequently, all subsequent assemblies used smaller stirrer bars with a faster rotation speed in the preparation setups.

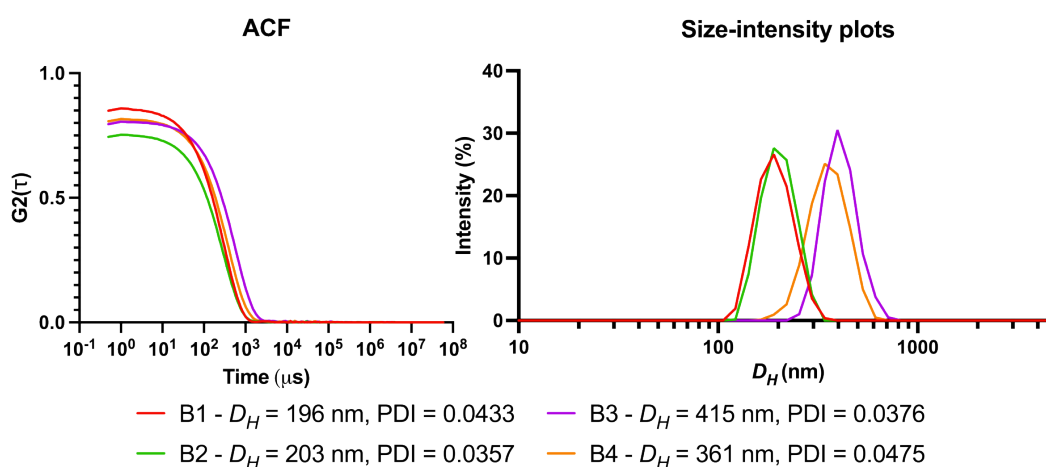


Figure 4.7 – Size variation of different batches of PECs-F3 ($[n^+/n^-] = 0.750$ ratio), monitored with DLS. B1, B2, B3 and B4 are used to represent batch numbers. PECs were prepared in 15 mM HEPES buffer (pH 7.45). The results are presented as an average of 3 technical replicates for each sample.

Prior to further analysis of selected PECs, transmission electron microscopy (TEM) was used to investigate the morphological properties (*i.e.*, size and shape) of produced PECs particles. For this purpose, an optimized PECs-F3 ($[n^+/n^-] = 0.750$) were selected, representing the least aggregated formulation based on the DLS data. To ensure that the pH of the assembly environment was maintained at 7.45, HEPES buffer was used when preparing PECs, so that Poly-P2 and PolB were present in their charged states.

Unfortunately, an abundance of buffer in the samples can lead to crystal formation that can be seen in TEM micrographs. These buffer crystals can obscure the particles, making it difficult to analyze their size and shape. As a result, a different batch of PECs-F3 ($[n^+/n^-] = 0.750$) was prepared using Milli-Q water instead of HEPES buffer. To ensure that colloidal particles were still present after the assembly with Milli-Q water, DLS analysis was repeated (Figure 4.8a), which was followed by TEM (Figure 4.8b, c).

The use of Milli-Q water instead of the HEPES buffer did not result in a degradation of the size distributions obtained with DLS. ACF curve (Figure 4.8a) was smooth with no indication of aggregation, $D_H = 267$ nm, which was only 30 nm lower than the average hydrodynamic radii of PECs-F3 in HEPES. Considering D_H of different batches of PECs-F3 ranged from 196 - 415 nm (Figure 4.7) the difference in 30 nm can be attributed more towards batch to batch variation.

The same PECs-F3 sample was then analyzed with TEM (Figure 4.8b, c). On the basis of TEM micrographs, a range of spherical particles could be easily identified. The particles' average diameter was 79 nm (D_{TEM}) and was based on the sizes of 75 nanoparticles, which were measured twice (in their longest and shortest diameters), with PDI calculated from a total of 150 measurements (Figure 4.8b, c). The average size the particles obtained from TEM images was 188 nm lower than the results obtained via DLS. This significant difference in diameter measurements can be related to the differences in TEM and DLS techniques as well as the dependence of PECs on the aqueous environment.

In DLS, the hydrodynamic radius (D_H), is representative of the 3D size of the particles in solution, which includes the diffuse layer surrounding it. On the contrary, TEM is conducted on a dried sample, creating a two-dimensional image of the three-dimensional shape of the electron-dense core of the sample. This differentiation is crucial considering that the assembly of PECs depends on the presence of solvent molecules between its components (PoIB and Poly-P2). Consequently, the size of PECs would decrease dramatically when dried, as observed in the TEM micrographs (Figure 4.8b).³⁴ Solvent evaporation, results in changes in surface tension that can cause particles to break down into smaller pieces, thus decreasing the average particle size compared to DLS measurement.¹⁶ This process was not uniform across the TEM grid, leading to the creation of particles with varying sizes, which can be seen by contrasting Figures 4.8b with 4.8c. This phenomenon was observed for other PECs-like systems.^{7,35} Nevertheless, the key information about particle morphology *i.e.*, their spherical shape, was confirmed with TEM. Additional characterization data of PECs such as FTIR and UV-Vis can be found in Supporting information, Figures S4.29, S4.30.

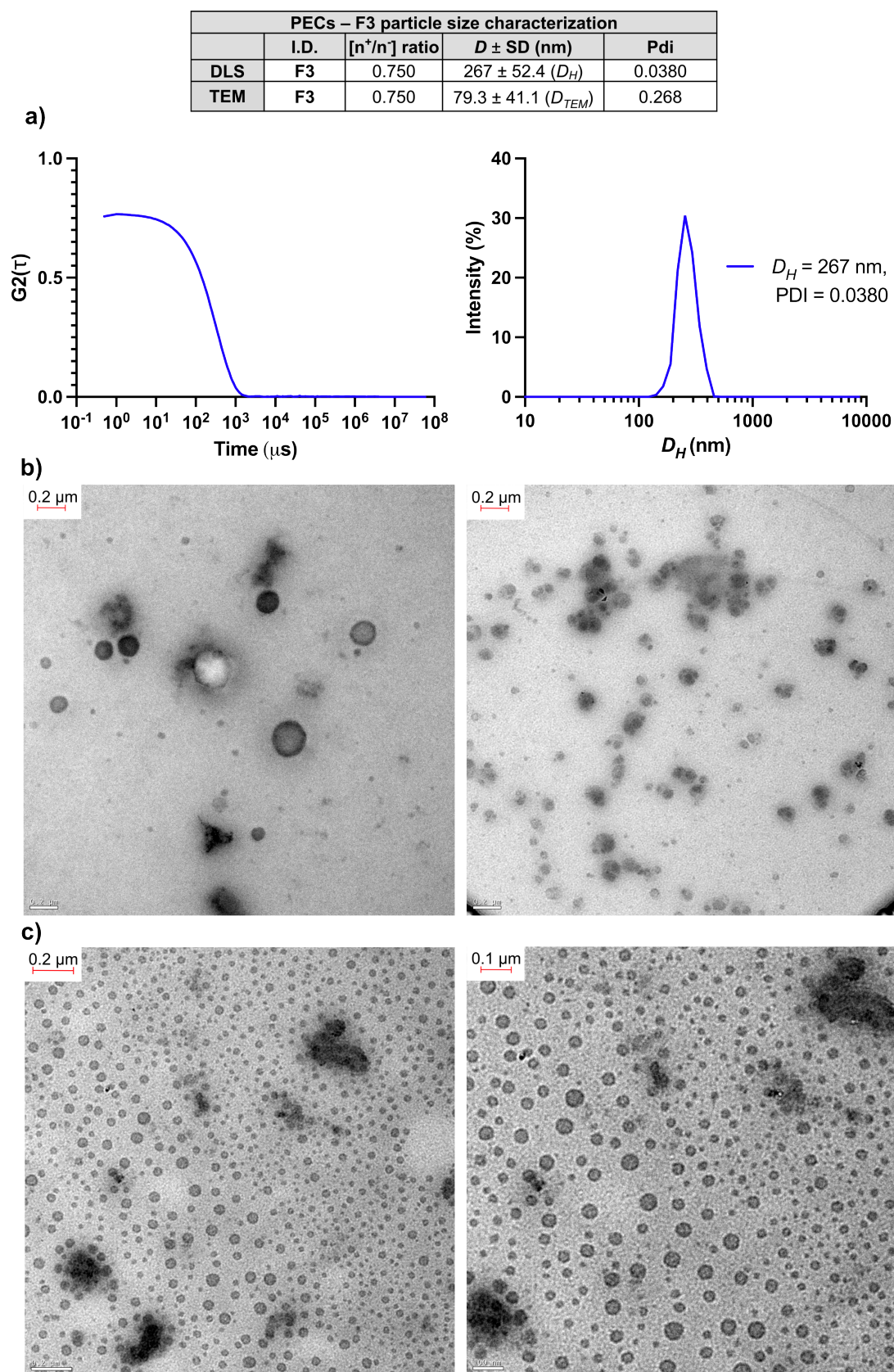


Figure 4.8 – a) DLS results of PECs-F3 ($[n^+/n^-] = 0.750$ ratio) prepared in Milli-Q water. The results are presented as an average of 3 technical replicates for each sample. b,c) TEM micrographs of the selected PECs-F3 ($[n^+/n^-] = 0.750$ ratio) prepared in Milli-Q water, $n = 1$.

4.4.2 Estimation of encapsulation efficacy of Polymyxin B in PECs

Once the size characteristics of the PECs formulations were determined using DLS and TEM, the encapsulation efficacy of PolB within these nanoparticles was explored. To monitor the encapsulation of PolB, a fluorescamine-based fluorogenic test was selected because it provides information on the number of primary amines present in PECs solutions. Fluorescamine is capable of reacting with any of the primary amine groups present, forming fluorescent conjugates that emit a signal at $460 \text{ nm} \pm 10 \text{ nm}$ when excited at 355 nm. With a higher degree of encapsulation of PolB within PECs, a lower number of primary amine groups (from Dab residues of PolB - Figure 4.9) would be available to form a fluorescent conjugate with fluorescamine, and as a result, the intensity of emission would decrease (Figure 4.9).

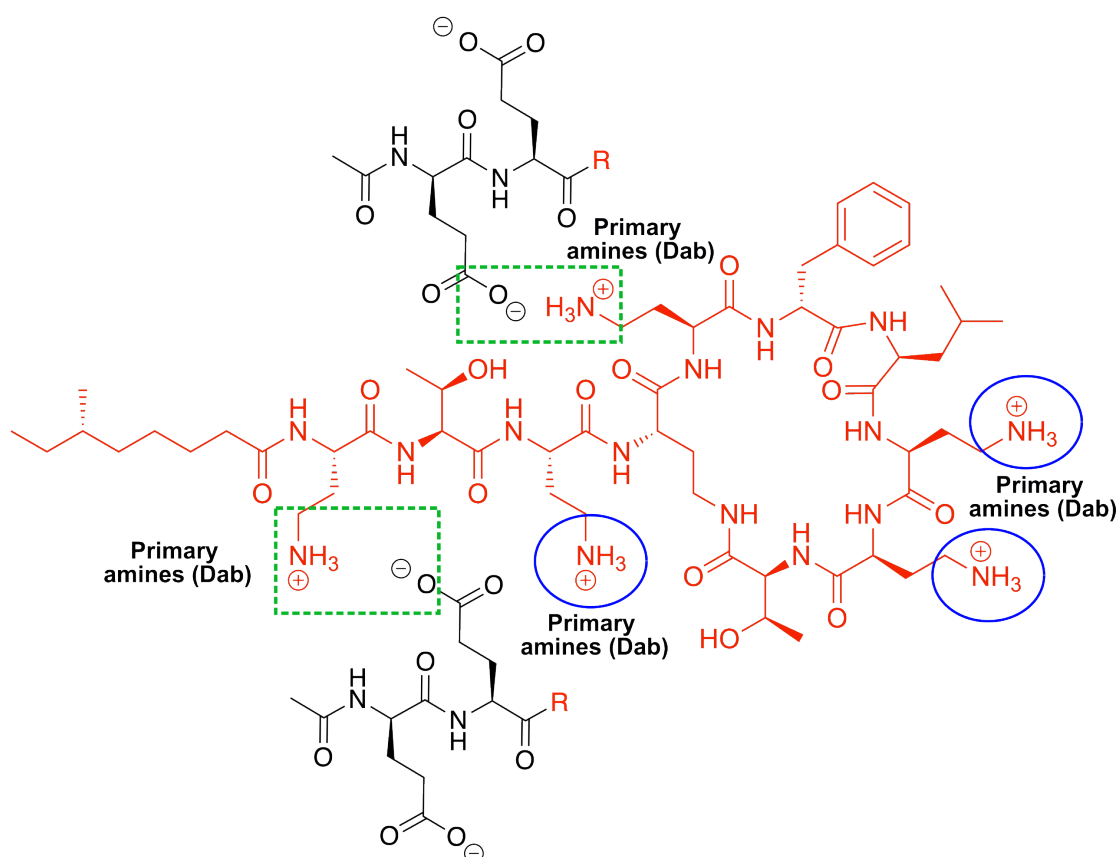


Figure 4.9 – Schematic representation of PolB encapsulation using Poly-P2, R - represents the rest of Poly-P2 chemical structure. Dab - diaminobutyric acid.

To estimate the amount of available PolB in PECs, a standard curve of PolB-fluorescamine conjugates was established (Figure S4.31a). Consequently, after obtaining the emission intensity data (Figure S4.31b and c) for the fluorescamine-PECs conjugates, the results were converted into the concentration of available PolB using the standard curve equation. The equation 4.4 was then used to calculate the degree

of encapsulation efficacy of PolB in PECs (Figure 4.10):

$$\frac{[mg \times mL^{-1}]_{total PolB} - [mg \times mL^{-1}]_{available PolB}}{[mg \times mL^{-1}]_{total PolB}} \times 100 \quad (4.4)$$

The quantity of PolB loaded was expressed in milligrams per milliliter (mg/mL) instead of millimolar (mM), as this is a more common unit for expressing the concentration of a drug in a solution ($\mu\text{g/mL}$ are also used), particularly when evaluating the minimum inhibitory concentration (MIC), which would be important during the discussion of antimicrobial activity of the delivery system.

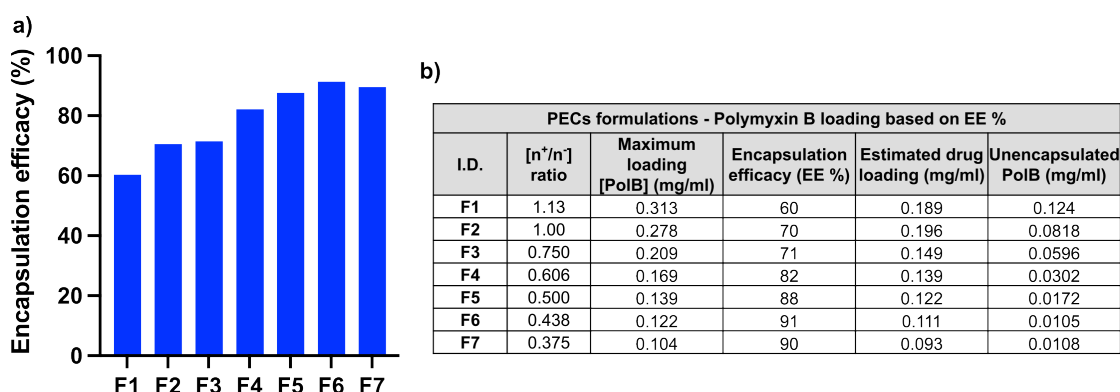


Figure 4.10 – a) Estimated encapsulation efficacy of PolB in PECs using fluorescamine assay. b) Polymyxin B loading in each PECs formulation, based on encapsulated efficacy. The results are presented as an average of 3 technical replicates for each sample.

F6 had the maximum encapsulation efficacy of 91 %, while the lowest values of 60 % and 70 % were for formulations with $[n^+/n^-] \geq 0$ (Figure 4.10a). Furthermore, as the amount of PolB added decreased from F1 (0.313 mg/mL) to F7 (0.104 mg/mL), the encapsulation efficacy predictively increased, since the Poly-P2 concentration remained constant for all formulations (Figure 4.10a). Although samples with $[n^+/n^-] < 0.750$ had better encapsulation efficacy, they also had a lower estimated drug loading (EE * max. loading - Figure 4.10a, b), which would have a negative effect on the antimicrobial efficacy of the PECs system. In comparison, the estimated maximum loading of PolB - 0.196 mg/mL (Figure 4.10b) was achieved at a charge ratio of 1.00 (F2), followed by F1,3,4,5,6 and F7. However, an excess of unencapsulated Polymyxin B such as in F1 (0.124 mg/mL) and F2 (0.082 mg/mL) would potentially lead to increased toxicity of the delivery system (Figure 4.10b) due to the presence of unshielded PolB molecules, which have strong hemolytic activity towards mammalian cells.³⁶ Therefore, we expected that with higher encapsulation efficiency (EE), the toxicity of Polymyxin B would reduce, when loaded into PECs. This expectation arises from the shielding effect provided by the anionic Poly-P2, which would neutralize the cationic residues of Polymyxin B. For

instance, when comparing a dose of 0.209 mg/mL of Polymyxin B Sulfate with PECs-F3 (*i.e.*, the same 0.209 mg/mL PolB loading), the toxicity of PECs-F3 would likely be up to 70% lower than that of free Polymyxin B. It is important to clarify that a dedicated experiment investigating cytotoxicity is required to fully understand the toxicological profiles of these PECs (PolB:Poly-P2), for example MTT (3-(4,5-Dimethylthiazol-2-yl)-2,5-Diphenyltetrazolium Bromide) assay. This is because the toxicity of PolB is not solely associated with its charge but also with other structural elements of the peptide therapeutic, such as its fatty acid tail.² Moreover, Poly-P2 on its own and its degradation products could potentially contribute to the toxicity of the system as well.

Interestingly, the size characteristics of PECs (Section 4.4.1) can be correlated with the data on encapsulation efficacy. For example, formulations F1 and F2 produced particles with the highest degree of aggregation (Figure 4.4), while also having the lowest EE. These data confirmed that at $[n^+/n^-] \geq 0$, the amount of added PolB exceeded the encapsulation capacity of Poly-P2 polymer, resulting in the formation of neutral particles that fluctuated in solution. In contrast, F4 - 8 had the highest EE but the number of colloidal particles produced was significantly lower, making again PECs with a charge ratio of 0.750 (F3) the most balanced formulation.

4.4.3 Investigating physiological stability and dominant interactions in selected PECs

One of the key challenges of using PECs *in-vivo* (this includes delivery into lungs and skin) would be stability of the particles under physiological osmolality conditions *i.e.*, 154 mM NaCl and temperature, 37 °C.^{7,8} The electrostatic interactions that usually stabilize PECs can be disrupted by adding ions such as Na⁺ and Cl⁻, which create repulsive forces that cause the particles to swell and even fully disassemble. However, electrostatics are not the only forces that contribute to the stability of PECs. H-bonding and hydrophobic interactions also play a role in keeping the electrolytes together and providing stability under physiological conditions.

Therefore, it was important to study the physiological stability of the formulated PECs. For this purpose, DLS was used as a means to monitor colloidal properties of the selected PECs. For this experiment, the most balanced formulation F3 ($[n^+/n^-] = 0.750$) was selected and tested against the least balanced formulation F1 ($[n^+/n^-] = 1.13$). The particles were incubated in a 154 mM NaCl solution for 4 hours at 37 °C, with aliquots taken every 1 hour for size analysis (Figure 4.11).

The ACF curves for both PECs-F1 and F3 showed a significant increase in particle size (*i.e.*, swelling) after being incubated in a 154 mM NaCl solution, which was

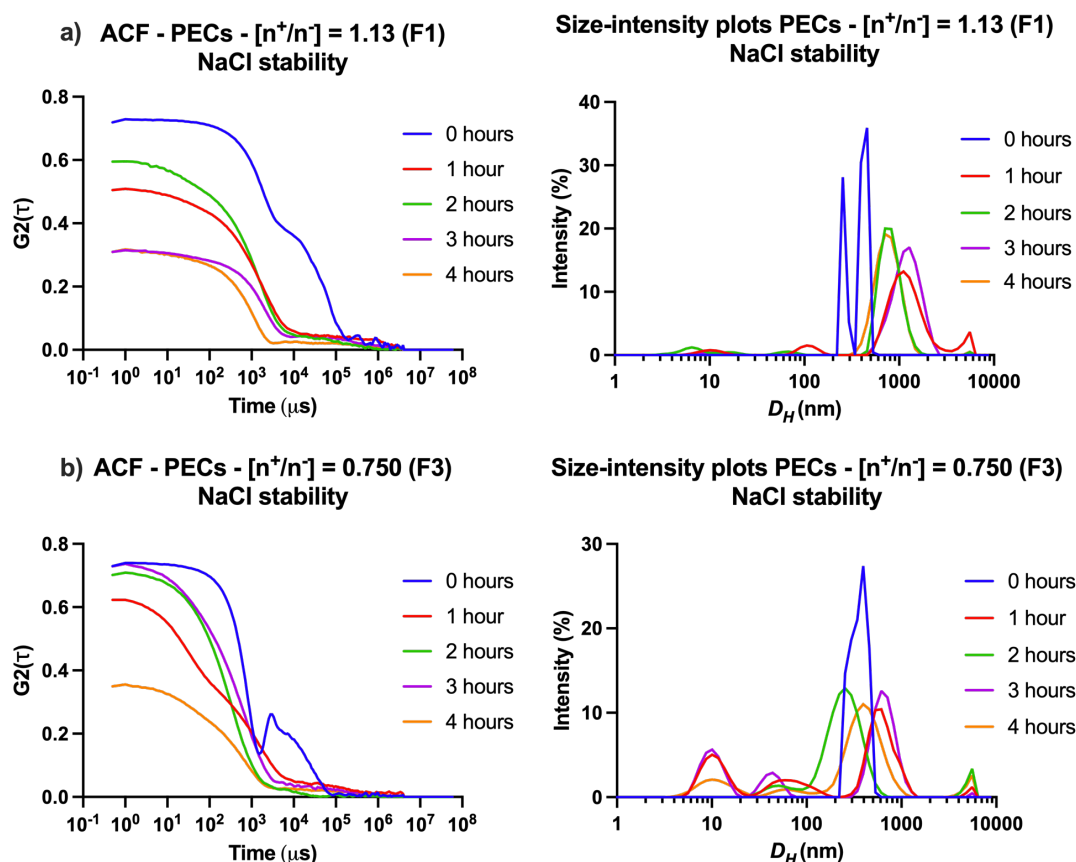


Figure 4.11 – Summary of **DLS** size-intensity plots as well as autocorrelation functions (**ACF**) of **PECs** nanoparticles with $[n^+/n^-]$ = a) 1.13 (F1) and b) 0.750 (F3) in presence of 154 mM NaCl at 37 °C over 4 hours. The results are presented as an average of 3 technical replicates for each sample.

evidenced by a long decay ($10^5 \mu\text{s}$ for F1 and $10^3 \mu\text{s}$ for F3, Figure 4.11a) of the **ACF** curves at T0. Interestingly, the extent of swelling was greatest at T0, which then decreased rapidly during the course of the incubation. Consequently, when **PECs** were added to the NaCl solution, swelling began to occur rapidly, leading to disassembly of the particles, as shown by the sharp decrease in the correlation coefficient of the **ACF** curves: for F3 from 0.73 to 0.35, and for F1 from 0.72 to 0.31 (Figure 4.11a and b). The size-intensity graphs for F3 and F1 revealed the formation of smaller particles in the range of 10 - 100 nm, which can be attributed to the disassembly products *i.e.*, **PolB** and **Poly-P2**. As anticipated, F1 ($[n^+/n^-]$ = 1.13) swelled more than F3 ($[n^+/n^-]$ = 0.750) at T0 due to increased electron repulsion caused by a higher concentration of polyelectrolyte (*i.e.*, **PolB**) in the particle suspension.³² However, neither **PECs**-F1 nor F3 were completely disassembled within four hours, as the **DLS** data revealed the presence of colloidal particles *i.e.*, size distributions were found. This implied that electrostatics were not the only forces at work in the formation and stability of these particles.

Therefore, in order to determine the dominant interactions that stabilize and promote the formation of **PECs** from **Poly-P2** and **PolB**, an additional stability experiment was conducted. This time, only **PECs** with a charge ratio of 0.750 (F3) were used, representing the most balanced formulation. Following a previously reported procedure,³⁷ freshly prepared **PECs**-F3 were incubated at 37 °C for 24 hours in 100 mM NaCl, **Tween 20**, **EDTA**, and Urea solution. A concentration of 100 mM was chosen because it was different from that of 154 mM NaCl (physiological conditions) and provided an additional data point to investigate the stability of **PECs**. Subsequently, the **DLS** technique was used to assess the extent of the change in the particle size distributions (Figure 4.12). Each of the 100 mM solutions of NaCl, **Tween 20**, **EDTA**, and urea probed for different dominating interactions: NaCl disrupts electrostatic bonds; **Tween 20**, a polysorbate-type nonionic surfactant disturbs hydrophobic interactions; **EDTA** inhibits metal ligation by chelating metals; Urea is known to form strong H-bonding interactions.

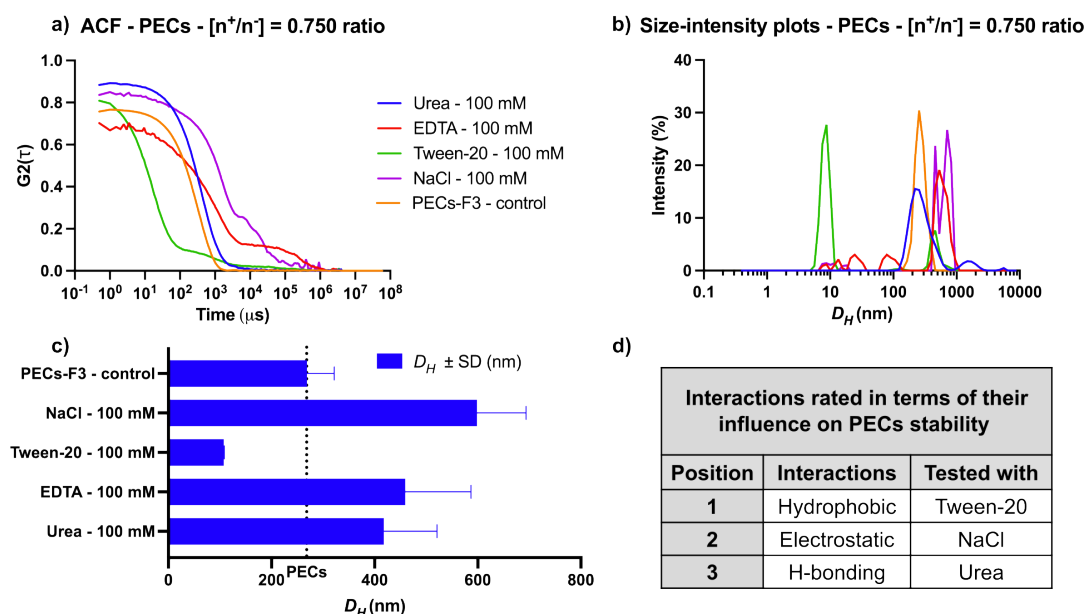


Figure 4.12 – Summary of **DLS** data: a) autocorrelation functions (**ACF**) as well as b) size-intensity plots of **PECs** nanoparticles with $[n^+/n^-] = 0.750$ (F3) in presence of 100 mM Urea, **EDTA**, **Tween 20** and NaCl at 37 °C after 24 hours of incubation. c) Comparison of hydrodynamic radii (D_H) for **PECs** after incubation with 100 mM Urea, **EDTA**, **Tween 20** and NaCl. d) Interactions rated in terms of their influence on **PECs** assembly and stability. The results are presented as an average of 3 technical replicates for each sample.

The least destabilizing effect on the size distributions of **PECs** was observed with Urea, resulting in the creation of aggregates with size 500 - 1000 nm (Figure 4.12b). This was likely caused by several particles binding to each other through H-bonding with urea. On the contrary, incubation with **Tween 20** led to mostly complete disassembly of **PECs** as can be seen by the creation of particle size of around 10 nm (Figure

4.12b,c), which highlighted that hydrophobic interactions between **Poly-P2** and **PolB** play a crucial role in their assembly and stability. These results were surprising but not unexpected, as both **PolB** and **Poly-P2** contain hydrophobic moieties in their chemical structure that represent amino acids such as Phe, Gly, Ala, Leu and also by the presence of the fatty acid tail in the drug.

As **PECs** do not rely on metal coordination for their assembly, the addition of **EDTA** did not cause particle disassembly. Instead, **PECs** swelled (size increased by 192 nm) as a result of electrostatic repulsion between the carboxylate groups of **Poly-P2** and the acid groups of **EDTA** (Figure 4.12 c). Similarly, when placed in a NaCl solution, the **PECs** particles swelled, doubling in size (from 267 to 600 nm) as a result of the electrostatic repulsion between the polyelectrolytes and the Na⁺ and Cl⁻ ions. It appeared that **PECs** were not as easily disassembled when exposed to 100 mM NaCl for 24 hours compared to 154 mM NaCl for 4 hours. These results were expected since the salt concentration was considerably lower than under physiological conditions (154 mM). However, **PECs** did not completely lose colloidal characteristics when incubated with 100 mM **EDTA** and NaCl, which can be attributed to the stabilizing hydrophobic interactions between **Poly-P2** and **PolB**.

Stability testing revealed that a variety of interactions, such as hydrophobic, hydrogen bonding, and electrostatic, are all involved to some extent in the formation and stabilization of **PECs**. However, the **PolB** and **Poly-P2**-based **PECs** are mainly stabilized by hydrophobic and electrostatic interactions (Figure 4.12d). Depending on the environmental conditions (e.g. pH, salt concentration, temperature), one of these interactions will be more influential than the other. This is why under physiological salt concentration (154 mM NaCl) **PECs** with a charge ratio of 0.750 (F3) did not fully disassemble. Nevertheless, in 154 mM NaCl solution the **PECs**-F3 nanoparticles swelled significantly, which can also lead to an uncontrolled release of Polymyxin B.^{7,32} Consequently, causing an unnecessary increase in the cytotoxicity of the delivery system. Therefore, it was important to look for simple ways to improve the physiological stability of the selected **PECs** without completely reinventing the delivery system.

4.4.3.1 Enhancing physiological stability of **PolB**:**Poly-P2** **PECs** nanoparticles

To improve the resistance of the **PECs** system towards physiological osmolality (*i.e.*, 154 mM NaCl), the strength of stabilizing interactions (*i.e.*, electrostatic and hydrophobic) between **PolB** and **Poly-P2** had to be increased.

Electrostatic forces can be strengthened by increasing the charge density of either of the polyelectrolytes. However, that would have required the synthesis of a new

anionic polymer with a more densely packed structure (e.g., star polymer) and a new peptide sequence (e.g., with more anionic residues). An alternative 'non-invasive' approach was to incorporate a multi-binding molecule, such as Tannic Acid (TA), to act as a cross-linker between PolB and Poly-P2. In this way, no changes would be required to the current formulations of PECs, considerably simplifying the optimization procedures.

Tannic Acid is a polyphenol that is renowned for its ability to create strong hydrophobic, H-bonding, and electrostatic interactions with a variety of molecules, including antimicrobial peptides (AMPs), as a result of the chemical features of the catechol and gallol groups (Figure 4.13).^{6,38,39} At acidic pH, gallol groups are protonated, which promotes the formation of H-bonds with more electronegative atoms, such as carbonyl oxygen in the amide bonds or nitrogen in the amide bond of the peptide.^{40,41} Opposite happens at pH > 8, where gallol groups in Tannic Acid change from an uncharged state to anionic, allowing it to form strong electrostatic interactions with other electrolytes (Figure 4.13). Consequently, Tannic Acid's characteristics make it a potential cross-linker between PolB and Poly-P2 by binding them together with hydrophobic and electrostatic interactions at physiological pH. This would result in strengthening of the stabilizing interactions between the three components, PolB, Poly-P2, and TA. Therefore, the resistance of PECs towards physiological salt concentration would be significantly improved.

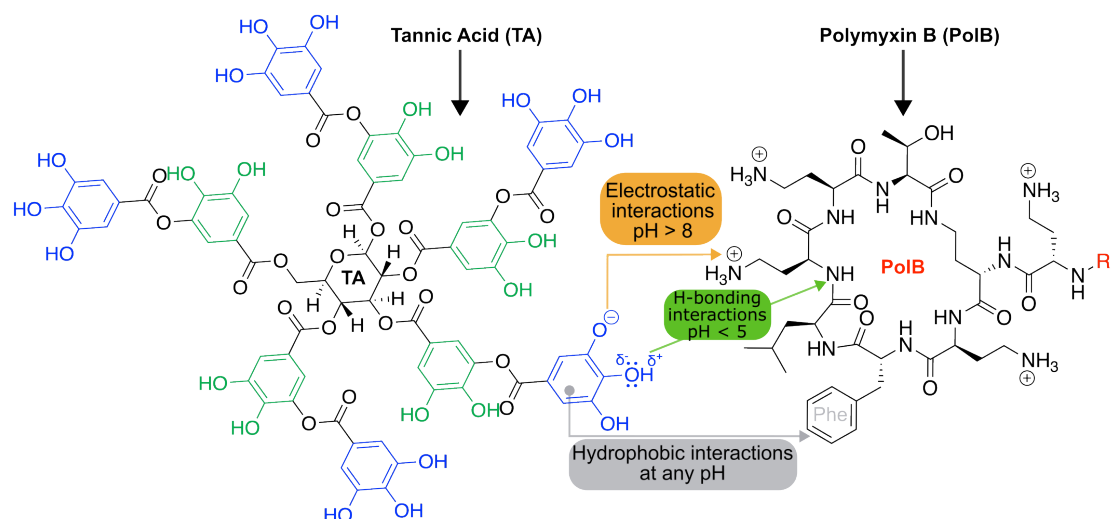


Figure 4.13 – Schematic representation of multi-binding properties of Tannic Acid (TA) with Polymyxin B (PolB) used as an example. R₁ - represents the rest of the chemical structure of Polymyxin B.

The synthesis of PECs with TA consisted of two steps. The first step was to assemble PECs-F3 without TA, followed by DLS analyses that verified the presence of particles (the detailed assembly of particles is discussed in Section 4.3.3). The second step was to add 5 μ L of a TA solution (0.02351 mM) to the PECs-F3 solution and let

them mix for 24 hours. The concentration and quantity of TA added (5 μ L, 0.02351 mM) were based on previous studies in which TA was successfully used to assemble nanoparticles composed of polyphenols and a variety of polypeptides.⁴² After the assembly of PECs-F3 + TA (referred to as PECs-N2), DLS, and ζ -potentials were used to investigate the size distributions and surface charge of the obtained nanoparticles (Figure 4.14).

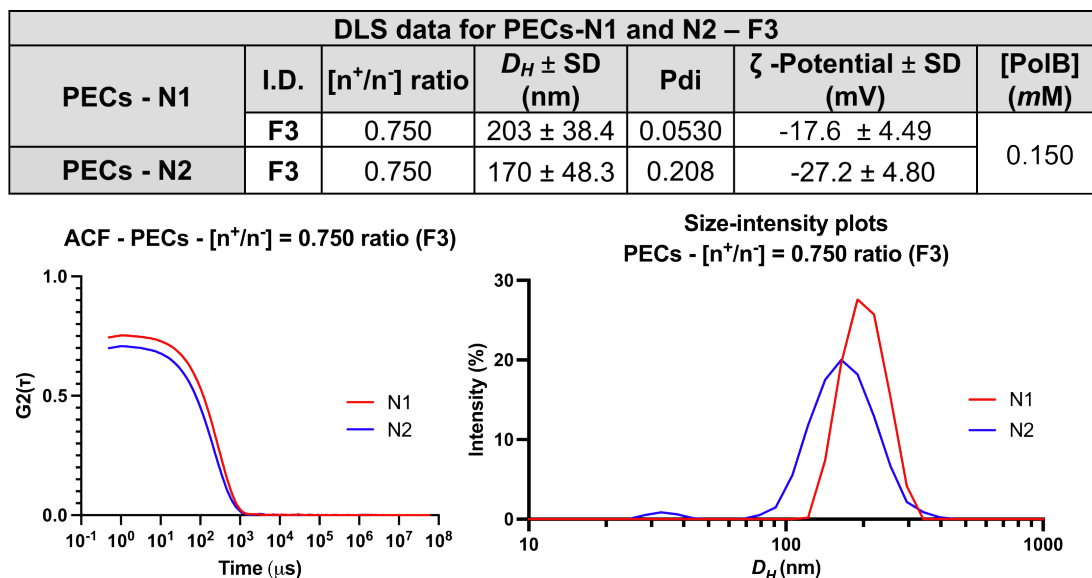


Figure 4.14 – Summary of DLS autocorrelation functions (ACF), size-intensity plots and ζ -potential data of PECs-F3 (PECs-N1) and PECs-F3 + TA (PECs-N2) nanoparticles with [n⁺/n⁻] = 0.750 (F3). The results are presented as an average of 3 technical replicates for each sample.

The addition of TA led to a decrease in particle size by 33 nm (from 203 to 170 nm), which was indicated by a faster decay of the autocorrelation function (Figure 4.14). This showed that TA increased the cross-linking between PoIB and Poly-P2, making the components closer together and decreasing the size of the particles. Simultaneously, it is probable that any unencapsulated PoIB formed separate PECs with TA, which is why a minor peak was observed at 30 nm, causing the PDI of the main peak to increase from 0.0530 to 0.208 (Figure 4.14). Theoretically, TA should have a strong binding affinity to PoIB due to electrostatic and hydrophobic forces, leading to the destabilization of interactions between PoIB and Poly-P2. Consequently, a considerable decrease in the correlation coefficient and multimodal size distributions would have been observed in the DLS data. However, this was clearly not the case for PECs-F3 + TA with DLS data that were only slightly different from PECs-F3 without TA, indicating good compatibility of PoIB and Poly-P2 with polyphenol.

Compared to size distributions, the ζ -potentials for PECs-F3 + TA experienced a more significant change, decreasing from -17.6 to -27.2 mV with the addition of Tannic

Acid. These results suggest that TA binds to the surface of PECs, which consists mainly of **Poly-P2**. At a pH of 7.45, two gallol groups³⁰ in TA, would be deprotonated, leading to an increase in the overall negative charge (as seen in Figure 4.14). Although both TA and **Poly-P2** were negatively charged, they did not cause particle disassembly, as a result of electrostatic repulsion. This meant that attractive interactions of **Poly-P2** and TA such as hydrophobic and H-bonding, dominated over repulsive electrostatic interactions.

Following the formation of PECs-F3 + TA, the physiological stability of the particles was tested using the same procedure as for PECs without TA (Section 4.4.3). In summary, PECs-F3 + TA were incubated for 4 hours in a 154 mM NaCl solution maintained at 37 °C. Stability aliquots were collected every hour and analyzed using DLS, monitoring changes in size distributions (Figure 4.15).

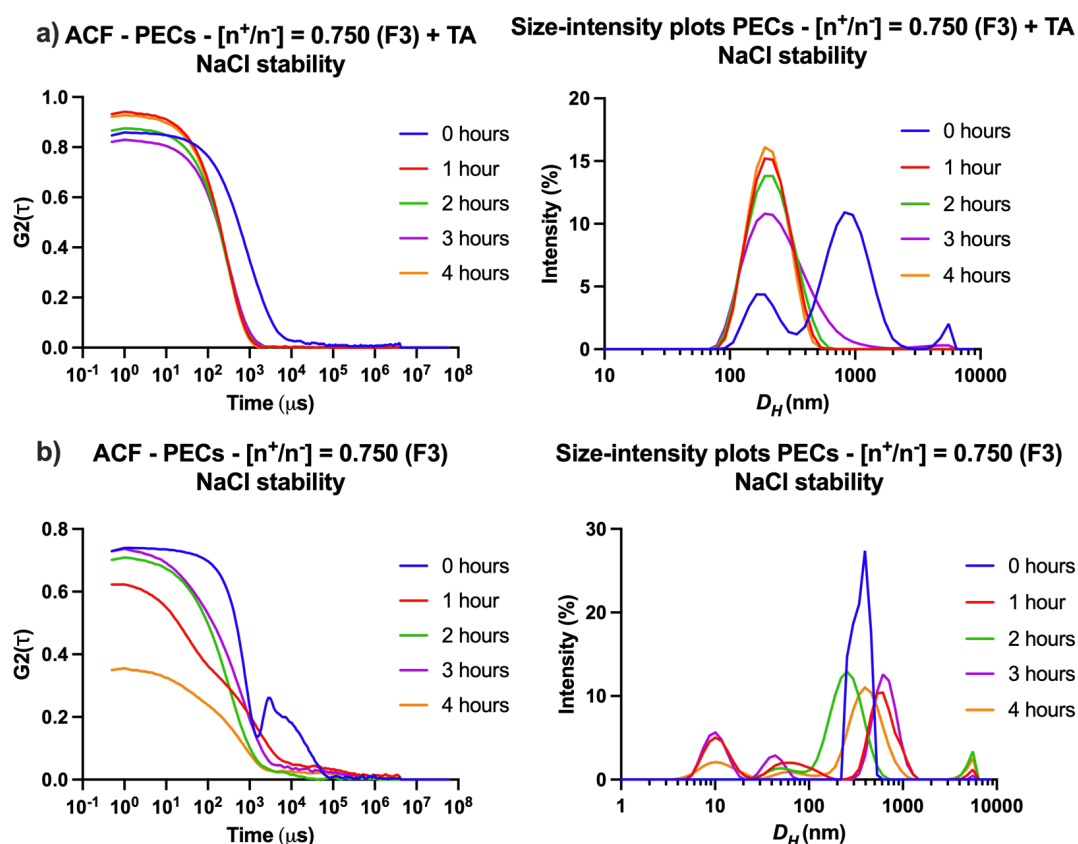


Figure 4.15 – Summary of DLS size-intensity plots as well as autocorrelation functions (ACF) of PECs nanoparticles with $[n^+/n^-] = 0.750$ (F3) a) with added Tannic Acid (TA), b) without added Tannic Acid (TA) in presence of 154 mM NaCl at 37 °C over 4 hours. The results are presented as an average of 3 technical replicates for each sample.

The behavior of the size distributions of PECs-F3 + TA (Figure 4.15a) was completely different from PECs-F3 without TA (Figure 4.15b). ACF of PECs-F3 + TA fluctuated between 0.8 and 0.9 (Figure 4.15a), but never decreased to 0.38 as in the case

of PECs-F3 without TA (Figure 4.15b), indicating minimal changes in the concentration of particles between time points. Size-intensity plots of PECs-F3 + TA became increasingly monomodal as the experiment progressed, in contrast to the multimodal plots observed for PECs-F3 without TA (Figure 4.15b). At the beginning of the stability experiment (T0), the size-intensity plot of PECs-F3 + TA showed that the sample contained three different size-distributions (D_H): at 220, 1000, and 5560 nm. After an hour of incubation in 154 mM NaCl, peaks at 1000 and 5560 nm disappeared for the duration of an experiment, while the intensity of the peak at 220 nm increased from 4 to 15 % (Figure 4.15a). The behavior observed suggested that the peaks at 1000 and 5560 nm were likely aggregates that were destabilized by the presence of NaCl ions, resulting in the formation of unaggregated particles at 220 nm. This was because NaCl ions shielded the charges of PolB, TA and Poly-P2, reducing the strength of electrostatic interactions and, in the case of PECs-F3 + TA, improving the size distributions (*i.e.*, lower polydispersity) by reducing aggregate formation. Compared to PECs-F3 without TA, the presence of NaCl salt had an excessive destabilizing effect, because the attractive interactions (H bonding, hydrophobic, and electrostatic) in that system are weaker, leading to particle disassembly (Figure 4.15b). Given that stabilizing interactions between PolB and Poly-P2 were found to be hydrophobic and electrostatic in nature, it is highly likely that TA strengthened them, thus preventing the loss of colloidal structure in 154 mM NaCl.

Taken together, these findings suggested that PECs consisting of PolB and Poly-P2 are not completely electrostatic in nature, with hydrophobic interactions playing a significant role in both particle assembly and stability. Furthermore, the addition of a strong binding agent such as TA can dramatically increase the physiological stability of these PECs, without completely changing their size characteristics. However, excessive physiological and colloidal stability of the delivery system, such as PECs, can be detrimental, as it can cause inadequate enzymatic breakdown and thus slow drug release, reducing its antimicrobial activity.^{6,8,39} Therefore, it was important to compare the enzymatic degradation properties of PECs-F3 with and without added Tannic Acid enhancement.

4.4.4 Evaluation of enzyme degradation properties of PolB:Poly-P2 PECs nanoparticles

The same enzyme degradation procedure was used for PECs as for testing polymers Poly-P1 and Poly-P2 (as outlined in Section 4.3.7), to ensure consistency in experimental protocols and comparability of the data. For this experiment, two sets of PECs with $[n^+/n^-] = 1.13$ ratio (F1) and $[n^+/n^-] = 0.750$ ratio (F3) with and without added

Tannic Acid were used. PECs-F1 were added to the test as the least balanced system (*i.e.*, negative control) to observe if there were differences in enzyme degradation properties compared to the optimized formulation F3. All of the PECs samples were prepared fresh using an identical assembly procedure (Section 4.3.3). As mentioned in Chapter 2 (2.4.3), thermolysin was used instead of *P.aeruginosa* protease (LasB) due to commercial unavailability of the later.^{43–45} For monitoring the extent of enzyme degradation, an optimized fluorogenic protocol based on a fluorescamine assay was used, following the exact procedure mentioned in Section 4.4.2. For a period of five hours, aliquots of the reaction were taken every hour and the activity of thermolysin was measured. The emission intensities were then normalized (Figure 4.16) to those generated by a model peptide, **P3** ($\text{H}_2\text{N-LA-NH}_2$), a simplified version of the GLA peptide sequences that had been broken down by the enzyme.

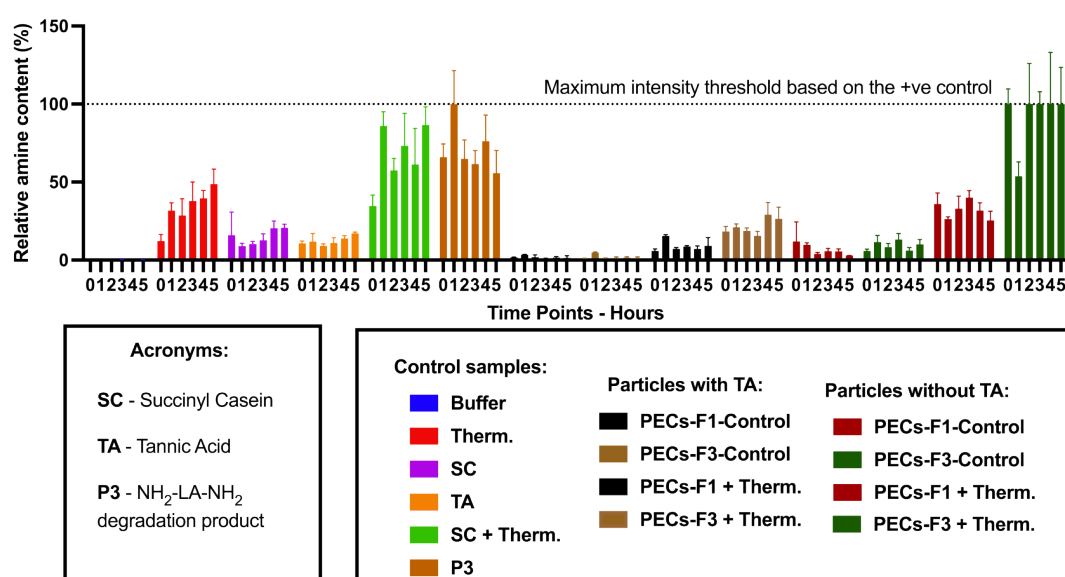


Figure 4.16 – Relative amine content (%) in samples of thermolysin-responsive PECs evaluated in this work. The relative amine content was calculated from fluorescamine conjugates formed following incubation of PECs with $[\text{n}^+/\text{n}^-] = 1.13$ ratio (F1) and $[\text{n}^+/\text{n}^-] = 0.750$ ratio (F3) with enzymes for 5 hours and normalized to the fluorescence observed with a model degradation peptide. Emissions normalized for HEPES, CaCl_2 , $\text{Na}_2\text{B}_4\text{O}_7$ buffer (Buffer), Thermolysin as enzyme control (Therm.), succinyl casein (SC) as a control for enzymatic activity, degradation peptide $\text{H}_2\text{N-LA-NH}_2$ (**P3**) as a control to normalize fluorescence intensity. All substrates were evaluated in the absence and presence of thermolysin. Incubation time: 5 hours, $n = 3$. For unnormalized data, see Figure S4.32.

The relative amine content of the PECs particles treated with thermolysin was significantly higher than that of the non-enzyme treated particles (labeled as PECs-Control in Figure 4.16), which increased over the course of the experiment. Furthermore, fluorescence data revealed the presence of primary amines in solution of non-enzyme-treated PECs which stayed relatively constant throughout the experiment for each of the controls. The presence of primary amines in control samples of PECs was attributed to

fluorescamine conjugates formed with unencapsulated Polymyxin B (as was explored in Section 4.4.2), since PECs were used without any purification (e.g., pelleting).

Of the two PECs formulations (PECs-F1 and PECs-F3), PECs-F3 degraded the most, reaching 100% (27% for PECs-F3 + TA) of the relative amine content within the first two hours of the experiment, while F1 only managed to reach a maximum of 40% (9% PECs-F1 + TA) (Figure 4.16). These differences could be attributed to the way the particles formed. In the case of F1, the particles were present in an aggregated state, surrounded by the largest amount of unencapsulated PolB (0.124 mg/mL, Figure 4.10) out of all formulations. When particles are aggregated, they are larger in size, which means that the total surface area of all the particles combined is less than that of non-aggregated, well-dispersed particles (such as in PECs-F3). Consequently, the amount of available Poly-P2 on the surface of the particles in colloidal dispersions of PECs-F1 is lower than in PECs-F3, resulting in a lower degree of degradation. It should be noted that the enzymatic breakdown of Poly-P2 in PECs would also cause the release of Polymyxin B, increasing emission intensities. The design of the enzyme degradation experiment did not consider the release of PolB, which is why a separate PolB release experiment was conducted, which is discussed in Section 4.4.5.

Interestingly, the samples with added Tannic Acid had a much lower relative amine content than those without it. For example, the relative amine content of PECs-F3 + TA at 5 hours was 27 %, while for PECs-F3 it was 100 %, a difference of 73% (Figure 4.16). This dramatic difference between PECs with and without TA can be attributed to two potential causes. First, TA quenches the fluorescence of fluorescamine conjugates as a result of its polyphenolic nature, leading to a decrease in the intensity of the emissions.⁴⁶ Second, due to the presence of TA on the surface of PECs (i.e., coating), it hinders Poly-P2 molecules from the enzyme, leading to slow or minimal degradation.

Ideally, the fluorogenic tests should have been redone specifically for PECs + TA so that all control samples, including the model peptide P3 include TA so that the signal is suppressed for all samples in the experiment. It is difficult to tell whether the degree of signal reduction would be consistent across all samples since the way TA interacts with fluorescamine conjugates can vary depending on the substance it is interacting with.⁴⁶ For instance, TA can use phenolic groups to attach themselves to the surface of PECs, while it can also interact with thermolysin in the degradation experiment.

Therefore, instead of relying on fluorescence to monitor the enzymatic degradation, ζ -potentials were used as an alternative method to monitor enzyme degradation of PECs. As Poly-P2 shell surrounding PolB is hydrolyzed by thermolysin, the concentration of primary amines on the surface of the particles would increase due to the degradation products of Poly-P2 and increased availability of PolB amine groups. At a

reaction pH of 7.45, primary amines will be predominantly protonated (e.g., **PolB** would have +5 charge at pH 7.45),³⁰ leading to an increase in the surface charge of the degraded **PECs** particles. Therefore, ζ -potentials of the degraded **PECs** are expected to become more positive with degradation. It is important to note that this experiment focused on the magnitude of the charge change for each sample, rather than comparing individual values.

Following exactly the same enzyme degradation procedure as described in Section 4.3.7, **PECs**-F3 samples with and without **TA** were incubated with thermolysin for a total of 6 hours. At regular intervals of two hours for a total of four time points, aliquots of a reaction mixture were analyzed for ζ -potentials (Figure 4.17).

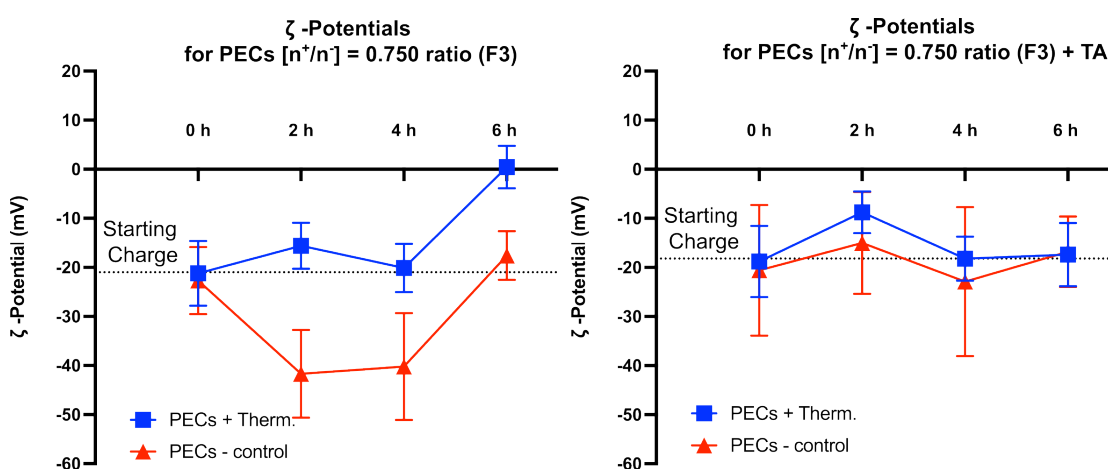


Figure 4.17 – Enzymatic degradation of **PECs** with $[n^+/n^-] = 0.750$ a) without b) with Tannic Acid (**TA**) monitored with ζ -potentials. Incubation time: 6 hours, 3 technical replicates were recorded for each sample. For enzyme degradation procedure see Section 4.3.7.

Both samples with and without **TA** had an increase in charge (*i.e.*, became more positive) of ζ -potentials (Figure 4.17). Consequently, this additionally confirmed that both systems are susceptible to thermolysin degradation. However, **PECs**-F3 without **TA** had a significantly greater charge difference between T0 (-21.2 mV) and T6 (0.428 mV) = 21.6 mV compared to T0 (-18.8 mV) and T6 (-17.4 mV) = 1.4 mV of **PECs**-F3 + **TA** (Figure 4.17). Interestingly, the greatest increase in charge from -20.1 to 0.428 mV for **PECs**-F3 without **TA**, occurred only in the last two hours of an experiment, suggesting that enzymatic degradation was slowed down for a minimum of 4 hours. This could be due to the fact that the enzyme needs time to locate and access the cleavable site since the **PECs** are much larger than the enzyme itself (**PECs**-F3, estimated Mw (**DLS**) = 8.84×10^5 kDa, thermolysin Mw = 34.6 kDa). Therefore, an incubation period of 4 four hours was required.

In contrast, ζ -potentials for **PECs** + **TA** did not change significantly (1.4 mV difference between T0 and T6) throughout the experiment, which confirmed that Tannic Acid

blocked **Poly-P2** from being accessible to thermolysin. Therefore, the lower emission intensities observed in the flurogenic test for the **PECs** + **TA** samples were not just due to **TA** suppressing the signal but also because **TA** prevented the **Poly-P2** layer from being degraded by the enzyme. In general, **TA** effectively formed a protective coating around the **PECs** (**PolB** + **Poly-P2**), which significantly improved the physiological stability of these particles but at the expense of their enzyme degradability. Consequently, **PECs** + **TA** system was not suitable for the development of the enzyme-responsive **AMP** delivery system and was therefore not considered for further evaluation.

4.4.5 *In-vitro* release of Polymyxin B from PolB:Poly-P2 PECs nanoparticles

After evaluating the enzyme-responsive properties of PECs, the next step was to investigate the enzyme-induced release of Polymyxin B from PECs-F3 ($[n^+/n^-] = 0.750$ ratio). For this purpose, a previously reported dialysis method was modified to suit the current PECs system (Figure 4.18).⁷

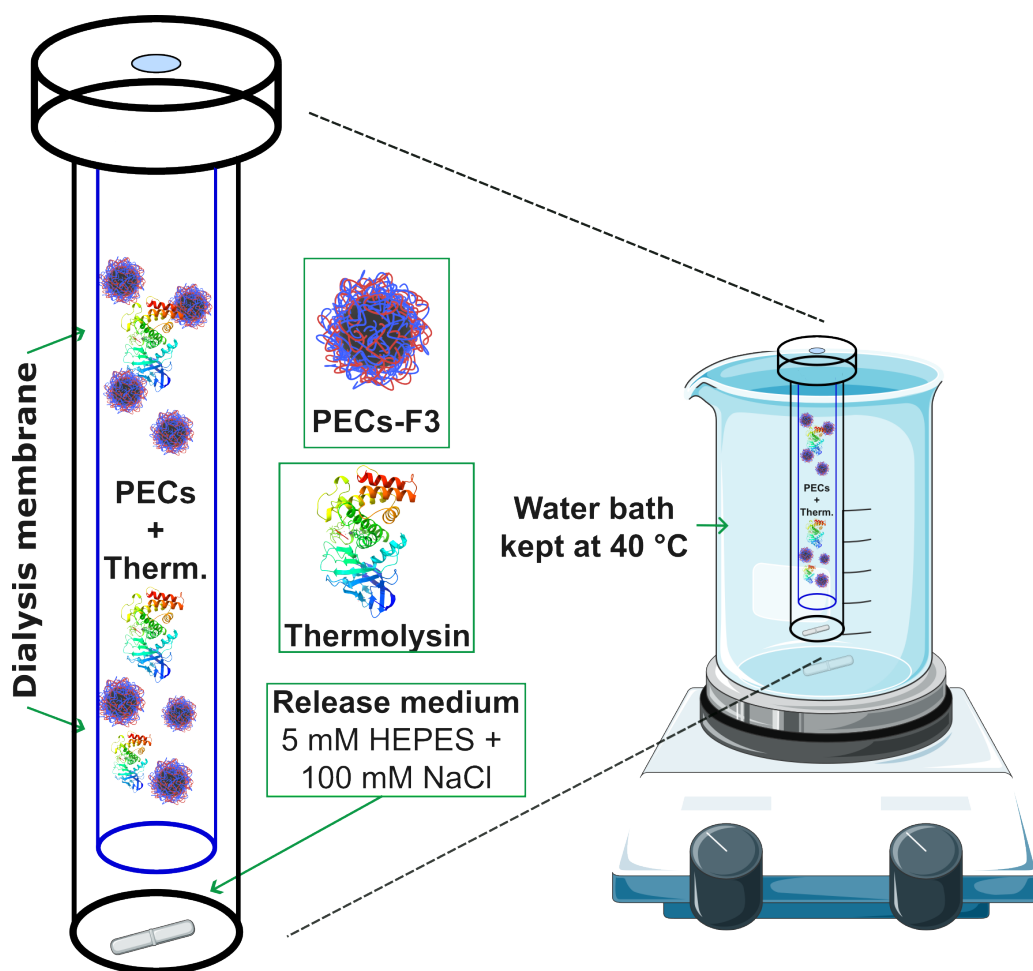


Figure 4.18 – Schematic representation of a dialysis set-up for investigating enzyme-induced Polymyxin B release from PECs-F3. Therm. - thermolysin.

To begin, PECs and thermolysin solutions were placed inside the dialysis membrane (Figure 4.18), which was dialyzed against 14 mL of 5 mM HEPES buffer supplemented with 100 mM NaCl to mimic physiological salt concentration. Furthermore, samples such as PECs-F3 without thermolysin and free Polymyxin B solution (0.209 mg/mL, same as in PECs-F3) were also dialyzed using an identical method in separate membranes. The purpose of using PECs-F3 without the added enzyme was to explore the release of PolB under physiological osmolality and to compare it with the enzyme-induced release. The efficacy of the dialysis membranes to pass PolB was

monitored using a **PolB** solution with a concentration of 0.209 mg/mL (labeled as Free **PolB** in Figure 4.20) and then compared to the release from **PECs**. Throughout the experiment, the dialysis systems were heated to 40 °C using an external water bath (Figure 4.18) that replicated the hypothermia conditions caused by bacterial infection in the human body.^{19–21} At regular time intervals, 1 mL of dialysate was removed for analysis and replaced with a fresh **HEPES** solution (with added NaCl), to maintain the total volume within the dialysis system constant. Since the colloidal stability of **PECs** was never tested at 40 °C, **DLS** analysis of **PECs**-F3 was performed at three different temperatures: 37, 40, and 50 °C prior to the release study (Figure 4.19).

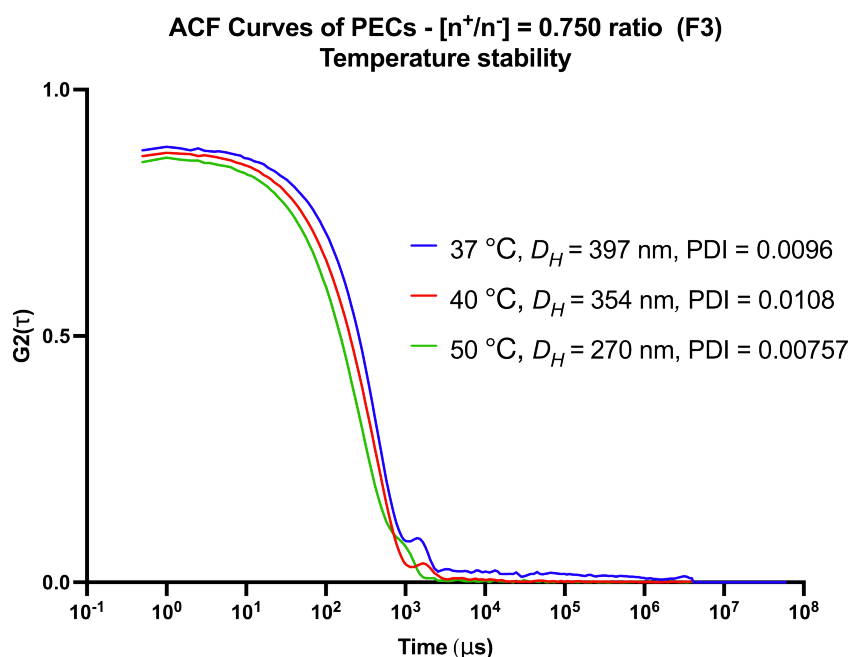


Figure 4.19 – Thermal stability of **PECs**-F3 ($[n^+/n^-] = 0.750$ ratio), monitored with **DLS**. The results are presented as an average of 3 technical replicates for each sample as an **ACF** curves.

With an increase in temperature, **PECs** hydrodynamic radii decreased from the average of 397 to 270 nm. This can be explained by the stronger hydrophobic interactions between **PolB** and **Poly-P2** due to the displacement of water molecules at higher temperatures, which caused the components of the nanoparticles to come closer together. This phenomenon is not new and was observed for proteins and other hydrophobic polymers.^{47,48} The **PDI** of the particles was not greater than 0.0108, suggesting that the integrity of the colloidal structure was not affected by increased temperatures.

It is worth noting that the pH of water, which is the primary medium of **PECs** suspensions, is temperature-dependent.⁴⁹ As the temperature rises, the pH of water tends to become more acidic due to increased concentration of hydrogen ions, caused by

dissociation of water molecules.⁴⁹ At acidic pH (for example at pH 4.0) some of the glutamic acid side-chains of **Poly-P2** (pKa of glutamic acid side chains is ≈ 4.25) would be protonated, consequently leading to reduction of the electrostatic attraction to cationic **PolB** molecules. As result of this the hydrodynamic radii of the particles would increase due to reduced cross-linking between the **Poly-P2** and **PolB** which is contrary to what was observed in the **DLS** data presented in Figure 4.19. Moreover, in the case of the **PECs** discussed in this work, an aqueous buffer (*i.e.*, **HEPES**) was employed to mitigate pH fluctuations, thereby maintaining the pH around the 7.45 mark. Consequently, changes in temperature are expected to have minimal effects on the pH of **PECs** suspensions and as a result should not have a significant impact on the hydrodynamic radii. Therefore, with the assurance that **PECs** would not rapidly disassemble at 40 °C, an experiment was carried out to evaluate their Polymyxin B release properties.

To monitor the concentration of released Polymyxin B in a dialysate, a fluorescamine assay was used following the same procedure as for the identification of the encapsulation efficacy of **PolB** in **PECs** (Section 4.4.2). The measured emission intensities were normalized to the fluorescence of the fluorescamine-**PolB** sample (0.0373 mg/mL - maximum concentration of **PolB** in dialysate), which represented the total concentration of **PolB** that was assumed to pass through the membrane, assuming 100% encapsulation efficacy (Figure 4.20a). The encapsulation efficacy determined in Section 4.4.2 was not used for normalization purposes, as the **PECs** used in the release experiment were not purified in any way, so unencapsulated **PolB** was still present in the particle solutions that were added to the dialysis membrane.

First, **PolB** release from **PECs-F3** without thermolysin was investigated. During the 24-hour period, the relative amine content in a dialysate of **PECs-F3** reached a maximum of 45 % (Figure 4.20a), representative of the drug release under physiological conditions. However, only 26 % of the total amine content was present in the dialysate after five hours of reaction, which can be explained by the release of unencapsulated **PolB** - 29 %, according to the encapsulation efficiency of **PECs-F3** (71 %). Consequently, the rest 19 % (= 45 - 26 %) of the relative amine content can be directly related to **PolB** released as a result of swelling caused by presence of NaCl salt in dialysate. These results nicely follow the results of the physiological stability tests (Section 4.4.3), where **PECs-F3** partially disassembled after 4 hours of incubation under 154 mM NaCl and 37 °C. This implies that stabilizing (*e.g.*, hydrophobic) interactions are responsible for keeping **PolB** and **Poly-P2** together, thus reducing the uncontrolled release of Polymyxin B.

PECs-F3 were then treated with thermolysin, which resulted in a notable increase in relative amine content to 84 % just after 5 hours of incubation, reaching a maximum of

Enzyme-responsive release from PECs - $[n^+/n^-] = 0.750$ (F3)

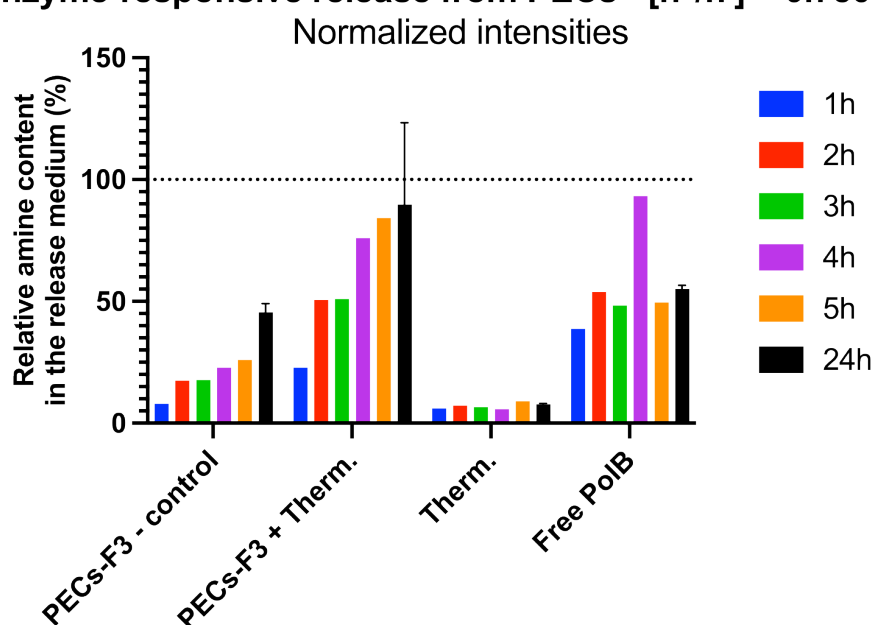


Figure 4.20 – Relative amine content (%) in the dialysate collected during the enzyme-induced release experiment, which is representative of the release of Polymyxin B (PolB) from PECs with $[n^+/n^-] = 0.750$ ratio (F3). Emission intensities were normalized to the fluorescence of fluorescamine-PolB (0.0373 mg/mL), a total concentration of PolB which was presumed to pass (100 %) through the dialysis membrane. Thermolysin control (Therm.) was also included, which represents the relative amine content of thermolysin-fluorescamine adducts. A sample of PolB (Free PolB) with a concentration of 0.209 mg/mL was used to monitor the efficacy of the dialysis membrane to pass PolB. Incubation time: 24 hours. Time points collected at 1,2,3,4,5 and 24 hours, $n = 3$. For unnormalized data, see Figure S4.33.

89 % at the end of the test. This result is 44 % higher than the solution of the non-enzyme treated PECs-F3 under the same conditions. Interestingly, the increase in the relative amine content of the thermolysin-treated PECs was more gradual (T1,2,3,4,5,24 = 23, 51, 51, 76, 84 and 89 %) compared to the previous enzyme degradation experiment (Figure 4.16), where 100 % was reached in one hour from T1 to T2. These differences can be attributed to the use of a dialysis membrane in the release experiment, which created an additional barrier through which PolB and product of Poly-P2 degradation must pass before it can be detected in a dialysate.

To test the efficacy of the dialysis membrane in passing the drug, a sample of free Polymyxin B (0.209 mg/mL), representing the maximum drug loading of PECs-F3, was dialyzed under the same conditions as PECs (labeled as free PolB in Figure 4.20). As illustrated in Figure 4.20, PolB gradually passed through the membrane, reaching a maximum release of 93 % within 4 hours of an experiment, indicating that at least 7 % of PolB was still retained in the membrane. Furthermore, these results confirmed that the rate at which free PolB travels through the membrane was not instantaneous and, as a result, should be taken into account when considering the release profile of PolB.

For example, if complete degradation of **PECs** (100 %) occurred within 1 hour of the experiment (*i.e.*, based on enzyme degradation data), it would take another 3 hours for **PolB** to reach its maximum concentration in the dialysate. Surprisingly, after 4 hours, the relative amine content of free Polymyxin B decreased, probably due to the drug entering back into the membrane. Nevertheless, the release dynamics of free **PolB** through the dialysis membrane was similar to that observed for **PECs-F3** with thermolysin added, again confirming that the delivery system is enzyme-responsive.

The same data on the relative amine content were then used to estimate the cumulative % release of Polymyxin B in the release medium (*i.e.*, converting relative amine content into the amount of **PolB** (mg) in a dialysate) (Figure 4.21). From Figure 4.21 it can be clearly seen that **PECs-F3 + Therm.** followed a similar release trend to the free **PolB** sample, reaching 100 % of the total drug content within 4 hours. Compared to non-enzyme treated **PECs-F3**, they released only 57 % of the total drug content during 5 hours of the experiment. However, it is important to remember that enzymatic degradation would lead to the creation of **Poly-P2** degradation products with the primary amine groups, which would also increase the concentration of amines in the release medium. Since fluorescamine is not selective with which amines to react, the emission intensities seen would not directly correlate with the amount of **PolB** present in the release medium, so the results of cumulative release are overestimated. Therefore, to clarify whether Polymyxin B was present in a dialysate, **HPLC** analyses were performed on the collected samples of the release medium.

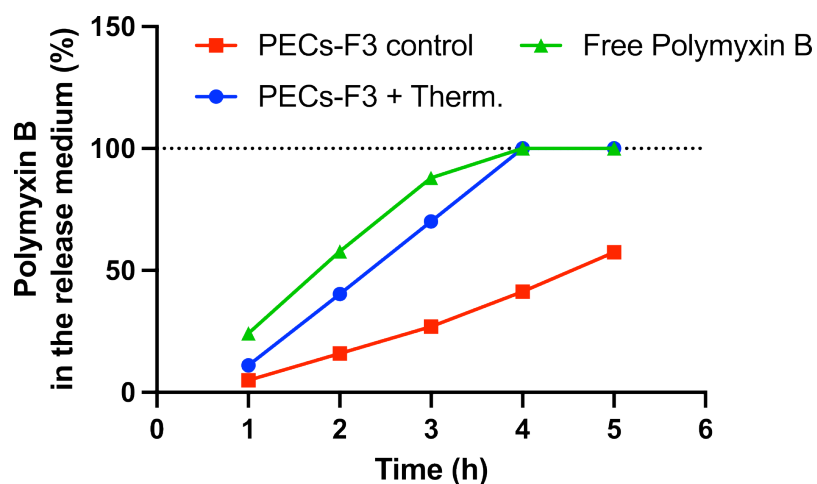


Figure 4.21 – Polymyxin B content in a dialysate collected during the enzyme-induced release experiment, data based on relative amine content from Figure 4.20, $n = 1$.

An adaptation of the analytical method developed by J. Hoogmartens and co-workers was used for the identification of the Polymyxin B content in the dialysate.^{8,22} Prior to analyzing the dialysate samples, a reference chromatogram of Polymyxin B sulfate (in water) was established at a concentration of 0.0250 mg/mL (Figure 4.22). Being a

biologically produced substance, Polymyxin B represents a mixture of peptides with different length fatty acid tails,²² which are different batch-to-batch, so it was challenging to compare the chromatograms found in the literature with those obtained in our laboratory. Therefore, all determinations of the presence of PolB in the dialysate were based on the chromatogram in Figure 4.22, which featured two peaks at 1.89 and 3.73 min that were identified as reference peaks of Polymyxin B. It is important to note that the exact nature of the peaks at 1.89 and 3.73 min could not be confirmed without mass spectrometry data. Consequently, HPLC analysis of dialysate samples was not used to determine the concentration of released PolB. Instead, it was used to give a general indication of whether PolB release had occurred, which could confirm or contradict the fluorescence data regarding PolB release. In addition, HEPES samples containing NaCl were also examined, which were representative of the release medium. The HPLC analysis showed that the PolB peak at 1.89 minutes would co-elute with the HEPES + NaCl mixture and should be carefully monitored in dialysate samples (Figure 4.22).

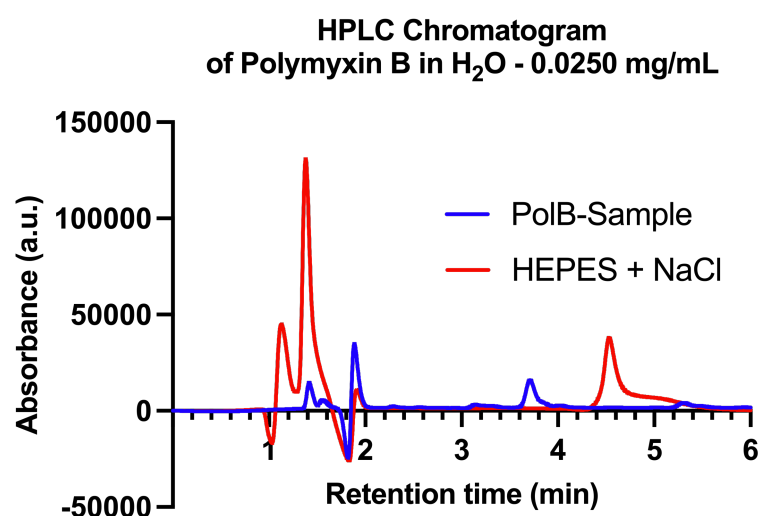


Figure 4.22 – RP-HPLC chromatograms of a control sample of Polymyxin B sulfate in water at a concentration of 0.0250 mg/mL overlaid with chromatograms of HEPES buffer with added NaCl for reference. $n = 1$.

Subsequently, 1 mL of dialysate from the six-time points (1 - 5 and 24 hours) was analyzed with HPLC, producing chromatograms that were overlaid on top of each other for easier comparison of the peak size and area, as indicated in Figure 4.23. Of the two reference peaks of PolB (at 1.89 and 3.73 min), only the peak at 1.89 min was identifiable in the dialysate samples. Another peak was observed at 4.80 minutes, which was associated with the Polymyxin B peak that was previously seen at 3.73 minutes in a reference sample (Figure 4.23). Notably, both peaks at 1.89 and 4.80 min were also present in PolB-control sample (0.0373 mg/mL), which represented the maximum concentration of PolB that can be released from PECs-F3 into the dialysate, assuming

100 % encapsulation efficacy. The intensity and area of the peaks increased over the course of the reaction (based on visual analysis), particularly between 5 and 24 hours, with the peak at 1.89 minutes reaching the highest intensity (31495 a.u. in Figure 4.23). Therefore, based on the visual evaluation of the reference peaks at 1.96 and 4.80 min, the PolB content in the dialysate increased with enzymatic degradation, which confirmed the primary fluorescence data from the enzyme-degradation experiment.

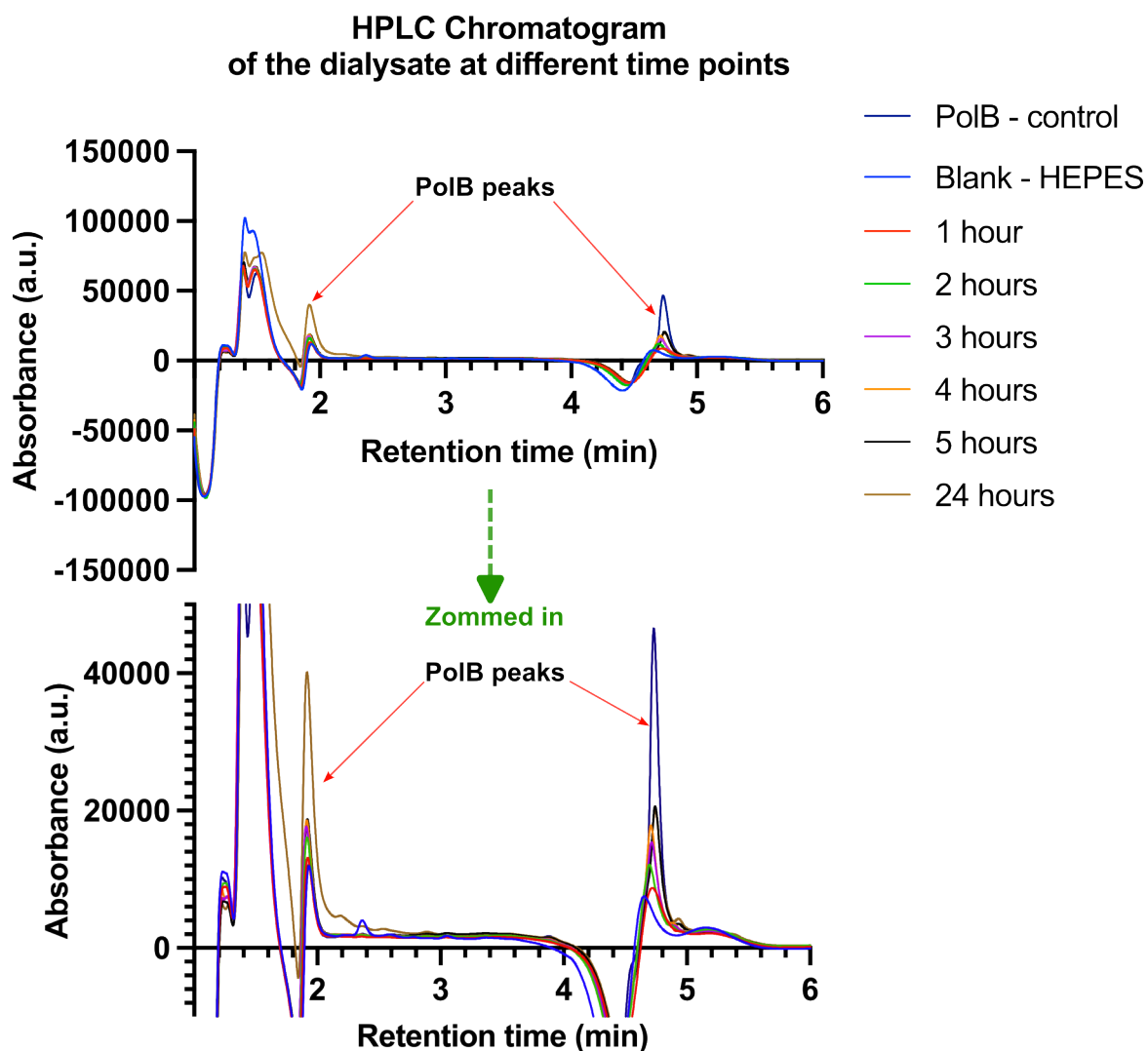


Figure 4.23 – RP-HPLC chromatograms of dialysate samples at 1 - 5 and 24 hours from *in-vitro* release study, including PolB (0.0373 mg/mL) and HEPES control samples. $n = 1$.

In summary, the *in-vitro* release experiment demonstrated that PECs-F3 released PolB in both scenarios with and without added enzyme. Release from non-enzyme treated PECs-F3 was attributed to swelling, caused by the presence of salts under simulated physiological conditions. This was expected and followed the previous physiological stability results discussed in Section 4.4.3. With the addition of thermolysin,

the rate of **PolB** release was increased 5 times (comparing the gradients of the graphs in 4.21), releasing 100 % of its payload (41 % for non-enzyme treated PECs-F3) in 4 hours, resulting in an estimated concentration of **PolB** in the release medium of 0.0373 mg/mL. Although **HPLC** analysis of **PolB** cannot be used to calculate the drug content in dialysate and can be considered inconclusive, when combined with fluorescence data, it confirmed the release of **PolB** from the PECs. It is also worth reminding that the **Poly-P2** structure was designed to incorporate an active release mechanism, where the product of **Poly-P2** degradation repels cationic **AMP**, expelling the drug from the particle. Based on the **PolB** release data, the design of **Poly-P2** polymer was successful in achieving effective drug release, which should translate into high antimicrobial activity of these systems against *P.aeruginosa*. Therefore, the next step was to investigate the antimicrobial efficacy of these **PECs** particles against *P.aeruginosa*.

4.4.6 Antimicrobial activity of **PolB**:**Poly-P2** PECs nanoparticles against *P. aeruginosa*

Comparing the antimicrobial activity of different agents is typically done by measuring their minimum inhibitory concentration (**MIC**). **MIC** is the lowest concentration of an antimicrobial agent that prevents visible bacterial growth. Consequently, lower **MIC** values indicate stronger antimicrobial activity. In the case of Polymyxin B, it was found to be highly effective in inhibiting the growth of *P. aeruginosa*, with **MIC** values ranging from 0.5 to 2 $\mu\text{g/mL}$.² An *in-vitro* release experiment (Section 4.4.5) indicated that the majority of **PolB** used in the assembly of PECs-F3 was released during the experiment. That makes the concentration of Polymyxin B in the dialysate = 37.7 $\mu\text{g/mL}$, which is 7 times higher than the **MIC** of free **PolB**. However, the release experiment did not demonstrate whether the released **PolB** maintained its antimicrobial activity after being encapsulated with **Poly-P2**.

Therefore, a dedicated antimicrobial efficacy test was performed to assess the **MIC** of the selected **PECs** against a model pathogen *P. aeruginosa*. For this, a broth microdilution method was selected, which was used successfully before for the identification of **MIC** of different **AMPs**.²³ For this experiment, two sets of **PECs** were selected with PECs-F3 ($[n^+/n^-] = 0.750$) representing the most stable and PECs-F1 ($[n^+/n^-] = 1.13$) representing the least stable nanoparticle system. Furthermore, the free Polymyxin B solution was also tested and used as a benchmark to compare. Consequently, selected **PECs** and free **PolB** solutions were added at pH 7.4 to the two *P. aeruginosa* cultures of a normal pathogenic strain (**ATCC**-47085) and a multidrug-resistant (**MDR**) strain (**FADDI**-PA067). First, bacterial growth curves were generated at varying concentrations of **PECs** and **PolB** including bacteria without **PolB** (negative control) by graphing

the optical density at 630 nm (OD_{630}) over time. The OD_{630} values of the samples at the time when the exponential growth of the bacteria was complete (i.e., late exponential phase, Figure S4.35a, S4.36a) were normalized to the OD_{630} of the negative control (set as 100 %), expressed as relative bacterial growth (%) (Figure S4.35b, S4.36b). The percentage of relative bacterial growth was then plotted against theoretical PolB concentration found in the sample and linear regression analysis was used to determine the MIC (Figure S4.35 c - e, S4.36 c - e). The minimum inhibitory concentration (MIC) was determined as the concentration where there was only 10% relative bacterial growth according to linear regression and used to compare the antimicrobial activity between samples (Figure 4.24).

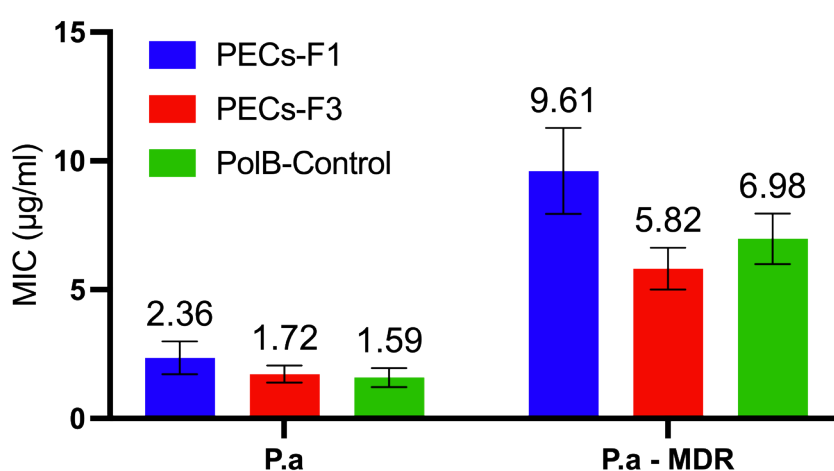


Figure 4.24 – The MIC of PECs-F1 and PECs-F3 including free Polymyxin B (PolB-Control) against normal pathogenic *P.aeruginosa* (ATCC-47085 - P.a) and MDR (FADDI-PA067 P.a - MDR) strains. For the OD_{630} plots see S4.35 and S4.36. MIC were derived from the linear regression analysis of the relationship between percentage of relative bacterial growth against theoretical PolB concentration, which is shown in Figures S4.35 c - e and S4.36 c - e. Data is presented as mean and \pm standard deviation of two replicates.

The results of the tests showed that all PECs had strong antimicrobial activity against both types of *P. aeruginosa* strains, with MIC values on average four times higher for the MDR strain (Figure 4.24). It is anticipated that bacteria with developed resistance will be able to protect themselves through a variety of antimicrobial mechanisms, thus requiring higher concentrations of the drug to inhibit their growth.⁵⁰ PECs-F3 had the lowest MIC (i.e., highest antimicrobial activity) of the two PECs, 1.72 $\mu\text{g/mL}$ compared to 2.36 $\mu\text{g/mL}$ of PECs-F1 (difference of 0.64 $\mu\text{g/mL}$) (Figure 4.24). At first, this result may seem unexpected, as neither of the particle solutions was purified (i.e., pelleting), which meant that suspension of PECs-F1 had higher drug loading of PolB (313 $\mu\text{g/mL}$) than PECs-F3 (209 $\mu\text{g/mL}$). However, in the case of PECs-F1 ($[n^+/n^-] = 1.13$ ratio) neutral aggregates were formed due to charge neutralization during the assembly of the particles (discussed in Section 4.4.1). This neutralization of the cationic

charges of **PolB** (like any other **AMP**) would lead to a decrease in its antimicrobial activity.⁵¹ This is why the difference between the **MIC** of PECs-F1 and PECs-F3 (3.79 $\mu\text{g/mL}$) is even more pronounced against the **MDR** *P. aeruginosa* strain.

PECs-F3 had the **MIC** (1.72 $\mu\text{g/mL}$) closest to that of a free **PolB** sample (1.59 $\mu\text{g/mL}$) against normal pathogenic strain, which confirmed that Polymyxin B was effectively released from the particles. The higher **MIC** of PECs-F3 compared to the free drug can be explained by the presence of various degradation products of **Poly-P2**, some of which are positively charged (**DP-2**, Figure 4.25). These degradation products could disrupt (*i.e.*, compete with **PolB**) the binding of Polymyxin B to bacterial membranes and subsequent destabilization of these membranes.

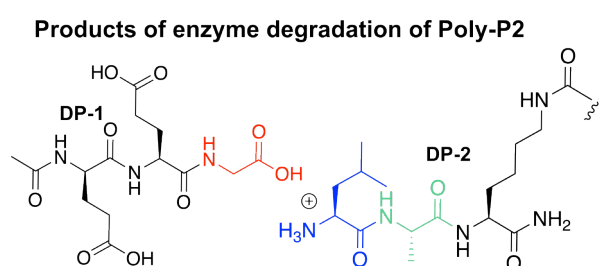


Figure 4.25 – Chemical structures of proposed enzyme degradation products of **Poly-P2** polymer with peptide side chain.

Although the antimicrobial effectiveness of **Poly-P2** on its own was not evaluated, its degradation product, **DP-2**, could exhibit some antimicrobial properties due to its positive charge. However, it is likely that this activity would be significantly lower compared to **PolB**, mainly due to the considerably smaller multivalency and the absence of amphipathic properties (*i.e.*, presence of polar and hydrophobic domains) of **AMPs**, which are important for **PolB**'s antimicrobial mechanism of action.⁵² On the other hand, the presence of cationic degradation products (*i.e.*, **DP-2**) could explain why the PECs-F3 **MIC** was lower than that of the **PolB** sample (5.82 compared to 6.98 $\mu\text{g/mL}$ presented in Figure 4.24) against the **MDR** strain. Potentially, resistant mechanisms of *P. aeruginosa* were not as effective against **DP-2**, which led to slightly better antimicrobial activity of PECs-F3.

In summary, the preliminary results of antimicrobial activity tests showed that the developed **PECs** consisting of **PolB** and **Poly-P2** were highly effective in inhibiting the growth of both *P. aeruginosa* **MDR** and non-**MDR** strains, indicating high antimicrobial efficacy of these nanoparticles. Moreover, the fact that **PECs** were highly antimicrobially active validated the results of the release experiment confirming that Polymyxin B was released from the particles. However, such high antimicrobial activity could potentially lead to significant toxicity against healthy cells in the host organism. Therefore, an obvious next step would be to assess how the toxicity of the created **PECs** in their

inactive (*i.e.*, non-degraded) state compares to the toxicity of free [PoIB](#). For this purpose, a cell viability assay such as MTT (3-(4,5-Dimethylthiazol-2-yl)-2,5-Diphenyltetrazolium Bromide) or LIVE/DEAD assay would be a suitable candidates.

4.5 Conclusions

In this Chapter, we investigated the encapsulation of an FDA-approved AMP, Polymyxin B, within enzyme-responsive PECs nanoparticles. As an encapsulation component, an enzyme-degradable anionic polymer, **Poly-P2** (developed in Chapter 2) was used. To find the most optimized formulation in terms of colloidal stability and drug loading, eight PECs formulations were created with different ratios of PolB to **Poly-P2** (*i.e.*, $[n^+/n^-]$).

Based on DLS analysis, formulation of PECs-F3 with $[n^+/n^-] = 0.750$ consistently produced size distributions with minimal aggregation, while also having the highest estimated Polymyxin B loading of 0.149 mg/mL (71 % encapsulation efficacy). Moreover, according to the encapsulation efficacy data, shielding of the cationic charges of PolB in PECs-F3 may contribute to 71 % reduction in cytotoxicity of the AMP. The assembled PECs-F3 nanoparticles had a hydrodynamic radii (D_H) between 196 and 430 nm with a low PDI of 0.03 - 0.05. TEM was used to confirm the morphology and size of PECs-F3. The particles were found to be spherical in shape, but their size decreased significantly when dried, resulting in an average diameter of 79.3 nm.

To test the stability of particles under physiological conditions (*i.e.*, physiological osmolality), PECs were incubated in 154 mM NaCl solution. Under physiological osmolality, PECs-F3 swelled but did not completely lose colloidal integrity as a result of strong hydrophobic interactions between **Poly-P2** and PolB. To improve the physiological stability of PECs-F3, a strong multi-binding agent in the form of Tannic Acid (TA) was successfully added (PECs-F3), producing particles with slightly smaller D_H of 171 nm. PECs-F3 + TA had excellent resistance to the presence of NaCl, significantly improving the physiological stability of the delivery system.

However, as a result of TA coating the **Poly-P2**, it effectively switched off the enzyme degradation properties of PECs, making the system only weakly enzyme-responsive, degrading by 27 % in 5 hours. In contrast, PECs-F3 without TA reached complete degradation (100 %) in only 2 hours of testing. These degradation results were translated into the *in-vitro* release performance of PECs-F3, where an estimated 100 % of Polymyxin B was released in 4 hours, 43 % more than the non-enzyme treated PECs-F3. Finally, the antimicrobial efficacy of PECs-F3 against *P. aeruginosa* pathogen was assessed. In particular, MIC of PECs-F3 against *P. aeruginosa* (1.72 $\mu\text{g/mL}$) was close to that of free Polymyxin B (1.59 $\mu\text{g/mL}$). In conclusion, this Chapter presented the assembly of PECs nanoparticles from enzyme-responsive polymer **Poly-P2** and FDA-approved AMP, Polymyxin B. These PECs successfully released the encapsulated Polymyxin B under enzymatic degradation, effectively inhibiting *P. aeruginosa* pathogen.

Ultimately, this Chapter proves that it is possible to assemble enzyme-degradable **PECs** particles, loaded with an FDA-approved **AMPs**, which can effectively release sufficient amount of the antimicrobial for bacterial inhibition. Consequently, the logical next phase of the project involves optimizing the delivery system for *in-vivo* applications, which includes pulmonary and topical delivery. However, before proceeding to *in-vivo* studies, it is essential to evaluate and optimize additional properties of the delivery system. These include assessing toxicity towards healthy cells, conducting additional antimicrobial testing against non-specific pathogens (such as *Escherichia coli*), and examining the stability of the particles in various delivery formats such as in wound dressing and nebulized forms.

4.6 Supporting information

Table 4.3 – Summary of DLS data for the PECs-N1 and PECs-N2 (PECs-N1 + Tannic Acid (TA)) formulations evaluated in this work. Average data is presented from 3 technical replicates \pm standard deviation ($n = 3$). For autocorrelation functions (ACF), see Figure S4.26 and for size-intensity plots, see Figure S4.27.

DLS data for PECs-N1 and N2							
	I.D.	$[n^*/n]$ ratio	$D_H \pm SD$ (nm)	Pdi	Z-Ave (nm)	ζ -Potential $\pm SD$ (mV)	[PoIB] (mM)
Before the addition of TA (PECs - N1)	F1	1.130	259 \pm 32.9	0.0161	901	-9.09 \pm 3.34	0.227
	F2	1.00	216 \pm 40.6	0.0353	409	-12.4 \pm 3.20	0.202
	F3	0.750	222 \pm 108	0.237	57.4	-17.6 \pm 4.49	0.150
	F4	0.606	283 \pm 194	0.472	82.7	-7.52 \pm 12.6	0.123
	F5	0.500	281 \pm 158	0.318	74.4	-17.6 \pm 8.53	0.101
	F6	0.438	98.3 \pm 48.4	0.243	226	-16.3 \pm 6.83	0.0884
	F7	0.375	286 \pm 179	0.391	92.6	-15.2 \pm 8.28	0.0758
	F8	0.125	302 \pm 121	0.159	94.8	-17.4 \pm 11.0	0.0253
After addition of TA (PECs - N2)	F1	1.130	208 \pm 67.0	0.103	189	-9.39 \pm 7.21	0.227
	F2	1.000	110 \pm 38.0	0.116	98.7	-9.30 \pm 7.95	0.202
	F3	0.750	170 \pm 97.0	0.325	69.1	-27.2 \pm 4.80	0.150
	F4	0.606	327 \pm 185	0.320	61.5	-35.9 \pm 6.35	0.123
	F5	0.500	280 \pm 136	0.237	67.7	-31.9 \pm 10.7	0.101
	F6	0.438	288 \pm 175	0.368	57.7	-28.0 \pm 10.6	0.0884
	F7	0.375	344 \pm 188	0.297	58.3	-27.0 \pm 16.2	0.0758
	F8	0.125	338 \pm 191	0.320	68.7	-22.4 \pm 10.9	0.0253

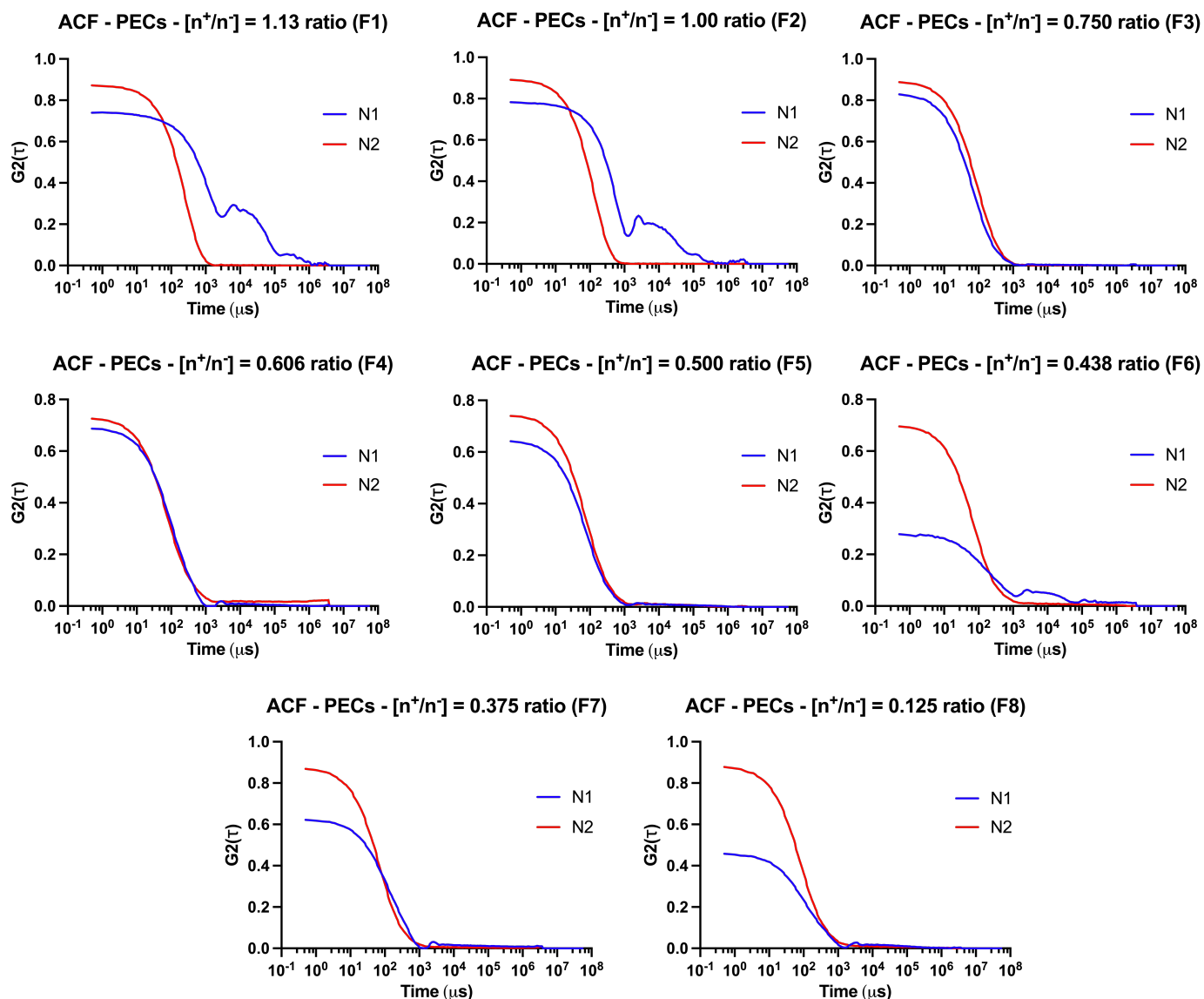


Figure S4.26 – Summary of DLS autocorrelation function (ACF) curves of PECs nanoparticles prepared with Poly-P2 and PolB at $[n^+/n^-]$ ratios of 1.13, 1.00, 0.750, 0.606, 0.500, 0.438, 0.375, 0.125. **N1** - ACF curves directly after 24 hours of mixing, **N2** - ACF curves directly after 24 hours following the addition of Tannic Acid (TA). The results are presented as an average of 3 technical replicates for each sample.

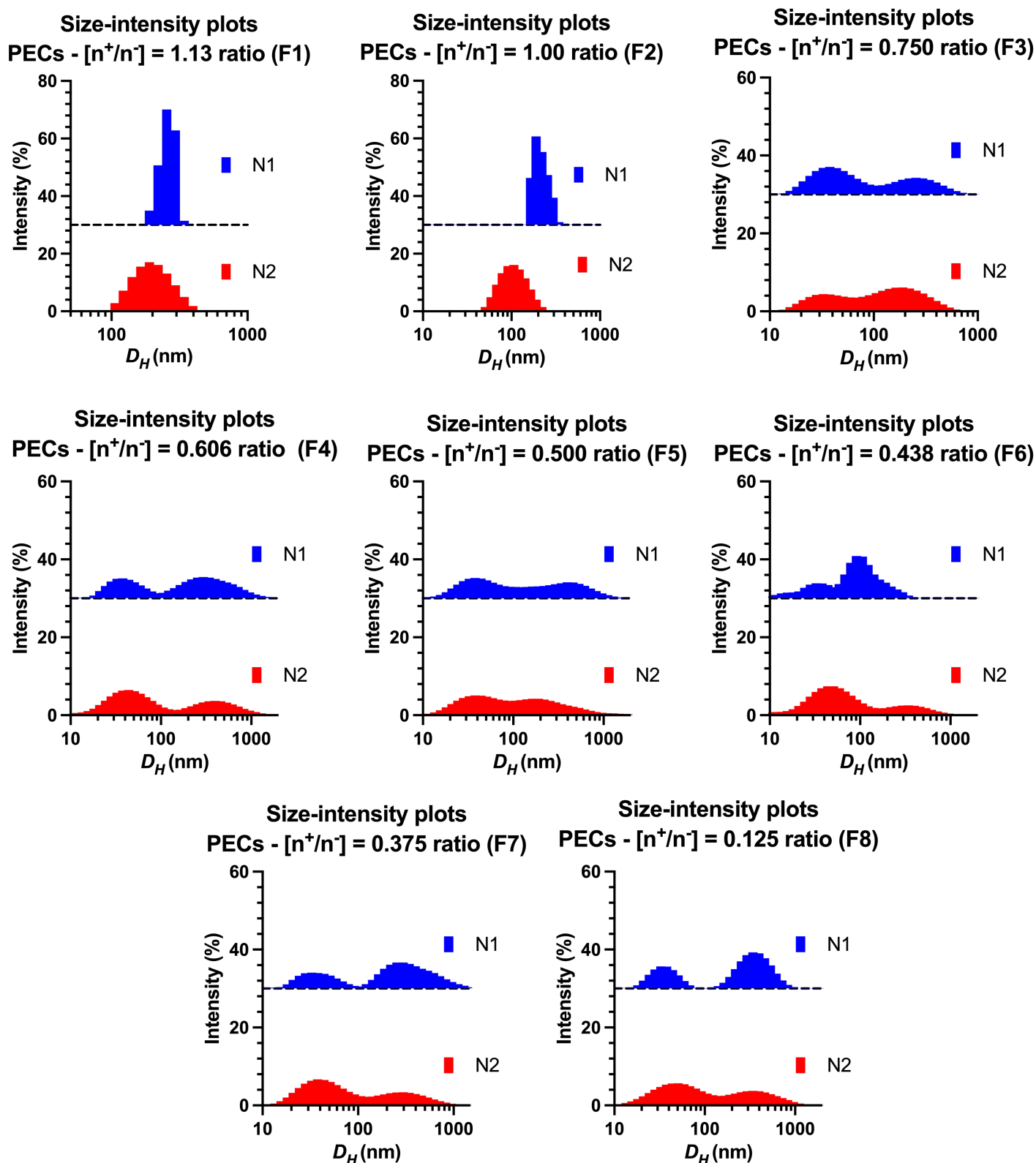


Figure S4.27 – Summary of DLS size-intensity plots of PECs nanoparticles prepared from Poly-P2 at $[n^+/n^-]$ ratios of 1.13, 1.00, 0.750, 0.606, 0.500, 0.438, 0.375, 0.125. **N1** - size-intensity plots directly after 24 hours of mixing, **N2** - size-intensity plots directly after 24 hours following the addition of Tannic Acid (TA). The results are presented as an average of 3 technical replicates for each sample.

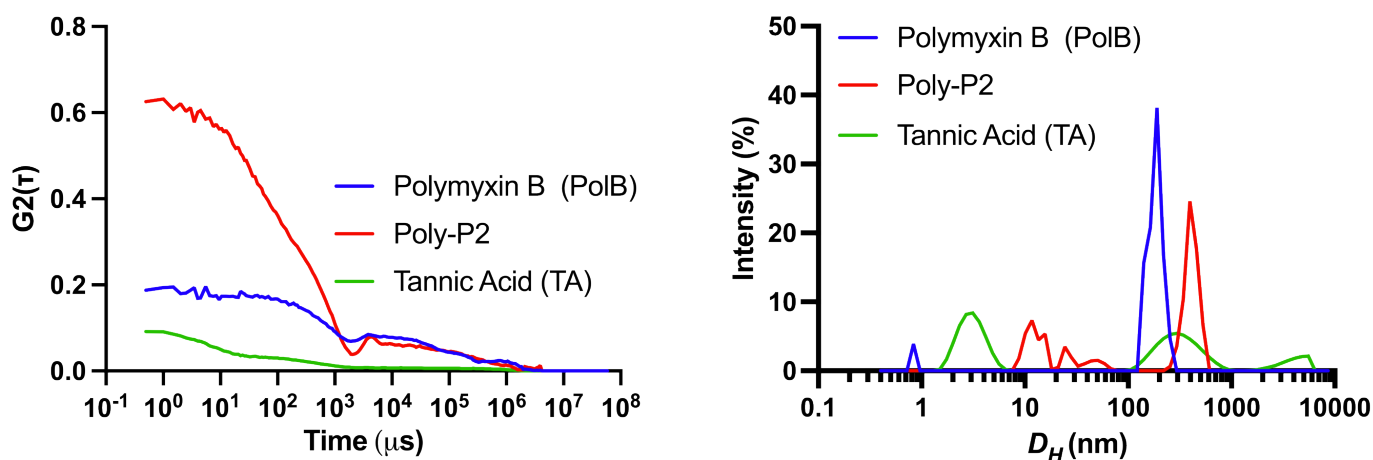


Figure S4.28 – DLS data for the samples of controls: Polymyxin B (PolB), Poly-P2 and Tannic Acid (TA) in 10 mM HEPES solution at pH 7.45. The results are presented as an average of 3 technical replicates for each sample.

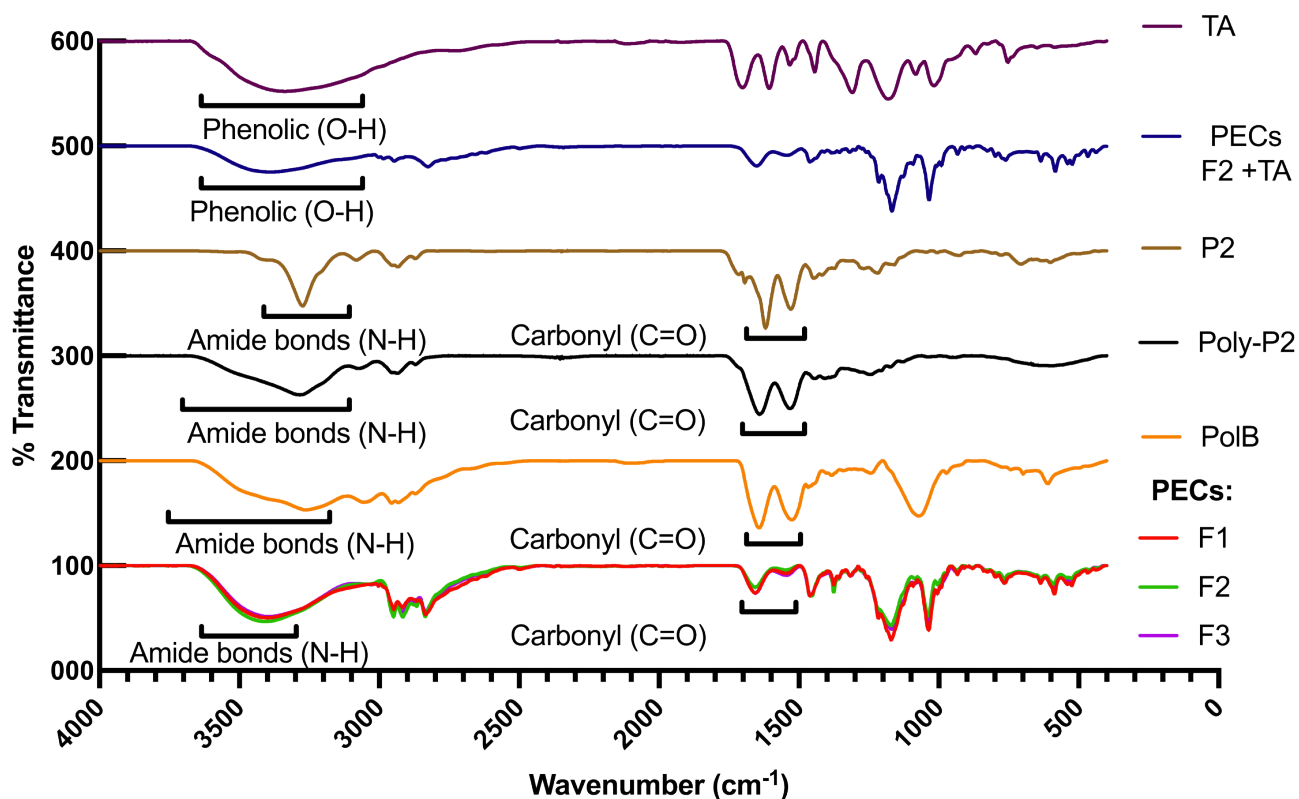


Figure S4.29 – FTIR spectra of Tannic Acid (TA), free drug Polymyxin B (PolB), peptide monomer P2, enzyme degradable polymer Poly-P2, PECs + TA with $[n^+/n^-] = 1.00$ ratio (F2), PECs with $[n^+/n^-] = 1.13$ ratio (F1), $[n^+/n^-] = 0.750$ ratio (F3). $n = 1$.

UV-Vis spectra

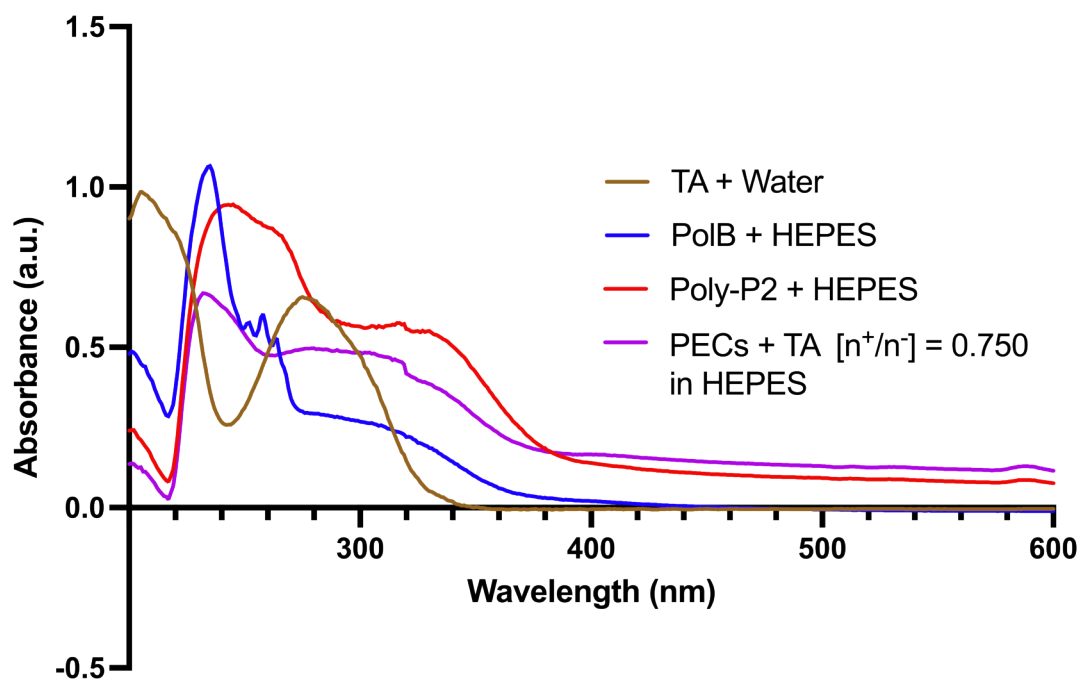


Figure S4.30 – UV-Vis spectra of Tannic Acid (TA), Polymyxin B (PolB), polymer with enzyme-degradable peptide side chain (Poly-P2) and PECs + TA with $[n^+/n^-] = 0.750$ ratio. $n = 1$.

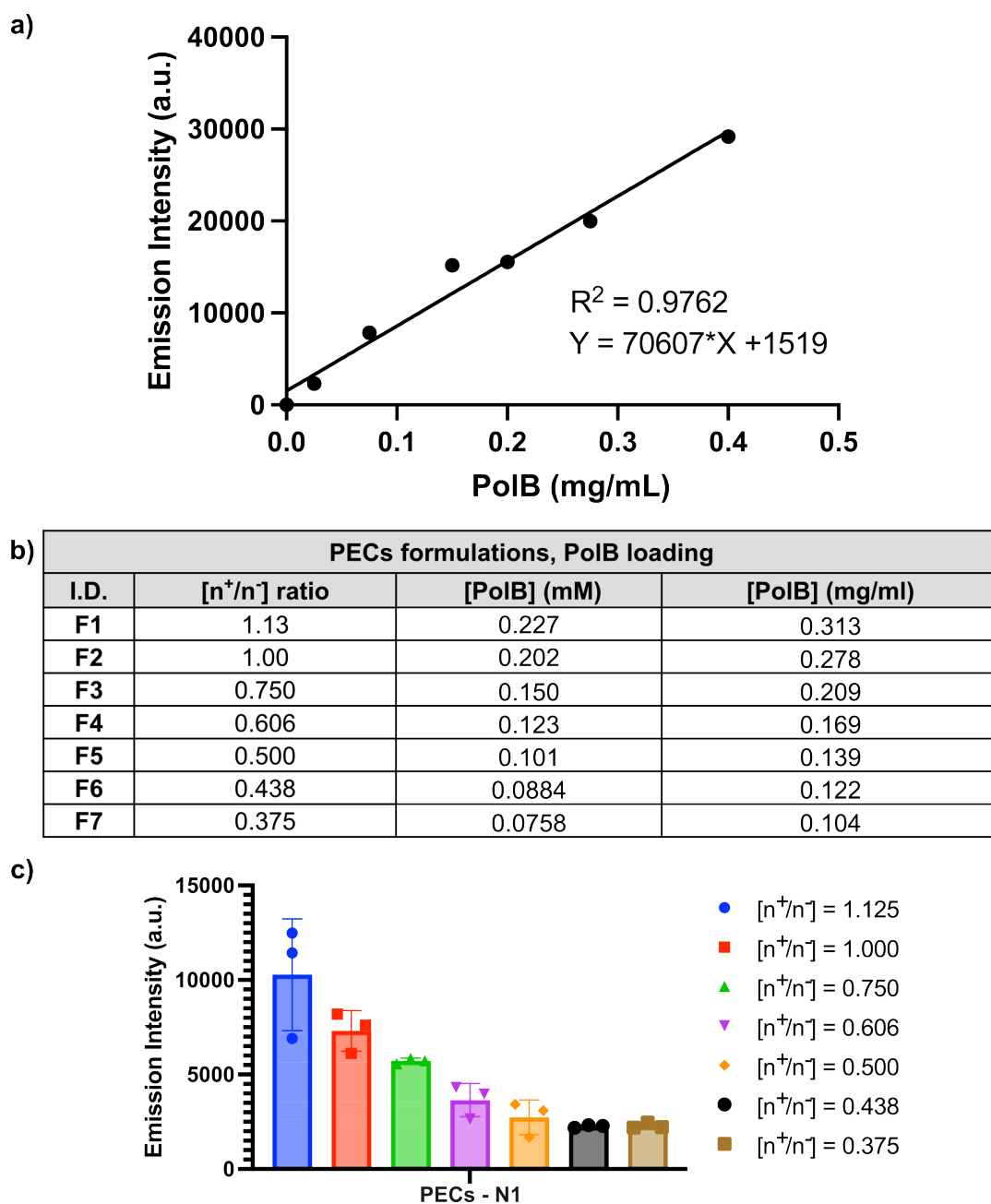
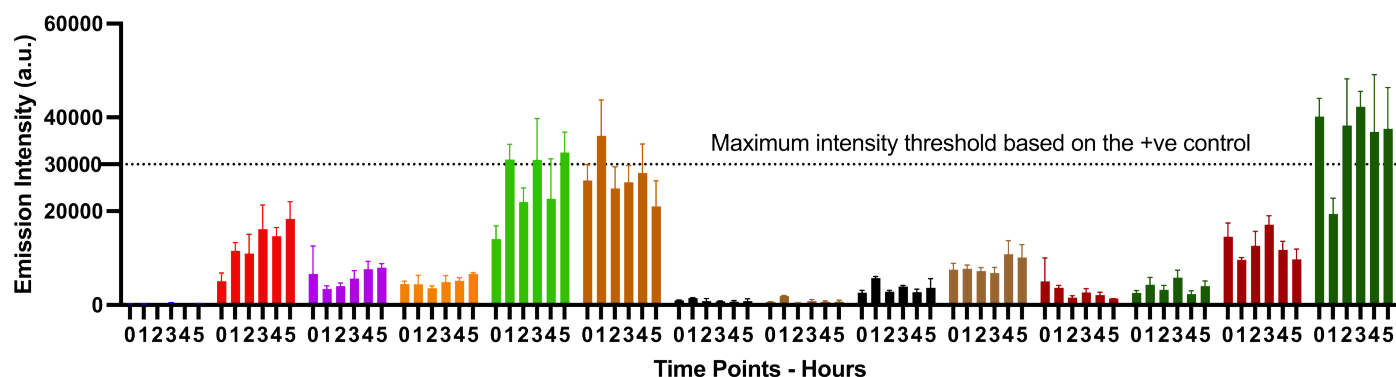


Figure S4.31 – a) The standard curve of Free Polymyxin B-fluorescamine conjugates based on 7 Polymyxin B standards at different concentrations, $n = 3$. b) Polymyxin B concentration in each formulation of PECs. c) Emission Intensity of fluorescamine conjugates for PECs prepared with different PolB concentrations *i.e.*, at different $[n^+/n^-]$ ratios. $n = 3$.

Emission intensity of fluorescamine conjugates from PECs degradation



Acronyms:		Control samples:		Particles with TA:	Particles without TA:
SC	- Succinyl Casein	Buffer		PECs-F1 - Control	PECs-F1 - Control
TA	- Tannic Acid	Therm.		PECs-F3 - Control	PECs-F3 - Control
P3	- NH ₂ -LA-NH ₂ degradation product	SC		PECs-F1 + Therm.	PECs-F1 + Therm.
		TA		PECs-F3 + Therm.	PECs-F3 + Therm.
		SC + Therm.			
		P3			

Figure S4.32 – Emissions intensity (λ_{exc} 365 nm, λ_{em} 470 nm) of fluorescamine conjugates formed for HEPES, CaCl₂, Na₂B₄O₇ buffer (Buffer), Thermolysin as enzyme control (Therm.), succinyl casein (SC) as a control for enzymatic activity, degradation peptide H₂N-LA-NH₂ (P3) as a control to normalize fluorescence intensity, enzyme-responsive PECs: PECs-F1 ($[n^+/n^-] = 1.13$), PECs-F3 ($[n^+/n^-] = 0.750$). All substrates were evaluated in the absence and presence of thermolysin. Incubation time: 5 hours. $n = 3$.

Enzyme-responsive release from PECs - $[n^+/n^-] = 0.750$ Non-normalized intensities

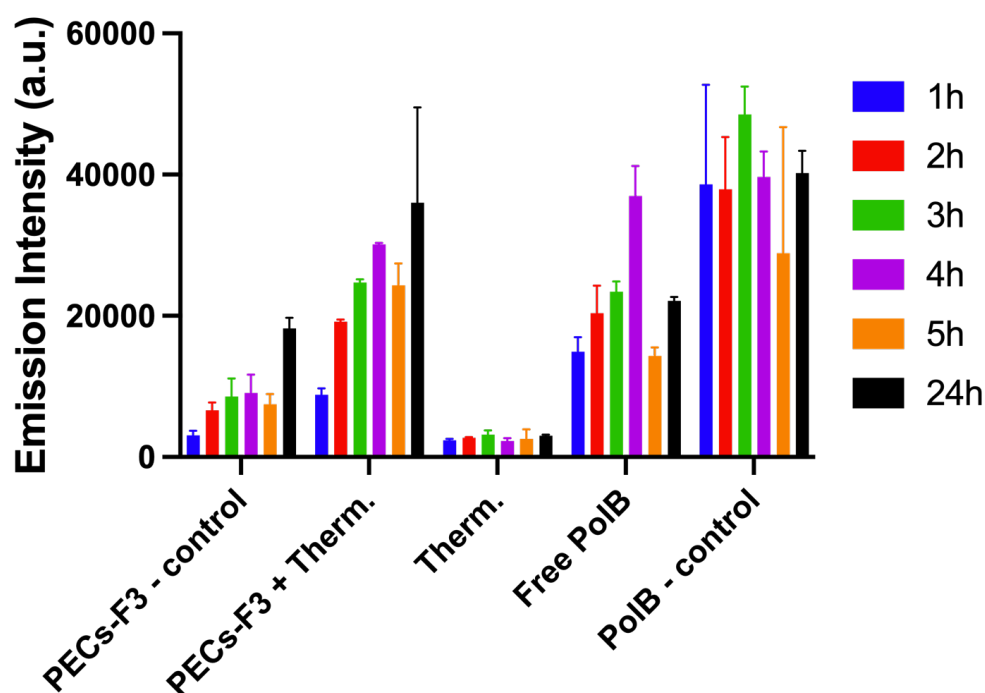


Figure S4.33 – Emissions intensity (λ_{exc} 365 nm, λ_{em} 470 nm) of fluorescamine conjugates found in the dialysate during the enzyme-induced release experiment, which are representative of the release of Polymyxin B (PolB) from PECs with $[n^+/n^-] = 0.750$ ratio (F3). Thermolysin control (Therm.) was also included, which represents the emission intensity caused by the thermolysin-fluorescamine adducts. A sample of PolB (Free PolB) with a concentration of 0.209 mg/mL was used to monitor the efficacy of the dialysis membrane to pass PolB. Incubation time: 24 hours. Time points collected at 1,2,3,4,5 and 24 hours, $n = 3$.

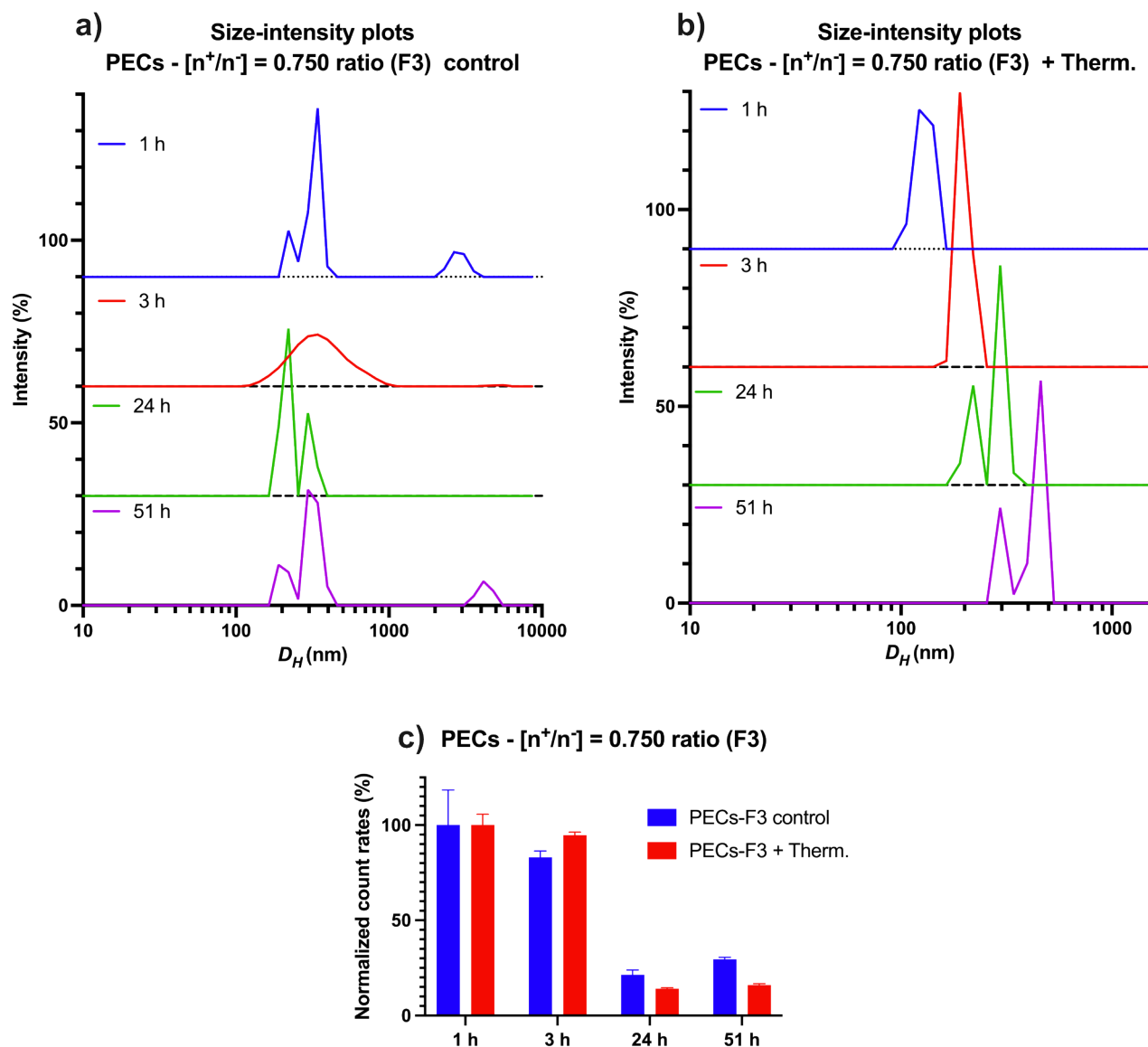


Figure S4.34 – Additional data from *in-vitro* release experiment. **DLS** Size-Intensity distributions of PECs-F3 $[n^+/n^-] = 0.750$ suspensions inside the dialysis membrane over time points = 1,3,24 and 51 hours. a) PECs-F3 control, without added thermolysin, b) PECs-F3 + thermolysin. c) Normalized count rates of PECs-F3 and PECs-F3-control samples inside the dialysis membrane over time points = 1,3,24 and 51 hours. The results are presented as an average of 3 technical replicates for each sample.

Growth curve of *P.aeruginosa* (ATCC-47085)

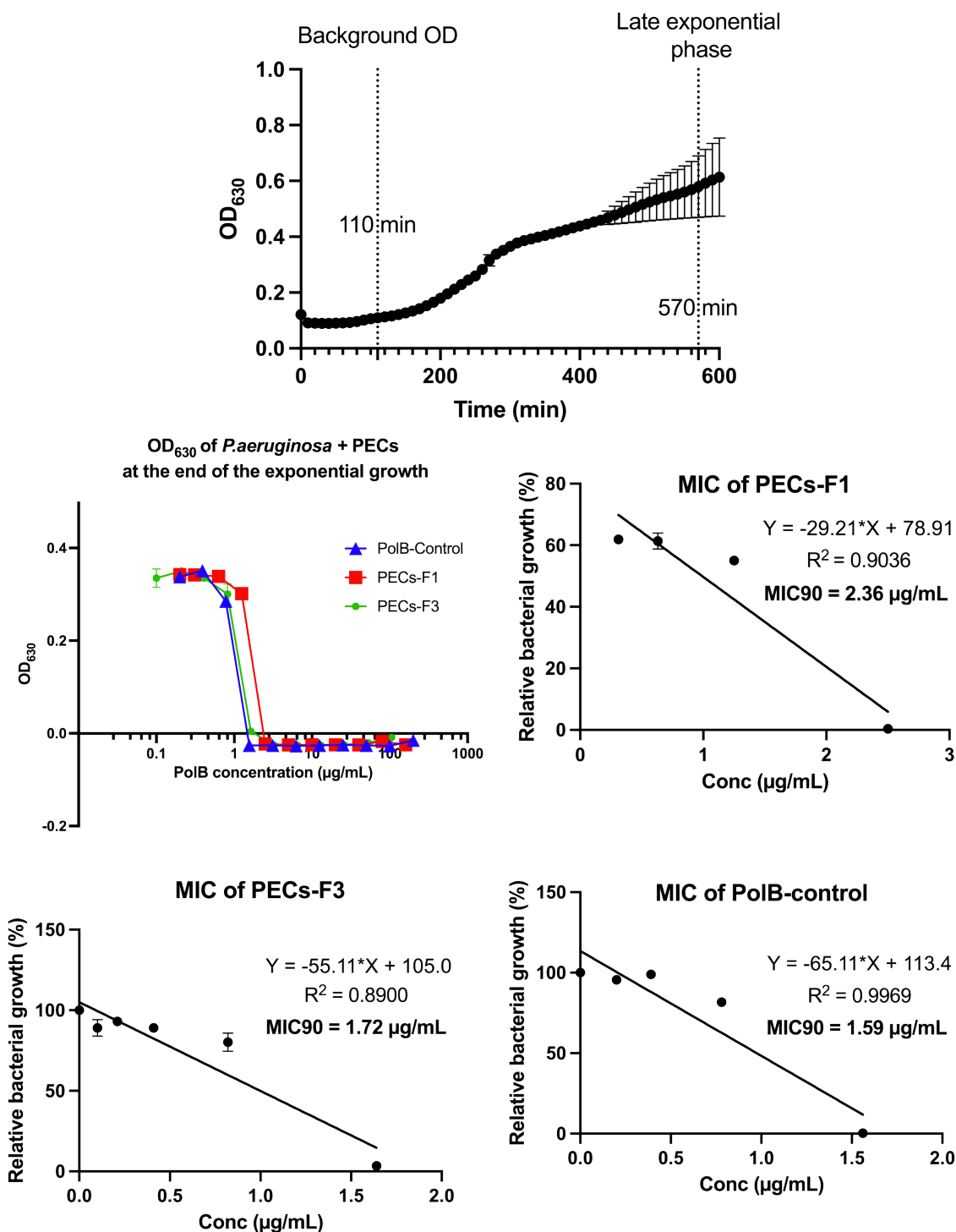


Figure S4.35 – a) Growth curve (OD_{630}) of *P.aeruginosa* (ATCC-47085) in the absence of PECs and PolB, representing negative control. b) OD_{630} at 570 min of PECs-F3, PECs-F1 and PolB-control samples at different drug content concentrations (serial two-fold dilutions). c - e) Relative bacteria growth of samples (%) at different drug content and linear regression analysis for determining MIC. The results are shown as means \pm standard deviations ($n = 2$).

Growth curve of *P.aeruginosa* (FADDI-PA067)

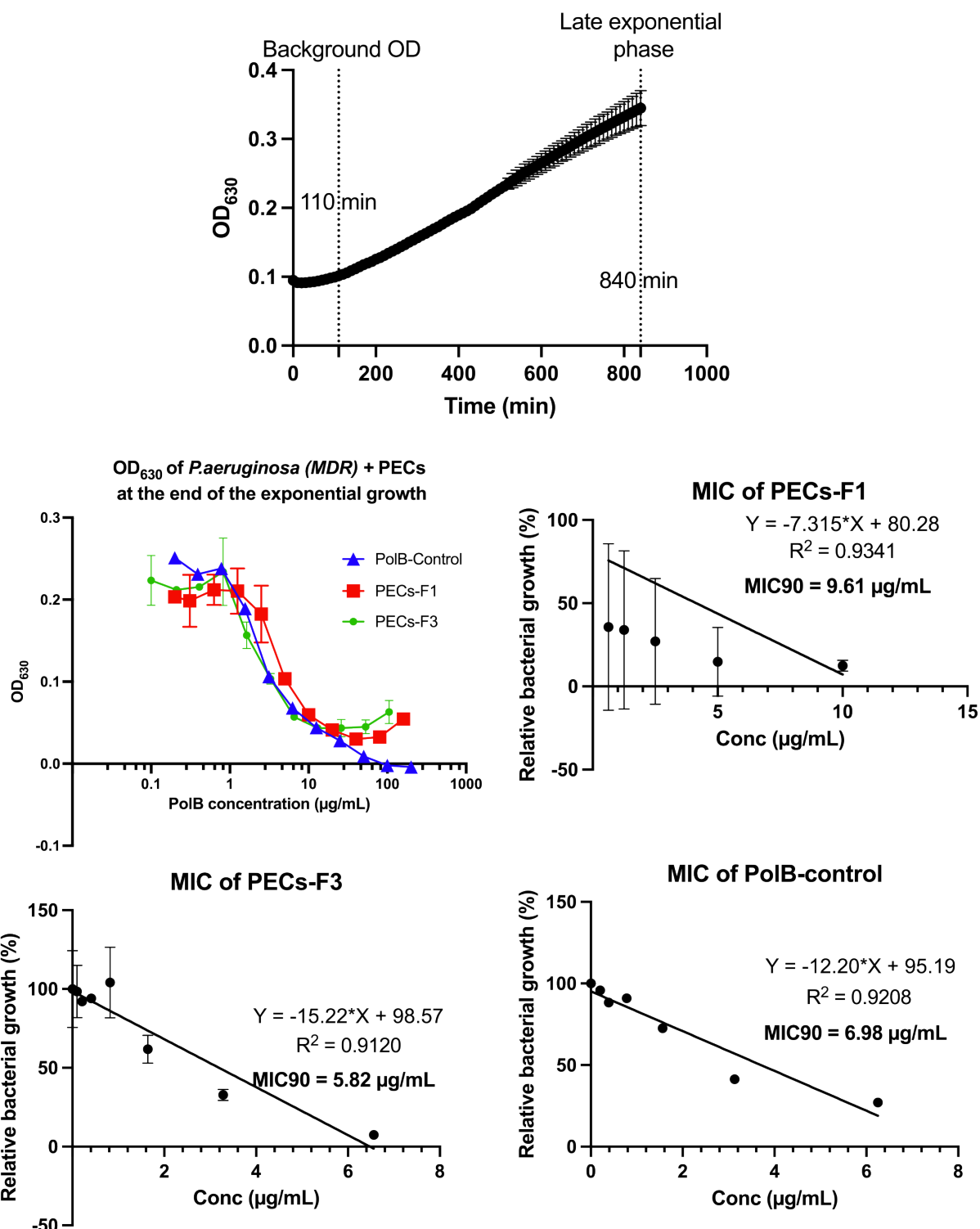


Figure S4.36 – a) Growth curve (OD₆₃₀) of MDR *P.aeruginosa* (FADDI-PA067) in the absence of PECs and PolB, representing negative control. b) OD₆₃₀ at 840 min of PECs-F3, PECs-F1 and PolB-control samples at different drug content concentrations (serial two-fold dilutions). c - e) Relative bacteria growth of samples (%) at different drug content and linear regression analysis for determining MIC. The results are shown as means ± standard deviations (*n* = 2).

4.7 References

- [1] A. Antropenko, F. Caruso and P. Fernandez-Trillo, *Macromolecular Bioscience*, 2023, e2300123.
- [2] *Polymyxin Antibiotics: From Laboratory Bench to Bedside*, ed. J. Li, R. L. Nation and K. S. Kaye, Springer Cham, 2019, vol. 1145.
- [3] A. C. Gales, A. O. Reis and R. N. Jones, *Journal of Clinical Microbiology*, 2001, **39**, 183–190.
- [4] R. L. Nation and J. Li, *Current Opinion in Infectious Diseases*, 2009, **22**, 535–543.
- [5] M. E. Falagas and S. K. Kasiakou, *Critical Care*, 2006, **10**, year.
- [6] I. Zhuk, F. B. Jariwala, A. Attygalle, Y. Wu, M. Libera and S. Sukhishvili, *ACS nano*, 2014, **8**, 7733–7745.
- [7] I. Insua, S. Majok, A. F. A. Peacock, A. M. Krachler and F. Fernandez-Trillo, *European Polymer Journal*, 2017, **87**, 478–486.
- [8] I. Insua, L. Zizmare, A. F. A. Peacock, A. M. Krachler and F. Fernandez-Trillo, *Scientific Reports*, 2017, **7**, 9396.
- [9] M. Chai, Y. Gao, J. Liu, Y. Deng, D. Hu, Q. Jin and J. Ji, *Advanced Healthcare Materials*, 2020, **9**, 1901542.
- [10] T. Pham, P. Loupias, A. Dassonville-Klimpt and P. Sonnet, *Medicinal Research Reviews*, 2019, **39**, 2343–2396.
- [11] J. Aparicio-Blanco, N. Vishwakarma, C.-M. Lehr, C. A. Prestidge, N. Thomas, R. J. Roberts, C. R. Thorn and A. Melero, *Drug Delivery and Translational Research*, 2024, 1–10.
- [12] R. Lakshminarayanan, E. Ye, D. J. Young, Z. Li and X. J. Loh, *Advanced Healthcare Materials*, 2018, **7**, 1701400.
- [13] Z. Lei and A. karim, *Journal of Veterinary Pharmacology and Therapeutics*, 2021, **44**, 281–297.
- [14] T. Hatakeyama, H. Kohzaki and N. Yamasaki, *Analytical Biochemistry*, 1992, **204**, 181–184.

- [15] I. Insua, E. Lamas, Z. Zhang, A. F. A. Peacock, A. M. Krachler and F. Fernandez-Trillo, *Polymer Chemistry*, 2016, **7**, 2684–2690.
- [16] S. Bhattacharjee, *Journal of Controlled Release*, 2016, **235**, 337–351.
- [17] B. A. S. B. M. Bruce A. Koeppen, *Renal Physiology*, Elsevier, 6th edn., 2013.
- [18] S. Udenfriend, S. Stein, P. Böhlen, W. Dairman, W. Leimgruber and M. Weigle, *Science (New York, N.Y.)*, 1972, **178**, 871–872.
- [19] R. Medzhitov, *Nature*, 2008, **454**, 428–435.
- [20] R. Medzhitov, *Cell*, 2010, **140**, 771–776.
- [21] O. Takeuchi and S. Akira, *Cell*, 2010, **140**, 805–820.
- [22] J. A. Orwa, A. V. Gerven, E. Roets and J. Hoogmartens, *Journal of Chromatography A*, 2000, **870**, 237–243.
- [23] S. J. Lam, N. M. O'Brien-Simpson, N. Pantarat, A. Sulistio, E. H. H. Wong, Y.-Y. Chen, J. C. Lenzo, J. A. Holden, A. Blencowe, E. C. Reynolds and G. G. Qiao, *Nature Microbiology*, 2016, **1**, 1–11.
- [24] S. Spoljaric, Y. Ju and F. Caruso, *Chemistry of Materials*, 2021, **33**, 1099–1115.
- [25] M. Björnmalm, K. J. Thurecht, M. Michael, A. M. Scott and F. Caruso, *ACS Nano*, 2017, **11**, 9594–9613.
- [26] Y. Huan, Q. Kong, H. Mou and H. Yi, *Frontiers in Microbiology*, 2020.
- [27] A. Thakur, A. Sharma, H. K. Alajangi, P. K. Jaiswal, Y.-b. Lim, G. Singh and R. P. Barnwal, *International Journal of Biological Macromolecules*, 2022, **218**, 135–156.
- [28] S. Azarmi, W. H. Roa and R. Löbenberg, *Advanced Drug Delivery Reviews*, 2008, **60**, 863–875.
- [29] J. S. Patton and P. R. Byron, *Nature Reviews Drug Discovery*, 2007, **6**, 67–74.
- [30] ChemAxon, *Calculations of degree of protonation were done using Marvin Protonation Plugin, version 19.10.0*, ChemAxon, 2023.
- [31] K. L. Niece, A. D. Vaughan, D. I. Devore, D. I. Devore and D. Devore, *Journal of Biomedical Materials Research Part A*, 2013, **101A**, 2548–2558.
- [32] I. Insua, A. Wilkinson and F. Fernandez-Trillo, *European Polymer Journal*, 2016, **81**, 198–215.

- [33] I. Insua, M. Petit, L. D. Blackman, R. Keogh, A. Pitto-Barry, R. K. O'Reilly, A. F. A. Peacock, A. M. Krachler and F. Fernandez-Trillo, *ChemNanoMat : chemistry of nanomaterials for energy, biology and more*, 2018, **4**, 807–814.
- [34] H. Friedrich, P. M. Frederik, G. de With and N. A. J. M. Sommerdijk, *Angewandte Chemie International Edition*, 2010, **49**, 7850–7858.
- [35] S. Wang, Y. Yu, H. Li, Y. Huang, J. Wang, J. Wang, Q. Jin, Q. Jin and J. Ji, *Journal of polymer science*, 2022, **60**, 2289–2297.
- [36] A. P. Zavascki, L. Z. Goldani, J. Li and R. L. Nation, *Journal of Antimicrobial Chemotherapy*, 2007, **60**, 1206–1215.
- [37] J. Chen, S. Pan, J. Zhou, Z. Lin, Y. Qu, A. Glab, Y. Han, J. J. Richardson and F. Caruso, *Advanced Materials*, 2022, **34**, 2108624.
- [38] J. Song, Y. Ju, T. H. Amarasena, Z. Lin, S. Mettu, J. Zhou, M. A. Rahim, C.-S. Ang, C. Cortez-Jugo, S. J. Kent and F. Caruso, *ACS Nano*, 2021, **15**, 10025–10038.
- [39] S. A. Abouelmagd, N. H. A. Ellah, O. Amen, A. Abdelmoez and N. G. Mohamed, *International Journal of Pharmaceutics*, 2019, **562**, 76–85.
- [40] H. Ejima, J. J. Richardson, K. Liang, J. P. Best, M. P. van Koeeverden, G. K. Such, J. Cui and F. Caruso, *Science (New York, N.Y.)*, 2013, **341**, 154–157.
- [41] J. Zhou, Z. Lin, Y. Ju, M. A. Rahim, J. J. Richardson and F. Caruso, *Accounts of Chemical Research*, 2020, **53**, 1269–1278.
- [42] Y. Han, R. P. M. Lafleur, J. Zhou, W. Xu, Z. Lin, J. J. Richardson and F. Caruso, *Journal of the American Chemical Society*, 2022, **144**, 12510–12519.
- [43] K. Morihara and T. Hiroshige, *Archives of Biochemistry and Biophysics*, 1971, **146**, 291–296.
- [44] K. Morihara, H. Tsuzuki and T. Oka, *Biochimica et Biophysica Acta (BBA) - Enzymology*, 1973, **309**, 414–429.
- [45] M. A. Durá and B. Franzetti, 2013, 1638–1645.
- [46] X. Liu, W. Zhang, C. Yang, Y. Yao, L. Huang, S. Li, J. Wang and Y. Ji, *Microchimica Acta*, 2019, **186**, 247.
- [47] Q. Sun, Y. Fu and W. Wang, *Chemical Physics*, 2022, **559**, 111550.
- [48] C. M. Beliciu and C. I. Moraru, *Journal of Dairy Science*, 2009, **92**, 1829–1839.

- [49] P. Atkins, J. de Paula and J. Keeler, *Atkins' Physical Chemistry*, Oxford University Press, 12th edn., 2023.
- [50] S. Qin, W. Xiao, C. Zhou, Q. Pu, X. Deng, L. Lan, H. Liang, X. Song and M. Wu, *Signal Transduction and Targeted Therapy*, 2022, **7**, 199.
- [51] S. Li, Y. Wang, Z. Xue, Y. Jia, R. Li, C. He and H. Chen, *Trends in Food Science & Technology*, 2021, **109**, 103–115.
- [52] T. Velkov, P. E. Thompson, R. L. Nation and J. Li, *Journal of Medicinal Chemistry*, 2010, **53**, 1898–1916.

Chapter 5

Conclusions

The rapid growth of antibiotic resistance to commonly used antibiotics in healthcare is a major problem, especially for Gram-negative pathogens, as the rate of resistance surpasses the development of new antimicrobial agents. A potential solution is the re-examination of older or less commonly used antimicrobial agents. One such class of antibiotics is antimicrobial peptides, which have high potency against a wide range of priority Gram-negative pathogens such as *P.aeruginosa*. However, many AMPs are associated with toxicity and poor stability *in-vivo*, resulting in low biocompatibility of these agents. A potential solution to address these limitations involves the utilization of stimuli-responsive drug delivery systems for antimicrobial peptides (AMPs) (Introduction - Chapter 1). The charged nature of AMPs makes encapsulation with anionic polyelectrolytes an appealing, simple, and effective solution, which has been investigated by various research teams to create stimuli-responsive polyelectrolyte complexes (PECs) loaded with AMPs (Introduction - Chapter 1). Only a few studies have used more specific bacterial stimuli, such as enzymes. This approach would enable creation of a finely-tuned and highly specific delivery systems for AMPs with the potential to reduce the number of side-effects and limitations associated with these drugs.

Therefore, the overall goal of this Thesis was to explore the feasibility of creating enzyme-responsive PECs for the delivery of an FDA-approved AMPs *i.e.*, Polymyxin B. *P. aeruginosa* was selected as the target pathogen due to its wide range of resistance mechanisms, particularly against conventional antibiotics, making it a challenging organism to treat. Consequently, to ensure that the delivery of AMP was triggered solely by the presence of the pathogen, the encapsulating component needed to respond specifically to LasB. LasB is the protease secreted by *P. aeruginosa* which effectively degrades protein in the tissues, promoting the spread of the pathogen throughout the host body.¹ Furthermore, to ensure both high antimicrobial efficacy and clinical relevance, Polymyxin B was used in the assembly of delivery system without any chemical modifications. This Thesis was structured in such a way that Chapters 2 and 3 concentrated on the synthesis of various enzyme-responsive polymers, while Chapter 4 explored the assembly of PECs using these materials with Polymyxin B.

In Chapter 2, we synthesized two new enzyme-degradable polymers, **Poly-P1** and **Poly-P2**. These polymers had a brush-like structure with a poly(methacrylamide) backbone and anionic LasB-responsive peptide side chains. This design was an evolution of previously reported systems, intended to improve the encapsulation and drug release efficacy of AMPs from polyelectrolyte nanoparticles.^{2,3} Both polymers were readily degraded by thermolysin, an enzyme with selectivity similar to LasB, which demonstrated excellent sensitivity of **Poly-P1** and **Poly-P2** towards *P. aeruginosa*. This results indicated suitability of **Poly-P1** and **Poly-P2** for our goal of creating an enzyme-responsive PECs delivery system.

In Chapter 3, we investigated a different type of polymer backbone with inherent responsiveness to external stimuli, namely poly(acetylenes). These polymers are examples of dynamic helical polymers, which can change their helical structure in response to external triggers, potentially even leading to the breakdown of the backbone. Consequently, it was proposed that different encapsulation polymers with improved sensitivity to bacterial stimuli can be created by combining the enzyme-responsive peptide sequences developed in Chapter 2 with the dynamic helical properties of poly(acetylenes). Three different peptide sequences (**P4**, **P5** and **P6/7**) with different acetylene groups were successfully synthesized using different coupling methodologies. However, none of the attempts to polymerize acetylene-containing peptides using Rh-based catalysts were successful. Reasons for unsuccessful polymerizations were attributed to three potential causes. First, the presence of metal coordinating impurities (*i.e.*, primary amines, carboxylate groups), even after the peptides were purified, poisoned the metal catalyst, leading to a lack of monomer conversion. Second, the use of low monomer concentrations in the polymerization reactions, which was not enough to initiate the formation of the poly(acetylene) backbone. Lastly, in the monomers (**P6/7**) with a larger number of H-bonding groups (*i.e.*, amides), overly stable secondary structures competed with the formation of a helical backbone, thus preventing polymerization.

In Chapter 4, the assembly of enzyme-responsive **PECs** was investigated by combining cationic Polymyxin B with an enzyme-degradable polyanion. **Poly-P2** was chosen over **Poly-P1** due to its higher multivalency, which was expected to improve the encapsulation efficacy and stability of polyelectrolyte nanoparticles. The mixing of polyanion **Poly-P2** and Polymyxin B at different charge ratios ($[n^+/n^-]$) produced **PECs** nanoparticles with varying physiological stability and encapsulation efficacy. Out of eight different formulations **PECs-F3** with $[n^+/n^-] = 0.750$ were determined to be the most optimized due to their low particle aggregation and the highest Polymyxin B loading of 0.149 mg/mL. An indirect assessment based on encapsulation efficacy data suggested that when encapsulated inside **PECs-F3**, Polymyxin B may exhibit up to a 71 % reduction in toxicity effects. Under simulated physiological conditions (*i.e.*, 154 mM NaCl at 37 °C), **PECs** particles swelled but did not completely disassemble, which was attributed to the strong hydrophobic interactions between **PolB** and the anionic polymer, **Poly-P2**. Subsequently, an attempt was made to enhance physiological stability of the particles by incorporating a multi-binding agent, Tannic Acid into the **PECs**. **PECs** with **TA** had significantly improved physiological stability compared to **PECs** without **TA** but at the cost of their enzyme-degradability. The *in-vitro* release of **PECs-F3** demonstrated that 100% of Polymyxin B was released in 4 hours. This release rate was 43 % higher than that of the non-enzyme-treated **PECs-F3**, demonstrating the remarkable effectiveness of the active delivery system. The excellent drug release performance of **PolB:Poly-P2**

PECs was then reflected in high antimicrobial activity against *P. aeruginosa*. The lowest MIC of PECs-F3 was 1.72 $\mu\text{g/mL}$, comparable to that of the free drug Polymyxin B, 1.59 $\mu\text{g/mL}$, indicating their potential for the treatment of priority pathogens such as *P. aeruginosa*.

Therefore, the outcome of this Thesis is the development of a prototype bacteria-specific delivery system based on PECs for clinically relevant AMPs, which is poised to simplify the clinical translation of such delivery systems. To the best of our knowledge, these PECs represent the first example of an enzyme-responsive (*i.e.*, bacteria specific), delivery system utilizing an FDA-approved AMP for treatment of *P. aeruginosa*. Previous efforts to create polyelectrolyte-based delivery systems for clinically approved AMPs often involved compromises between antimicrobial efficacy and physiological stability characteristics. However, in this project, we successfully incorporated a highly effective drug release mechanism without sacrificing the physiological stability of the assembled PECs through the use of an enzyme-degradable encapsulating polymer with brush-like structure.

Moreover, the methods, outcomes, and design principles presented in this work hold promise for the enzyme-responsive delivery of other charged therapeutics, such as anticancer and nucleic acid drugs. Importantly, certain charged drugs like PoIB were demonstrated to be used without the need for chemical modifications, which should make the clinical applicability of these delivery systems much simpler. The highly modular nature of the synthesis methods used in this Thesis (*i.e.*, SPPS and FRP) allows the creation of custom materials with degradation properties tailored to specific enzymes (*i.e.*, disease markers). The simplicity of the PECs assembly streamlines the optimization process, allowing more time for exploration of additional properties and features of the delivery system.

Throughout the project, a variety of challenges were encountered. Some of these were successfully addressed (*e.g.*, the coupling of methacrylate groups), while others require further exploration. This is especially true for Chapter 3, where none of the acetylene-containing peptides were polymerized. With more time and the availability of the necessary starting materials, optimal polymerization conditions can be identified. For instance, the use of improved purification procedures, such as automatic fraction collection in preparative LC-MS would help to eliminate the presence of catalyst-inhibiting side-products, which were one of the major obstacles in the polymerization of acetylene-containing peptides. With respect to **P4** peptide, a version with fully protected carboxylate side chains needs to be synthesized (*e.g.*, using an acid-labile resin such as 2-Chlorotrityl chloride) and its polymerization attempted. Additionally, for **P5**, polymerizations at a higher monomer concentration (*e.g.*, 0.200 M) can be carried out,

which was not possible at the time. For **P7**, the key to successful polymerizations is to reduce the strength of the H-bonds while at the same time maintaining interactions, which can stabilize the helical conformation. One way to weaken H-bonding is by using a more polar solvent such as **DMF** or **ACN** with lower monomer concentrations (*i.e.*, below the critical self-assembly concentration between 0.0294 - 0.0588 M). Alternatively, the propargyl + urea group in **P7** can be removed and replaced with propargyl chloroformate, which could reduce the ability of the **P6/7** sequences to pre-organize in non-polar solvents to a level that is not disruptive to the formation of the poly(acetylene) backbone.

Another aspect of the project that requires further investigation is the physiological stability of **PECs**. Under osmotic pressure, **PECs** swelled and passively released up to 57 % of Polymyxin B, which could lead to high toxicity of these particles in biological environments. The addition of strongly binding agents, such as Tannic acid, improved physiological stability but at the cost of enzyme degradation properties. To improve the physiological stability of the particles, while preserving enzyme-degradation properties, an alternative binding agent with weaker affinities to the components of **PECs** can be tried, for example, Epigallocatechin gallate. Furthermore, the mixing order of the polyelectrolytes can also be further investigated; instead of adding the binding agent after the main assembly of **PECs** (**PolB:Poly-P2**), it can be mixed together with the main polyelectrolytes. Changes in the binding agent and assembly order could potentially result in **PECs** particles with stronger internal cross-linking between components, while also having an enzyme-degradable shell, which can be accessed by the enzyme.

It is also important to highlight that **PECs** are not exempt from the phenomenon of biomolecule adsorption in the biological environments, leading to the formation of a protein 'corona' around the particle.⁴⁻⁶ Therefore, the ability to control the physical-chemical properties (such as size, charge, and surface chemistry) of the particles is crucial for optimizing their behavior in a biological system.^{6,7} As previously mentioned in Section 4.4.1, while the self-assembly methodology for assembling **PECs** may limit control over particle size, surface properties such as charge and chemical characteristics (*e.g.*, hydrophobicity) can be manipulated primarily through the design of the encapsulation polymer. For example, for **Poly-P2** polymer used in assembly of **PECs**, it contains both anionic groups (*i.e.*, COOH) and hydrophobic groups (*i.e.*, -GLA-), thus the accumulated corona would likely be formed from proteins with a combination of hydrophobic and electrostatic domains. The chemical properties of **Poly-P2** can be easily changed by modifying the amino-acid sequence for example adding more hydrophilic character with coupling of histidine residue or attaching a nonfouling groups (*e.g.*, polyethylene glycol (PEG)).^{5,6,8,9} In any scenario the interaction of **PECs** with biological fluids (*e.g.*, using mouse serum) should be studied potentially before transitioning into *in-vivo* mouse model studies.^{5,10}

Furthermore, the toxicity towards mammalian cells of the **PECs** delivery system consisting from **PolB** and **Poly-P2** was not investigated. Understanding the toxicological profile of such **PECs** would be important in evaluating the efficacy of these nanoparticle to prevent the systematic exposure towards the toxic effects of **AMPs**. Therefore, a dedicated experiment (e.g., cell viability assays **MTT** and LIVE/DEAD assay or toxicity *in-vivo*) probing the toxicity of the assembled **PECs** (**PolB:Poly-P2**) particles should be carried out before transitioning to *in-vivo*.

In addition, it was not possible to accurately quantify the amount of **PolB** released under enzymatic degradation using the obtained **HPLC** method. This was because the chromatograms of the **PolB** control samples were different from those reported in the literature and without mass detection, the identity of the peaks seen in the dialysate was unknown. Therefore, to quantify the amount of released **PolB** an **HPLC** method more suitable for detecting **PolB** *in vitro* can be used, such as the method developed by Nation and colleagues, which includes mass detection.¹¹

In the early stages of the Thesis, two potential target applications of enzyme-responsive **PECs** for treating *P. aeruginosa* infections were proposed: delivery into the lungs and topical application as wound dressings. In both scenarios, encapsulating **AMPs** within enzyme-degradable **PECs** is expected to reduce unnecessary proteolytic degradation of the drug, thereby increasing drug retention and reducing dosing requirements. Consequently, the enzyme-specific release of **AMPs** can potentially reduce the rate of development of drug-resistant bacterial strains.^{12–15} For pulmonary delivery, it is crucial to assess the aerodynamic size and stability of the **PECs** (**PolB:Poly-P2**) after nebulization or in dry powder state.^{16,17} Although the outcome of the stability experiment is difficult to predict, it is highly likely that, due to the soft nature (*i.e.*, low rigidity) of **PECs**, particles could partially disassemble under drying, resulting in loss of encapsulation efficacy of the delivery system.¹⁶ Alternatively, nebulization might be a more optimal option for pulmonary delivery as particles would still be present in liquid state, preserving their colloidal structure. For topical administration, **PECs** can serve as an antimicrobial coating in wound dressings for treating burn or chronic wounds, particularly where *P. aeruginosa* growth is prevalent.¹⁸ In wounds, the stratum corneum layer of the skin is impaired, significantly reducing the need for strict control over particle size for deeper penetration into skin layers.¹⁸ Unlike pulmonary delivery, no mechanical treatment of the particle solution (such as drying or nebulization) would be necessary, thereby reducing the possibility of particle degradation. Hypothetically, **PECs** (**PolB:Poly-P2**) particle suspensions could be combined with traditional wound dressings by wetting the dressing with the colloidal solution. As a result, antimicrobial wound dressings are expected to exhibit a stronger and longer-lasting antimicrobial effect, leading to reduced development of antimicrobial resistance in *P. aeruginosa* strains compared to traditional

antimicrobial dressings. Consequently, the recovery time from chronic and burn wound infections should be significantly lowered overall.

In summary, this Thesis aimed to evaluate the key characteristics and attributes of **PolB:Poly-P2 PECs** such as size, charge, physiological stability, enzyme degradability, enzyme-induced drug release, and initial antimicrobial activity. The following section outlines the potential avenues for future work:

- Explore new designs of the encapsulating polymer (including the peptide sequence). Specifically, investigate controlled polymerization techniques to create polymers with various architectures (e.g., star, block, cyclic, and dendritic) and sizes, investigating how the characteristics of the polymer (e.g., size, graft density, hydrophobicity) affect the degradation and release profiles of the final **PECs**.
- Evaluate the toxicity and biocompatibility of **PolB:Poly-P2 PECs** towards mammalian cells and compare with Polymyxin B toxicity, using a dedicated cytotoxicity assay (e.g., LIVE/DEAD assay).
- Assess the selectivity of **PECs** toward *P. aeruginosa in-vitro*, by incubating particles with microorganisms that are not expected to cause polymer degradation, such as *E. coli*.
- Test the antimicrobial efficacy of these **PECs in-vivo** using mouse models. This would demonstrate whether the antimicrobial activity of the particle system would remain effective in the biological environment.
- Investigate the physiological stability of **PolB:Poly-P2 PECs in-vitro** in the presence of human leukocyte elastase by incubating particles in human serum.
- Attempt assembly of **PECs** with other charged therapeutics, including synthetic **AMPs**. This study would provide an indication of the versatility of this delivery system and evaluate its suitability for other areas of drug delivery.
- Explore the stability and antimicrobial activity of **PECs** prepared in various delivery formats, such as in gels/creams, wound dressings and nebulized forms.

5.1 References

- [1] S. Bleves, V. Viarre, R. Salacha, G. P. Michel, A. Filloux and R. Voulhoux, *International Journal of Medical Microbiology*, 2010, **300**, 534–543.
- [2] I. Insua, E. Lamas, Z. Zhang, A. F. A. Peacock, A. M. Krachler and F. Fernandez-Trillo, *Polymer Chemistry*, 2016, **7**, 2684–2690.
- [3] I. Insua, M. Petit, L. D. Blackman, R. Keogh, A. Pitto-Barry, R. K. O'Reilly, A. F. A. Peacock, A. M. Krachler and F. Fernandez-Trillo, *ChemNanoMat : chemistry of nanomaterials for energy, biology and more*, 2018, **4**, 807–814.
- [4] M. P. Monopoli, C. Åberg, A. Salvati and K. A. Dawson, *Nature Nanotechnology*, 2012, **7**, 779–786.
- [5] P. C. Ke, S. Lin, W. J. Parak, T. P. Davis and F. Caruso, *ACS Nano*, 2017, **11**, 11773–11776.
- [6] J. Cui, J. J. Richardson, M. Björnmalm, M. Faria and F. Caruso, *Accounts of chemical research*, 2016, **49**, 1139–1148.
- [7] S. Naahidi, M. Jafari, F. Edalat, K. Raymond, A. Khademhosseini and P. Chen, *Journal of Controlled Release*, 2013, **166**, 182–194.
- [8] C.-M. J. Hu, R. H. Fang, B. T. Luk and L. Zhang, *Nanoscale*, 2014, **6**, 65–75.
- [9] C. Allen, N. Dos Santos, R. Gallagher, G. Chiu, Y. Shu, W. Li, S. Johnstone, A. Janoff, L. Mayer, M. Webb and M. Bally, *Bioscience Reports*, 2002, **22**, 225–250.
- [10] T. Lima, K. Bernfur, M. Vilanova and T. Cedervall, *Scientific Reports*, 2020, **10**, 1129.
- [11] S.-E. Cheah, J. B. Bulitta, J. Li and R. L. Nation, *Journal of Pharmaceutical and Biomedical Analysis*, 2014, **92**, 177–182.
- [12] T. Pham, P. Loupias, A. Dassonville, Klimpt and P. Sonnet, *Medicinal Research Reviews*, 2019, **39**, 2343–2396.
- [13] J. Aparicio-Blanco, N. Vishwakarma, C.-M. Lehr, C. A. Prestidge, N. Thomas, R. J. Roberts, C. R. Thorn and A. Melero, *Drug Delivery and Translational Research*, 2024, 1–10.

- [14] R. Lakshminarayanan, E. Ye, D. J. Young, Z. Li and X. J. Loh, *Advanced Healthcare Materials*, 2018, **7**, 1701400.
- [15] Z. Lei and A. karim, *Journal of Veterinary Pharmacology and Therapeutics*, 2021, **44**, 281–297.
- [16] J. C. Sung, B. L. Pulliam and D. A. Edwards, *Trends in Biotechnology*, 2007, **25**, 563–570.
- [17] J. S. Patton and P. R. Byron, *Nature Reviews Drug Discovery*, 2007, **6**, 67–74.
- [18] R. K. Thapa, D. B. Diep and H. H. Tønnesen, *Acta Biomaterialia*, 2019, **103**, 52–67.